Structure-activity relation of ivermectin:

a Positive Allosteric Modulator of the human P2X4 receptor

Jessica Lauren Meades

Thesis submitted for the degree of Doctor of Philosophy

University of East Anglia
School of Biological Sciences
May 2023

Declaration

I verify that the work presented in this thesis is my own original work and has not been previously submitted for a degree at this or any other university. Where work by other authors has been included, their work has been fully cited and referenced.

In line with the regulations for submission for a degree of Doctor of Philosophy at the University of East Anglia, this thesis has a word count of approximately 53,000 words, which includes all footnotes and references, but excludes the title page; table of contents; list of figures and tables; abbreviations; acknowledgments and the appendix.

Abstract

Ivermectin (IVM) is as a positive allosteric modulator of the P2X4 receptor, a ligand-gated ion channel activated by ATP. Various features restrict IVM as a viable pharmacological tool for P2X4 receptor modulation, including its ability to bind and modulate other mammalian ion channels. Moreover, IVM's binding site and mode of action at the P2X4 receptor has yet to be fully elucidated. Lack of selective modulators for P2X4 channels has hindered research advancement, despite the growing evidence implicating P2X4 as a feasible therapeutic target in several cardiovascular and neurological disorders.

In this study, a library of IVM-analogues was investigated, and the structure-activity relationship was examined by calcium influx assays in 1321N1 cells stably expressing the human P2X4 receptor. Pharmacologically characterising these compounds has allowed ranking of potency and efficacy, and the chemical features of IVM that produce effects at P2X4 to be determined. Such features include redundancy of the large disaccharide moiety and positioning of carbon chains in the spiroketal group. The novel chemical information determined will be useful in the development of more efficacious and potent positive allosteric modulators of P2X4. Another objective of this study was to perform a selectivity screen of the IVM analogues against the GABA(A) receptor. Each compound was screened as an agonist of the GABA(A) receptor at two fixed concentrations (1 µM and 10 µM) using the FLIPR membrane potential assay in L(tk-) cells stably expressing the human recombinant GABA(A) (α1β3γ2) receptor. Two of the 33 compounds screened were identified as having selectivity towards the human P2X4 receptor over the GABA(A) receptor. The information gained from this screen will aid in the discovery and design of novel compounds for selective targeting of P2X4 receptors for future medications.

The P2X4 receptor is highly expressed in vascular endothelial cells. Multiple studies have linked activation of this receptor to the regulation of vascular tone by promoting flow-dependent vasodilation in blood vessels. To test this hypothesis, pressure myography studies were performed on the isolated second-order mesenteric arteries of male mice. This provides an *ex vivo* model to study the effect of IVM in the vasculature at physiological pressures and rates of luminal flow. In this study, IVM was found to significantly potentiate flow-mediated vasodilation in pre-constricted mouse mesenteric arteries. Since IVM is known to enhance P2X4 function, this data suggests that P2X4 receptors are involved in the flow-sensitive mechanism that regulates blood pressure. This demonstrates the therapeutic potential of positive modulation of P2X4 in the treatment of cardiovascular diseases such as hypertension or ischemia.

Table of Contents

List of Figures

Chapter 1

Chapter 2

Chapter 3

Chapter 4

Chapter 5

List of Tables

Abbreviations

IVM	Ivermectin
IVM-B1a	Ivermectin B1a
IVM-B1b	Ivermectin B1b
ABM	Abamectin
DRM	Doramectin
EPM	Eprinomectin
SLM	Selamectin
MBM	Milbamectin
NEM	Nemadectin
MOX	Moxidectin
ATP	Adenosine 5'-triphosphate
Ach	Acetylcholine
ADP	Adenosine diphosphate
AUC	Area under the curve
AUD	Alcohol use disorder
BDNF	Brain-derived neurotrophic factor
BSS	Buffered Saline Solution
Ca^{2+}	Calcium Ions
$CaCl_2$	Calcium chloride
CNS	Central nervous system
CO_2	Carbon dioxide
DEX	Dexamethasone
DMEM	Dulbecco's Modified Eagle Medium
DMSO	Dimethyl sulfoxide
EC	Endothelial cells
EC_{50}	Half maximal effective concentration
ECD	Extracellular domain
EDTA	Ethylenediaminetetraacetic acid
E_{max}	Maximal response/efficacy
ER	Endoplasmic reticulum
FBS	Fetal Bovine Serum
FLIPR	Fluorometric imaging plate reader
FMP-dye	Fluorescent membrane potential dye
FXR	Farnesoid X receptor
GABA	Gamma-aminobutyric acid
GABA(A)R	Gamma-aminobutyric acid type A receptor
GIRK	G protein-coupled inwardly-rectifying potassium channels
GluCl	glutamate-gated chloride channels
GlyR	Glycine receptors
GPCRs	G-protein coupled receptors
HBSS	Hanks Balanced Salt Solution
HEPES	4-(2-hydroxyethyl)-1-piperazineethanesulfonic acid

HF	Heart failure
HUVECs	Human umbilical vein endothelial cells
IC_{50}	Half maximal inhibitory concentration
KCl	Potassium chloride
KH_2PO_4	Potassium dihydrogen phosphate
KPSS	Potassium Physiological Saline Solution
LB	Loading buffer
$MgCl_2$	Magnesium chloride
$MgSO_4$-$7H_2O$	Magnesium sulfate heptahydrate
mRNA	Messenger ribonucleic acid
Na_2HPO_4	Disodium phosphate
nAChR	Nicotinic acetyl-chloride receptors
NaCl	Sodium Chloride
NAFLD	Non-alcoholic fatty liver disease
$NaHCO_3$	Sodium bicarbonate
NAM	Negative allosteric modulator
NaOH	Sodium hydroxide
NLRP3	NOD-like receptor 3
NO	Nitric oxide
PAM	Positive allosteric modulator
PBS	Phosphate buffered saline
PE	Phenylephrine
PPADS	Pyridoxalphosphate-6-azophenyl-2',4'-disulfonic acid
PSS	Physiological Saline Solution
RA	Rheumatoid arthritis
RT	Room temperature
RyR	Ryanodine receptor
SBS	Salt buffered saline
SEM	Standard error of the mean
SERCA	Sarcoendoplasmic reticulum calcium transport ATPase
SR	Sarcoplasmic Reticulum
Tg	Thapsigargin
TMD	Transmembrane domain
TNF-α	Tumour Necrosis Factor-alpha
UDP	Uridine diphosphate
UTP	Uridine triphosphate
WT	Wild-Type

Acknowledgements

Firstly, I would like to acknowledge and give thanks to my supervisor Prof Samuel Fountain, who made this work possible. His guidance, support and encouragement has helped me to see the project to completion and moulded me into a better researcher. I would also like to thank my secondary supervisor Prof Mark Searcy for his support and advice which has helped me to better interpret and understand the medicinal chemistry side of the project. I would also like to thank the BBSRC doctoral training partnership and my industrial partner Merck Sharp & Dohme (MSD), for funding my research project.

I would like to give thanks to the entire Fountain lab, with special thanks to Anna Fortuny Gomez, Sonia Paz Lopez, Michelle Fletcher and Estela Perez Santamarina. I feel lucky to have such a brilliant and supportive group of friends in my life. Anna, you have always been there for me, throughout the good and the bad times and I will be forever grateful that I was able to experience this journey with you. I would also like to extend my thanks to Maria Del Carmen Glez-Montelongo, who patiently taught me how to use the pressure myograph and was always happy to help me throughout my project.

I would also like to acknowledge my friends Lisa and Hollie. Both of you have helped me to de-stress, whether its scuba diving in Greece or bouldering every Wednesday night at highball. I would also like to thank my friends Rachael and Joe, who helped me to stay positive throughout the pandemic through our weekly game and quiz nights.

Finally, I would like to thank my family for their unwavering support and love throughout my project. I would especially like to thank my parents for believing in me and supporting me every step of the way.

Chapter 1. Introduction

1.1 Purinergic signalling

The discipline of purinergic signalling was first instigated when the macromolecule adenosine triphosphate (ATP), otherwise known as the energy currency of eukaryotic cells, was recognised to play an important role as an extracellular signalling molecule. This concept was first proposed following the accidental discovery by Burnstock and his team of the existence of non-adrenergic non-cholinergic transmission when studying nerve signalling in the guinea-pig taenia coli in the 1960s (Burnstock, 2006). However, the neurotransmitter remained elusive until the early 1970s when Burnstock demonstrated that ATP could satisfy the criteria for a neurotransmitter and first coined the phenomenon "purinergic signalling" in a review two years later (Burnstock et al., 1970; Burnstock, 1972). Despite providing strong evidence that purines could act as neurotransmitters his theory was controversial. ATP already had an established role in energy metabolism and DNA/RNA synthesis and therefore was an unlikely candidate for such widespread extracellular communication (Burnstock, 2006). A few years later, support for his purinergic signalling hypothesis arose with the recognition of two families of purine receptors that could bind to these neurotransmitters: the P1 receptors, selective to adenosine, and the P2 receptors, selective to ATP and adenosine diphosphate (ADP) (Burnstock and Ralevic, 1998).

The P2 receptor family was later subdivided into two families due to major differences in receptor pharmacology. These two families of receptors were designated the names P2X (ionotropic receptors) and P2Y (metabotropic receptors), which comprised ligand-gated ion channels and G-protein coupled receptors, respectively (Burnstock & Kennedy, 1985). However, it was not until the receptors were cloned and characterised in the early 1990s that the hypothesis was fully accepted (Burnstock, 2006). These purine and pyrimidine receptors are now known to be expressed across many cell types in the body and have been implicated in an ever-growing number of physiological processes and disease states. As a result, interest from the scientific community to fully understand these receptors has grown and they are now regarded as highly interesting and understudied therapeutic targets.

1.1.1 P1 receptors

P1 receptors are G-protein coupled receptors (GPCRs) sensitive to adenosine, as such they are often referred to as adenosine receptors. Four subtypes of P1 receptor have been cloned: A1, A2A, A2B, and A3. Like other GPCRs, P1 receptors are characterised by seven putative transmembrane spanning regions with the N-terminus on the extracellular side, and the C-terminus on the cytoplasmic side of the membrane (Burnstock, 2007). P1 receptors are involved in the adenosine 3',5'-cyclic monophosphate (cAMP) pathway. Specifically, activation of the A1 and A3 subtypes inhibits adenylyl cyclase and consequently a decrease in the secondary messenger cAMP, while activation of A2A and A2B activates adenylyl cyclase and promotes cAMP formation. This in turn regulates the activity of cAMP-dependant protein kinase, which mediates downstream cellular effects by phosphorylation of target proteins. P1 receptors have been linked to the regulation of many physiological processes

involving blood flow, immune response, and synaptic activity in the central nervous system (Jacobson and Gao, 2006). Although, the molecule adenosine is arguable the most recognised for its role in sleep through the activation of A1 receptors and the effects of a well-known A1 antagonist – caffeine – in the nervous system (Burnstock, 2007).

1.1.2 P2Y receptors

As with the P1 receptors, P2Y receptors are also a type of GCPR and are reported to respond to a range of mononucleotides such as ADP, ATP, UDP, or UTP. In total eight subtypes of P2Y receptor have been identified: P2Y1, P2Y2, P2Y4, P2Y6, P2Y11, P2Y12, P2Y13 and P2Y14 (Burnstock, 2007). Crystal structures of the P2Y1 and P2Y13 receptors confirmed they share similar structural architecture to other solved GCPRs, including seven transmembrane regions connected to three large intracellular and extracellular loops (Kügelgen and Hoffmann, 2016). Based on pharmacology and structure, the P2Y superfamily is split into two structurally distinct families, referred to as P2Y1-like and P2Y12-like receptors. The receptors of the first subfamily, the P2Y1-like receptors, consist of the P2Y1, P2Y2, P2Y4, P2Y6 and P2Y11 receptors and are Gq-coupled receptors. Activation of these receptors stimulates phospholipase C production and a release of calcium from intracellular stores. The other subfamily, the P2Y12-like receptors, consists of P2Y12, P2Y13, and P2Y14 and signal primarily through Gi proteins. Downstream signalling events induce inhibition of adenylate cyclase activity and subsequent reduction in cAMP production (Kügelgen & Hoffmann, 2016; Jacobson et al., 2020).

1.1.3 P2X receptors

P2X receptor channels are a family of ligand-gated ion channels that are activated through the binding of adenosine triphosphate (ATP). These ion channels are found embedded into the membrane of a diverse array of cell types and are permeable to a range of monovalent (potassium, K^+ and sodium, Na^+) and divalent (calcium, Ca^{2+}) cations (Franklin et al., 2014). P2X channels can exist as homo or heterotrimers from a repertoire of seven peptide subunits (P2X1-7), although very little is known about the heteromeric composition or function of these receptors (North, 2002; Oken et al., 2022). The gating of P2X receptors usually consists of ATP binding resulting in receptor activation, a desensitisation step and a rapid deactivation phase after ATP is removed. The main differences between the P2X receptors is there sensitivity to ATP, and desensitization kinetics (Coddou et al., 2011). The homomeric P2X1 and P2X3 receptors are known to be rapidly desensitising (milliseconds), whilst P2X2, P2X4 and P2X7 are slow desensitizing (North, 2002). P2X1 and P2X4 receptors are the most sensitive to ATP with sub-micromolar potency values. High concentrations of ATP (millimolar) are required to activate P2X7 receptors, making them the least sensitive P2X subtype. P2X2, P2X3 and P2X5 (exon 10 containing) exhibit moderate sensitivity to ATP, and P2X6 is considered a silent receptor in humans (Coddou et al., 2011; Illes et al., 2021; King et al., 2022).

Despite only sharing 30-50% sequence identify, all members of the P2X family share a similar three-dimensional structure. This consists of a large cysteine-rich extracellular domain where ATP binds and two transmembrane domains (TM1 and TM2) with short intracellular amino and carboxyl termini (Burnstock, 2006). Upon ATP binding a conformational change within the transmembrane domain

triggers the cation-selective pore to open, allowing the passage of ions and subsequent depolarisation of the cell, triggering downstream signalling events (Samways et al., 2014). These receptors are ubiquitously expressed across the human body including in the cardiovascular, nervous and immune systems and have been implicated in a range of physiological conditions such as pain processing, smooth muscle contraction and inflammation (Surprenant and North, 2009).

1.2 The P2X4 receptor

The P2X4 receptor is a ligand-gated ion channel that belongs to the P2X family. It shares many characteristics with the other subtypes, including its three-dimensional structure, topology and ability to bind ATP, but varies in its expression pattern, selectivity and binding kinetics. There is growing evidence to suggest that P2X4 plays an important role in many pathophysiological processes, including hypertension, neuro-inflammation, and neuropathic pain, making it a very interesting drug target.

1.2.1 Structure and channel opening

In 2009, the first homomeric P2X crystal structure was solved, the apo (unbound) closed state of the truncated zebrafish P2X4 (zfP2X4) receptor, confirming the trimeric architecture of the P2X receptor family (Figure 1.1) (Kawate et al., 2009). The crystal structure revealed three subunits, each resembling the shape of a leaping dolphin, that come together to form the P2X4 receptor (see Figure 1.2). Kawate et al. (2009) used this analogy to describe the structural components of each subunit. This included the body, head, dorsal fin and right and left flippers for the large extracellular domain, and the tail (fluke) of the dolphin corresponding to the two transmembrane domains (TM1 and TM2) attached to intracellular amino and carboxyl termini. Furthermore, inspection of the crystal structure revealed the presence of three lateral fenestrations or portals, linker regions in the interface between the extracellular domain and transmembrane domain. Based on the structure, Kawate et al. (2009) suggested two pathways by which ions might access the pore. The first hypothesis was the lateral pathway, where the lateral fenestrations would change shape and provide an access point for ions to enter the pore. The second hypothesis was that ions would access the pore using a central pathway through the ectodomain of the receptor via three vestibules (upper, central and extracellular) (Kawate et al., 2009). A few years later, the first hypothesis (the lateral pathway) was validated by Gouaux and Hattori (2012), who stated that the central pathway via the upper and central vestibule is too small for ion permeation.

To activate the channel, ATP must bind to the ATP-binding site. The subsequent publication of the open, ATP-bound state of the zfP2X4 receptor revealed three ATP-binding pockets located in the extracellular domain (ectodomain) of the receptor (Figure 1.1) (Gouaux and Hattori, 2012). This discovery, coupled with other biochemical and functional studies, has greatly improved our understanding of where ATP binds and how ATP-binding results in channel gating (Chataigneau et al., 2013). Previous mutagenesis studies investigating highly conserved residues within the extracellular loop of the receptor have identified specific residues critical for ATP recognition, including K70, K72, K316, N296, R298 and K319 (zfP2X4 numbering) (Habermacher et al., 2016). The proximity of these

residues to the ATP binding site was confirmed by X-ray crystallography of the ATP-bound zfP2X4 receptor (Gouaux and Hattori, 2012). In the extracellular domain, these residues form a tight cluster that is located within an intersubunit binding pocket between the upper body (head and left flipper) of one subunit and lower body (dorsal fin) of an adjacent subunit. The crystal structure also revealed that the adenine base of ATP was buried deep in the hydrophobic binding pocket and that the negatively charged phosphate tail adopted a U-shaped conformation. This unusual positioning of ATP in the binding pocket is thought to be stabilised by highly conserved polar and basic residues through extensive hydrophilic interactions (Gouaux and Hattori, 2012). Due to the trimeric nature of P2X receptors, three interfaces exist between the three subunits, allowing space for up to three ATP-binding pockets. It has been proposed that the binding of the first ATP molecule positively influences the binding of subsequent ATP molecules in a mechanism known as positive cooperativity and that at least two molecules of ATP are required for receptor activation (Jiang et al., 2003; Chataigneau et al., 2013).

Once ATP binds, the head and dorsal fin domains of the receptor undergo a conformational change to accommodate the ATP molecule. Consequently, ATP pushes the left flipper outward, which is structurally connected to the lower body and causes a conformational change that reverberates down the channel, resulting in the separation of the three subunits. This separation causes expansion of the three lateral portals, allowing ions to enter and collect within the extracellular vestibule at the entrance of the pore. Subsequent conformational changes in the transmembrane helices (TM1 and TM2) expand the diameter of the pore and allows ions to transverse the membrane (Gouaux and Hattori, 2012; Chataigneau et al., 2013). An early study employing patch-clamp photometry to measure fractional calcium currents (Pf%) identified P2X4 receptors as the most permeable to calcium ions (Egan and Khakh et al., 2004; Samways et al., 2014). Thus, upon activation of P2X4 the cell undergoes depolarisation and a rise in intracellular calcium, implicating P2X4 in a wide range of calcium-dependent signalling pathways (Samways et al., 2014). In addition, multiple studies have suggested that upon prolonged exposure to ATP, P2X2, P2X4 and P2X7 receptors can undergo “pore-dilation” and become more permeable to large cationic ions such as N -methyl-D-glucamine (NMDG). However, the physiological role of this proposed change in channel pore size and increased permeability to larger cations remains unclear and warrants further investigation (Stokes et al., 2017; Kanellopoulos et al., 2021).

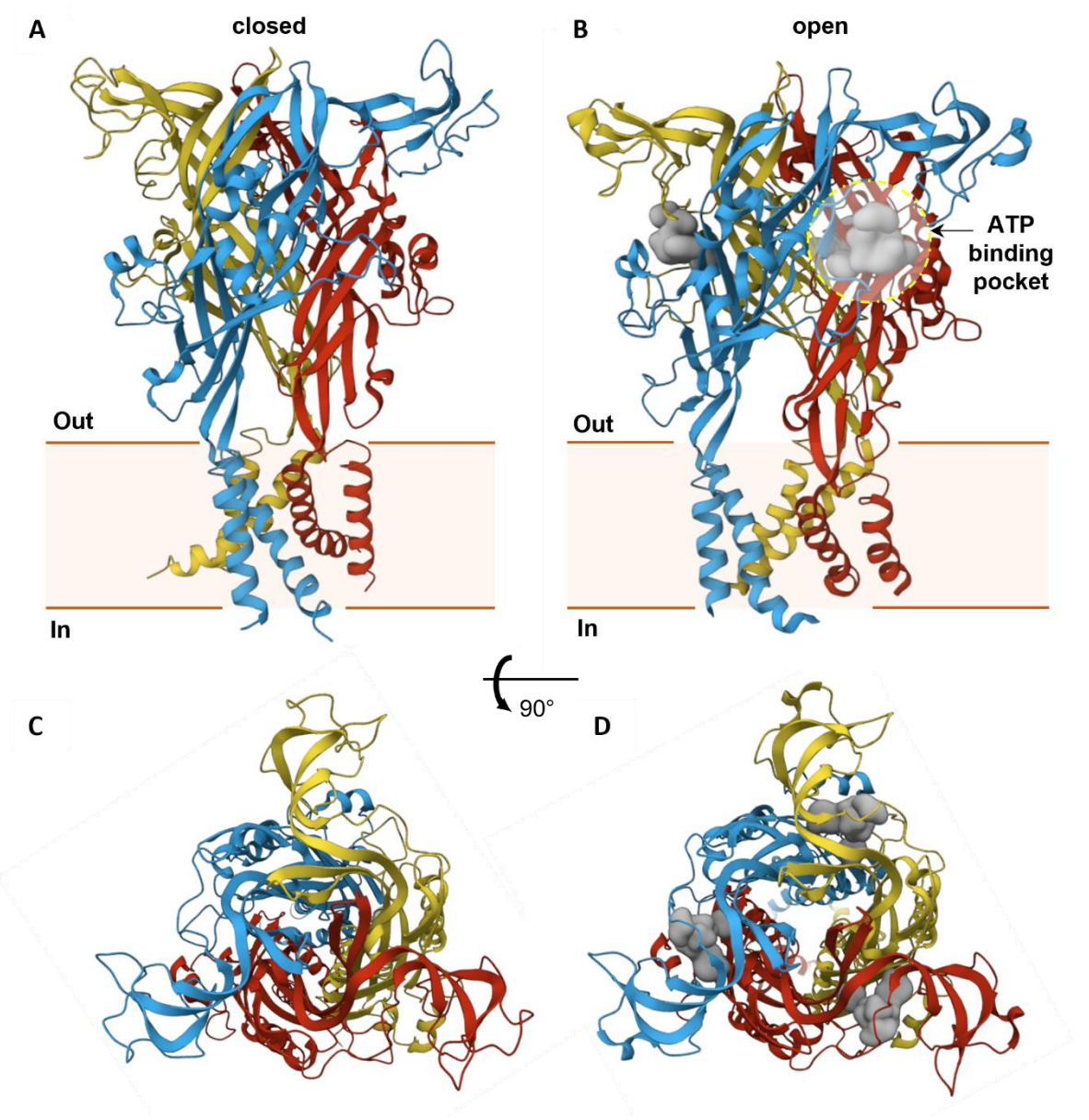

Figure 1.1. Crystal structure of the zfP2X4 receptor in the closed and open, ATP-bound state. (A) Side-view of the homomeric zfP2X4 receptor in the closed and (B) open, ATP-bound state. Each of the three subunits is displayed in a separate colour (blue, red, and yellow). The ATP molecule is displayed as a grey surface. Orange bars represent the plasma membrane. (C) Top view (extracellular side) of the closed and (D) open, ATP-bound receptor pore. Structure was obtained from the SWISS-MODEL Repository (PDB accession number 4DW1 (open) and 4DW0 (closed)).

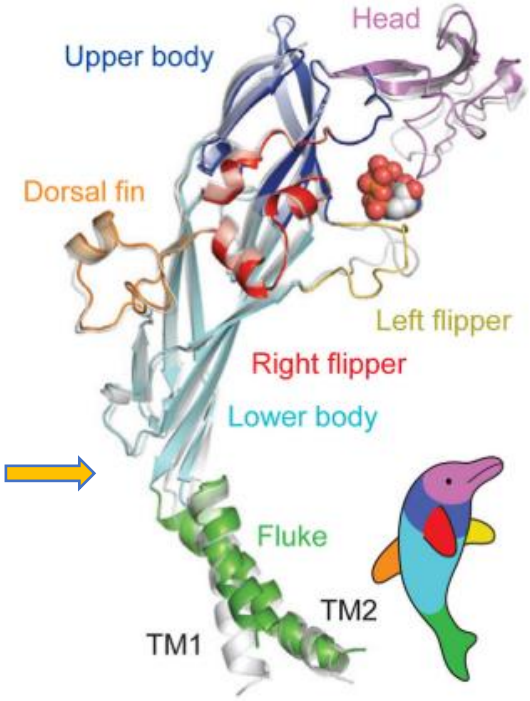

Figure 1.2. Crystal structure of an individual subunit of the zfP2X4 receptor. A comparison of zfP2X4 crystal structure to the features of a dolphin. Each structural feature is assigned a name and colour corresponding to its representative part on the dolphin. The yellow arrow indicates the relative position of the lateral portals. Image modified from Gouaux and Hattori, (2012).

1.2.2 Subcellular localisation and trafficking

The cellular distribution of the P2X receptor family varies, with some predominantly localised at the cell surface, and others within the endoplasmic reticulum or intracellular compartments such as late endosomes and lysosomes (Robinson and Murrell-Lagnado, 2013). Building evidence suggest that P2X4 receptors undergo rapid internalisation from the plasma membrane and are predominantly expressed in endolysosomal compartments across many cell types, including macrophages, microglia, and endothelial cells (Suurväli et al., 2017). Figure 1.3 demonstrates the process of trafficking and recycling of the P2X4 receptor. It is now understood that P2X4 internalisation is mediated by motifs in the amino and carboxyl terminus of the receptor, as mutations of these motifs disrupt receptor endocytosis (Qureshi et al., 2007). Further studies revealed that the rapid internalisation of the P2X4 receptor was dependent on AP2 and dynamin/clathrin-dependent processes (Robinson and Murrell-Lagnado, 2013; Stokes et al., 2017). The extent to which P2X4 receptors are recycled between the plasma membrane and intracellular compartments depends on several factors, including the cell type and environmental conditions (Qureshi et al., 2007).

Amongst the P2X subtypes, P2X4 receptors are predominantly expressed in macrophages, vascular endothelial cells, and microglial cells and, as such, have been implicated in many physiological processes. However, to respond to ATP and promote downstream signalling events, the P2X4 receptor must be expressed at the plasma membrane. Studies have demonstrated that in cultured primary cell lines, including vascular endothelial cells and microglial cells, P2X4 receptors are predominantly localised in the lysosome, making them difficult to study. Qureshi et al. (2007) were the first the suggest a novel mechanism to increase P2X4 receptor expression at the plasma membrane by exposing cells to stimuli that promote lysosome exocytosis. Since then, other groups have activated cells through exposure to certain stimuli, such as pro-inflammatory cytokines in vascular endothelial cells, or lipopolysaccharide in macrophage cells, triggering trafficking of the P2X4 receptor to the cell membrane (Tang et al., 2008; Toulme et al., 2010).

In addition, the pH of lysosomes has been linked to the regulation of P2X4 receptors (Figure 1.3). Lysosomes are acidic organelles (pH 4.6) (Xu and Ren, 2015). However, P2X4 receptors can remain stable and resist degradation in these proteolytic environments due to seven N-linked glycosylation sites (Qureshi et al., 2007). Studies have shown the P2X4 receptors can be regulated by luminal pH within lysosomes suggesting that P2X4 receptors also play a role in the regulation of lysosomal calcium and fusion events (Sophocleous et al., 2022).

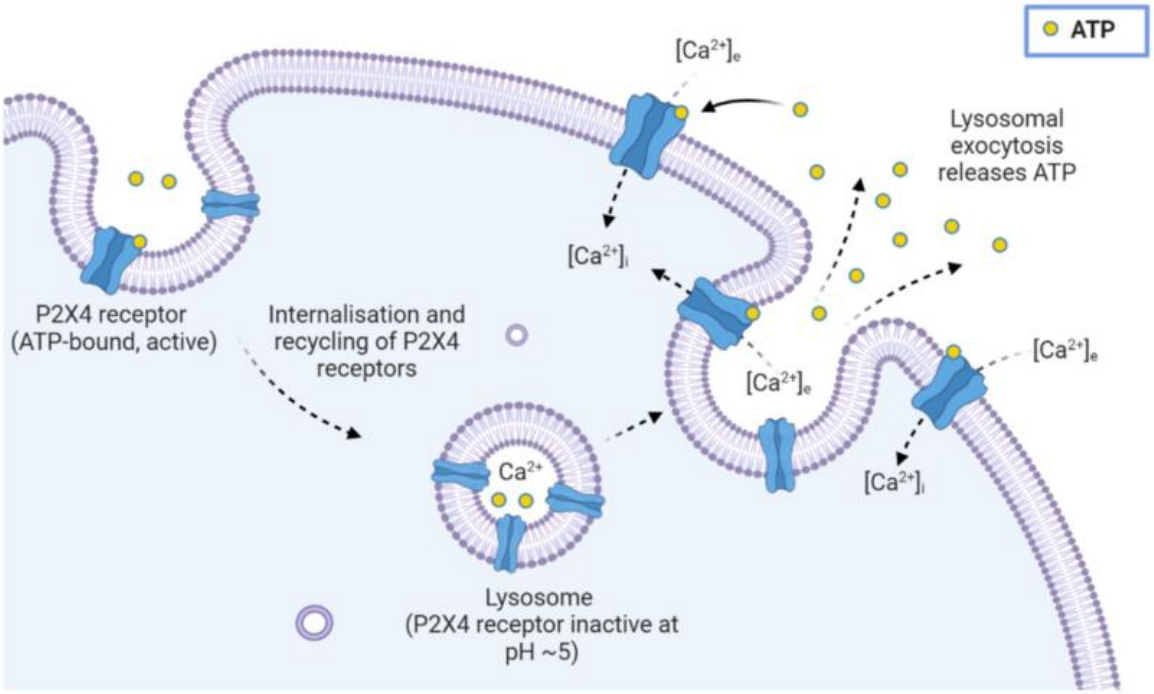

Figure 1.3. Trafficking of the P2X4 receptor. P2X4 receptors are expressed at the cell surface as well as subcellular compartments such as late endosomes and lysosomes. P2X4 receptors undergo rapid internalisation from the cell membrane by endocytosis to subcellular compartments before being recycled back to the plasma membrane. The luminal pH of lysosomes regulates the activity of P2X4 receptors, suggesting these receptors play a role in the regulation of lysosomal calcium and fusion events. The extent of which P2X4 is trafficked to and from the plasma membrane is dependent upon the cell type and environmental conditions. Image obtained from Sophocleous et al. (2022).

1.2.3 Pharmacology of the P2X4 receptor

1.2.3.1 Agonists

The main agonist that acts on all subtypes of the P2X receptor is adenosine 5'-triphosphate (ATP). The P2X4 receptor is one of the most sensitive to ATP and is functional at sub-micromolar concentrations. In the late-1990s electrophysiological studies were conducted on rat P2X4 receptor, and it was revealed that, when the rat P2X4 cDNA was transfected in *Xenopus oocytes*, it is activated by ATP > 2-methylthio-ATP > CTP >α,β-meATP > dATP (Soto et al., 1996). The agonist profile for human P2X4 receptor expressed in *Xenopus oocytes* was found to reflect this agonist profile (Garcia-Guzman et al., 1997). The molecule BzATP and diadenosine polyphosphate (AP4A and AP5A) have also been identified as partial agonists for the mammalian P2X4 receptor (Bianchi et al., 1999; Bowler et al., 2003; Stokes et al., 2011). It is important to note that none of the described agonists are selective to the P2X4 subtype.

1.2.3.2 Antagonists

For many years researchers have struggled to study the P2X4 receptor due to a lack of selective drug targeting. Until recently, researchers relied on broad-spectrum P2 antagonists such as pyridoxalphosphate-6-azophenyl-2',4'-disulfonic acid (PPADS) and suramin. Both antagonists display activity at the human P2X4 receptor, with suramin being a relatively weak antagonist with IC_{50} values of 178.1 μM (Garcia-Guzman et al., 1997). On the other hand, PPADs was able to fully inhibit the human ortholog with IC_{50} values of 27.5 μM and 9.6 μM when expressed in *Xenopus oocytes* and HEK293 cells, respectively (Garcia-Guzman et al., 1997; Jones et al., 2000). Interestingly, rat P2X4 receptors are insensitive to both antagonists, with mouse P2X4 also being insensitive to suramin (Garcia-Guzman et al., 1997; Jones et al., 2000; North and Surprenant, 2000). The ATP derivate 2',3'-O-(2,4,6- trinitrophenyl)-ATP (TNP-ATP) is also considered a non-selective broad-spectrum antagonist of human P2X4 receptor. Studies have found TNP-ATP to inhibit human P2X4 in a competitive manner with IC_{50} values of 1.4μM and 1.5μM when expressed in HEK293 (Balazs et al., 2013) and astrocytoma cells (Abdelrahman et al., 2017), respectively. However, TNP-ATP has been shown to display much greater potency as an inhibitor of P2X1 and P2X3 receptors (North and Jarvis, 2013).

In the last decade, the list of available antagonists for the human P2X4 receptor has been growing, with some compounds presenting better selectivity over the other P2X subtypes. This includes two phenoxazine derivatives N-(benzyloxycarbonyl)phenoxazine (PSB-12054) and N-(p-methylphenylsulfonyl)phenoxazine (PSB-12062) which were found to have IC_{50} values of 0.189 μM and 1.38 μM, respectively, at the human P2X4 receptor in astrocytoma cells (Hernandez-Olmos, 2012). PSB-12054 was found to have good selectivity over other human P2X subtypes (P2X1, P2X2, P2X3 and P2X7), whilst PSB-12062 was identified as a selective P2X4 antagonist with equal potency in mouse and rat P2X4 receptors. Both compounds demonstrated an allosteric mechanism of action (Hernandez-Olmos, 2012). Another selective antagonist is 5-(3-bromophenyl)-1,3-dihydro-2H-benzofuro[3,2-e]-1,4-diazepin-2-one (5-BDBD), first reported to completely inhibit the human P2X4 receptor with moderate potency (IC_{50} = 0.3 – 1.5 μM) (Balázs et al., 2013; Abdelrahman et al., 2017;

Bidula et al., 2022), but was also found to be a less potent inhibiter of mouse and rat P2X4 receptors (Abdelrahman et al., 2017). There is some controversy in the literature around how 5-BDBD inhibits the P2X4 receptor, with some studies stating that it acts as a competitive inhibitor, and others demonstrating that it modulates the receptor via an allosteric site (Abdelrahman et al. 2017). Recently, molecular docking analysis revealed a potential allosteric site, supporting the theory that 5-BDBD acts as a negative allosteric modulator (NAM) of the human P2X4 receptor (Bidula et al., 2022).

Recently, the phenylurea derivative BX430 (1-(2,6-dibromo-4-isopropyl-phenyl)-3-(3-pyridyl)urea) was discovered to be a highly selective non-competitive inhibitor of the human P2X4 receptor. Patch-clamp studies demonstrated that BX430 was highly potent (IC_{50} = 0.54μM) with no inhibitory effect on the mouse or rat P2X4 receptor (Ase et al., 2015). The same group proposed a putative allosteric binding site for BX340 in the ectodomain of the human P2X4 receptor and attributed BX430's high selectivity across the P2X orthologs to a single amino acid (Ile-312) which forms part of the docking site (Ase et al., 2019).

Furthermore, some studies have highlighted the potential role of antidepressants as P2X4 antagonists, including paroxetine, a serotonin reuptake inhibitor clinically used for the treatment of chronic pain (Nagata et al., 2009). Paroxetine was shown to inhibit P2X4-mediated currents and calcium increases in rat (IC50 = 2.45 μM) and human P2X4 receptors (IC_{50} = 1.87 μM) in astrocytoma cells (Nagata et al., 2009. Abdelrahman et al. (2017) supported this by confirming direct inhibition of the human P2X4 receptor in astrocytoma cells (IC_{50} = 4.81 μM) and categorised paroxetine as a NAM. However, unlike BX430, the inhibitor action of paroxetine appeared to be non-selective, as it has been shown to inhibit the P2X7 receptor with an IC_{50} value of 24 μM in HEK293 cells (Dao-ung et al., 2015). In addition, studies by Li and Fountain (2012) reported that the HMG-CoA reductase inhibitor, Fluvastatin, inhibited the activity of human P2X4 receptors. However, the mode of inhibition does not involve direct modulation of the channel and is suspected to be a consequence of cellular cholesterol depletion and interference with receptor trafficking.

Recently, newly developed compounds have emerged in an attempt to design novel P2X4 receptor antagonists with improved potency and selectivity. A recent example is N-[4-(3-chlorophenoxy)-3-sulfamoylphenyl]-2-phenylacetamide (BAY-1797), identified as a potent and orally available antagonist that is selective to human (IC_{50} = 0.1 μM) and mouse P2X4 (EC_{50} = 0.2 μM) receptors over the other P2X subtypes (Werner et al., 2019). Moreover, inflammatory pain models in mice demonstrated that BAY-1797 exhibits both anti-inflammatory and antinociceptive effects *in vivo*, making it a promising drug target for the treatment of neuropathic pain (Werner et al., 2019).

Lastly, other negative modulators for the human P2X4 receptor have been identified. This includes the divalent cations copper (Cu^{2+}) and mercury (Hg^{2+}), both of which have been shown to inhibit ATP-evoked currents in rat P2X4 receptors (Coddou et al., 2005). Likewise, the trace metals zinc (Zn^{2+}) and cadmium (Cd^{2+}) have been shown to inhibit rat P2X4 receptors, but only at high concentrations (>100 μM). In contrast, at low micromolar concentrations Zn^{2+} and Cd^{2+} can potentiate rat P2X4 receptors.

(Acuña-Castillo et al., 2000). In addition, high concentrations of protons have been shown to negatively modulate the human P2X4 receptor, with complete inhibition occurring in acidic environments (pH <7) (Clarke et al., 2000). The biological significance of pH-regulated modulation of the P2X4 receptor is supported by the fact that these receptors are predominantly localised in lysosomes which are highly acidic organelles (pH 4.6) and, therefore, could be regulating P2X4 activity (Xu and Ren, 2015; Sophocleous et al., 2022). Lastly, ethanol has also been shown to act as a NAM of the rat P2X4 receptor, which can be antagonised by the positive modulator ivermectin (Franklin et al., 2014).

1.2.3.3 Positive allosteric modulators

Positive allosteric modulators (PAMs) are a group of compounds that can bind to allosteric sites on a receptor and enhance the receptor's response to a stimulus. Allosteric sites are distinct from the orthosteric site where endogenous agonists would bind. In drug discovery, identifying and characterising these sites is important as they are under less evolutionary pressure than orthosteric agonist-binding sites and therefore have the potential to exhibit great selectivity between receptor subtypes (Weinhausen et al., 2022). Typically, PAMs are characterised into three types depending on how they affect the actions of the natural agonist. Type I, which increases agonist efficacy; Type II, which shifts the agonist concentration-response curve to the left, thus increasing agonist potency; or Type I/II, which exhibits both effects (Stokes et al., 2020).

In P2X4 receptor research, relatively few PAMs have been identified, and those with more recognition are derived from natural products. The most well-studied is ivermectin (IVM), a large semisynthetic avermectin derived from the natural fermentation products of *Streptomyces avermitilis*, a soil bacterium (Khakh et al., 1999; Priel and Silberberg, 2004). IVM has been shown to potentiate P2X4-mediated currents and slow receptor deactivation in humans (Priel and Silberberg, 2004) and rats (Khakh et al., 1999) with an EC_{50} value of 250 nM for both species. IVM can also increase P2X4 receptor sensitivity to ATP (decreases ATP EC_{50} value), making it a Type I/II PAM (Khakh et al., 1999; Priel and Silberberg, 2004; Jelínková et al., 2006; Gao et al., 2015; Stokes et al., 2020). The action and proposed binding site(s) of IVM at P2X4 receptors, as well as other mammalian receptors, is further explored in section 1.3. In addition to IVM, other avermectins and the milbemycin, moxidectin, have also been reported to act as PAMs of the P2X4 receptor (Asatryan et al., 2014; Huynh et al., 2017).

Recently, 'steroid-like' compounds derived from the root of a medical plant (*Panax ginseng*), termed ginsenosides, have been shown to potentiate P2X4-mediated currents and intracellular Ca^{2+} concentrations in a similar manner to IVM (Dhuna et al., 2019). Specifically, two ginsenosides, metabolite compound K (CK) and Rd were demonstrated to be equipotent at potentiating human P2X4 responses in HEK293 cells, with EC_{50} values of 7.5 µM and 8.5 µM, respectively. Ginsenoside CK was also found to cause a leftward shift in the concentration-response curve to ATP in addition to increasing the maximum response elicited by ATP, making ginsenoside CK a Type I/II PAM. However, these compounds are not subtype-selective and have stronger potentiating action at P2X7 receptors (Helliwell et al., 2015). Investigations into the putative binding pocket revealed that both CK and Rd

might be binding in a large hydrophobic crevice within the central vestibule of the P2X4 receptor (Bidula et al., 2019). The molecular model was based on earlier modelling and mutagenesis work investigating the allosteric site of ginsenosides in P2X7 receptors, which share similar channel architecture. This allosteric site is different from the predicted IVM binding site, which is hypothesized to bind to the transmembrane (TM) domain and interact with residues at the TM-ectodomain interface (Jelínková et al., 2006; Silberberg et al., 2007; Popova et al., 2013). In addition, a recent study found that synthetic testosterone derivates, specifically testosterone butyrate and testosterone valerate, can increase the sensitivity of the rat P2X4 receptor to ATP, making them Type II PAMs (Sivcev et al., 2019). Interestingly, Sivcev et al. (2019) demonstrated that these derivates could antagonise the effect of IVM on P2X4 channel deactivation, suggesting an overlapping allosteric binding site. The same group also investigated the ability of bile acids, natural steroid compounds derived from cholesterol, and found lithocholic acid to be an effective Type II PAM of the rat P2X4 receptor at low micromolar concentrations (Sivcev et al., 2020).

Lastly, trace metals have been shown to act as PAMs of the P2X4 receptor. In cellular biology, trace metals are essential to life, with zinc (Zn^{2+}) being the most abundant trace metal found in the body. These metals are released from the synapses following membrane depolarisation and interact with neuronal ion channels, including voltage-gated and ligand-gated channels (Mathie et al., 2006). Two of these trace metals, specifically zinc (Zn^{2+}) and cadmium (Cd^{2+}), have also been shown to potentiate the ATP-evoked current in rat P2X4 receptors (Garcia-Guzman et al., 1997; Acuna-Castillo et al., 2000; Coddou et al., 2005). Recently, a study by Latapiat et al. (2017) hypothesised that the putative binding site for Zn^{2+} at the P2X4 receptor resides in the ectodomain, distinct from IVMs proposed binding site within the TM domain, and that the joint application of both modulators had an additive effect on ATP-mediated currents. Conversely, other trace metals, specifically copper (Cu^{2+}) and mercury (Hg^{2+}), have the opposite effect and can inhibit P2X4 responses (Coddou et al., 2005). Overall, the full extent of trace metal modulation at the P2X4 receptors has yet to be explored, as well as their effect on the other P2X subtypes (Acuña-Castillo et al., 2000).

1.2.4 Biological roles of the P2X4 receptor

The P2X4 receptor makes an interesting therapeutic target due to its wide-tissue distribution linking it to many physiological processes in the body (Figure 1.4). Expression includes the central nervous system in microglial cells, the immune system in macrophages and high expression in cardiomyocytes and vascular endothelial cells in the cardiovascular system. As such, changes in P2X4 expression and function have been associated with many disease states, such as neuropathic pain, cardiovascular disease, and inflammation, as well as neurodegenerative disorders and alcohol use disorders (Sophocleous et al., 2022).

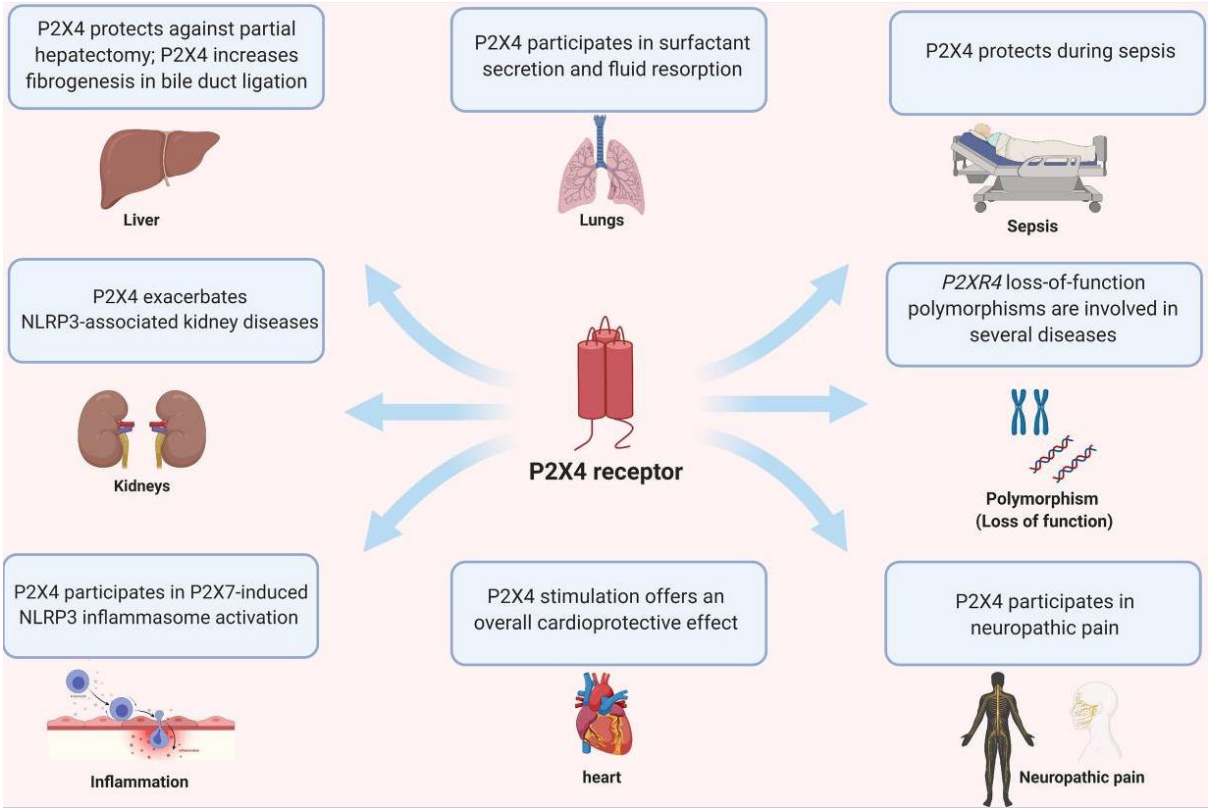

Figure 1.4. The multiple effects of P2X4-mediated signalling on different organs and diseases. Image obtained from Kanellopoulos et al. (2021).

1.2.4.1 Central nervous system

The first identified physiological role of P2X4 receptors was the regulation of synaptic transmission between neurons and glial cells after studies demonstrated widespread expression in both neurons and microglial cells in the central and peripheral nervous system (Stokes et al., 2017). However, great interest in the role of the P2X4 receptor in the central nervous system (CNS) comes from its involvement in neuropathic pain transmission. Neuropathic pain is a reaction of the nervous system to nerve damage and can be triggered by many factors, such as infection, bone compression in cancer or a dysfunctional nervous system. Neuropathic pain is characterised by spontaneous pain, hyperalgesia (abnormal sensitivity to pain), and tactile allodynia (pain hypersensitivity). The development of new treatments to target neuropathic pain is of great clinical interest as neuropathic pain is often resistant to currently available analgesics, such as nonsteroidal anti-inflammatory drugs and opioids (Tsuda et al., 2013).

Following peripheral nerve injury (PNI), microglial cells become activated by damaged sensory neurons which in turn upregulates gene expression of the P2X4 receptor (Tsuda et al., 2013; Stokes et al., 2017). Extracellular ATP then activates the P2X4 receptor and triggers the synthesis and release of brain-derived neurotrophic factor (BDNF) from microglial cells. BDNF release is thought to cause the downregulation of the neuronal potassium-chloride transporter 2 (KCC2), expressed in dorsal horn neurons, altering the anion gradient. The subsequent increase in intracellular chloride switches the effects of GABA form hyperpolarising to depolarising (inhibition to excitation). This causes hyperexcitability of the dorsal horn and in turn gates neuropathic pain (Ulmann et al., 2008; Tsuda et al., 2013; Stokes et al., 2017). The first to demonstrate the importance of P2X4 in neuropathic pain and tactile allodynia was Tsuda et al. (2003) by blocking P2X4 receptor expression using antisense oligonucleotides. A later study supported this by generating transgenic P2X4 knockout mice that were resistant to peripheral nerve injury-induced tactical allodynia, confirming that P2X4 plays a role in pain processing (Ulmann et al., 2008). This work has led to extensive research in purinergic signalling and pain transmission, including driving the development of antagonists that can selectively target the P2X4 receptor. As discussed earlier, some of the more recent drug candidates include BAY-1797 and antidepressants such as paroxetine, both of which have been shown to inhibit P2X4 receptor function. (Werner et al., 2019).

Recently there has been a shift in focus on the role of P2X4 receptors in the CNS from pain transmission to neurodegeneration. Neuroinflammation is the inflammation of nervous tissue, mediated by the release of pro-inflammatory cytokines and secondary messengers. In neurodegenerative diseases such as Parkinson's disease and multiple sclerosis, microglial activation and inflammatory mediator release is central to disease progression (Stokes et al., 2017). Given P2X4 receptor up-regulation and involvement in microglial pathways, a new focus has been placed on its role in neuroinflammation. For example, Parkinson's disease is characterised by a depletion of dopamine in the brain. In P2X4 knockout mice, a deficit in dopamine-associated behaviours was observed, including motor control and sensorimotor gating (Khoja et al., 2016). Conversely, the same study demonstrated that in a

dopamine depletion mouse model, the use of ivermectin, a positive modulator of the P2X4 receptor, enhanced induced motor behaviour in the presence of L-DOPA, a derivate of dopamine. These findings link P2X4 receptors to the dopamine neurotransmission in the brain and suggest positive modulation of P2X4 receptors could be a potential avenue for the treatment of Parkinson's disease (Khoja et al., 2016; Warnecke et al., 2020). In addition, in a mouse model of multiple sclerosis, ivermectin has been used to potentiate P2X4 receptor function and improve oligodendrocyte-mediated remyelination of neurons (Zabala et al., 2018).

Lastly, several studies have begun to investigate the role of P2X4 receptors in alcohol use disorder (AUD) which is a chronic brain disease that is characterised by compulsive heavy drinking (Burton et al., 2016). At present, ethanol is known to increase extracellular adenosine levels, resulting in the ataxic and sedative effects of alcohol (Asatryan et al., 2011). Ethanol is also known to inhibit ATP-evoked currents in P2X receptors expressed in *Xenopus oocytes,* with P2X4 receptors being the most alcohol-sensitive P2X subtype (Xiong et al., 2000; Davies et al., 2005; Asatryan et al., 2010). As discussed earlier, P2X4 receptor modulation is linked to dopamine neurotransmission within neurons and glial cells of the CNS. The mesolimbic dopamine pathway, otherwise known as the reward pathway, is known to play an important role in alcohol consumption and addiction (Franklin et al., 2014). Later studies discovered that ivermectin could reduce the alcohol-drinking behaviour in mice and reverse the inhibitory effect of alcohol *in vitro* by binding to an overlapping allosteric binding site within the TMD of the P2X4 receptor (Franklin et al., 2014). Overall, these findings suggest that P2X4 modulation is involved in alcohol drinking behaviour and that potentiating P2X4 function using avermectins, including ivermectin and moxidectin, could be a potential treatment for AUD (Huynh et al., 2019).

1.2.4.2 Cardiovascular research

In the cardiovascular system, P2X4 has been shown to participate in the regulation of vascular tone and cardiac function and therefore is likely to play a role in heart failure and ischaemic stroke, as well as vascular disease states, such as hypertension and atherosclerosis.

Early work by Yamamoto et al. (2000a) first highlighted the role of P2X4 receptors in modulating the cardiovascular system. They were the first to demonstrate P2X4 receptors as the most abundantly expressed P2X subtype in human vascular endothelial cells (ECs), including pulmonary and coronary arteries (Yamamoto et al., 2000a). ECs are in direct contact with blood flow and have been shown to respond to changes in shear stress generated by blood flow via ATP release and calcium signalling events. Yamamoto et al. (2000a) demonstrated that P2X4 receptors were responsible for the sustained phase of calcium release caused by ATP-induced calcium influx by knocking out P2X4 function in vascular ECs using antisense oligonucleotides. This suggested that P2X4 receptors act as a signal transducer for shear stress by allowing the influx of calcium into the cell interior. As a result, nitric oxide synthase is activated, which leads to the production of the vasodilator, nitric oxide (NO), causing the blood vessels to dilate and blood pressure to be reduced (Yamamoto et al., 2000b) (Figure 1.5). Later work by Yamamoto et al. (2006) supports this theory by monitoring the responses of P2X4

knock-out mice to changes in blood flow. They found that endothelial cells in P2X4 knock-out mice did not exhibit flow-induced influx of calcium or subsequent production of NO. Furthermore, P2X4 knock-out mice showed a significant increase in blood pressure compared to wild-type mice, indicating that P2X4 channels are key players in the regulation of vascular tone and thus provide interesting drug targets for the regulation of blood pressure disorders (Yamamoto et al., 2006).

Furthermore, the maintenance of this P2X4-mediated vasodilatory mechanism has been shown to be very important for maintaining vascular homeostasis. The P2X4 gene has four nonsynonymous single-nucleotide polymorphisms (SNPs). One SNP involves an amino acid change from a tyrosine to a cysteine at position 315 in the protein sequence and is thought to interfere with the ATP binding pocket and cause a loss of channel function (Stokes et al., 2011). At the cellular level, Stokes et al. (2011) demonstrates a significant reduction in ATP-evoked currents in mutated P2X4 receptors and patients that carried the mutation exhibited increased pulse pressure. These observations are consistent with the hypothesis that the P2X4 receptor plays a critical role in endothelium-mediated vasodilation as reduced endothelial NO release would account for the reduced large atrial compliance and increased pulse pressure that is in seen in carriers of the P2X4 mutation, all of whom are at considerably greater risk of developing cardiovascular disease.

At present, the most abundant P2X receptors expressed in human heart tissue at the mRNA level are P2X4-7 (Musa et al., 2009). Among the P2X receptors, building evidence points towards the cardiac P2X4 receptor as having an important physiological role, that of stimulating increased contractibility in cardiac myocytes and intact heart. A study performed in intact hearts of transgenic mice with cardiac-specific overexpression of P2X4 receptor showed enhanced basal and P2 agonist (2-meSATP) induced contractibility over WT mice, with no evidence of heart failure (HF) (Hu et al., 2001). Furthermore, in WT mice ventricular myocytes, the agonist-induced current was partially insensitive to blockage by P2 antagonist suramin and susceptible to potentiation by IVM and Zn^{2+}. Since P2X4 is the only P2X receptor known to be potentiated by IVM and resistant to blockage by suramin, these findings support the importance of P2X4 receptors in cardiac myocytes (Shen et al., 2006).

Furthermore, the ionotropic receptors have also been shown to have a beneficial, protective function against the progression of HF. For example, transgenic overexpression of the P2X4 receptor was found to improve the survival and cardiac function of calsequestrin (CSQ) overexpressing mice, a model for HF (Yang et al., 2004). In addition, transgenic P2X4 animals showed a salutary phenotype and improved survival after myocardial infarction (Sonin et al., 2008). This suggests that P2X4 receptors have an important role in enhancing cardiac performance and mediating cardioprotection in HF. At present, the cellular mechanism at which P2X4 receptors enhance this contractile state in cardiomyocytes is unknown. The design and development of novel modulators that can target P2X4 selectively could provide the tools needed to fully elucidate the functional role and mechanism of this receptor in cardiomyocytes and the heart.

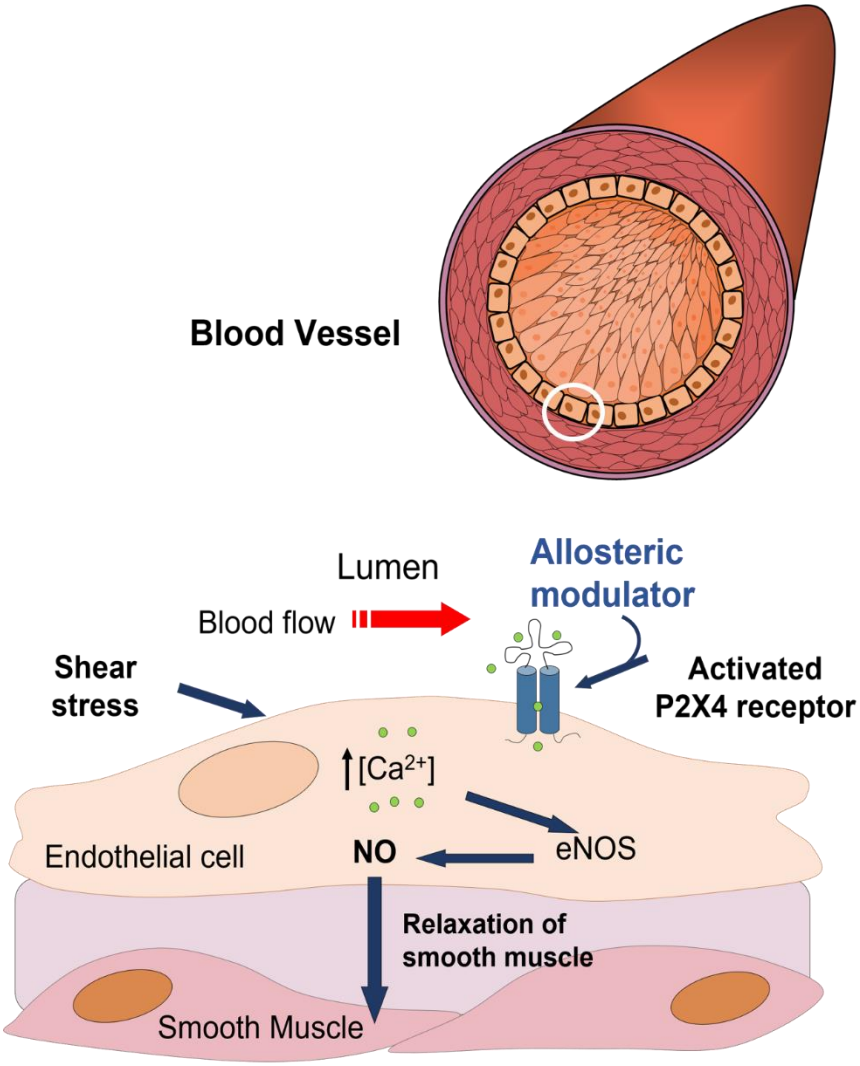

Figure 1.5. P2X4 receptor activation is a potential pathway for the release of nitric oxide (NO) in vascular endothelial cells. In vascular endothelial cells, P2X4 receptors are activated by the release of the native agonist ATP in response to shear stress. Activated P2X4 receptors facilitate the influx of calcium and increase eNOS activity. This leads to the increased production of the potent vasodilator NO, which diffuses into smooth muscle cells, causing them to dilate and blood pressure to decrease (reduction in vascular tone).

1.2.4.3 Immune system

Building evidence supports the critical role of P2X4 receptors in the immune system, with multiple studies linking P2X4 receptor modulation with neuropathic pain transmission and neuroinflammation, both of which are mediated by microglial cell activation. In accordance with this, P2X4 receptors have been found to have widespread distribution in the cells of the immune system, including lymphocytes, dendritic cells, macrophages, and glial cells (Sophocleous et al., 2022).

Recent work has linked P2X4 receptor activation with the regulation of inflammasome production. Inflammasomes are multi-protein complexes that assemble in the cytosol of immune cells after detecting infection and stress (Kanellopoulos et al., 2021). Activation of inflammasomes leads to downstream inflammatory signalling events, such as the release of pro-inflammatory cytokines, including interleukin-1β (IL-1β) and interleukin-18 (IL-18). One of the most well-studied inflammasomes is the NOD-like receptor 3 (NLRP3), which is linked to plaque formation in atherosclerosis, rheumatoid arthritis and acute kidney injury (Han et al., 2020). Previous studies have suggested that P2X4 and P2X7 receptors interact to modulate NLRP3-inflammasome activation. For example, Sakaki et al. (2013) demonstrated that in dendritic cells, P2X4-induced Ca^{2+} responses were required for P2X7-dependant cytokine release and subsequent inflammation. Likewise, in a mouse model of ischemic acute kidney injury, activation of the P2X4 receptor worsens the condition by potentiating renal tubular necrosis, NLRP3-inflammasome activation and apoptosis (Han et al., 2020). In addition, P2X4 receptors have been linked to joint inflammation associated with rheumatoid arthritis (RA). In a mouse model of arthritis, inhibition of the P2X4 receptor led to a decrease in inflammasome formation (NLRP1) in the arthritic joints of mice and, consequently, a reduction in cytokine production (IL-1β) (Li et al., 2014). Together, these *in vivo* studies demonstrate the role of P2X4 receptors in inflammation and propose P2X4 attenuation as a potential route in the treatment of acute kidney injury and RA through the inhibition of inflammasome formation and stunted release of pro-inflammatory cytokines.

Lastly, P2X4 modulation has been linked to the defence of sepsis-causing bacteria in mice models (Csoka et al., 2018). Microphage and monocytes are known to play an important role in the body's immune responses against sepsis, and the expression of P2X4 receptors in these immune cells has been well-documented in humans and rodents (Bowler et al., 2003; Layhadi et al., 2018). Recently, the potentiation of P2X4 receptors with ivermectin has been shown to be protective against sepsis-induced organ failure and inflammation. Treatment with ivermectin increased bacteria-killing macrophages and improved animal survival in a P2X4-dependent manner (Csoka et al., 2018). This demonstrates the protective role of P2X4 receptors in sepsis-related pathologies and presents a novel drug target for the treatment of sepsis, a life-threatening response to infection (Kanellopoulos et al., 2021).

1.3 Ivermectin (IVM), a PAM of the P2X4 receptor

Ivermectin (IVM) is best known for its use in human and veterinary medicine as an anti-parasitic drug and is derived from the natural product avermectin. In parasites, IVM acts as an irreversible agonist of glutamate-gated chloride channels (GluCl), promoting the influx of chloride ions through these channels, paralysing muscle activity and preventing feeding (Omura, 2008; Crump and Omura, 2011). IVM is known to bind with high affinity to GluCl (nM concentrations), making it selectively toxic to parasites (Wolstenholme & Rogers, 2005). However, it is now understood that IVM can act as an agonist or allosteric modulator or both at multiple mammalian ion channel targets, albeit at lower affinity (µM concentrations), including α-7 nicotinic acetylcholine receptors (α-7 nAChR) (Krause et al., 1998) and γ-aminobutyric acid type A receptor (GABA(A)R) (Krusek and Zemkova, 1994). In the late 1990s, IVM was reported to potentiate, but not activate, the purinergic channel P2X4 (Khakh et al., 1999).

Further research revealed IVM to be selective to the P2X4 receptor over the other six P2X subtypes (P2X1-7). Because of this reason, IVM has been used extensively as a pharmacological tool to study and isolate P2X4 activity across various *in vitro* and *in vivo* model systems for health and disease states. However, there have been contradictory reports about whether IVM is truly selective to the P2X4 receptor subtype. Nörenberg et al. (2012) reported that the human P2X7 receptor could also be potentiated by IVM. However, Schneider et al. (2017) could not replicate these results and observed no potentiation of P2X7-dependant current in response to pre-incubation with 3 µM IVM in *Xenopus oocytes* expressing human P2X7 receptor. Likewise, a recent study published by Weinhausen et al. (2022) observed no potentiation of the ATP-evoked calcium response in 1321N1 cells expressing human P2X7 receptors. It is generally agreed that IVM is selective to P2X4 over the other P2X receptor subtypes.

Despite the publication of the open and closed zfP2X4 crystal structure, the specific location of IVMs allosteric binding site(s) and the underlying mechanism of action at the P2X4 receptor remains unknown. However, numerous studies have pinpointed a potential binding site within the transmembrane region of the receptor (Figure 1.6) and proposed multiple hypotheses on how IVM might exert its PAM effects.

1.3.1 Allosteric binding site(s)

The first study to investigate the action of IVM on P2X4 channels was published by Khakh et al. (1999), demonstrating that IVM could potentiate the ATP-evoked currents in P2X4 channels by increasing the gating efficiency and slowing the rate of deactivation. A pioneering study by Priel and Silberberg (2004) supported this by attributing these two distinct effects on P2X4 to IVMs ability to bind two individual binding sites. The theory states that the binding of IVM to a higher affinity site amplifies the ATP-evoked current by increasing the efficacy of ATP and reduces channel desensitisation during sustained ATP application, whereas binding to a lower affinity site stabilizes the open conformation of the channel and thereby slows the rate of current deactivation. Since IVM is a highly lipophilic molecule,

the paper also states that IVM may need to partially embed in the membrane to reach its allosteric binding site(s) (Priel and Silberberg, 2004; Jelinkova et al., 2006; Zemkova et al., 2015). Single-channel recordings found that IVM prolonged channel open time and the probability of channel opening, suggesting that IVM binds more favourably with the open state of the channel (Priel and Silberberg, 2004; Silberberg et al., 2007).

This mechanism of action was supported in later studies suggesting that, rather than binding close to the orthosteric site within the extracellular domain of P2X4, IVM interacts with residues lining the transmembrane helices. It was also suggested that, in agreement with Priel and Silberberg (2004), the binding of IVM is allosteric in nature and adds that by binding to the transmembrane regions, IVM is interfering with the rearrangement of the TM domains and channel gating, similar to what is observed in the IVM-bound crystal structure of GluCL (Jelínková et al., 2006; Silberberg et al., 2007; Hibbs and Gouaux, 2011). To investigate the likeliness of IVM reaching the proposed hydrophobic binding site between the TM domains, Silberberg and colleagues (2007) performed a spin-down assay where IVM, as well as its analogue doramectin (DRM), were shown to partition into phospholipid vesicles. This supported the idea that IVM could interact with the TM regions of P2X4, which are thoroughly embedded in the lipid membrane (Silberberg et al., 2007). However, as opposed to IVM having direct action on the P2X4 receptor, as suggested by Priel and Silberberg (2004), a report by Toulme et al. (2006) suggested that IVM causes potentiation of ATP-evoked currents in P2X4 by increasing the number of cell surface receptors. The study demonstrated that P2X4 was continuously recycled via clathrin/AP2-mediated endocytosis and that disruption of this mechanism could completely abolish the potentiation of ATP-evoked current by IVM. Swiftly after this theory was published, Silberberg et al. (2007) were quick to demonstrate that IVM did not alter the number of P2X4 channels at the cell surface and was interacting with P2X4 directly via an allosteric mechanism (Silberberg et al., 2007). Asatryan et al. (2010) also found no change in surface expression levels of P2X4 in oocytes after incubation with IVM, indicating that IVM directly interacts with the P2X4 receptor (Asatryan et al., 2020). A few years later and a study by Stokes et al. (2013) supported Toulme's theory by blocking P2X4 internalisation and observing an abolished potentiation of ATP-induced currents in the presence of IVM. However, Stokes et al. (2013) proposed a compromise and suggested that, although these theories appear to oppose each other, it may be possible for IVM to both stabilise the open-state of the receptor and prevent internalisation via endocytosis. This would result in increased surface expression as more receptors are inserted into the membrane, promoting an observable increase in ATP-evoked current from P2X4 receptor channels. Another theory to support this dual effect of IVM states that the drug rescues the receptor from desensitisation by invoking an IVM-dependent transition from an open to dilated state of the channel pore. This temporarily prolongs the sensitisation state, rescuing the receptor from desensitisation and subsequent internalisation (Zemkova et al., 2015).

Further evidence to support the theory that IVM binds via the TM domain was provided using chimeric receptors and site-directed mutagenesis (Silberberg et al., 2007; Zemkova et al., 2014). Previous

studies have shown that IVM is only effective when applied extracellularly (Priel and Silberberg, 2004), suggesting that the allosteric site is located in the extracellular domain. However, gain-of-function experiments using IVM-sensitive (P2X4) and IVM-insensitive (P2X2) chimeras demonstrated that transferring both TM domains of P2X4 to P2X2 was enough to transfer sensitivity to IVM, whereas transferring the ectodomain alone was not enough (Silberberg et al., 2007). This suggested that the P2X4-TM helices are important for IVM-mediated effects on channel activity.

Previous work on rat P2X4 channels identified the extracellular **Val49–Val61** region as important for the deactivating effect of IVM and alanine-substitutions in this region identified two P2X4-specific residues (**Val60** and **Trp50**) as critical for this action of IVM. The group also mutated the P2X4-specific residue **Val357**, found at the C-terminal end of TM2, and likewise was found to be important for IVMs effect on receptor deactivation. Specifically, in the presence of IVM, the deactivation time constant was significantly reduced for mutants **Trp50** and **Val357**, and enhanced for the **Val60** mutant when compared to WT P2X4 (Jelínková et al., 2006). Silberberg et al. (2007) also supported the view that IVM binds more favourably between the open conformations of the two TM helices. Tryptophan scanning mutagenesis studies identified a series of important residues at the lipid-protein interface that significantly reduces IVM modulation when mutated to tryptophan, including **Val47**, **Tyr42**, **Val43** and **Ile39** in TM1 and **Gly340**, **Gly342**, **Ley345** and **Val348** in TM2. This group was the first to suggest that the hydrophobic nature and shape of the binding crevice are more important for IVM binding (Silberberg et al., 2007). Jelínkova et al. (2008) went on to identify further specific P2X4-TM residues thought to play a role in IVM binding via cysteine-scanning mutagenesis, including **Arg33**, **Gln36**, **Leu40**, **Val43**, **Val47** and **Trp50** in TM1 and **Asn338**, **Leu346**, **Ala349**, **Cys353**, and **Ile356** belonging to TM2, all of which are predominantly hydrophobic non-polar residues. This agrees with the hypothesis that IVM partitions into the membrane and binds to the receptor via an allosteric interaction involving both TM helices located at the protein-lipid interface (Silberberg et al., 2007; Jelínkova et al., 2008; Zemkova et al., 2014). Furthermore, Zemkova et al. (2014) supported the theory that three IVM binding sites may exist in the P2X4 receptor, first proposed by Silberberg et al. (2007), with each IVM molecule binding between two neighbouring subunits. This is due to P2X4s trimeric nature and the fact that a single mutation of the previously mentioned residues does not fully eliminate the effect of IVM on current amplification or channel deactivation (Silberberg et al., 2007; Zemkova et al., 2014).

Furthermore, research into the inhibitory effects of ethanol on P2X4 receptors found evidence of an overlapping binding pocket for IVM and ethanol (Asatryan et al., 2008, Popova et al., 2010). Mutagenesis studies and molecular docking simulations identified this putative binding picket at the TM-ectodomain interface, lined with the residues **Trp46** and **Trp50** (TM1) and **Asp331**, **Met336** (TM2) (Kawate et al., 2009; Asatryan et al., 2010, Popova et al., 2013). This site is located close to the lateral fenestrations or “portals”. These linker regions form a bridge between the ectodomain to the TM domain and, upon ATP binding, undergo a conformational change that allows the ions to gain access to the pore, reaching 8Å in diameter in the holo state. This would provide a large space for IVM to bind and stabilise the receptor in the open state (Hattori and Gouaux, 2012; Popova et al 2013).

This agreed with Samways et al. (2012), who had found in the previous year that the conserved acidic residues **Glu51** and **Asp331**, which form part of the lateral portals, were important for IVM sensitivity at the P2X4 receptor. Interested in understanding if allosteric drugs could change the Ca^{2+} current in ligand-gated ion channels, Samways et al. (2012) was able to demonstrate for the first time that IVM, whilst potentiating ATP-evoked currents, reduced the contribution of calcium to the ATP-evoked current (fractional calcium current or pf%) in native and recombinant P2X4 receptors. Encouraged by their results, the group also employed site-directed mutagenesis to study how IVM might be exerting this effect. It was shown that removal of the negatively charged residue **Glu51**, located at the extracellular end of TM1, attenuated the effects of IVMs (reduced pf% and prolonged deactivation). The paper suggests that IVM changes the topology of the lateral portals which hinders Ca^{2+} influx through the pore, a process that is dependent on the fixed negative charge of **Glu51** (Samways et al., 2012). To further probe the role of these portal regions in the mechanism of IVM modulation, alanine and serine replacement mutagenesis was employed on residues within this region. This work found four highly conserved aromatic residues (**Tyr195**, **Phe198**, **Phe200** and **Phe330**) that can influence IVMs ability to sensitise the P2X4 receptor to ATP and prolong deactivation of ATP-gated currents (Figure 1.6). The data suggests that these residues that line the lateral fenestrations of P2X4 play a critical role in channel gating and thus influence IVMs ability to modulate channel opening (Gao et al., 2015).

Recently, two molecular docks of IVM bound to the P2X4 receptor were published around the same time with similar docking conformations and support the involvement of many residues previously identified to be involved with IVM action (Latapiat et al., 2017 and Pasqualetto et al., 2018). Much of the evidence supports the hypothesis that IVM inserts between two adjacent subunits and directly influences the re-arrangement of the TM domain during channel gating.

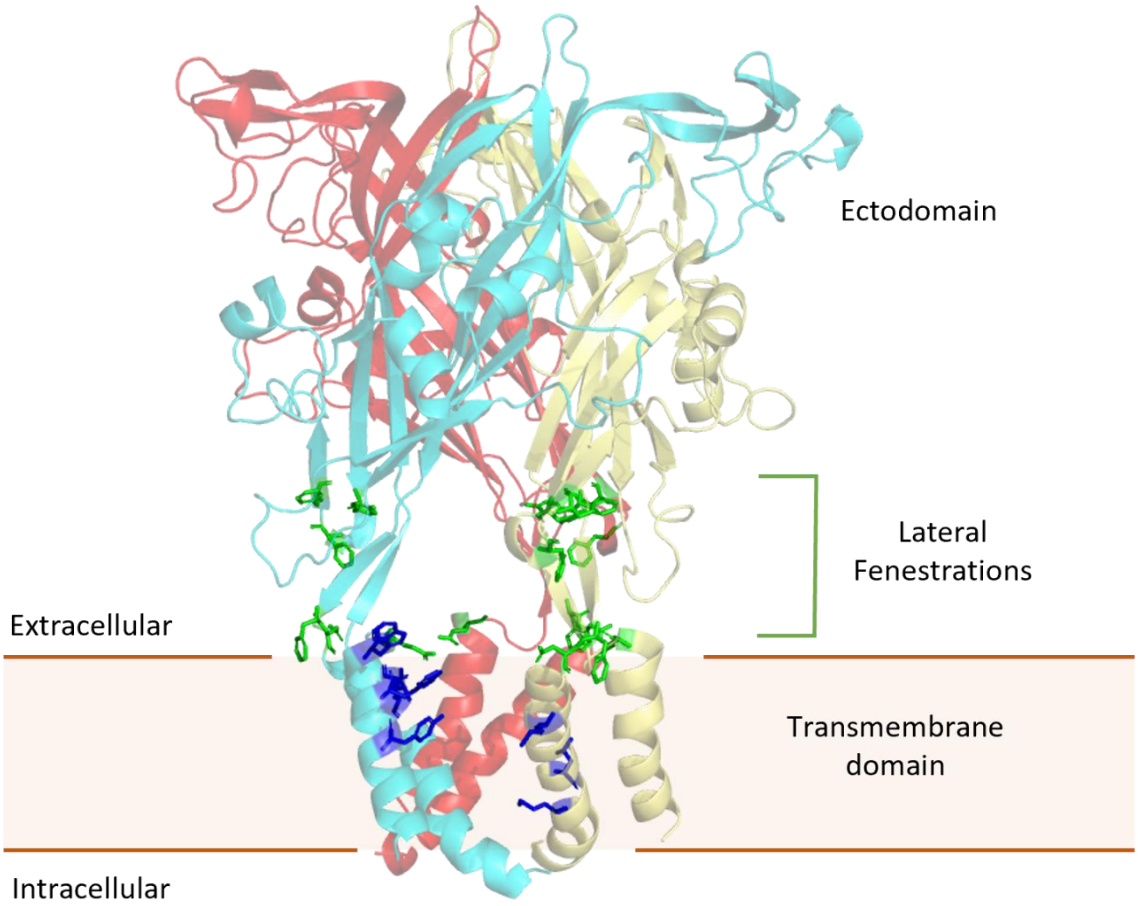

Figure 1.6. Critical amino acid residues involved in IVM binding and modulation of the P2X4 receptor. A side-view of the homomeric zfP2X4 receptor in the open state. Each of the three subunits is displayed in a separate colour (blue, red and yellow). At present, the IVM-bound crystal structure has yet to be solved. Based on current mutagenesis work and molecular modelling approaches IVM is suspected to bind between two adjacent subunits with the extracellular-TM domain interface, interacting with the upper region of TM1 and TM2 of one subunit (light blue subunit) and the lower region of TM2 in the adjacent subunit (yellow subunit) (Pasqualetto et al., 2018). Key residues suspected to be involved in IVM binding and action at the rat P2X4 receptor have been highlighted within the transmembrane domain (dark blue) and the lateral fenestrations (green), shown here at the corresponding position in the zfP2X4 receptor. Structure was obtained from the SWISS-MODEL Repository (PDB accession number 4DW1).

1.3.2 IVM and other molecular targets

As discussed earlier, ivermectin can activate and/or modulate multiple mammalian targets in addition to the P2X4 receptor. This includes members of the cys-loop receptor ion channel superfamily, specifically GABA(A) receptors (Adelsberger et al., 2000), glycine receptors (GlyR) (Shan et al., 2001), and α-7 nicotinic acetylcholine receptor (α-7 nAChR) (Krause et al., 1998). Investigations into the activity of IVM at other mammalian receptors were first encouraged by the fact that the cys-loop receptors were very structurally similar to GluCl, the target receptor of IVM in parasites, as well as reports of adverse side effects in animals and humans following IVM treatment. This included low blood pressure and neurological symptoms such as depression and coma (Chandler et al., 2018). These harmful neurological effects result from IVM targeting GABA(A) receptors in the CNS. However, IVMs modulatory action is not restricted to pentameric receptors, as evidenced by its PAM activity at the P2X4 receptor as well as other structurally unrelated targets, summarised in Figure 1.7. Many of the above-mentioned channels, transporters and receptors are considered important therapeutic targets. Therefore, understanding the full scope of IVMs modulatory effects in mammals is critical for the design and development of novel drugs that can target these receptors with improved selectivity and thus reduced side effects.

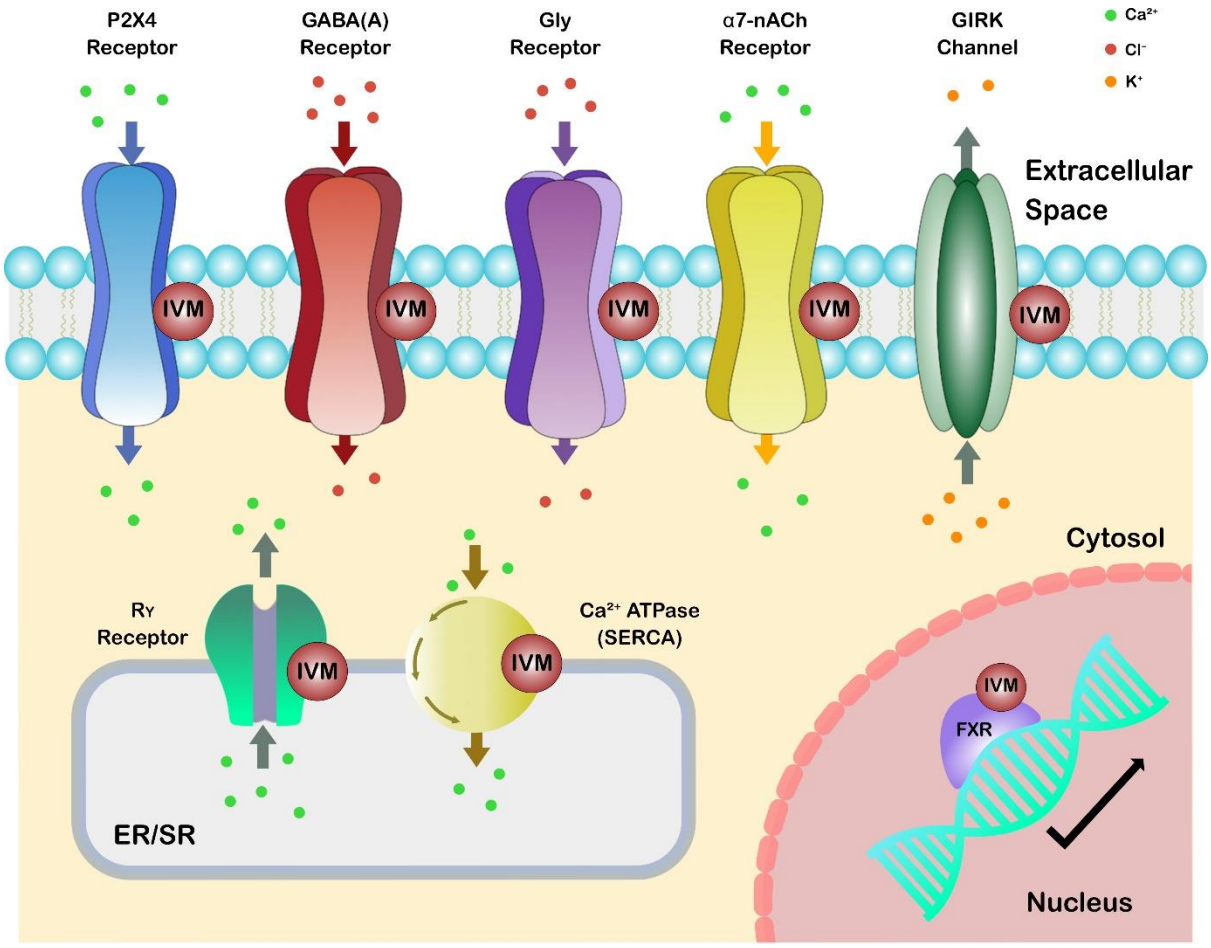

Figure 1.7. Ivermectin and its molecular targets in mammalian cells. IVM is known to activate and/or modulate several ion channels, receptors and transporters, including the P2X4 receptor and Cys-loop receptors (γ-aminobutyric acid receptor (GABA(A)R); glycine receptor (GlyR) and α7 nicotinic acetylcholine receptor (α7-nAChR)). IVM can also interact with GIRK channels; the nuclear receptor FX; ryanodine receptors (RyR) at the endoplasmic/sarcoplasmic reticulum (ER/SR) and the Ca^{2+}-ATPase (SERCA) transporter.

1.3.2.1 Cys-loop receptors

Interestingly, IVM has been found to activate and modulate GABA(A)R (Adelsberger et al, 2000; Krůšek & Zemková, 1994) and the GlyR (Shan et al, 2001). Both of these channels mediate fast inhibitory neurotransmitter transmission in the brain and are permeable to anions. Early research found that IVM could activate the GABA(A)R at high (μM) concentrations and at low concentrations (<0.1 μM) bind to a novel high-affinity site and potentiate the native GABA-mediated Cl^- currents in mouse hippocampal neurones (Krusek and Zemkova, 1994). Later studies showed that IVM activates mammalian α1β2γ2 GABA(A) receptors with relatively low potency compared to GluCl (EC_{50} of 2.3 μM and 140nM, respectively) (Adelsberger et al., 2000; Chen and Kubu, 2018). Whole-cell recordings also revealed that the rise-time and decay of ivermectin-activated currents were decidedly slower than those of GABA-activated currents and that IVM inhibited desensitisation of the receptor (Zemkova et al., 2014). This suggests that IVM and GABA activated the channel independently resulting in different kinetic properties.

Likewise, at the GlyR IVM acts as an irreversible agonist at high (μM) concentrations and a potentiator of glycine-gated currents at low concentrations (<30 nM) (Shan et al., 2001). This is not entirely surprising since the glycine receptor is very closely related to the GABA(A) receptor. Furthermore, Shan et al. (2001) demonstrated that IVM and Glycine bind via a structurally distinct mechanism as the binding affinity for IVM is not affected by mutations to the glycine binding domain (Shan et al. 2001; Zemkova et al. 2014). In the case of the excitatory receptors in the Cys-loop superfamily, it was found that IVM alone does not activate α7 nAChR current but, at high concentrations (30 μM), acts as a PAM molecule and potentiates the ACh-evoked currents (Krause et al., 1998 and Collins and Millar, 2010).

In the last decade, steady research, including crystal structures, site-directed mutagenesis and molecular modelling, has paved the way to uncovering how IVM binds and exerts its effect on Cys-loop receptors. Cys-loop receptors are composed of 5 subunits arranged in a ring formation to form a central pore that spans the membrane. Each subunit has a large extracellular domain (ECD) containing the ligand-binding domain; a transmembrane domain (TMD), characterised by four membrane spanning helices (M1-M4) and an intracellular domain. In terms of crystal structures, there has been two Cys-loop receptors complexed with IVM published: *C.elegan* GluCl (Hibbs and Gouaux, 2011) and zebrafish and human GlyR (Du et al., 2015; Huang et al., 2017), which clearly show how IVM binds to the interface between the M1 and M3 subunit and stabilises the open state of the receptor.

For the GABA(A)R, despite having no IVM-bound structure published, mutagenesis and structural modelling suggest that IVM binds to a similar position in the TM region as GluCl and GlyR (Estrada-Mondragon and Lynch, 2015). Interestingly, many critical residues discovered for IVM binding to GlyRα3, are highly conserved in the α and γ subunits of GABA(A)R (Huang et al., 2017). This is consistent with functional data demonstrating that IVM could bind to three different interfaces (α1-β2, α1-γ2L, and γ2L-β2) in α1β2γ2L GABA(A)Rs (Estrada-Mondragon and Lynch, 2015). However, these binding sights are not equivalent and have different effects. For example, electrophysiological

recordings revealed that when IVM binds to the α1-β2 interface it can potentiate GABA-mediated currents but has no irreversible activating effect. Whereas, if IVM binds to the γ2L-β2 interface it has an irreversible activating effect which, based on docking simulations, is thought to be a result of stronger molecular interactions in the binding pocket (Mondragon and Lynch, 2015). Lastly, for the α7 nAChR, IVM is considered a type I PAM, meaning it can only potentiate peak agonist-induced responses. Although like GABA(A)R, no IVM-bound structure has been published, the use of α7/5-HT3 chimeras and computer docking simulations supports the hypothesis that IVM interacts with α7 nAChR via the TM region (Sattelle et al, 2009; Collins & Millar, 2010).

1.3.2.2 Ca^{2+}-ATPase and Ryanodine receptors

IVM is also believed to have putative potentiating and inhibiting effects on Ryanodine receptor (RyR) and Ca^{2+} ATPase in skeletal muscle, respectively (Ahern et al., 1999). RyR are channels located in sarcoplasmic/endoplasmic reticulum (ER/SR) and are responsible for the efflux of Ca^{2+} from internal stores in response to an action potential in skeletal/cardiac muscle resulting in contraction. To counteract RyR and trigger relaxation in skeletal muscle, the SR Ca^{2+} ATPase (SERCA) will pump the Ca^{2+} back into the SR (or ER in non-muscle cells) from the cytosol at the expense of ATP hydrolysis. This dual effect of IVM was first reported when IVM was found to reversibly activate rabbit skeletal muscle RyR channels at micromolar concentrations whilst inhibiting Ca^{2+} uptake in skeletal muscle SR via Ca^{2+}-ATPase (SERCA) at high (10 µM) concentration, thus promoting the elevation of cytosolic Ca^{2+} (Ahern et al., 1999). Furthermore, it was reported later that IVM was the most effective inhibitor in the micromolar range of the rabbit SERCA1 isoform (skeletal muscle) but could also inhibit the porcine (pig) brain SERCA2b isoform (smooth muscle) (Bilmen et al., 2002). This was supported by another study that found IVM could inhibit all three P-type mammalian ATPases (Ca^{2+} ATPase; Na^{+}, K^{+}-ATPase and H^{+}/K^{+}-ATPase) at micromolar concentrations (Pimenta et al., 2010).

These changes in intracellular Ca^{2+} can have detrimental effects inside a cell, and the forethought behind these studies is to express that IVM can interfere with this cellular process, albeit at much higher concentrations, and is indicative of the adverse effects of IVM if used at higher doses. For example, this could explain the side effects on muscular activity in animals given higher doses of IVM to treat parasitic infections (Lovell, 1990). These papers highlight the wide reach of the macrocyclic drug IVM and stress the importance of developing novel selective and potent analogues, either for targeting parasitic infections or other biological targets. This will reduce adverse side effects, especially if higher than usual doses are required for treatment (Pimenta et al., 2010).

1.3.2.3 GIRK Channels

Recently another target of IVM was identified, called the G protein-coupled inwardly-rectifying potassium channels (GIRK). These channels are directly activated by the downstream signalling of GPCRs and are modulated by the lipid phosphatidylinositol-4,5-biphosphate (PIP_2), typically as a result of inhibitory neurotransmission resulting in reduced neuronal excitability. A study found that one member of the mouse GIRK family (GIRK2), typically found in the brain, is activated by IVM (EC_{50} of 3.5 µM) but only in the presence of PIP_2 (Chen et al., 2017). This study also identified a critical amino

acid, Ile82, needed for the high efficacy of the IVM response and suggests the IVM binds between the transmembrane domain (TM1) and N-terminal cytoplasmic tail domain (CTD) of GIRK2. This contrasts with Cys-loop receptors and P2X4 channels, where IVM is thought to bind predominantly to the TM domains (Chen and Kubo, 2018). The IVM analogues abamectin, doramectin and eprinomectin were also tested, and it was found that all avermectins investigated activated GIRK2 channels in oocytes with ABM showing similar efficacy to IVM (Chen et al., 2017).

1.3.2.4 Farnesoid X receptor

Another target receptor identified was the human farnesoid X receptor (FXR), a nuclear receptor involved in metabolic regulation (Jin et al., 2013). The natural ligands to these receptors are bile acids and upon activation, these receptors are capable of promoting gene transcription by directly binding to the DNA. These genes are essential for lipid, glucose and bile acid homeostasis, and increasing evidence links these receptors to non-alcoholic fatty liver disease (NAFLD). This development has encouraged researchers to hunt for novel FXR agonists as a possible treatment of NAFLD (Jiao et al., 2015; Keely and walters, 2016). Interestingly, IVM was found to be a highly potent partial agonist of FXR (EC_{50}, 200nM), but, more importantly, treatment with IVM could downregulate glucose and cholesterol levels, as well as fat buildup in diabetic mice (Jin et al, 2013 and 2015). Investigation of IVM analogues at the rat FXR found, like IVM, the avermectins doramectin and abamectin (EC_{50}, 0.5µM and 1.25µM, respectively) to be partial agonists. These studies demonstrated the high selectivity and affinity of these avermectin analogues over the natural ligand, bile acids (micromolar concentrations), and suggest how they could be used as the scaffolds for the design of drugs that can treat the NAFLD via FXR signalling (Jin et al., 2013 and 2015; Chen and Kubo et al, 2018).

1.3.3 IVM and neurotoxicity

Although IVM is generally considered a safe anti-parasitic drug, there are reports of severe toxic neurological side effects in humans and animals. These neurological effects, including dizziness, depression, and coma, have been linked to accidental overdose or when the blood-brain barrier (BBB) is compromised, specifically through the dysfunction or absence of P-glycoproteins (Edwards et al., 2003; Chandler, 2018). The BBB consists of a physical barrier of endothelial cells that limits the passive transport of potentially toxic macromolecules into the brain (Kadry et al., 2020). P-glycoproteins play an integral role in maintaining the BBB by transporting molecules out of the brain. Since IVM is highly lipophilic, it has the potential to cross the BBB. However, IVM has a high affinity for the P-glycoprotein and thus does not readily reach high concentrations in the CNS. Deficiencies in the P-glycoprotein will disrupt this process, and the resulting neurological side effects are thought to be due to IVMs penetration of the CNS and modulation of GABA(A) receptors.

1.4 Aim and objectives

As made evident by the literature, P2X4 receptors have received growing attention in the last two decades due to their widespread tissue distribution and potential involvement in numerous physiological and pathophysiological processes. Despite this, lack of selective modulators, particularly positive modulators, of the P2X4 receptor has slowed research advancement. At present, ivermectin is the most well-known positive allosteric modulator of the human P2X4 receptor and, as such, is routinely used as a pharmacological tool to study and isolate the contribution of the P2X4 receptors to health and disease states. Growing evidence suggests that potentiating P2X4 receptor function is therapeutically beneficial for a number of cardiovascular, immunological, and neurological disorders, such as hypertension (via vasodilation of blood vessels), sepsis, alcohol use disorder (AUD), and neurodegenerative diseases such as Alzheimer's and multiple sclerosis. Therefore, IVM has been proposed as a structural platform for designing novel drugs to target these conditions, as well as other P2X4-mediated processes. However, IVM's structure-activity relationship (SAR) is unknown, the allosteric binding site(s) has yet to be fully elucidated, and IVM is known to modulate other mammalian ion channels, risking neurological side effects.

The main aim of this project is to aid in the development of novel drug candidates with improved potency, efficacy, and selectivity at the human P2X4 receptor. This was done by investigating the SAR of IVM-B1a against the human P2X4 receptor using a library of structural analogues. The effects of these compounds on P2X4 channel function would be assessed by intracellular calcium mobilisation measurements and ranked in terms of PAM activity (potency and efficacy) at the human P2X4 receptor. Each compound would then be statistically compared to the reference compound IVM-B1a, and any structure-activity trends would be documented and assessed to determine the SAR between IVM-B1a and the human P2X4 receptor. Another objective of this study was to perform a selectivity screen of the IVM analogues against the GABA(A) receptor. Each compound was screened as an agonist of the GABA(A) receptor using a membrane potential assay kit in L(tk-) cells stably expressing the human recombinant GABA(A) ($\alpha1\beta3\gamma2$) receptor. In addition, pressure myography was employed to investigating the effect of IVM on flow-mediated vasodilation in mouse mesenteric arteries. In doing so, this study sought to demonstrate the therapeutic potential of P2X4-targetted PAMs as treatments for hypertension and ischemia.

Chapter 2. Material and Methods

2.1 Drugs and reagents

A list of the IVM-analogues and commonly used drugs (agonists, antagonists, and modulators) used throughout this study are provided in Tables 2.1 and 2.2, respectively. All the IVM-analogues were dissolved in 100% dimethyl sulfoxide (DMSO) at a stock concentration of 10 mM and stored at -20°C. The final concentration of DMSO was 0.1% (v/v) for all experiments in the 1321N1 and L(tk-) cell lines, and 0.5% (v/v) for the HUVEC cells. The FLIPR Membrane Potential Red Assay Kit (FMP-Red-Dye) was purchased from Molecular Devices Corporation (Sunnyvale, CA).

Table 2.1. List of IVM-analogues used in this study.

Compound	Catalogue Number	Supplier	Molecular Weight (g/mol)	Purity (%)
Ivermectin B1a	18768	Cayman Chemical	875.1	>95.0
Ivermectin B1b	23824	Cayman Chemical	861.1	>96.0
Ivermectin	18898	Sigma-Aldrich	875.1	B1a ≥ 90.0 B1b ≤ 5.0
Abamectin	19201	Cayman Chemical	873.1	B1a 80.0 B1b 20.0
Doramectin	33993	Supelco	899.1	≥ 95.0
Eprinomectin	32526	Supelco	900.1	≥ 95.0 (Sum of B1a + B1b)
Selamectin	21529	Cayman Chemical	770	≥98.0
Milbemectin	22003	Cayman Chemical	535.7	≥95.0 (Sum of A3 and A4)
Moxidectin	33746	Supelco	639.819	≥ 95.0
Nemadectin	17454	Cayman Chemical	612.8	≥ 95.0
1	L-000652264-000N	Merck Sharp & Dohme (MSD)	905.143	N/A
2	L-000640549-001A	Merck Sharp & Dohme (MSD)	977.079	N/A
3	L-000642126-000M	Merck Sharp & Dohme (MSD)	889.1	N/A
4	L-000734873-000V	Merck Sharp & Dohme (MSD)	979.223	N/A
5	L-000448091-000S	Merck Sharp & Dohme (MSD)	1189.81	N/A
6	L-000427078-000V001	Merck Sharp & Dohme (MSD)	1217.88	N/A
7	L-000647991-000S	Merck Sharp & Dohme (MSD)	1159.39	N/A
8	L-002483136-000A	Merck Sharp & Dohme (MSD)	975.191	N/A
9	L-000676897-000G	Merck Sharp & Dohme (MSD)	891.116	N/A
10	L-000734922-000J	Merck Sharp & Dohme (MSD)	919.17	N/A
11	L-000650360-000Z	Merck Sharp & Dohme (MSD)	969.124	N/A

N/A = Not Applicable. Purity unknown.

All compounds were dissolved and stored in 100% DMSO at -20°C.

Table 2.1(cont). List of IVM-analogues used in this study.

Compound	Catalogue Number	Supplier	Molecular Weight (g/mol)	Purity (%)
12	L-000658990-000S	Merck Sharp & Dohme (MSD)	932.169	N/A
13	L-000638709-000R	Merck Sharp & Dohme (MSD)	875.117	N/A
14	L-000639622-000Z	Merck Sharp & Dohme (MSD)	861.09	N/A
15	L-000757724-000U	Merck Sharp & Dohme (MSD)	965.199	N/A
16	L-000708381-000G	Merck Sharp & Dohme (MSD)	911.098	N/A
17	L-000757723-000K	Merck Sharp & Dohme (MSD)	931.138	N/A
18	L-000428486-000D	Merck Sharp & Dohme (MSD)	1220.85	N/A
19	L-001267140-000W	Merck Sharp & Dohme (MSD)	875.117	N/A
20	L-000452066-000E	Merck Sharp & Dohme (MSD)	1245.84	N/A
21	L-000691983-000V	Merck Sharp & Dohme (MSD)	891.116	N/A
22	L-000638725-000R	Merck Sharp & Dohme (MSD)	889.144	N/A
23	L-000688800-000T	Merck Sharp & Dohme (MSD)	891.116	N/A
24	L-000643214-000G	Merck Sharp & Dohme (MSD)	891.116	N/A
25	L-000680742-000N	Merck Sharp & Dohme (MSD)	933.154	N/A
26	L-000640370-000C	Merck Sharp & Dohme (MSD)	975.191	N/A
27	L-000680900-000W	Merck Sharp & Dohme (MSD)	991.191	N/A

N/A = Not Applicable. Purity unknown.

All compounds were dissolved and stored in 100% DMSO at -20°C.

Table 2.2. List of drugs used in this study.

Compound	Function	Supplier	Vehicle	Final Conc.
ATP	P2X4 agonist	Abcam	Distilled Water	0.01-100 µM
Carbachol	Acetylcholine receptor *agonist*	Sigma	Distilled Water	30 µM
U46619	Thromboxane A2 (TP) receptor agonist	Tocris	DMSO	20-40 nM
Phenylephrine (PE)	Alpha-1 adrenergic receptor agonist	Sigma	Distilled Water	0.3 – 1 µM
GABA	Neurotransmitter	Sigma	Distilled Water	0.01-500 µM
Acetylcholine (Ach)	Neurotransmitter	Sigma	Distilled Water	10 µM
BX430	P2X4 allosteric antagonist	Tocris	DMSO	5 µM
Thapsigargin (Tg)	SERCA pump inhibitor	Santa- Cruz	DMSO	5 µM
Dexamethasone (DEX)	GABA(A) expression promoter	Sigma	Ethanol	1 µM
Tumour Necrosis Factor-alpha (TNF-α)	Cytokine	Sigma	Distilled Water	10 ng/mL
Fibronectin	Plasma protein	Fisher	Distilled Water	100 ug/mL

DMSO = dimethyl sulfoxide

2.2 Cell culture

2.2.1 Human 1321N1 astrocytoma cells

The 1321N1 human astrocytoma cell line is derived from the U-118MG, a parental line isolated from human malignant glioma (Pontén and Macintyre, 1968). The 1321N1 cell line was available in-house and is referred to in this study as the parental 1321N1 cell line.

Another cell line used in this study was the 1321N1 astrocytoma cell line expressing human P2X4 receptor. This cell line was derived from stably expressing the human P2X4 receptor gene into the parental 1321N1 astrocytoma cell line. This cell line was chosen because they have previously been shown to be devoid of endogenous P2X and P2Y receptors (Bianchi et al., 1999) and are a fast growing, adherent cell line, making them a good model to study the human P2X4 receptor. All 1321N1 astrocytoma cells were used between passages 2-30.

2.2.1.1 General maintenance

The 1321N1 astrocytoma cell line was maintained in Dulbecco's Modified Eagle Media (DMEM, catalog #BE15-604K, Lonza, UK) containing high glucose (4.5 g/L) with L-Glutamine supplemented with 10% (v/v) foetal bovine serum (FBS; HyClone^{TM}, UK) and 1% (v/v) penicillin- streptomycin solution (Lonza) containing a final concentration of 50 units/mL penicillin and 50µg/mL of streptomycin. Cells were maintained at 37°C and 5% CO_2.

2.2.1.2 Cell passage

The 1321N1 astrocytoma cell line is adherent and was cultured in T75 flasks with filtered caps (Thermo Scientific) kept in a humidifier incubator at 37°C with 5% Carbon dioxide (CO_2). Once cells had reached 70-80% confluency they were washed with 3 mL pre-warmed (37°C) phosphate buffered saline (PBS; Lonza) followed by treatment with 1.5 mL trypsin EDTA solution (Lonza) for 5 minutes in the humidifier incubator at 37°C. After incubation the culture vessel was gently tapped to help detach the cells from the bottom of the flask. When ≥ 90% of the cells had detached the enzymatic reaction was stopped by adding 3.5 mL of fresh pre-warmed (37°C) cell growth media. The cells were then centrifuged at 450 x g for 5 minutes at room temperature (RT). The supernatant was aseptically decanted without disrupting the pellet and the pellet was gently re-suspended in approximately 5 mL of fresh cell growth media. The total number of cells was determined using a haemocytometer and cells/mL was calculated. The cell suspension was either re-seeded to generate a fresh T75 flask and returned to the humidifier incubator (37°C, 5% CO_2) or seeded for experimental use.

2.2.1.3 Freezing and thawing

For cryopreserving cells were stored in a cryopreserving solution consisting of 60% DMEM, 30% FBS and 10% DMSO at a concentration of approximately 1.00 x 10^6 cells per mL. This was achieved by detaching the cells and centrifuging them using normal passaging procedure but re-suspending the cells in the cryopreserving solution. The solution was then dispensed into cryogenic storage vials (Nunc, Sigma-Aldrich) which were transferred to a cryo-freezing container (Thermo Scientific) and

stored at -80°C overnight. The frozen cells were then transferred to liquid nitrogen (-180°C) for long-term storage.

When the cells were needed for experimental use, they were removed from long-term storage and thawed in a 37°C water bath for approximately 2 minutes. The cells were then immediately diluted by adding the cell suspension to 4 mL of cell growth media and centrifuged at 450 x g for 5 minutes at RT. The supernatant was then decanted, and the pellet was re-suspended in 5 mL of fresh cell growth media before being transferred to a T75 flask with filter cap and left to incubate in a humidifier incubator at 37°C and 5% CO_2.

2.2.2 Mouse L(tk-) cells

The mouse L(tk-) cell line expressing human recombinant GABA(A) receptors (α1β3ɣ2) was provided by the industrial partner Merck Sharp & Dohme (MSD). The cell line originates from Brooks Life Sciences (now called Azenta Life Sciences), who retrieved and shipped the cell line from long-term storage to complete cell line expansion at Sampled. The mouse L(tk-) cell line is adherent and derived from fibroblast cells from mouse connective tissue. All L(tk-cells) were used between passages 2-20.

2.2.2.1 General maintenance

The GABA (α1β3ɣ2) L(tk-) cell line was kept in Dulbecco's Modified Eagle Media (DMEM, catalog #BE15-604K) containing high glucose (4.5 g/L) with L-Glutamine, supplemented with 10% (v/v) foetal bovine serum (FBS); 1% (v/v) penicillin-streptomycin solution containing a final concentration of 50 units/mL penicillin, 50µg/mL of streptomycin and 1 mg/mL Geneticin-G418 (Sigma-Aldrich).

2.2.2.2 Cell passage

The GABA (α1β3ɣ2) L(tk-) cells are adherent and were cultured in T75 flasks with filtered caps kept in a humidifier incubator at 37°C with 5% CO_2. The cell passage methods for the mouse L(tk-) GABA(A) (α1β3ɣ2) cell line were carried out as previous outlined for the 1321N1 astrocytoma cells (section 2.2.1.2), replacing 1321N1 cell culture media with the L(tk-) cell culture media.

2.2.2.3 Freezing and thawing

The mouse L(tk-) GABA(A) (α1β3ɣ2) cells were cryopreserved and thawed in a similar manner to 1321N1 cells (Section 2.2.1.3), replacing 1321N1 cell culture media with the L(tk-) cell culture media.

2.2.3 Human umbilical vein endothelial cells (HUVECs)

HUVECs are a well-known in-vitro model for understanding the role of vascular ECs in normal physiology and disease. HUVECs were purchased from PromoCell (Heidelberg, Germany) at passage 1-2 and were isolated from the vein of an umbilical cord from pooled donors. All HUVECs were used between passages 1-10.

2.2.3.1 General maintenance

HUVECs were cultured in Endothelial Cell Growth Medium (PromoCell) with Supplement Mix containing FBS and additional required nutrients (Promocell). 50 units/mL penicillin and 50µg/mL of streptomycin was also added.

2.2.3.2 Cell passage

HUVECs are adherent and routine culture work took place in T25 or T75 flasks with filtered caps (Thermo Scientific) kept in a humidifier incubator at 37°C with 5% CO_2. Once the cells reached 70-80% confluency they were washed and detached using a Detach Kit (PromoCell) according to the manufacturer's instructions. In detail, the culture medium was carefully aspired, and the cells were washed with HEPES BSS solution (PromoCell), agitating the vessel carefully for approximately 15 minutes. After aspiring the HEPES BSS solution, the cells were then detached by applying Trypsin/EDTA (PromoCell) at RT. As soon as the cells began to detach (approximately 5 minutes) the side of the vessel was gently tapped to loosen any remaining adherent cells. To reaction was then neutralized by adding the Trypsin Neutralization Solution (PromoCell) to the vessel. The cells were then transferred to a centrifuge tube and spin down at 220 x g for 3 minutes at RT. The supernatant was aseptically decanted, and the pellet was gently re-suspended in 1 mL of fresh growth medium. The cells were then counted using a haemocytometer and seeded at the required seeding density and returned to the humidifier incubator (37°C, 5% CO_2) for maintenance or seeded in a 96-well plate for experimental use. Fresh media changes were performed every 2-3 days.

2.2.3.3 Freezing and thawing

For cryopreservation the cells were counted and re-suspended in cryopreserving mixture at a concentration of approximately 1.00 x 10^6 cells per mL. The mixture consisted of 90% Endothelial Cell Growth Medium and 10% DMSO. The cells were then transferred to cryovials and immediately placed in liquid nitrogen storage (-180°C). To thaw the HUVEC cells, cryovials were transported on dry ice before being immersed in a water bath (37°C) for 2 minutes. The cells were then immediately transferred to a T25 flask containing pre-warmed cell media (37°C).

2.2.3.4 Tumour Necrosis Factor-alpha (TNF-alpha) pre-treatment

For some Ca^{2+} mobilisation assays the HUVECs were exposed to pre-treatment for 48 hours with TNF-alpha (10 ng/mL) to induce an inflammatory response and up-regulate the expression of the human P2X4 receptor. To achieve this, the stock TNF-alpha was resuspended in PBS under sterile conditions and added to the endothelial cell growth medium during cell seeding in the 96-well plate.

2.2.3.5 Fibronectin coating

Fibronectin-coated 96-well plates were used to promote the expression of human P2X4 receptors in HUVECs. Briefly, under sterile conditions fibronectin was diluted in PBS to 100 ug/mL and dispersed equally in the 96-well plate (50 µl per well). The plate was then left to air dry for 1-2 hours and any excess liquid was removed by aspiration. The fibronectin-coated 96-well plates were stored at 4°C.

2.3 Fluorescent measurements

2.3.1 Calcium mobilisation assay

Changes in intracellular calcium concentration were measured using the fluorescent Ca^{2+} indicator dye, Fura-2 AM (Abcam) (Grynkiewicz et al., 1985). This allowed for the measurement of intracellular Ca^{2+} mobilisation caused by the activation of purinergic receptors present in the 1321N1 astrocytoma and HUVEC cell line. Fura-2 AM is a membrane permeable indicator that can cross the cell membrane. Once inside the cell the acetoxymethyl (AM) moiety is cleaved by cellular esterases, trapping the Fura-2 ratiometric dye inside the cell. The excitation peak of the dye shifts between 363 nm to 335 nm upon binding of the dye to free Ca^{2+} in the cell. Fura-2 has a constant emission maximum of 510 nm, and the typical excitation wavelengths are 340 nm and 380 nm for Ca^{2+} bound and Ca^{2+} free Fura-2, respectively. The fluorescent ratio of the two emission signals (340/380) is directly proportional to the intracellular Ca^{2+} level. Measuring the ratio reduces the effects of dye leakage, photo bleaching and uneven dye loading, as opposed to using single wavelength dyes such as Fluo-8 to measure intracellular Ca^{2+} concentrations (Paredes et al., 2008).

2.3.1.1 Calcium mobilisation buffers

Salt Buffered Saline (SBS) physiological solution was prepared in deionised water and contained (mM): NaCl, 130; KCl, 5; $MgCl_2$, 1.2; $CaCl_2$, 1.5; D-glucose, 8 and HEPES, 10; pH was adjusted to 7.4 with NaOH. Loading Buffer (LB) was prepared from SBS supplemented with 0.01% (w/v) of pluronic acid and 2µg/mL of Fura-2 AM (Abcam, Cambridge, UK). Both buffer solutions were stored at 4 °C and used within one week of preparation.

2.3.1.2 Intracellular calcium measurements

Adherent cells (1321N1 astrocytoma and HUVEC cells) were diluted with cell growth media to $1.25x10^5$ cells/mL (25,000 cells per well) and added to the wells (200 µl) of a sterile 96-well, clear-bottomed plate (Thermo Scientific). Plates were incubated for 24 hours at 37°C in a humidified incubator (5% CO_2) to allow cells to adhere to the flask. The following day, growth media was carefully removed, and the cells were washed with 200 µl pre-warmed (37°C) salt buffered saline (SBS). The cells were then loaded with 200 µl pre-warmed (37°C) loading buffer (LB) containing Fura-2 AM dye (2µg/mL). The 96-well plate was then wrapped in aluminium foil due to the photosensitivity of Fura-2 and incubated for 1 hour at 37°C. After the incubation step the cells are washed twice with SBS buffer and loaded with fresh SBS buffer.

Where applicable, drug compounds, including IVM and its analogues, or respective vehicle controls were added to each column of the 96-well plate at regularly spaced 5-minute intervals at 37°C. As a result, all cells were preincubated with drug compound or vehicle control for approximately 30 minutes before Fura-2 fluorescence (excitation 340nm and 380nm, emission 510nm) was measured in the Flexstation-3 plate reader (Molecular Devices, UK). Following this incubation step the plate was transferred to the Flexstation-3 plate reader and, after 18 seconds, the appointed wells were challenged with 50 µl of agonist or buffer control, automatically transferred from a U bottom 96-well

plate (Thermo Scientific) to a final volume of 250 µl per well. For all experiments, cells were maintained at 37°C and fluorescent readings were taken every 3 seconds for 250 seconds. The ratio of excitation wavelengths for Fura-2 at 340 and 380 nm was then used to quantify the change in intracellular calcium levels which is represented as the F ratio (340/380), as detailed in section 2.3.1. Blank samples were also run to control for background fluorescence.

2.3.1.3 Data analysis for calcium mobilisation assay

The F ratio (340/380) values for all calcium mobilisation experiments were extracted for every time point as trace data (max-min), peak data and area under the curve (AUC) data using the SoftMax Pro 5.4.5 software (Molecular Devices). All data was analysed using Excel (Microsoft Corporation) and the OriginPro software 9.7 (2020; Originlab).

To control for experimental variation between repeats all concentration-response data was normalised to a respective control on each plate. In the 1321N1 astrocytoma cell line, all data contributing to the ATP concentration-response curves in the absence and presence of compound was normalised to the maximal ATP response (30 µM) and for the compound concentration-response curves, all data was normalised to the submaximal ATP response (300 nM). For the calcium mobilisation assays performed on HUVEC cells, all data was normalised to the maximal response at 100 µM ATP.

For the concentration-response relationships the normalised responses were plotted against Log10 agonist/compound concentration and individually fitted with the Hill1 equation. See below;

$$y = START + (END - START)\frac{x^n}{k^n + x^n}$$

Where K = Michealis constant and n = number of cooperative sites. The log EC_{50} values, corresponding to half maximal effective concentration, were generated from fitting the Hill1 equation and is equal to the K value.

2.3.2 FLIPR membrane potential assay

To assess GABA(A) receptor activity in the L(tk-) cell line, changes in the membrane potential were measured using the fluorometric imaging plate reader (FLIPR) membrane potential Red-Dye (product #R8126) purchased from Molecular Devices (Sunnyvale, CA).

This dye was incubated with the cells and redistributes across the plasma membrane in a voltage-dependent manner. Upon depolarisation of the cell, a membrane potential change triggers the movement of positively charged ions and the dye into the cell. This increases the fluorescent signal intensity and is an indirect method of ion channel activity. Conversely, the fluorescent signal decreases upon cell hyperpolarization (Baxter et al., 2002; Whiteaker et al., 2001).

The FLIPR membrane potential assay kit comes with two fluorescent membrane potential (FMP) dyes (FMP-Red-Dye and FMP-Blue-Dye), both of which have subtle chemical changes that can be more, or less, suitable for the chosen ion channel target. Based on past literature, the FMP-Red-Dye showed better performance at detecting membrane potential changes via the GABA(A) receptor with kinetic values similar to those observed in electrophysiological studies and thus was deemed more suitable for this assay (Joesch et al., 2008).

2.3.2.1 FLIPR assay buffer

The FLIPR assay buffer was Hank's buffer with 20 mM HEPES (HHBS) containing (mM): $CaCl_2$, 1.3; $MgCl_2$, 0.5; $MgSO_4$-$7H_2O$, 0.4; KCl, 5.3; KH_2PO_4, 0.4; $NaHCO_3$, 4.2; NaCl, 138; Na_2HPO_4, 0.3; D-glucose, 5.6; HEPES, 4.7; pH 7.0 adjusted with NaOH.

2.3.2.2 Membrane potential measurements

Prior to running any FLIPR experiments, the mouse L(tk-) GABA(A) (α1β3ɣ2) cell line was exposed to 1 µM dexamethasone (DEX), added directly to the culture medium in the T75 flask (0.5% ethanol), for 24 hours to induce GABA(A) receptor expression. The cell line was then seeded and cultured in sterile 96-well, clear-bottom plates (Thermo Scientific) to a final plating volume of 100 µl/well at a density of approximately $1.75x10^5$ (35,000 cells/well). The cells were incubated for 24 hours at 37°C in a humidified incubator (5% CO_2) to allow cell adhesion. The FMP-Red-Dye was reconstituted to 1x with 100 mL of assay buffer, as instructed by the supplier (Molecule devices).

The following day, the growth media was removed and replaced with 100 µl of pre-warmed (37°C) assay buffer before being loaded with 100 µl pre-warmed (37°C) assay buffer containing the FMP-Red-dye. The 96-well plate was then incubated for 1 hour at 37°C. After incubation, each plate was transferred to a Flexstation-3 plate reader (Molecular Devices) and basal fluorescence was measured for 150 seconds at excitation and emission wavelengths of 530 nM and 565 nM, respectively. After 30 seconds of baseline recording, 50 µl of stimulant (GABA), was added to each well at a range of concentrations (0.01 – 500 µM) to evaluate agonist activity. The same protocol was used to test IVM-B1a as an agonist (0.01 – 30 µM) and to screen the IVM-analogues for agonist activity at two fixed concentrations (1 µM and 10 µM). All assays were performed at 37°C and fluorescent readings were taken every 5 seconds for 300 seconds.

2.3.2.3 Data analysis for FLIPR membrane potential assay

For all FLIPR experiments, the fluorescent values (Ex/Em 530/565 nm) were extracted for every time point as trace data (max-min) and peak data using the SoftMax Pro 5.4.5 software (Molecular Devices). All data was analysed using Excel (Microsoft Corporation) and the OriginPro software 9.7 (2020; Originlab).

All fluorescent signals exhibited an abrupt drop in fluorescent signal intensity with the addition of any solution that slowly returned to baseline over time. This transient drop in signal is suspected to be a caveat of injecting a contrasting agent (assay buffer) into the well, effectively diluting the FMP-Red-

Dye and causing a drop in fluorescence. Therefore, each experimental plate contained DEX-treated wells that would be injected with assay buffer only (buffer control wells) and subtracted from all experimental values to account for this drop in fluorescence.

The blank-subtracted data was then normalised to reduce experimental variation between replicates. For the agonist (GABA or IVM) concentration-response curves, all data was normalised to the maximal agonist response. For the activity screen (IVM-analogues), all data was normalised to maximal GABA response (30 µM) on the plate. EC_{50} values were determined from concentration-response curves by individually fitting the Hill1 equation, shown in section 2.3.1.3.

2.4 Electrophysiology

2.4.1 Electrophysiology buffers

All buffers were prepared in deionised water and stored in aliquots at -20°C and then 4°C once used. Nanion external solution used to resuspend the cells contained (mM): NaCl, 140; KCl, 4; $MgCl_2$, 1; $CaCl_2$, 2; D-glucose, 5; HEPES, 10; pH 7.4. The internal solution contained (mM): CsF, 140; NaCl, 10; EGTA, 2; HEPES, 10; pH 7.3 and the standard external solution contained (mM): NaCl, 155; KCl, 3; $MgCl_2$, 1; $CaCl_2$, 1.5; HEPES, 10; pH 7.4. Lastly, the seal enhancer contained (mM): NaCl, 80; KCl, 3; $MgCl_2$, 10; $CaCl_2$, 35; HEPES, 10; pH 7.3.

2.4.2 Planar patch clamp

Planar-patch electrophysiology was employed to validate the 1321N1 cell line stably expressing the human P2X4 receptor. The 1321N1 cells were detached from T25 flasks using TrypLE and were resuspended at $1x10^6$ cells/mL in Nanion external solution. Planar patch-clamp was conducted using a Nanion port-a-patch system fitted with an 8-valve gravity fed perfusion panel. Experiments were made in whole-cell configuration with internal solution. Following Mega-Ohm (>200 MΩ) to Giga-Ohm seal formation, all recordings were performed in standard external solution.

Recordings were acquired using HEKA Patchmaster software and a HEKA EPC 10 amplifier. Data were sampled at 1 kHz and filtered at 10 kHz. Cells were held at -80mV in all experiments and kept at room temperature. Seal formation was enhanced by treatment with seal enhancer for a maximum of 2 minutes until stable seals were obtained and replaced with standard external solution. All solutions were 0.2-µm membrane filtered. The protocol consisted of perfusing the cell with ATP for 3 seconds at increasing concentrations (0.3 to 100 µM) followed by an 8-minute recovery period. Offline analysis was performed using Origin Pro software (version 2020; Originlab).

2.5 Animals

For this study C57BL/6 male mice (8-32 weeks old) were investigated. All animals were housed in the Biomedical Research Centre Disease Modelling Unit. The housing conditions were individually ventilated cages under a 12-hour light/dark cycle; temperature of 21°C +/- 2°C and Humidity 55% +/- 10%. Animals were killed in accordance with the schedule 1 method as detailed in the Animal

(Scientific procedures) Act 1986 by exposure to rising concentrations of carbon monoxide and dislocation of the neck.

2.6 Pressure myography

To better understand the role of P2X4 receptors in vascular homeostasis, the activity of IVM on flow-mediated vasodilation was investigated in the mesenteric arteries of male mice using pressure myography. This technique tracks the blood vessel diameter and is often used to study vascular tone under a range of physiological conditions.

2.6.1 Pressure myography buffers

All buffers were prepared in deionised water, prepared weekly, and stored at 4°C. Physiological Saline Solution (PSS) contained (mM): NaCl, 130; KCl, 4.7; KH_2PO_4, 1.2; $MgSO_4$-$7H_2O$, 1.2; $NaHCO_3$, 15; D-glucose, 5.5; EDTA, 0.03; $CaCl_2$, 1.6. The Ca^{2+} free buffer contained the same ingredients as PSS except for $CaCl_2$ was substituted for EGTA (2 mM). The high Potassium Physiological Saline Solution (KPSS) contained NaCl, 74.7; KCl, 60; KH_2PO_4, 1.2; $MgSO_4$-$7H_2O$, 1.2; $NaHCO_3$, 15; D-glucose, 5.5; EDTA, 0.03; $CaCl_2$, 1.6. Lastly, Hanks Balanced Salt Solution (HBSS) was used to wash the arteries and contained (mM): KCl, 5.3; KH_2PO_4, 0.4; NaCl, 137; Na_2HPO_4, 0.3; D-glucose, 5.6; HEPES, 10; pH 7.0 adjusted with NaOH.

2.6.2 Vessel mounting and equilibration

The abdominal cavity was opened via a small incision in the skin under the sternum and the mesenteric tissue was dissected out of the mouse. The isolated tissue was then washed in ice-cold Hanks buffer and the mesenteric bed was pinned flat in a dissection dish that contained Hanks solution at 4˚C. The second order mesenteric arteries were identified and isolated from the connective and adipose tissue under a dissection microscope (Leica S8 APO) using fine scissors and forceps. The vessels were cut into 2-4 mm segments with the arterial segment containing branching to identify the distal end and avoid damage by applying flow in the wrong direction. The arteries were then stored in Hanks solution at 4˚C until they were transferred to a temperature-controlled (37°C) myograph chamber (Pressure Myograph - 114P, Danish Myo Technology) (Figure 2.1). Prior to transferring the vessel, the system was purged with PSS that had been pre-heated (37°C) and bubbled with carbogen (5% CO2, 95% O2) for 30-minutes to remove any air bubbles which might damage the endothelium of the vessel. The vessel was then carefully transferred to the myograph chamber which contained 4 mL PSS solution and one side of the artery was manoeuvred over the tip of a glass cannula (Living systems, 175 – 200 µM) and secured using two double loops of nylon suture (DMT). Once secured at one end, the vessel was gently rinsed with PSS to remove any blood before the vessel was attached to the other glass cannula. Once mounted the chamber was refilled with fresh PSS solution to remove any cell debris and transferred to the microscope. The lid of the myograph chamber was then attached and, to maintain the pH at physiological range (pH 7.4), supplied with a continuous stream of gas (5% CO2, 95% O2). The microscope is connected to a camera that allows for the monitoring of the vessel diameter using the MyoVIEW 4 software.

To equilibrate the vessel, the vessel was perfused with pre-warmed (37°C) and pre-gassed PSS solution by opening the inflow and outflow tap, filling the vessel, and making it partially pressurised. A flow gradient was then applied with 20 mmHg at the inflow end and 5 mmHg at the outflow end for 2-3 minutes before the system was set to a no-flow state. The artery was then gradually pressurized over 60 minutes from 10 mmHg to 60 mmHg. During this time the micro-positioner for horizontal adjustment of one of the canulae was used to slowly stretch the vessel and avoid any buckling as the pressure increased. Any drops in intraluminal pressure where indicative of arterial leakage and the artery was either re-attached to the cannulas or discarded. Once the vessel was equilibrated the protocol could be initiated.

2.6.3 Pressure myography protocol

For these experiments the outer wall diameter of the vessel was monitored and recorded using a digital camera and the MyoVIEW 4 software. The typical diameter of the arteries was between 230-270 µm and the intraluminal pressure was maintained at 60 mmHg for all vessels. A slight pressure difference of 2 mmHg was constantly maintained during no flow conditions to prevent backflow and damaging the endothelium.

Once the vessel has been equilibrated, the artery was 'activated' by initiating a series of contractions using a high potassium buffer. This is important to test the function of the artery before initiating any experiments. The PSS in the chamber was removed and replaced with 60 mM KPSS to stimulate a contraction. After the contraction had stabilised, the artery was washed three times with 5 mL PSS buffer. The process was repeated at least three times or until baseline diameter was reached. If the artery was viable, it should contract quickly once the chamber is flooded with KPSS buffer and dilate quickly when washed with PSS buffer. Once the contractile function was tested the experiment could commence. The vessel was then incubated for 15 minutes with control (<0.1% DMSO) and pre-constricted to approximately 60% of the initial diameter upon the addition of U46619 (20-40 nM). A range of concentrations was used to achieve a similar degree of constriction despite differences in vessel diameter. Once stabilised (approximately 5 minutes), pressure differences of 4-10 mmHg between the inflow and outflow were introduced to simulate flow through the vessel. A range was used to achieve submaximal vasodilation (approximately 70% of the initial diameter) depending on the artery. After a 5-minute incubation time, the pressure difference returned to no flow conditions (2 mmHg) for another 5 minutes and the artery was washed three times with 5 mL PSS buffer to return to baseline diameter. This protocol was repeated at least twice for control conditions and twice with the 15-minute pre-incubation of IVM (3 µM; <0.1% DMSO) to assess the effect of IVM on flow-dependant vasodilation.

At the end of each experiment, endothelium viability was assessed by constriction with phenylephrine (PE) (0.3 – 1 µM) and dilation with acetylcholine (ACh) (10 µM). Vessels that failed to achieve >50% of the averaged maximal dilation (D_{max}) were considered damaged and not used in subsequent analysis. Finally, the artery was then bathed in Ca^{2+}-free buffer for 30 minutes to achieve maximal dilation

(D_{max}). All drugs were administered to the abluminal edge of the vessel wall via the lid and mixed by pipetting the solution up and down several times.

2.6.4 Data analysis for pressure myography

The outer wall of the artery was continuously monitored allowing the tracking of vasoconstriction and vasodilatory responses. All data points represent the mean diameter over 5-10 seconds ± SEM (n represents the number of animals). The percentage dilation was calculated as:

$$Dilation\ (\%) = \frac{D_{FLOW} - D_{BASELINE}}{D_{MAX} - D_{BASELINE}}\ X\ 100$$

where D_{MAX} is the peak diameter following a 30-minute incubation with Ca^{2+}-free buffer, $D_{BASELINE}$ is the diameter of the vessel pre-constricted with U4166, and D_{FLOW} is the diameter of the vessel during flow conditions. Statistical comparisons were performed using unpaired two-sample t-tests, with $p<0.05$ indicating statistical significance.

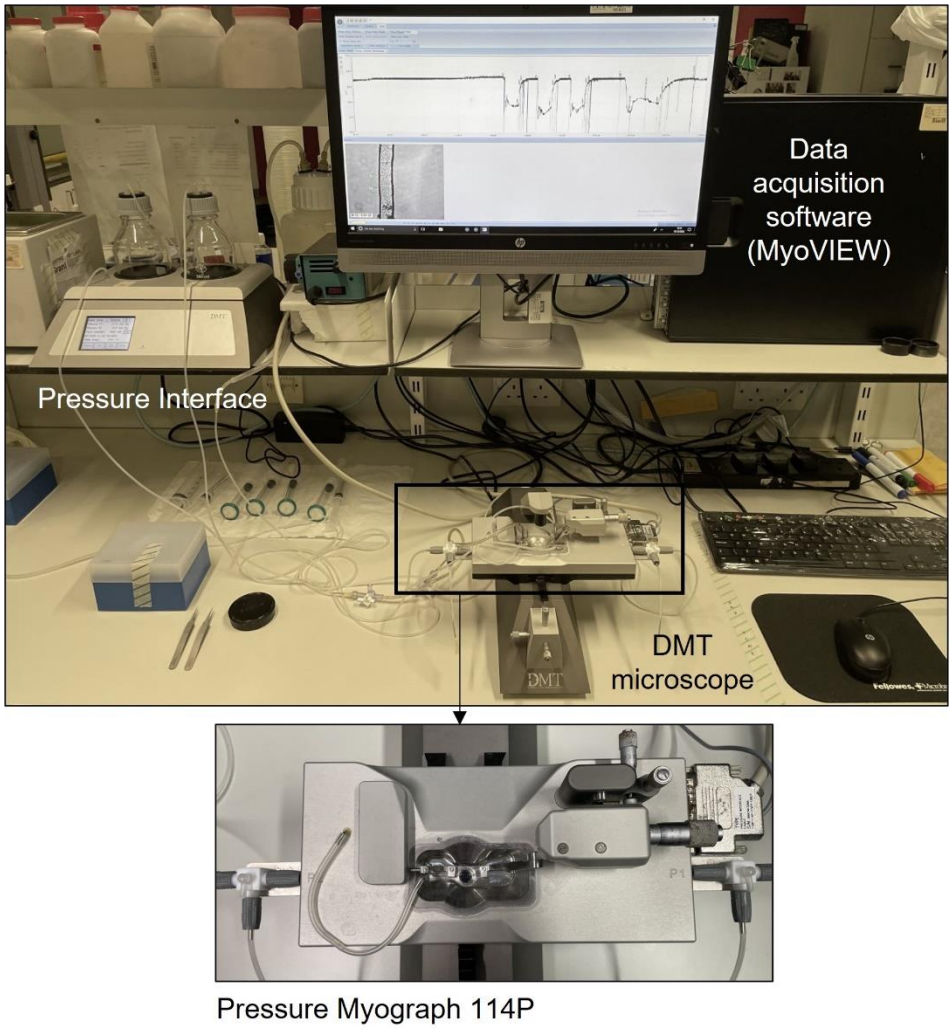

Figure 2.1. Pressure myography set-up with Pressure Interface and MyoVIEW software.

2.7 Statistical analysis

All data analysis was performed in Excel (Microsoft Corporation) and the OriginPro software 9.7 (2020; Originlab). Data was represented as mean ± SEM (standard error of mean) and with n representing the number of biological repeats (cells or mouse) and N representing technical repeats on the 96 -well plate.

To determine if the data was normally distributed a Shapiro-Wilk test was used and, if the data was normally distributed, a Levene's test for equal variance was performed. Normally distributed data was assessed using an unpaired two sample t-test or a one-way ANOVA followed by a post hoc Tukey test. If the data is not-normally distributed, then a Mann-Whitney test or a Kruskal-Wallis ANOVA followed by post hoc analysis was used. The threshold for statistical significance was $p<0.05$ throughout (*$p<0.05$, **$p<0.01$, ***$p<0.001$).

Chapter 3. Investigating the structure-activity relationship (SAR) and selectivity of a series of ivermectin analogues at the human P2X4 receptor

3.1 Introduction

Ivermectin (IVM), as detailed in the introduction (see section 1.3) is a positive allosteric modulator of the P2X4 receptor. The application of extracellular IVM is shown to potentiate ATP-evoked currents mediated by the human and rodent P2X4 receptor, as well as slow the rate of receptor deactivation (Khakh et al., 1999; Priel and Silberberg, 2004; Gao et al., 2015; Weinhausen et al., 2022). In addition, IVM is known to be selective for the P2X4 receptor over the other six P2X subtypes (P2X1-7). Because of this reason, IVM has been applied extensively as a pharmacological tool to study and isolate P2X4 activity in health and disease states and has been associated with a range of therapeutic benefits, including the treatment of hypertension and alcohol use disorder (AUD).

Although much information can be extracted from the published zfP2X4 crystal structure, predicting allosteric sites on the receptor remains extremely challenging. As such, the binding site(s) and the full mechanism of action for IVM at the P2X4 receptor have not been fully elucidated. Identifying and characterising the site(s) of IVM action would enable the design and development of novel small molecules and help to unlock the full therapeutic potential of P2X4 receptors.

Furthermore, IVM can activate and modulate multiple mammalian ion channel targets. This includes members of the cys-loop receptor superfamily, including GABA(A) receptors (Adelsberger et al., 2000) and as well as other structurally unrelated mammalian receptors. Notably, treatment with ivermectin has been reported to induce neurotoxicity in animals and humans, such as CNS depression and occasionally coma (Chandler et al., 2018). These adverse effects are likely accounted to IVM's broad-spectrum activity, specifically at GABA(A) channels which are key advocates for neurotoxic side effects. Therefore, understanding the full scope of IVMs modulatory effects at the GABA(A) receptor is critical for the design of novel drugs that can target the P2X4 receptor with improved selectivity and reduced risk of adverse side effects.

3.2 Aims

The main aim of this study was to investigate the structure-activity relationship between the human P2X4 receptor and IVM-B1a using a library of IVM-analogues. The specific objectives were as follows:

- Identify IVM-analogues that can target the P2X4 receptor with increased efficacy and potency.
- Define the general rules for the SAR of IVM-B1a at the P2X4 receptor.
- Identify IVM-analogues that can target P2X4 receptor with increased selectivity against the GABA(A) receptor.

3.3 Results

3.3.1 Effects of ATP on the P2X4 overexpressing astrocytoma cell line

3.3.1.1 Activation of human P2X4 receptor by ATP using fluorometric calcium assays

The cell line used in this study was an astrocytoma cell line (1321N1) overexpressing human P2X4 receptor. Since P2X4 channels are permeable to divalent cations, including Ca2+, P2X4 receptor activity was assessed by measuring the changes in intracellular Ca2+ using the Ca2+ indicator dye, Fura-2 AM. ATP is the most well-characterised full agonist of P2X4 receptors (Coddou et al., 2011), so initial experiments were designed to determine the potency and efficacy of ATP at the human P2X4 receptor when expressed in 1321N1 cells. An important aspect of the 1231N1 cell line is that it does not express any P2 receptors. Since ATP is not a P2X4-selective agonist, it was important to use a cell line that did not express any endogenous P2 receptors which could mask any P2X4-mediated responses.

As shown in Figure 3.1A, ATP could evoke concentration-dependent (0.01 – 300 µM) intracellular Ca^{2+} responses in 1321N1 cells stably expressing human P2X4 receptors, with maximal activity at 30 µM. To give confidence that this response is due to P2X4 activation, untransfected parental 1321N1 cells were stimulated with a maximal concentration of ATP (30 µM). As shown in Figure 3.1C, an ATP-evoked Ca^{2+} response could not be detected in the untransfected cells, giving assurance that the response is due to P2X4 activation. To control for cell viability, carbachol (100 µM), a drug that mimics the effect of acetylcholine, was also used to stimulate a P2X4-independent rise in intracellular Ca^{2+} through muscarinic acetylcholine receptors that are known to be expressed in these cells (Kitazawa et al., 2008). From the ATP concentration-response curve, the calculated EC_{50} and EC_{30} value was 0.5 ± 0.03 µM and 0.3 ± 0.02 µM, respectively (n=5). This agrees with reported ATP EC_{50} values using Ca^{2+} assays which range between 0.2 µM to 1 µM for human P2X4 receptors in 1321N1 cells (Bianchi et al., 1999; Abdelrahman *et al*., 2017; Sophocleous *et al.*, 2020;). The EC_{30} value was used in later experiments to test the ability of IVM and its analogues to potentiate the intracellular Ca^{2+} response as PAMS of the human P2X4 receptor. At low concentrations of ATP (0.01 and 0.03 µM), there was no amplification of the Ca^{2+} response. This suggests that the agonist concentration is not high enough to overcome the threshold concentration required to activate the human P2X4 receptor. In contrast, the application of high concentrations of ATP (100 and 300 µM) resulted in a reduction of intracellular Ca^{2+} response, which can suggest receptor desensitisation. This is reflected in the representative time-response trace (Figure 3.1B) which shows a rapid, transient increase in P2X4-mediated Ca^{2+} influx upon ATP (30 µM) application. The response then drops over time to a sustained elevated Ca^{2+} phase which could be due to the P2X4 receptors slow desensitisation kinetics (North and Surprenant, 2000).

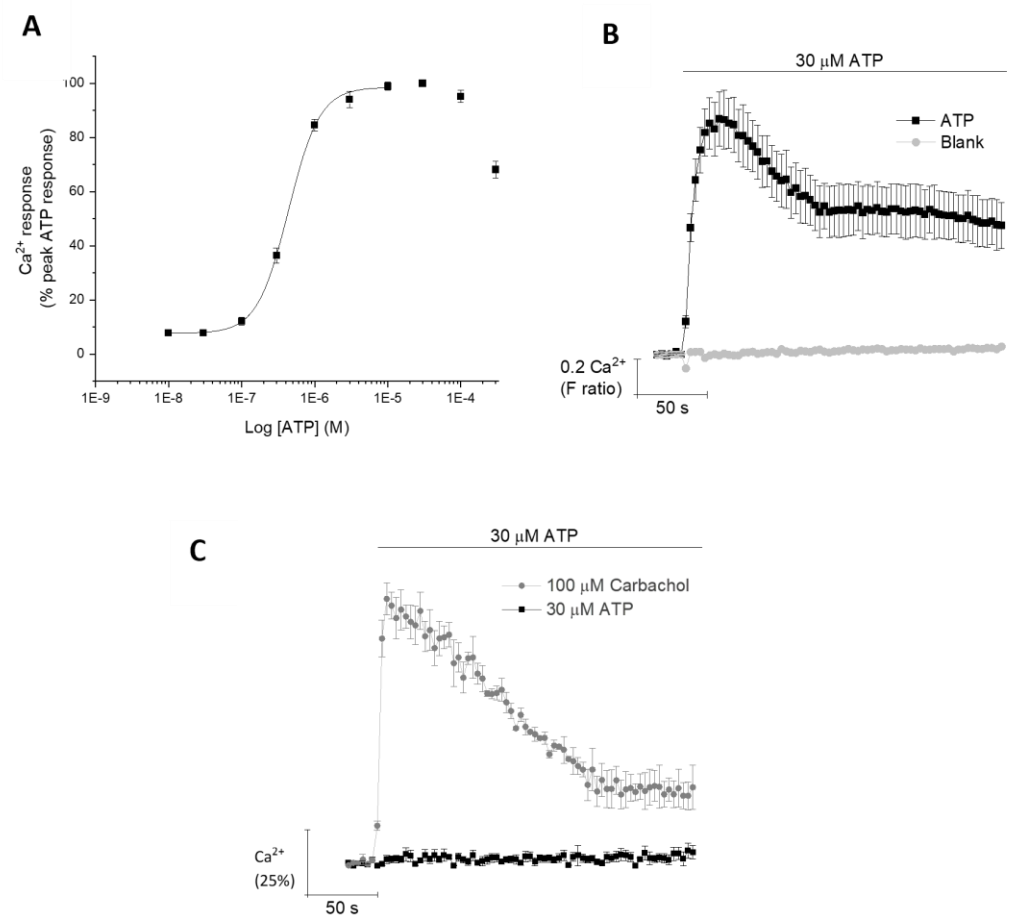

Figure 3.1. ATP elicited intracellular calcium response through human P2X4 receptors stably expressed in 1321N1 cells. (A) ATP concentration-response curve (0.01–300 μM) for human P2X4 receptors. All data was normalised to peak ATP response (30 μM) and fit to the Hill1 equation with the following EC_{50} value: 0.5 ± 0.03 μM (n=5). (B) Averaged time resolved intracellular Ca^{2+} responses upon application of 30 μM ATP to human P2X4 overexpressing 1321N1 cells over 250 seconds (n=5). (C) Averaged time-resolved traces showing the intracellular Ca^{2+} response elicited by 30 μM ATP and 100 μM carbachol (n=3). Data was normalised to either peak ATP response (30 μM) or peak carbachol response (100 μM). All data points are mean ± SEM.

3.3.1.2 Activation of human P2X4 receptor by ATP using planar patch-clamp electrophysiology

To support the pharmacological observations seen in the calcium assay, the 1321N1-hP2X4R cell line was further characterised using planar-patch clamp electrophysiology. ATP was applied at concentrations ranging from 0.3 to 100 µM. Activation of the P2X4-mediated currents was concentration-dependent, and representative currents elicited by various concentrations of ATP are shown in Figure 3.2A. At saturating concentrations of ATP (10 µM), the measured maximum current varied, ranging from -60 to -300 pA with a mean value of 206 ± 64 (SE) pA (n=5). For each cell, the inward current induced by increasing ATP concentrations was normalised to the value obtained with 10 µM ATP. Construction of a concentration-response curve to ATP was done for each cell, revealing EC_{50} values ranging from 1.04 µM to 5.30 µM with a mean value of 2.61 ± 1.0 µM ATP. For each ATP concentration, the normalised mean for all cells was plotted and fitted using the Hill1 equation to construct a final concentration-response curve, as shown in Figure 3.2B. The EC_{50} value compares well with the previously reported values of 1.4 µM (Jones et al., 2000) and 2.3 µM (Zemkova et al., 2015) for ATP in human and rat P2X4 receptors in HEK293 cells, respectively.

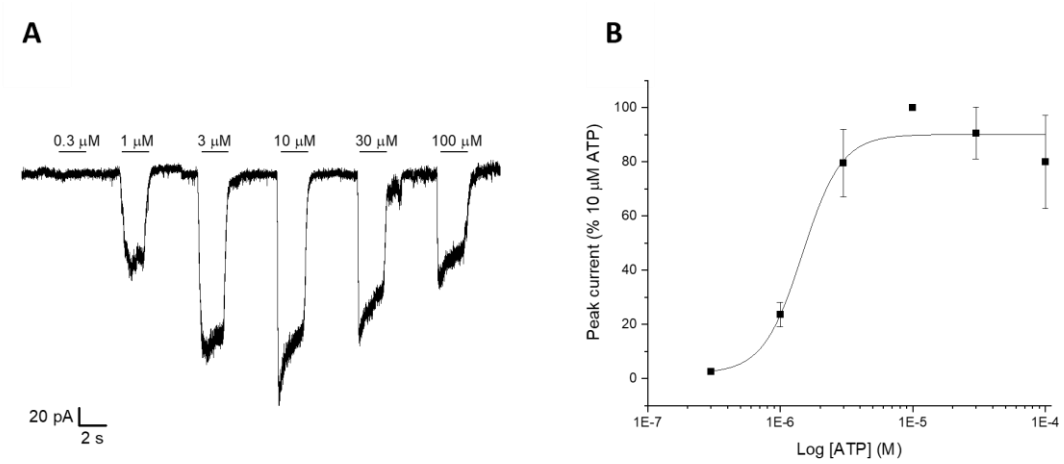

Figure 3.2. Activity of ATP on human P2X4 receptors stably expressed in 1321N1 cells. (A) Representative inward current elicited by application of ATP at different concentrations depicting a concentration-response relationship. The concentrations of ATP are indicated above the current traces. The horizontal bars indicate the beginning and duration of ATP application (3 seconds). Holding potential was -80mV. (B) Concentration-response curve for ATP activation. Data was normalised to peak ATP response (10 μM) and fit to the Hill1 equation with the following EC_{50} value: 2.61± 1.0 μM (n=5). All data points are mean ± SEM.

3.3.2 Pharmacological characterisation of ivermectin at the human P2X4 receptor overexpressing cell line

Before exploring the SAR of IVM using a series of analogues, IVM was first characterised in the 1321N1-hP2X4R cell line. Initial experiments were performed to confirm the mode of IVMs modulation and to determine potency (EC_{50}) and efficacy (E_{max}).

Since IVM and many of the analogues used in this study were insoluble in water, the compounds were dissolved in 100% dimethyl sulfoxide (DMSO), a widely used chemical solvent, at a stock concentration of 10 mM and stored at -20°C. The final concentration of DMSO for the drug compounds was 0.1% (v/v) in all experiments. Preliminary experiments were conducted to test whether the solvent influenced the magnitude of the ATP-evoked response. This involved pre-incubating the cells for 30 minutes with 0.1% DMSO (equivalent to compound incubation time) and stimulating them with a submaximal (0.3 µM) and maximal (30 µM) ATP concentration. Figure 3.3 shows no significant change in ATP-evoked Ca^{2+} response in relation to the control (no DMSO) for cells stimulated with either ATP concentration. This suggests that the solvent at 0.1% does not significantly affect the ATP-evoked Ca^{2+} response. From now on, every experimental plate was prepared at 0.1% DMSO.

To generate an IVM concentration-response curve, the cells were stimulated with submaximal ATP (ATP EC_{30} = 0.3 µM), and the rise in intracellular Ca^{2+} response was measured in the presence of various concentrations of IVM (0.03 – 10 µM). IVM significantly potentiated the ATP-induced Ca^{2+} response in a concentration-dependent manner. Peak activity was recorded at 3 µM, potentiating the fluorescence response to 555.90 ± 45.51% of the ATP-only response (n=5, $p<0.001$; Figure 3.4B). A representative Ca^{2+} time-response trace showing this potentiation of submaximal ATP (0.3 µM) in cells pre-incubated with IVM (3 µM) is shown in Figure 3.4C. The calculated EC_{50} value was 0.79 ± 0.07 µM, close to previously reported studies (Priel and Silberberg, 2004; Gao et al., 2015).

Figure 3.4D shows the ATP concentration-response curve in the presence and absence of 3 µm IVM. In the absence of IVM, ATP was an effective agonist at concentrations ranging from 0.01 µM to 30 µM, with an EC_{50} of 0.69 ± 0.05 µM. In cells preincubated with 3 µM IVM for 30 seconds, the magnitude of the intracellular Ca^{2+} response at saturating ATP concentrations (10 µM) increased to 195 ± 7%, a 2.1-fold potentiation by IVM. The representative Ca^{2+} time response trace in the presence and absence of 3 µM IVM upon stimulation with 0.3 µM ATP is represented in Figure 3.4E. The curve was also shifted to the left, reducing the ATP EC_{50} by 3.5-fold to 0.20 ± 0.02 µM ($p<0.001$; Table 3.1).

These observations suggest that IVM is a positive allosteric modulator of hP2X4 receptor. Not only does IVM increase the potency of ATP by shifting the curve, but it also increases the maximal efficacy of ATP. Specifically, IVM is a mixed type I/II PAM modulator (Stokes et al., 2020). This is consistent with prior studies that found IVM could enhance the amplitude of the ATP-induced currents at P2X4, as well as increase receptor sensitivity to ATP (Priel and Silberberg, 2004; Jelínková et al., 2006; Gao et al., 2015).

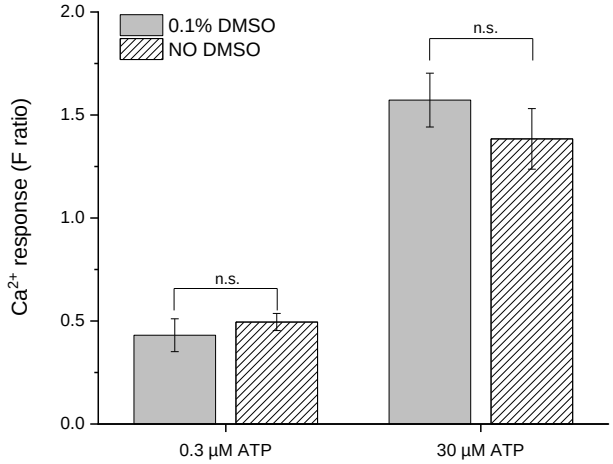

Figure 3.3. Tolerance of the ATP-evoked calcium response in 1321N1 hP2X4R overexpressing cells to 0.1% dimethyl sulfoxide (DMSO). Bar chart shows the effect on the magnitude of the intracellular Ca^{2+} response after a 30-minute incubation in the presence (grey bars) and absence (stripped bars) of 0.1% DMSO upon stimulation with ATP at submaximal (0.3 µM) and maximal (30 µM) concentrations (n=5). Each bar chart represents the mean of five independent biological assays; error bars are SEM. n.s: $p>0.05$ (not significant).

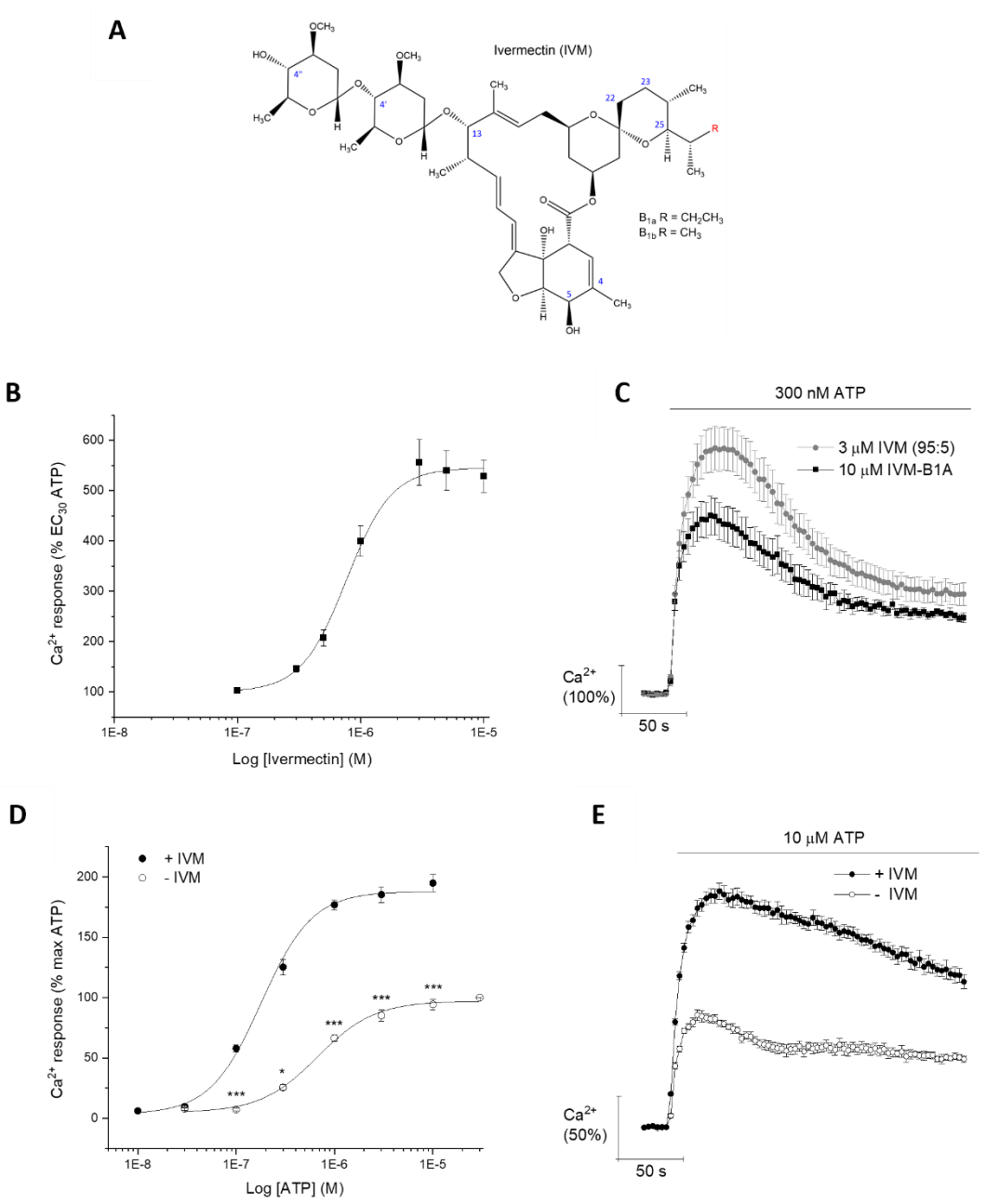

Figure 3.4. Activity of ivermectin (IVM) at the human P2X4 receptor in 1321N1 cells. (A) Chemical structure of IVM. Blue numbers represent the C-positions. (B and C) Concentration-response curve of IVM (0.1 – 10 µM; black squares) when the cells are stimulated with a submaximal ATP concentration (0.3 µM) and representative Ca^{2+} time-response trace demonstrating the potentiation of submaximal ATP-evoked Ca^{2+} response in the presence of 3 µM IVM. Data is normalised to peak control response (0.3 µM ATP) and represented as percentage control response (n=8). (D and E) ATP concentration-response curve (0.01 – 30 µM) in the presence (closed circles) and absence (open circles) of 3 µM IVM and representative Ca^{2+} time-response trace elicited by maximal ATP (10 µM) in the presence and absence of 3 µM IVM, respectively. Data is normalised to 30 µM ATP in the absence of IVM (n=5). Asterisks show significant differences between equivalent ATP concentrations in the presence verses the absence of IVM (*p<0.05, **p<0.01, ***p<0.001). All data points represent the mean ± SEM.

3.3.2.1 Investigating the individual homologues of ivermectin

Ivermectin is a semisynthetic derivate of avermectin B1 and consists of a mixture of two homologues: ivermectin B1a and B1b. These two homologues differ by one methyl group (CH_3) at the C25 side chain (R group): an ethyl group (CH_2CH_3) in the B1a form (Figure 3.5A) and a methyl group (CH_3) in the B1b form (Figure 3.5B). In this study, commercially available IVM was used with a reported composition of approximately 95% IVM-B1a and 5% IVM-B1b. Since IVM is a mixture of two compounds, it would be more precise to make chemical comparisons against the primary component IVM-B1a. In addition, most IVM-analogues tested have the ethyl B1a attachment in the R group. As a result, IVM-B1a was characterised to be the reference compound going forward rather than IVM, which is a blend of the two homologues. To avoid confusion throughout the study, IVM is only referred to when mentioning the mixture, while for the individual homologues the type of avermectin (B1a or B1b) is always indicated.

Figure 3.5C shows the concentration-response curve for IVM-B1a and IVM-B1b. As expected, both homologues elicited a concentration-dependent increase in intracellular Ca^{2+} levels. In the presence of submaximal ATP (0.3 µM), both IVM-B1a (10 µM) and IVM-B1b (3 µM) significantly potentiated the ATP-elicited Ca^{2+} response by 391.01 ± 40.37% (n=5; $p<0.01$) and 356.19 ± 51.52% (n=5; $p<0.001$) respectively (Table 3.2). The representative Ca^{2+} time-response curves in IVM-B1a (10 µM) and IVM-B1b (3 µM) treated cells upon stimulation with 0.3 µM ATP are shown in Figure 3.5D. Both homologues were found to be equally efficacious at potentiating the intracellular Ca^{2+} response but significantly less efficacious when compared to the mixed compound IVM ($p<0.05$ and $p<0.01$, respectively). However, the calculated EC_{50} values for IVM-B1a (EC_{50} = 1.04 ± 0.12 µm; n=5), IVM-B1b (EC_{50} = 0.93 ± 0.10 µM; n=5) and IVM (EC_{50} = 0.79 ± 0.07 µM; n=8) were comparable ($p>0.05$; Table 3.3).

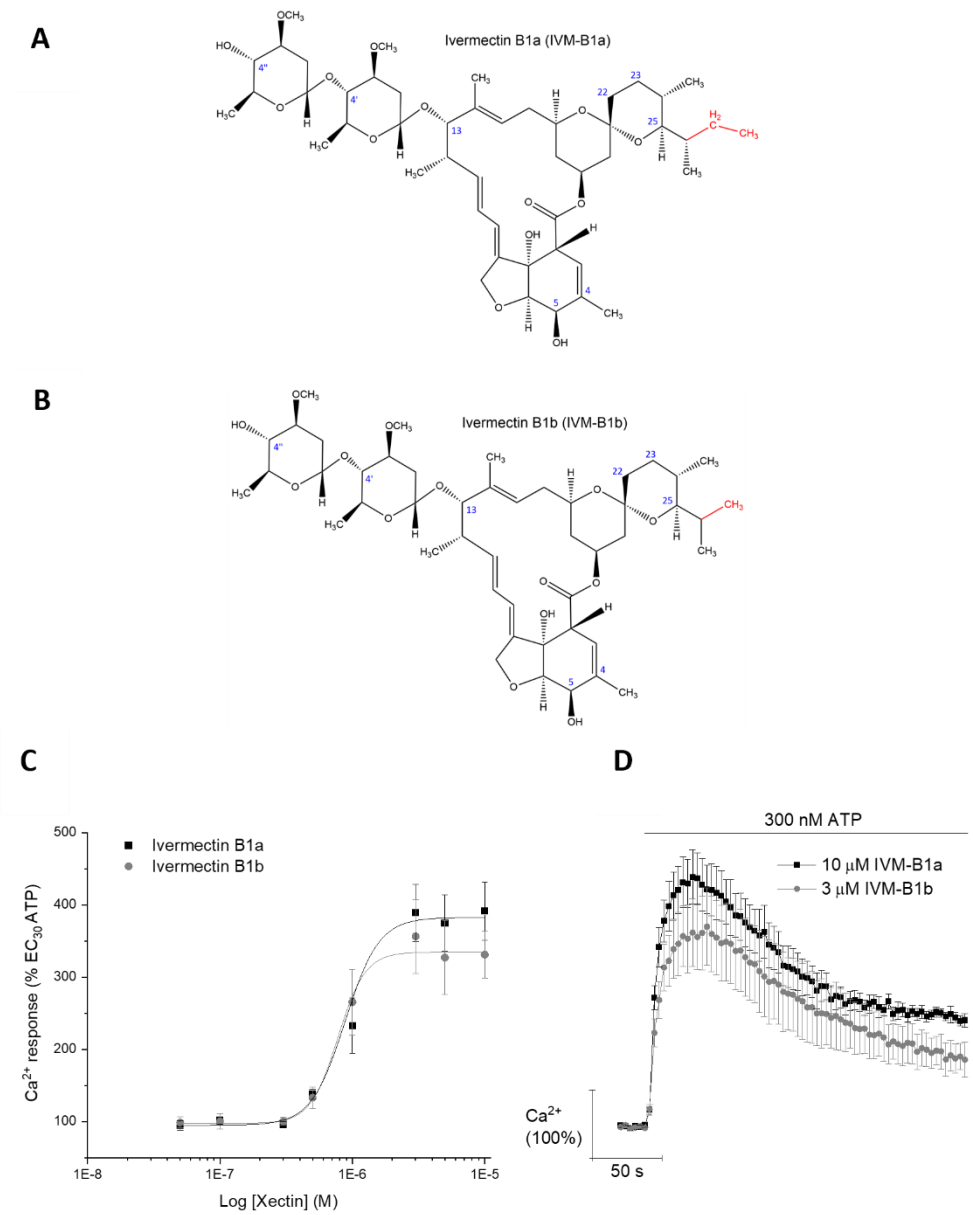

Figure 3.5. Activity of the ivermectin homologues (IVM-B1a and IVM-B1b) at the human P2X4 receptor in 1321N1 cells. (A and B) Comparison of the chemical structure of IVM-B1a (top) and IVM-B1b (bottom). Structural differences are highlighted in red. Blue numbers represent the C-positions. (C) Concentration-response curve of IVM-B1a (0.05 – 10 µM; black squares; n=6) compared to IVM-B1b (0.05 – 10 µM; grey circle; n=6) when the cells are stimulated with a submaximal EC_{30} ATP concentration (0.3 µM). (D) Representative Ca^{2+} time-response of IVM-B1a and IVM-B1b at maximal concentrations when stimulated with submaximal ATP (0.3 µM; n=6). Data is normalised to peak control response (0.3 µM ATP) and represented as percentage of control response. All data points represent the mean ± SEM.

3.3.3 Structure-activity relationship studies of IVM-B1a

To understand how structural modifications affect the potency and efficacy of IVM-B1a at the human P2X4 receptor, a library of 34 analogues was investigated. Most of the IVM-analogues explored in this study had structural changes in one or more regions of the molecule: R1, R2 and R3 (Figure 3.6). Of this compound library, several were commercially available and known positive allosteric modulators of P2X4 receptors. It should be noted that the chemical structure for IVM-B1a, as well as the commercial analogues, may not reflect the true stereochemistry of the molecule and therefore cannot be compared in this way. The remaining compounds, labelled **1**-**27**, were provided by the industrial partner, Merck Sharp & Dohme (MSD), and are not commercially available. The chemical structure for these compounds reflects the true stereochemistry of the molecule. A list of the compounds used in this study, including their chemical structures, can be found in Table A1 and A2 in the appendix.

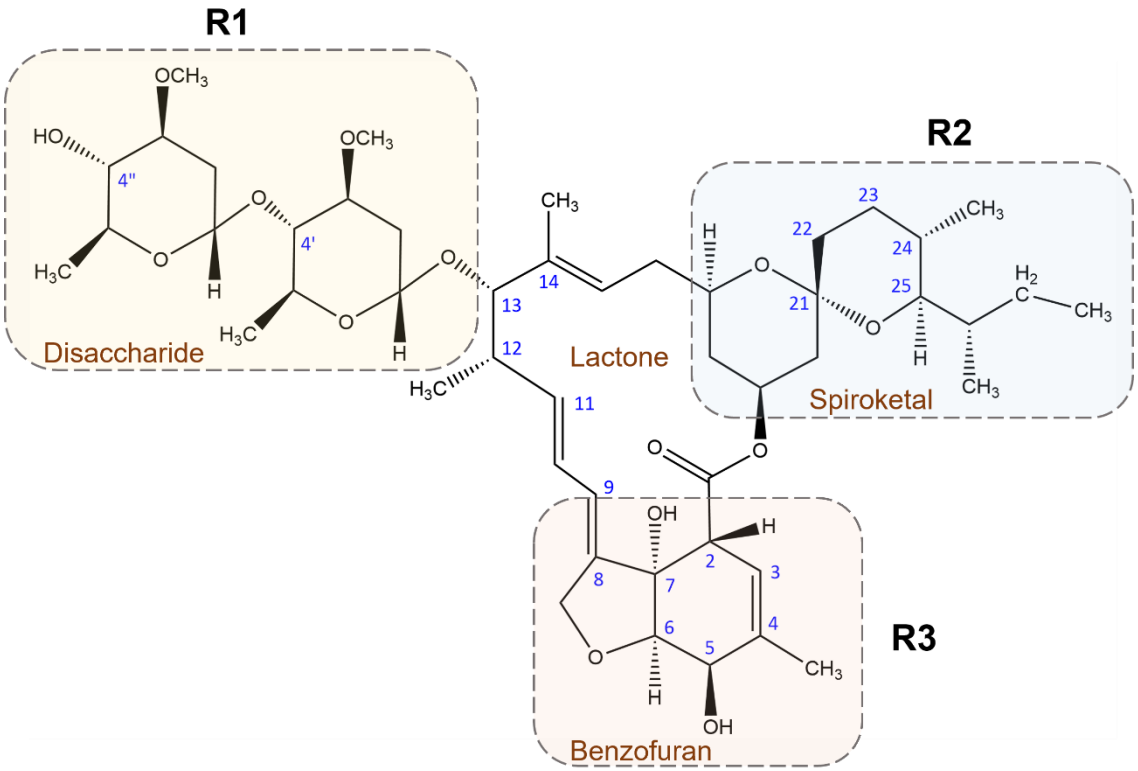

Figure 3.6. Chemical structure of IVM-B1a. The molecule is divided into three regions. The central 16-membered macrocyclic ring is the core structure present in all the IVM-analogues and connects the three variable substituent regions. These include the disaccharide moiety (R1), the spiroketal moiety (R2) and the benzofuran moiety (R3). Structural modifications to these regions give rise to all the IVM-analogues. Blue numbers represent the C-positions, based upon IVM-B1a numbering.

3.3.3.1 Effect of the commercial analogues on ATP concentration-response curves.

As reported earlier, IVM acts as a type I/II PAM modulator (Stokes et al., 2020) by increasing the potency and efficacy of the agonist ATP (Figure 3.4D). To confirm the type of modulation of the remaining commercial analogues (Table A1), an ATP concentration-response curve was constructed for each commercial compound, including ABM (Figure 3.13E), DRM (Figure 3.14E), EPM (Figure 3.33E), SLM (Figure 3.34E), MBM (figure 3.9E), MOX (Figure 3.35E) and NEM (Figure 3.36E). The effect of these compounds on ATP potency and efficacy was then assessed by comparing the concentration-response curves of ATP in the presence and absence of each compound at maximum concentration.

All the commercial analogues increased the potency of ATP, reducing the EC_{50} value, and increased the maximal efficacy of ATP, increasing the E_{max} value for the human P2X4 receptor. This was demonstrated by a left-ward shift in the concentration-response curve (potency) and an increase in maximum Ca^{2+} response (efficacy) compared to the untreated cells. A summary of all the results is shown in Table 3.1. All the commercial analogues produced a similar increase in ATP efficacy compared to untreated cells at approximately 200% of control response, i.e., a 2-fold potentiation in ATP-evoked Ca^{2+} response. However, the commercial analogues ABM (3 μM) and NEM (10 μM) promoted the most significant increase in ATP potency, reducing the ATP EC_{50} by 12.1-fold and 10.3-fold, respectively.

The remaining 27 compounds, plus the two homologues IVM-B1a and IVM-B1b, were not tested in this way since, given their structural similarity to IVM, they were expected to modulate P2X4 similarly to IVM and its commercial compounds.

Table 3.1. Activity of IVM and the commercial analogues on ATP concentration-response curves. The EC_{50} values and E_{max} values were calculated from ATP concentration-response curves. Data is presented as mean ± SEM (n=5-6).

Compound (Max Conc)	EC_{50} (µM) of ATP				E_{max} (%) of ATP		
	Without Compound	With Compound	Fold Increase α	Significance (p-value) β	With Compound γ	Fold Increase δ	Significance (p-value) ε
Ivermectin	0.70 ± 0.05	0.20 ± 0.02	3.5	<0.001	194.95 ± 7.04	2.07	<0.001
Abamectin	1.00 ± 0.08	0.08 ± 0.01	**12.1**	<0.001	212.51 ± 12.61	2.17	<0.01
Doramectin	0.75 ± 0.10	0.20 ± 0.02	3.8	<0.05	169.07 ± 7.29	1.76	<0.01
Eprinomectin	0.90 ± 0.08	0.17 ± 0.02	5.2	<0.001	197.35 ± 17.60	2.01	<0.01
Selamectin	1.46 ± 0.16	0.23 ± 0.02	6.4	<0.001	150.28 ± 6.06	1.57	<0.05
Milbemectin	1.21 ± 0.10	0.23 ± 0.02	5.3	<0.001	186.05 ± 9.26	1.86	<0.01
Moxidectin	0.92 ± 0.04	0.27 ± 0.02	3.4	<0.001	186.49 ± 7.73	1.96	<0.001
Nemadectin	1.01 ± 0.14	0.10 ± 0.01	**10.3**	<0.05	163.26 ± 2.36	1.69	<0.001

α = The relative fold change in ATP EC_{50} value with and without compound. **Bold** indicates a fold change greater than 10-fold.

β = p-value is the statistical comparison between ATP EC_{50} value with and without compound.

γ = Maximum compound concentration (1 – 10 µM) normalised to 30 µM ATP.

δ = The relative fold change in ATP E_{max} value with and without compound.

ε = p-value is the statistical comparison between maximum ATP with and without compound.

3.3.3.2 Investigating the potency and efficacy of the IVM-analogues

To test each compound, the cells were stimulated with submaximal ATP, corresponding to ATP EC_{30} (0.3 µM), and the rise in intracellular Ca^{2+} was measured in the presence of varying concentrations of compound (0.03 to 30 µM). Concentrations greater than 30 µM were not tested due to low solubility at these concentrations. To quantify the potentiating properties of these compounds, a concentration-response curve was constructed to determine EC_{50} and E_{max} values for each IVM-analogue at the human P2X4 receptor. This allowed for the ranking of the analogues according to their efficacy (Table 3.2) and potency (Table 3.3) for a clearer assessment of the effects of each compound on intracellular Ca^{2+} and subsequent SAR analysis.

In total, approximately 70% of the screened analogues were able to elicit an intracellular Ca^{2+} response significantly higher than the ATP-only control ($p<0.05$ vs. ATP 0.3 µM). A bar chart of this data showing the resulting E_{max} values ± SEM of each compound at maximal concentration ranging from 1 µM to 10 µM can be found in Figure 3.7. Eleven of the IVM-analogues did not significantly potentiate the intracellular Ca^{2+} response higher than ATP-only control (ATP 0.3 µM). These compounds were considered to have no activity at the P2X4 receptor under these tested conditions, represented by empty bars (Figure 3.7) and grey rows (Tables 3.2 and 3.3) ($p>0.05$ vs. ATP 0.3 µM). The remaining compounds were able to potentiate the intracellular Ca^{2+} response higher than ATP-only control ($p<0.05$), with several ranking significantly more efficacious than IVM-B1a ($p<0.05$).

For a comparison of compound potency, Figure 3.8 shows the calculated EC_{50} values for each compound and statistical significance compared to IVM-B1a. All compounds where a sigmoidal curve could not be fitted were labelled as n.d. since the EC_{50} value could not be determined. In total, four IVM-analogues were significantly more potent than IVM-B1a ($p<0.05$).

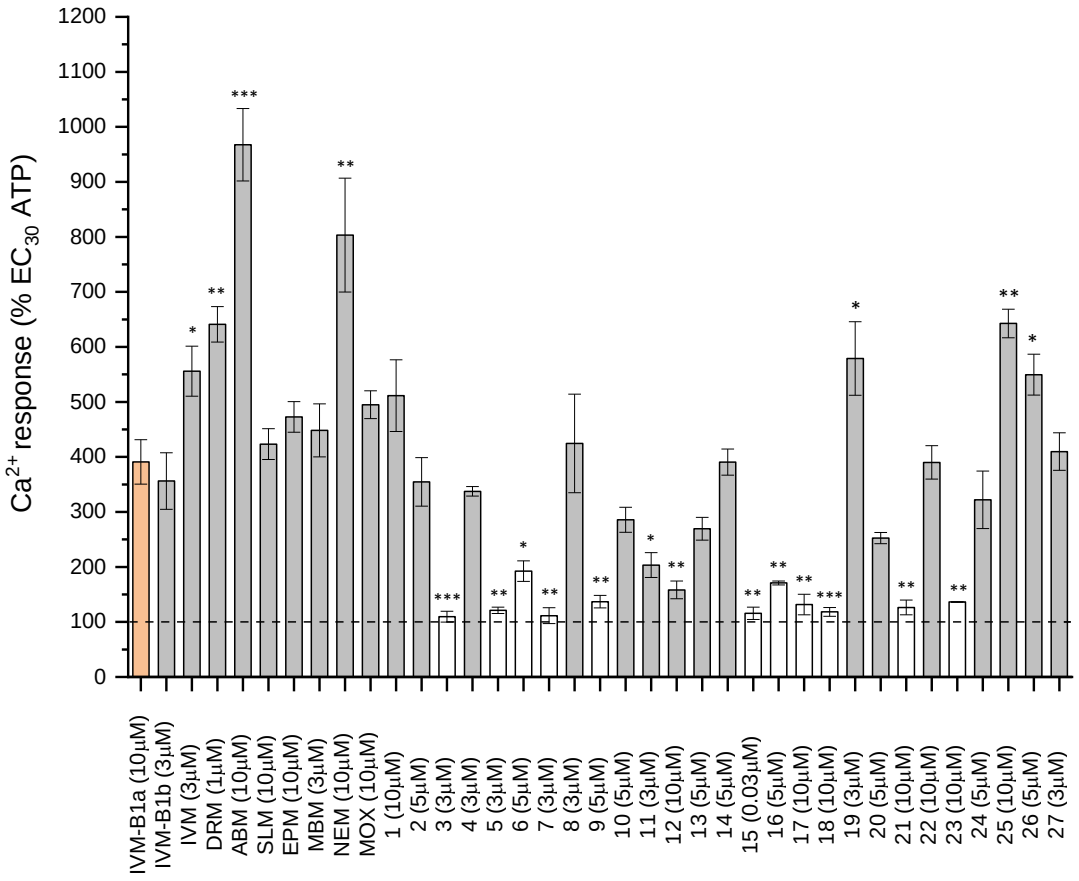

Figure 3.7. Activity of IVM-B1a and its analogues on ATP-evoked calcium response in 1321N1-hP2X4R cells. Bar chart showing the efficacy (E_{max}) of all IVM-analogues tested and the reference compound IVM-B1a (orange), as well as the concentration required to reach E_{max}. All cells were stimulated with submaximal ATP (0.3 µM) and normalised to peak control response (0.3 µM ATP). Compounds that did not potentiate the intracellular Ca^{2+} response significantly higher ($p>0.05$) than control response (100%) were considered to have no activity at the P2X4 receptor (white) (n=3-8). Asterisks show statistical significance relative to IVM-B1a efficacy (orange) at maximal concentration (*$p<0.05$, **$p<0.01$, ***$p<0.001$). Each bar represents the mean of at least three independent biological assays; error bars are SEM.

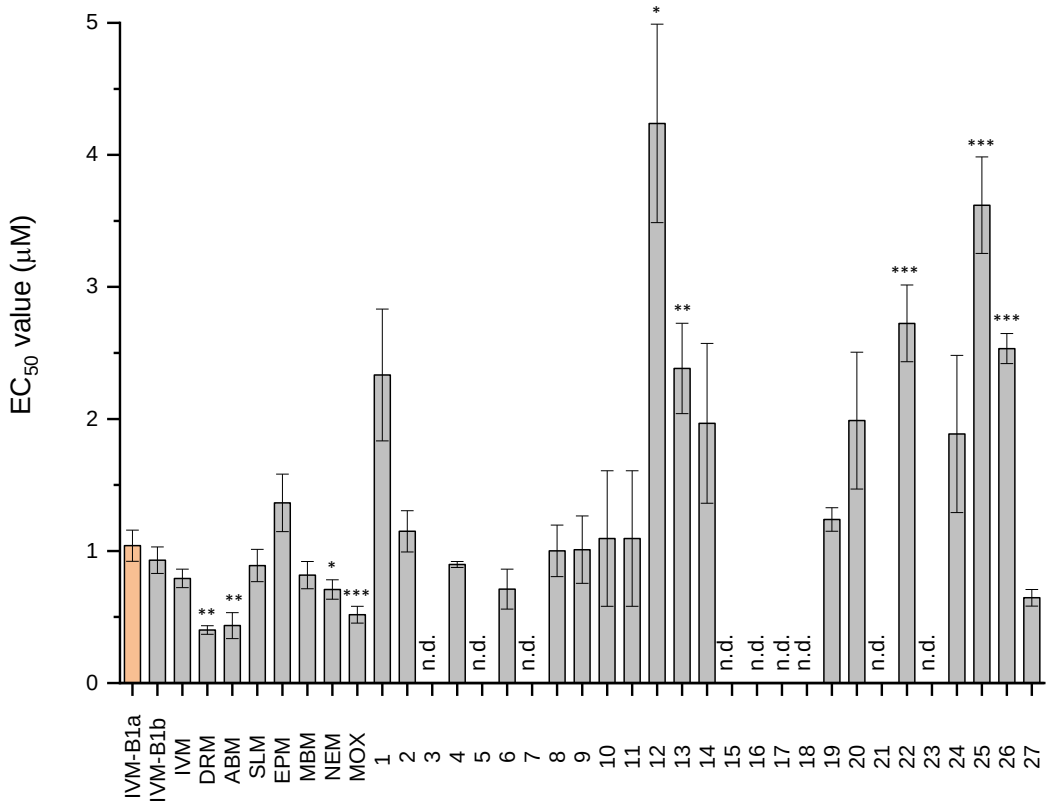

Figure 3.8. Comparison of EC_{50} values between IVM-B1a and its analogues in 1321N1-hP2X4R cells. EC_{50} values were determined from concentration-response curves generated from Ca^{2+} mobility assays (n=3-8). Asterisks show statistical significance relative to IVM-B1a potency (orange) (*<0.05, ** p<0.01, ***p<0.001). Each bar represents the mean of at least three independent biological assays; error bars are SEM. n.d. means an EC_{50} could not be determined.

Table 3.2. Summary of the effects of IVM-B1a (orange) and its analogues on the P2X4 response, ranked in terms of efficacy (E_{max}). The E_{max} values and EC_{50} values were calculated from individual concentration-response curves (n3-8). Data is presented as mean ± SEM.

Compound	Efficacy (Maximum Ca^{2+} Response/E_{max}) (%) (p-value) $^{\alpha}$	Potency (EC_{50}) (μM) (p-value) $^{\beta}$	Percentage IVM-B1a response
Abamectin	967.47 ± 65.76 (p<0.001)	0.44 ± 0.10 (p<0.01)	247
Nemadectin	803.40 ± 103.47 (p<0.01)	0.71 ± 0.07 (p<0.05)	205
25	642.62 ± 25.87 (p<0.01)	3.62 ± 0.37 (p<0.001)	164
Doramectin	641.01 ± 32.34 (p<0.01)	0.40 ± 0.03 (p<0.01)	164
19	578.92 ± 66.85 (p<0.05)	1.24 ± 0.09	148
Ivermectin	555.90 ± 45.51 (p<0.05)	0.79 ± 0.07	142
26	549.50 ± 37.13 (p<0.05)	2.53 ± 0.11 (p<0.001)	141
1	511.53 ± 65.10	2.33 ± 0.50	131
Moxidectin	491.91 ± 25.36	0.52 ± 0.06 (p<0.001)	127
Eprinomectin	472.634 ± 27.86	1.36 ± 0.22	121
Milbemectin	448.38 ± 48.22	0.82 ± 0.10	115
8	424.54 ± 89.50	1.00 ± 0.19	109
Selamectin	423.29 ± 28.08	0.89 ± 0.12	108
27	409.73 ± 34.03	0.65 ± 0.06	105
Ivermectin B1a	391.06 ± 40.37	1.04 ± 0.12	100
14	390.67 ± 23.80	2.79 ± 1.43	100
22	390.05 ± 30.21	2.72 ± 0.29 (p<0.001)	100
Ivermectin B1b	356.19 ± 51.52	0.93 ± 0.10	91
2	354.65 ± 44.23	1.15 ± 0.16	91
4	337.40 ± 8.66	0.90 ± 0.02	86
24	321.94 ± 52.22	1.89 ± 0.59	82
10	285.85 ± 22.69	1.01 ± 0.26	73
13	269.46 ± 20.84	2.34 ± 0.34 (p<0.01)	69
20	252.50 ± 10.11	1.99 ± 0.52	65
11	203.42 ± 22.69 (p<0.05)	1.01 ± 0.51	52
6	192.38 ± 18.66 (p<0.05)	0.71 ± 0.15	49
16	170.97 ± 3.60 (p<0.01)	n.d.	44
12	158.28 ± 16.00 (p<0.01)	4.24 ± 0.75 (p<0.05)	40
9	136.88 ± 11.39 (p<0.01)	n.d.	35
23	136.29 ± 0.60 (p<0.01)	n.d.	35
17	131.79 ± 18.63 (p<0.01)	n.d.	34
21	126.39 ± 13.54 (p<0.01)	n.d.	33
5	121.14 ± 5.63 (p<0.01)	n.d.	31
18	118.35 ± 7.91 (p<0.001)	n.d.	30
15	115.74 ± 11.10 (p<0.01)	n.d.	30
7	111.34 ± 14.42 (p<0.01)	n.d.	28
3	109.67 ± 9.88 (p<0.001)	n.d.	28

n.d. = not determined.

α = Efficacy compared to submaximal ATP response (% of 0.3 μM ATP response). P-value is the statistical comparison between efficacy (E_{max}) of respected compound and IVM-B1a.

β = p-value is the statistical comparison between potency (EC_{50}) of respected compound and IVM-B1a.

Table 3.3. Summary of the effects of IVM-B1a (orange) and its analogues on the P2X4 response, ranked in terms of potency (EC_{50}). The EC_{50} values and E_{max} values were calculated from individual concentration-response curves. Data is presented as mean ± SEM (n=3-8).

Compound	Potency (EC_{50}) (μM) (p-value) β	Efficacy (Maximum Ca^{2+} Response/E_{max}) (%) (p-value) α	Percentage IVM-B1a response
Doramectin	0.40 ± 0.03 (p<0.01)	641.01 ± 32.34 (p<0.01)	164
Abamectin	0.44 ± 0.10 (p<0.01)	967.47 ± 65.76 (p<0.001)	247
Moxidectin	0.52 ± 0.06 (p<0.001)	491.91 ± 25.36	127
27	0.65 ± 0.06	409.73 ± 34.03	105
Nemadectin	0.71 ± 0.07 (p<0.05)	803.40 ± 103.47 (p<0.01)	205
6	0.71 ± 0.15	192.38 ± 18.66 (p<0.05)	49
Ivermectin	0.79 ± 0.07	555.90 ± 45.51 (p<0.05)	142
Milbemectin	0.82 ± 0.10	448.38 ± 48.22	115
Selamectin	0.89 ± 0.12	423.29 ± 28.08	108
4	0.90 ± 0.02	337.40 ± 8.66	86
Ivermectin B1b	0.93 ± 0.10	356.19 ± 51.52	91
8	1.00 ± 0.19	424.54 ± 89.50	109
10	1.01 ± 0.26	285.85 ± 22.69	73
Ivermectin B1a	1.01 ± 0.51	391.06 ± 40.37	100
11	1.10 ± 0.51	203.42 ± 22.69 (p<0.05)	52
2	1.15 ± 0.16	354.65 ± 44.23	91
19	1.24 ± 0.09	578.92 ± 66.85 (p<0.05)	148
Eprinomectin	1.36 ± 0.22	472.634 ± 27.86	121
24	1.89 ± 0.59	321.94 ± 52.22	82
14	1.97 ± 0.60	390.67 ± 23.80	100
20	1.99 ± 0.52	252.50 ± 10.11	65
1	2.33 ± 0.50	511.53 ± 65.10	131
13	2.34 ± 0.34 (p<0.01)	269.46 ± 20.84	69
26	2.53 ± 0.11 (p<0.001)	549.50 ± 37.13 (p<0.05)	141
22	2.72 ± 0.29 (p<0.001)	390.05 ± 30.21	100
25	3.62 ± 0.37 (p<0.001)	642.62 ± 25.87 (p<0.01)	164
12	4.24 ± 0.75 (p<0.05)	158.28 ± 16.00 (p<0.01)	40
5	n.d.	121.14 ± 5.63 (p<0.01)	31
16	n.d.	170.97 ± 3.60 (p<0.01)	44
3	n.d.	109.67 ± 9.88 (p<0.001)	28
7	n.d.	111.34 ± 14.42 (p<0.01)	28
9	n.d.	136.88 ± 11.39 (p<0.01)	35
15	n.d.	115.74 ± 11.10 (p<0.01)	30
17	n.d.	131.79 ± 18.63 (p<0.01)	34
18	n.d.	118.35 ± 7.91 (p<0.001)	30
21	n.d.	126.39 ± 13.54 (p<0.01)	33
23	n.d.	136.29 ± 0.60 (p<0.01)	35

n.d. = not determined.

α = Efficacy compared to submaximal ATP response (% of 0.3 μM ATP response). P-value is the statistical comparison between efficacy (E_{max}) of respected compound and IVM-B1a.

β = p-value is the statistical comparison between potency (EC_{50}) of respected compound and IVM-B1a.

3.3.3.3 Structural modifications at R1 (Disaccharide)

Firstly, to investigate the effects of structural substitutions at the R1 region (disaccharide group), a group of four IVM-analogues was explored. Milbemectin (MBM), a commercial analogue, was one of the first to be tested. MBM is a class of milbemycin and is a mixture of two homologues: milbemycin A3 (30%) and milbemycin A4 (70%) (Figure 3.9A). MBM is identical to the reference compound IVM-B1a, except it lacks the disaccharide region (R1). Figure 3.9C presents the concentration-response curve of MBM compared to IVM-B1a, and Figure 3.9D shows the representative trace of Ca^{2+} elicited by each compound at maximum concentration. At submaximal ATP (0.3 µM), MBM (3 µM) was able to significantly potentiate the ATP-evoked Ca^{2+} response ($p<0.001$). The calculated EC_{50} and E_{max} for MBM (3 µM) was 0.82 ± 0.10 µM and 448.38 ± 48.22%, respectively (n=8). Overall, MBM is well tolerated and demonstrated similar effects on the ATP-evoked Ca^{2+} response as IVM-B1a, with no significant change in efficacy or potency ($p>0.05$). At high concentrations of MBM (≥5 µM), the cell loading values were significantly higher than cells pre-incubated with control buffer ($p<0.001$). These fluorescent measurements were taken by the FlexStaton-3 reader after a 30-minute incubation with either compound or buffer only, and before ATP-stimulation. This suggests that MBM may be affecting resting intracellular Ca^{2+} levels prior to ATP stimulation at high concentrations.

Figure 3.10C shows the concentration-response curve for compound **2**. This compound has a monosodium phosphate group addition to the disaccharide region (R1; C4") (Figure 3.10A). Compound **2** (5 µM) potentiated the ATP-evoked Ca^{2+} response ($p<0.01$) in a concentration-dependent manner to 354.65 ± 44.23% of vehicle control and has an EC_{50} value of 1.15 ± 0.16 µM (n=3), making it equally as efficacious and potent as IVM-B1a ($p>0.05$). The representative time-response trace (Figure 3.10D) illustrates an equally efficacious peak in intracellular Ca^{2+} level following application of ATP at approximately 50 seconds for both compound **2** (5 µM) and IVM-B1a (10 µM), which is then followed by a drop in response. The rate of decline appears faster for compound 2, which drops back to baseline level within 250 seconds, as opposed to IVM-B1a, which is still in the steady decline phase. In addition, at high concentrations (≥3 µM), the loading values for the cells exposed to compound **2** were significantly higher than those incubated with control buffer alone ($p<0.05$).

Compound **11** has a similar structural modification to the sugar moiety (R1), with the addition of a methyl phosphate group to carbon 4" (Figure 3.11A). The calculated EC_{50} value was 1.15 ± 0.16 µM (n=3), making it equally potent to IVM-B1a ($p>0.05$; Table 3.3). At maximal concentration, compound **11** (3 µM) could significantly potentiate the ATP-evoked Ca^{2+} response ($p<0.01$) but only to 52% of the IVM-B1a response (203.42 ± 22.69% vs. 391.06 ± 40.37%, respectively; n=3-6; $p<0.05$; Figure 3.11C). At high concentrations (≥5 µM) of compound **11**, the loading values for the cells were significantly higher than those incubated with control buffer alone ($p<0.05$).

Lastly, Figure 3.12C shows the concentration-response curve and representative trace of ATP-evoked Ca^{2+} response at maximal concentration for compound **26**. Compound **26** is structurally identical to IVM-B1a, except it has a succinic acid addition to the end of the disaccharide region (R1; C4") (Figure

3.12A). The highest potentiation was recorded at 5 µM at 549.50 ± 37.13% of vehicle control response (n=3, $p<0.001$) and was significantly higher than the reference compound at 141% of IVM-B1a response ($p<0.05$). The calculated EC_{50} value was 2.53 ± 0.11 µM (n=3), making compound **26** significantly less potent than IVM-B1a ($p<0.001$).

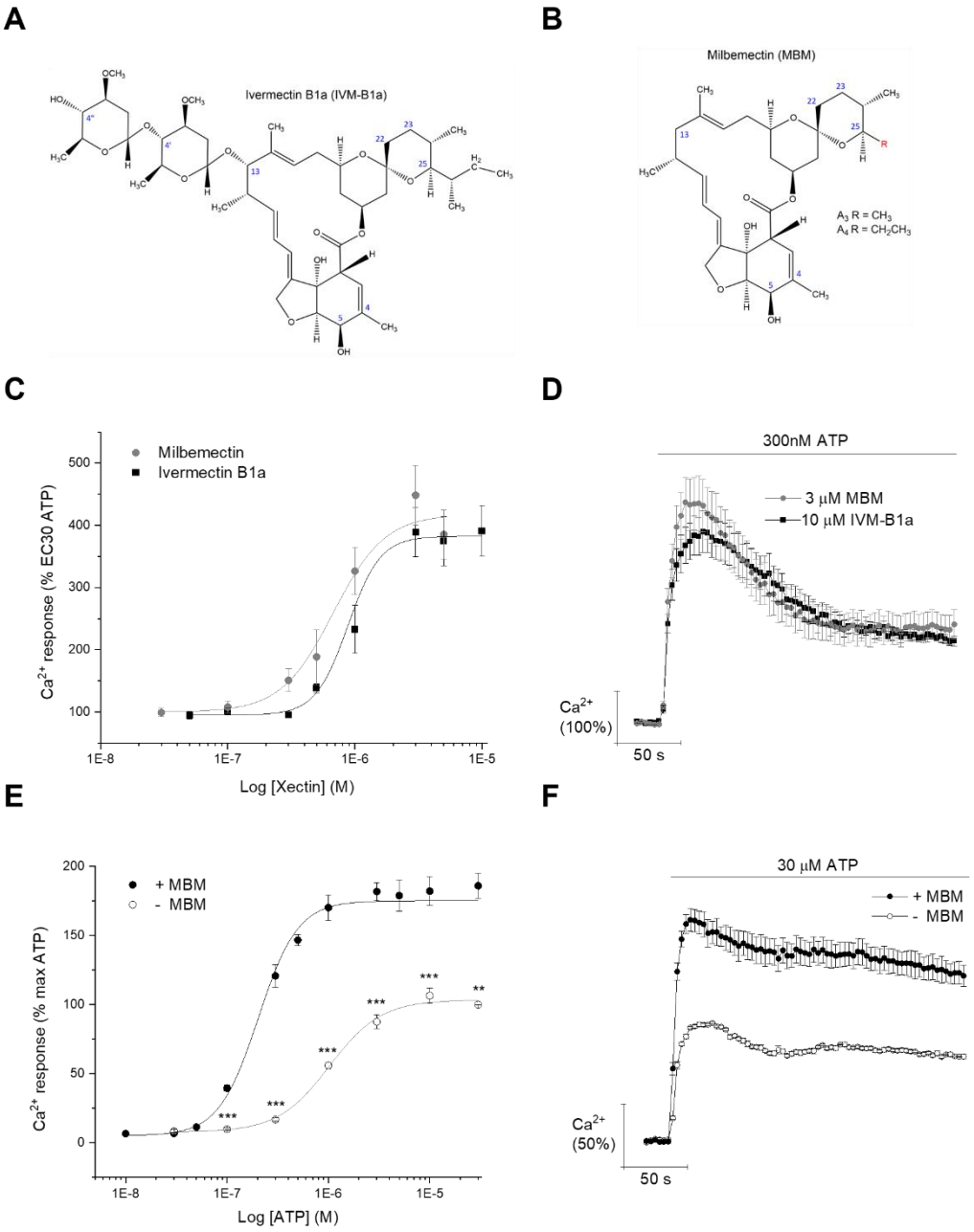

Figure 3.9. Effects of milbemectin (MBM) on the human P2X4 receptor response in 1321N1 cells. (A and B) Comparison of the chemical structure of IVM-B1a (left) and MBM (right). Structural differences are highlighted in red. Blue numbers represent the C-positions. (C and D) Concentration-response curve of MBM (0.03 – 5 µM; grey circles; n=8) compared to IVM-B1a (0.05 – 10 µM; black squares; n=6) when the cells are stimulated with a submaximal ATP concentration (0.3 µM) and representative Ca^{2+} time-response trace of MBM and IVM-B1a at maximal concentrations, respectively. Data is normalised to peak control response (0.3 µM ATP) and represented as percentage of control response. (E and F) ATP concentration-response curve (0.01 – 30 µM) in the presence (closed circles) and absence (open circles) of 3 µM MBM and representative Ca^{2+} time-response trace elicited by maximal

ATP (30 µM) in the presence and absence of 3 µM MBM, respectively. Data is normalised to 30 µM ATP in the absence of MBM (n=5). Asterisks show significant differences between equivalent ATP concentrations in the presence verses the absence of MBM (*$p<0.05$, **$p<0.01$, ***$p<0.001$). All data points represent the mean ± SEM.

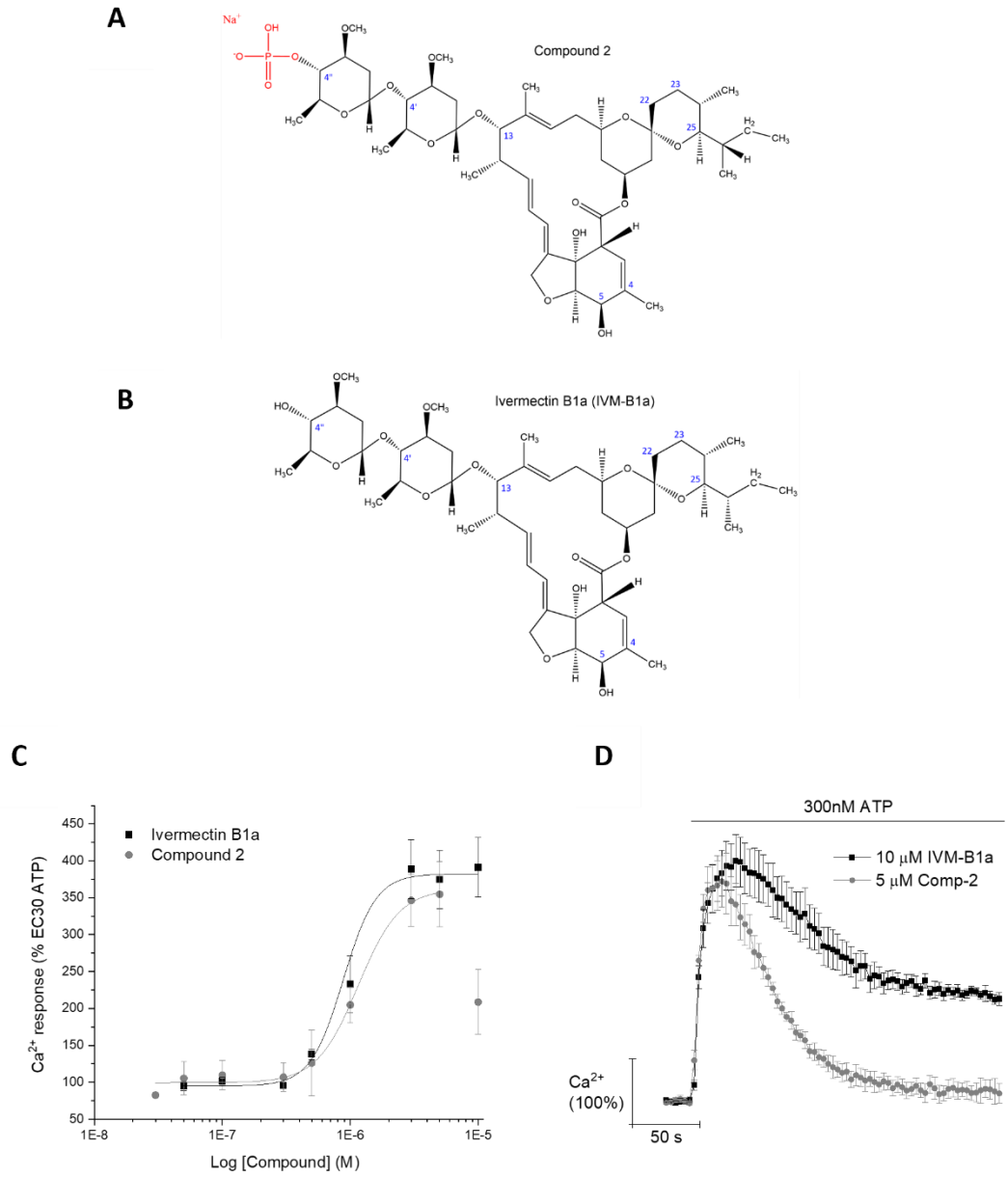

Figure 3.10. Effects of compound 2 on the human P2X4 receptor response in 1321N1 cells. (A and B) Comparison of the chemical structure of compound 2 (top) and IVM-B1a (bottom). Structural differences are highlighted in red. Blue numbers represent the C-positions. (C) Concentration-response curve of compound 2 (0.03 – 10 µM; grey circles; n=3) compared to IVM-B1a (0.05 – 10 µM; black squares; n=6) when the cells are stimulated with a submaximal EC_{30} ATP concentration (0.3 µM). (D) Representative Ca^{2+} time-response of compound 2 (n=3) and IVM-B1a (n=6) at maximal concentrations when stimulated with submaximal ATP (0.3 µM). Data is normalised to peak vehicle control response (0.3 µM ATP) and represented as percentage of vehicle control response. All data points represent the mean ± SEM.

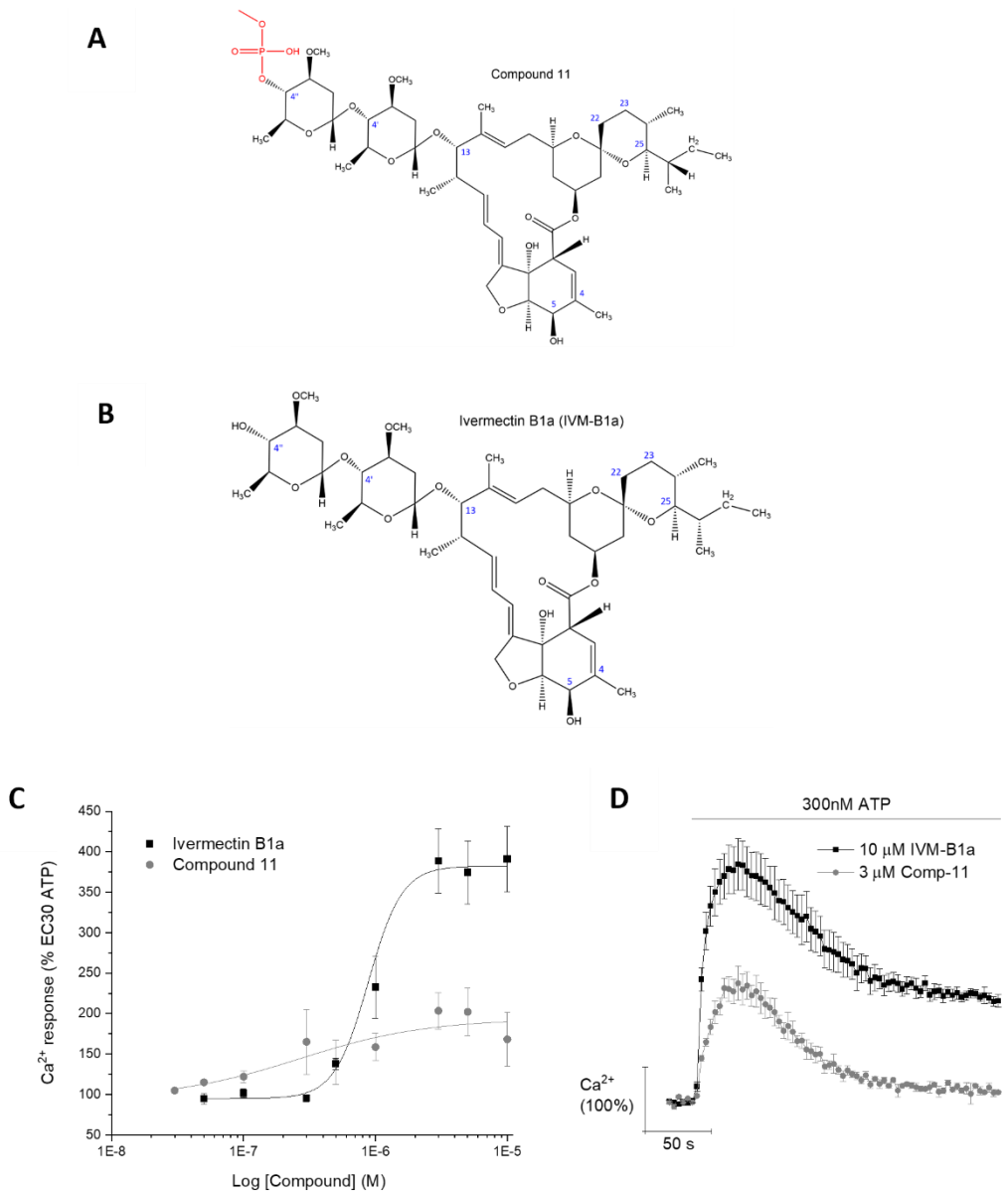

Figure 3.11. Effects of compound 11 on the human P2X4 receptor response in 1321N1 cells. (A and B) Comparison of the chemical structure of compound 11 (top) and IVM-B1a (bottom). Structural differences are highlighted in red. Blue numbers represent the C-positions. (C) Concentration-response curve of compound 11 (0.03 – 10 µM; grey circles; n=3) compared to IVM-B1a (0.05 – 10 µM; black squares; n=6) when the cells are stimulated with a submaximal EC_{30} ATP concentration (0.3 µM). (D) Representative Ca^{2+} time-response of compound 11 (n=3) and IVM-B1a (n=6) at maximal concentrations when stimulated with submaximal ATP (0.3 µM). Data is normalised to peak vehicle control response (0.3 µM ATP) and represented as percentage of vehicle control response. All data points represent the mean ± SEM.

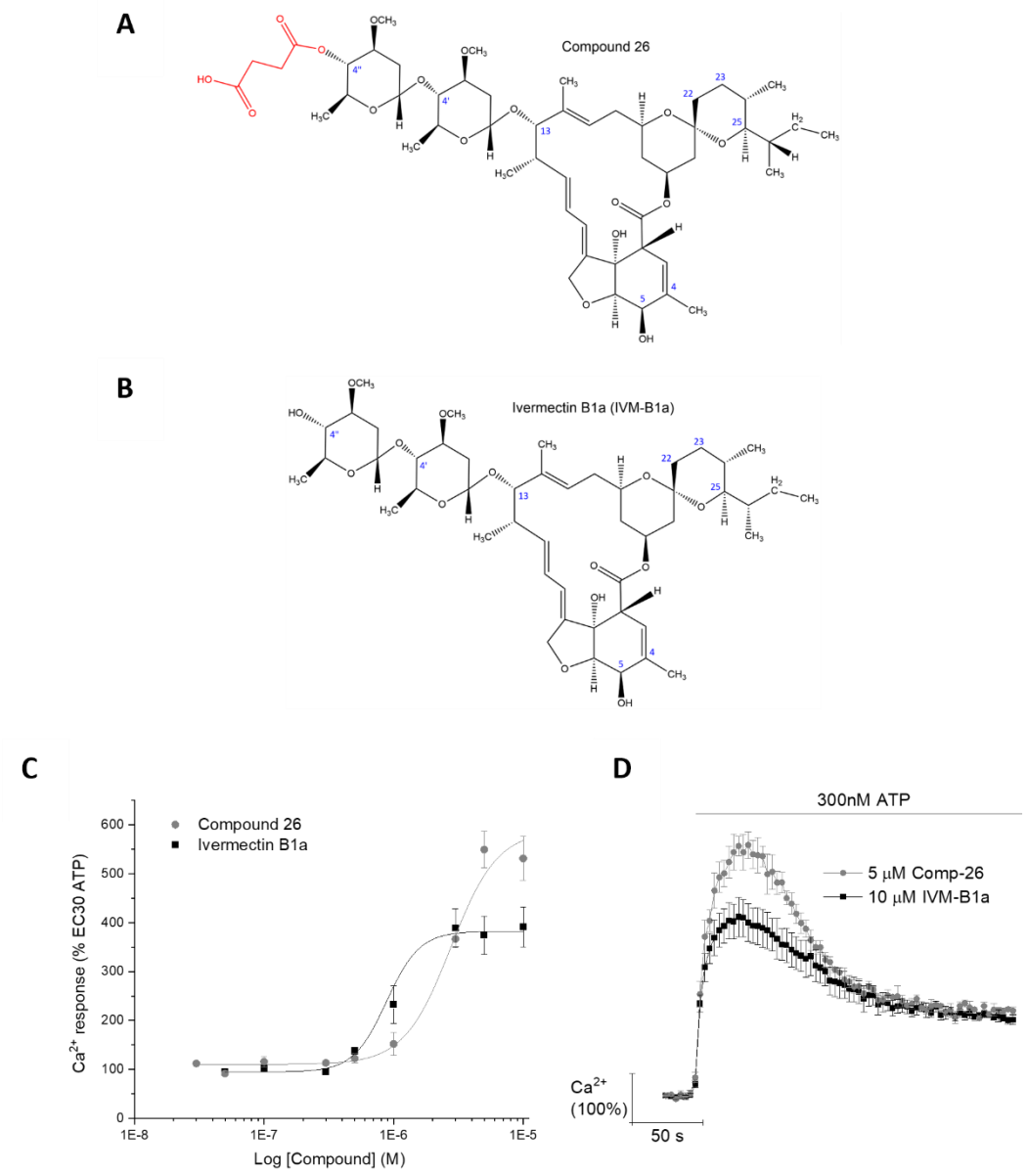

Figure 3.12. Effects of compound 26 on the human P2X4 receptor response in 1321N1 cells. (A and B) Comparison of the chemical structure of compound 26 (top) and IVM-B1a (bottom). Structural differences are highlighted in red. Blue numbers represent the C-positions. (C) Concentration-response curve of compound 26 (0.03 – 10 µM; grey circles; n=3) compared to IVM-B1a (0.05 – 10 µM; black squares; n=6) when the cells are stimulated with a submaximal EC_{30} ATP concentration (0.3 µM). (D) Representative Ca^{2+} time-response of compound 26 (n=3) and IVM-B1a (n=6) at maximal concentrations when stimulated with submaximal ATP (0.3 µM). Data is normalised to peak vehicle control response (0.3 µM ATP) and represented as percentage of vehicle control response. All data points represent the mean ± SEM.

3.3.3.4 Structural modifications at R2 (Spiroketal)

Next, to investigate the effects of structural modifications to the R2 region (spiroketal group), a series of thirteen IVM-analogues were explored. The first to be tested are the two commercial avermectins, abamectin (ABM) and doramectin (DRM). ABM shares a similar structure to IVM-B1a, the difference being the double bond in the C22-C23 position (Figure 3.13A). ABM is a mixture of two homologues, with the major component (B1a) compromising more than 80%. DRM is also closely related to IVM-B1a but has a cyclohexane group at the C25 position and, like ABM, a double bond in the C22-23 position (Figure 3.14A).

Figure 3.13 presents the concentration-response curve of ABM and IVM-B1a overlayed and representative ATP-evoked Ca^{2+} trace for both compounds at maximal concentration. At submaximal ATP (0.3 µM), ABM (10 µM) was able to potentiate the ATP-evoked Ca^{2+} response to 967.47 ± 65.76% (n=7; p<0.001). This is significantly higher than IVM-B1a, at 247% of the IVM-B1a response, making ABM significantly more efficacious than IVM-B1a at maximal concentration and the highest-ranking compound tested for efficacy overall (p<0.001; Table 3.2). ABM was also significantly more potent than IVM-B1a, with a calculated EC_{50} value of 0.44 ± 0.10 µM (n=7), compared to 1.01 ± 0.51 µM (n=6), respectively (p<0.01). Similarly, DRM could potentiate the ATP-evoked Ca^{2+} response in a concentration-dependent manner, with maximum potentiation recorded at 1 µM at 641.01 ± 32.34% (n=5; p<0.01; Figure 13.14C). As illustrated in the time-response trace (Figure 3.14D), DRM is significantly more efficacious than IVM-B1a, reaching 164 % of the IVM-B1a response at the maximum concentration (p<0.01). However, the response begins to drop off at higher concentrations (3, 5, and 10 µM), as opposed to IVM-B1a, which plateaus out. Likewise, the EC_{50} for DRM was calculated to be 0.44 ± 0.03 µM (n=5); making it significantly more potent than IVM-B1a and the highest-ranking compound for potency (p<0.01; Table 3.3).

Two of the compounds investigated, compound **13** (Figure 3.15A) and **19** (Figure 3.16A), are stereoisomers of each other, in that they have the same molecular formula and connectivity but differ in their spatial arrangement (bond directions). They could also be stereoisomers of IVM-B1a, although this is impossible to say without knowing the true stereochemistry of IVM-B1a. Between compounds **13** and **19**, one chiral centre is experiencing an enantiomeric change in the ethyl group in the side chain of C25. This enantiomeric change leads to two largely different effects on ATP-evoked Ca^{2+} response in the cell. Firstly, both compounds could potentiate the response in a concentration-dependent manner, with maximum potentiation observed at 5 µM for compound **13** (269.46 ± 20.84 %; n=4; p<0.05; Figure 3.15C); and at 3 µM for compound **19** (578.92 ± 66.85%; n=3; p<0.001; Figure 3.16C). However, compound **19** was significantly more efficacious than IVM-B1a (p<0.05), reaching 148% of the IVM-B1a response, while compound **13** was not significantly different from IVM-B1a (p>0.05). In terms of potency, compound **19** was close in ranking to IVM-B1a with an EC_{50} of 1.24 ± 0.09 µM (n=3; p<0.05), while for compound **13**, there was a significant loss in potency compared to IVM-B1a (2.34 ± 0.34 µM vs. 1.01 ± 0.51 µM, respectively; n=4-6, p<0.01). In addition, at the highest

concentration tested (10 µM), the loading values for the cells exposed to compound **13** were significantly higher than those incubated with control buffer ($p<0.01$).

Compound **14** has the same structure as the minor component of IVM (IVM-B1b), which has a methyl group (CH_3) attached to the C25 side chain (Figure 3.17A). The highest potentiation was recorded at 5 µM at 390.67 ± 23.80%of vehicle control response ($n=3$; $p<0.05$), and the calculated EC_{50} value was 1.97 ± 0.60 µM ($n=3$). In comparison to IVM-B1a, compound **14** did not differ significantly in terms of potency or efficacy ($p>0.05$, Figure 17C), and neither was it significantly different from IVM-B1b in either ranking ($p>0.05$; Table 3.2 and 3.3).

The following eight compounds investigated all have structural modifications at the C23 position in the spiroketal group. Three of them showed activity against the human P2X4 receptor, and the remaining five showed no activity (did not significantly potentiate the ATP-evoked Ca^{2+} response), suggesting they do not act as modulators for the P2X4 receptor at the concentration range tested. Compound **1** (10 µM) was one of the three compounds that showed activity and has a methyl group and a hydroxyl group addition to the C23 position (Figure 3.18A). Compound **1** was able to potentiate the Ca^{2+} response to 511.53 ± 65.10% in cells stimulated with submaximal ATP (0.3µM) ($n=4$; $p<0.001$ Figure 3.18C). From the concentration-response curve, the EC_{50} value was calculated to be 2.33 ± 0.50 µM ($n=4$), making compound **1** less potent than IVM-B1a but not to a statistically significant extent ($p<0.05$). The shift in efficacy and potency was even more pronounced between IVM-B1a and compound **25**, which has a methyl ester group attached to the C23 position, as demonstrated in Figure 3.19A. In the presence of submaximal ATP (0.3 µM), compound **25** potentiates the Ca^{2+} response to 642.62 ± 25.87% ($n=3$; $p<0.01$; Figure 3.19C), a significant jump in efficacy at 164% of IVM-B1a response ($p<0.01$). Additionally, the calculated EC_{50} value was 3.62 ± 0.37 µM ($n=3$), making it significantly less potent than IVM-B1a ($p<0.001$). The last of the active compounds with modifications restricted to the spiroketal region is compound **12**, possessing an acetamide at the C23 position (Figure 3.20A) and having a relatively poor biological effect. At the highest concentration tested, compound **12** (10 µM) was able to potentiate the ATP-evoked Ca^{2+} response by 158.28 ± 16.00 ($p<0.05$) but suffered a significant reduction in maximal response in comparison to IVM-B1a (10 µM), at 40% of the IVM-B1a response ($p<0.01$; Figure 3.20C). Likewise, a shift in the concentration-response curve demonstrated a significant decrease in compound potency with a calculated EC_{50} of 4.24 ± 0.75 µM compared to IVM-B1a ($p<0.05$).

Finally, five of the investigated compounds had little or no effect on ATP-evoked Ca^{2+} response at the concentrations tested. The intolerable structural modifications included a carbonyl group (compound **3**; Figure 3.21A); two fluorine atoms (compound **16**; Figure 3.22A), and a hydroxyl group (compound **9**, **21** and **23**; Figure 3.23A; 3.24A and 3.25A, respectively) to the C23 position. The last three compounds (compound **9**, **21** and **23**) differ in stereochemistry. This is indicated by the different bond types within the disaccharide group (oxygen bridges) and within the spiroketal group at carbon 23 and the side chain of carbon 26.

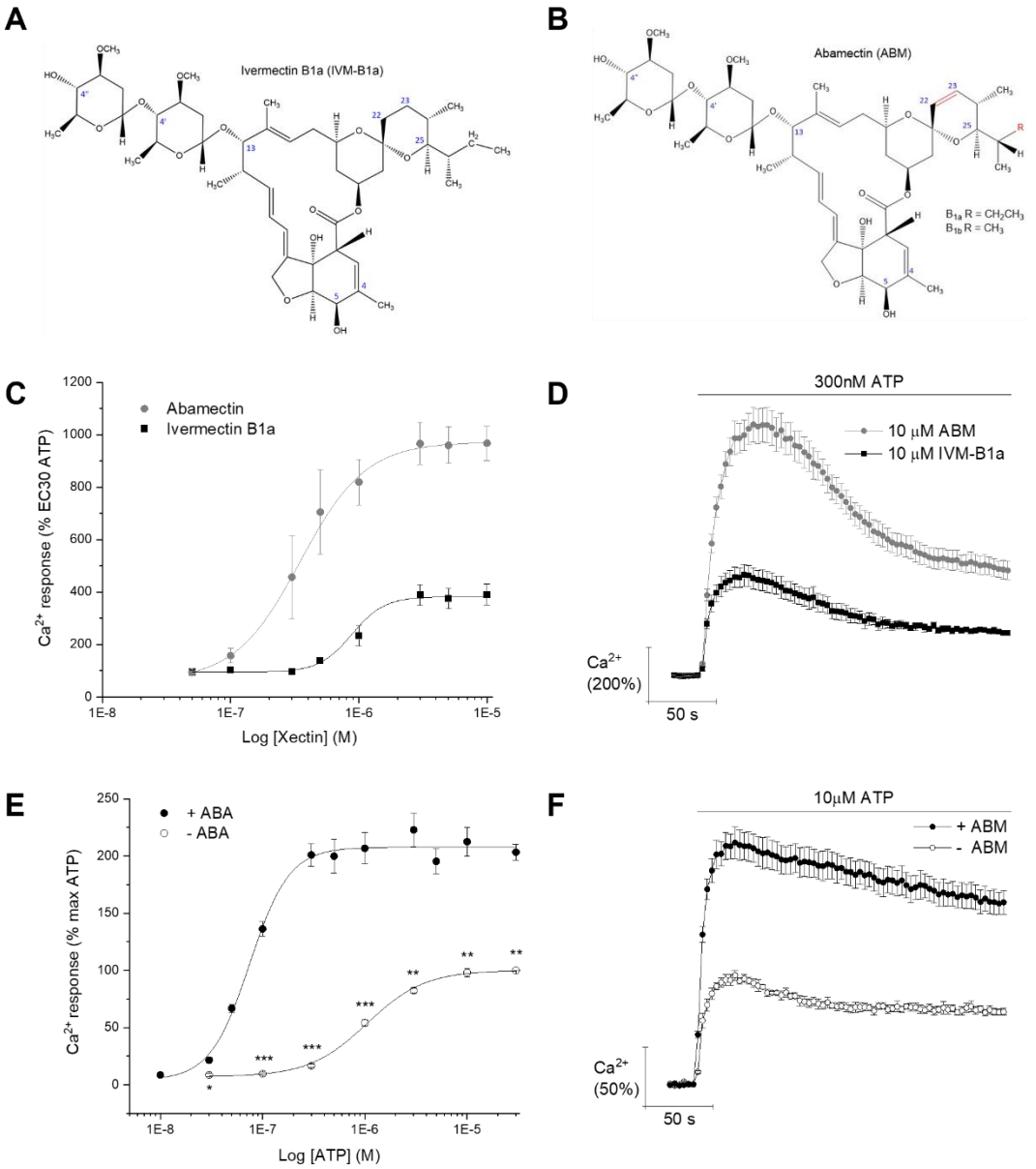

Figure 3.13. Effects of abamectin (ABM) on the human P2X4 receptor response in 1321N1 cells. (A and B) Comparison of the chemical structure of IVM-B1a (left) and ABM (right). Structural differences are highlighted in red. Blue numbers represent the C-positions. (C and D) Concentration-response curve of ABM (0.03 – 10 µM; grey circles; n=7) compared to IVM-B1a (0.05 – 10 µM; black squares; n=6) when the cells are stimulated with submaximal EC_{30} ATP (0.3 µM) and representative Ca^{2+} time-response trace of ABM (10 µM) and IVM-B1a (10 µM) at maximal concentrations, respectively. Data is normalised to peak vehicle control response (0.3 µM ATP) and represented as percentage of vehicle control response. (E and F) ATP concentration-response curve (0.01 – 30 µM) in the presence (closed circles) and absence (open circles) of 3 µM ABM and representative Ca^{2+} time-response trace elicited by maximal ATP (10 µM) in the presence and absence of 3 µM ABM, respectively. Data is normalised to 30 µM ATP in the absence of ABM (n=6). Asterisks show significant differences between equivalent

ATP concentrations in the presence verses the absence of ABM (*p<0.05, **p<0.01, ***p<0.001). All data points represent the mean ± SEM.

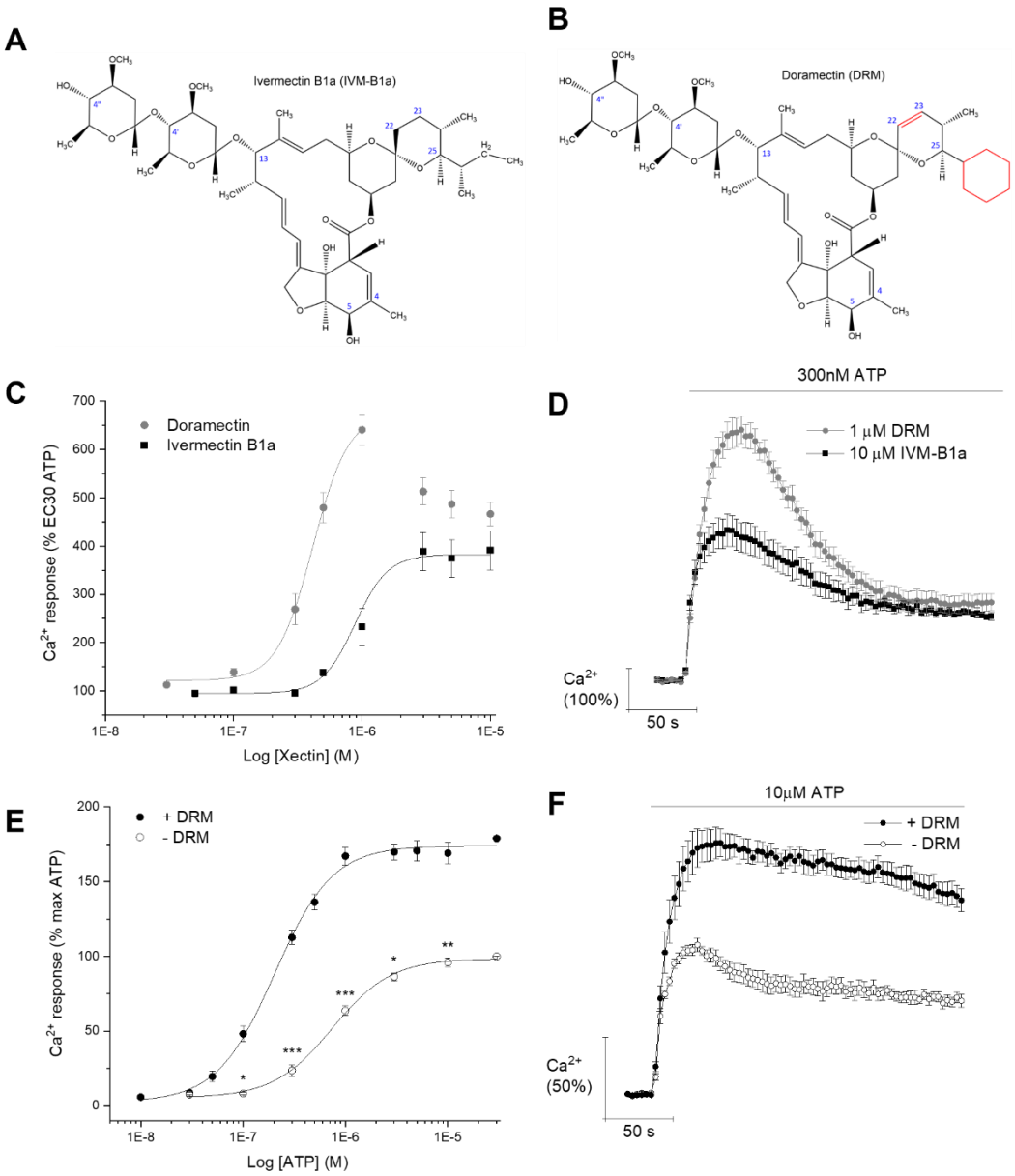

Figure 3.14. Effects of doramectin (DRM) on the human P2X4 receptor response in 1321N1 cells. (A and B) Comparison of the chemical structure of IVM-B1a (left) and DRM (right). Structural differences are highlighted in red. Blue numbers represent the C-positions. (C and D) Concentration-response curve of DRM (0.03 – 10 µM; grey circles; n=5) compared to IVM-B1a (0.05 – 10 µM; black squares; n=6) when the cells are stimulated with a submaximal EC_{30} ATP concentration (0.3 µM) and representative Ca^{2+} time-response trace of DRM (1 µM) and IVM-B1a (10 µM) at maximal concentrations, respectively. Data is normalised to peak vehicle control response (0.3 µM ATP) and represented as percentage of vehicle control response. (E and F) ATP concentration-response curve (0.01 – 30 µM) in the presence (closed circles) and absence (open circles) of 1 µM DRM and representative Ca^{2+} time-response trace elicited by maximal ATP (10 µM) in the presence and absence of 1 µM DRM, respectively. Data is normalised to 30 µM ATP in the absence of DRM (n=5). Asterisks

show significant differences between equivalent ATP concentrations in the presence verses the absence of DRM (*p<0.05, **p<0.01, ***p<0.001). All data points represent the mean ± SEM.

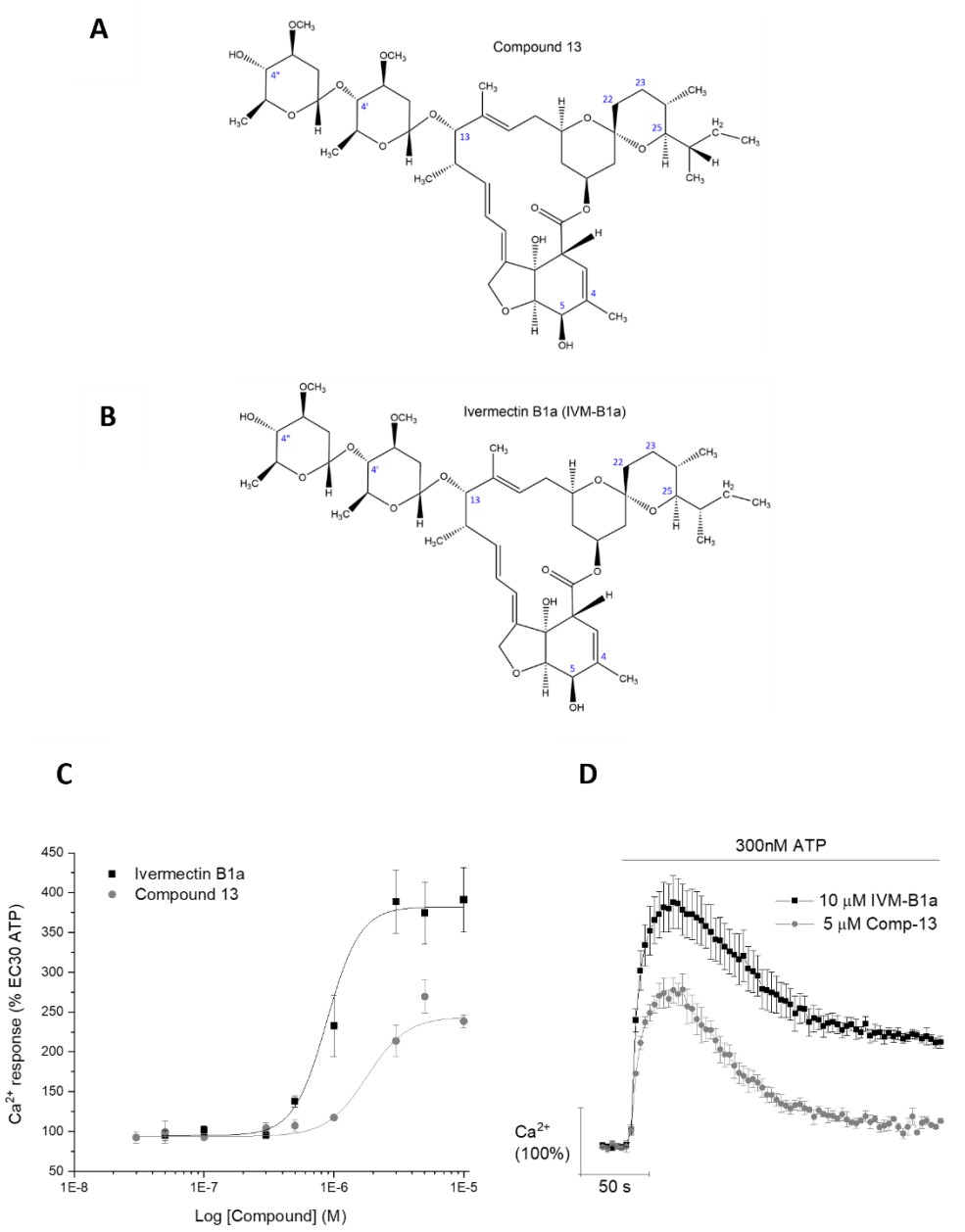

Figure 3.15. Effects of compound 13 on the human P2X4 receptor response in 1321N1 cells. (A and B) Comparison of the chemical structure of compound 13 (top) and IVM-B1a (bottom). Blue numbers represent the C-positions. (C) Concentration-response curve of compound 13 (0.03 – 10 µM; grey circles; n=4) compared to IVM-B1a (0.05 – 10 µM; black squares; n=6) when the cells are stimulated with a submaximal EC_{30} ATP concentration (0.3 µM). (D) Representative Ca^{2+} time-response of compound 13 (n=4) and IVM-B1a (n=6) at maximal concentrations when stimulated with submaximal ATP (0.3 µM). Data is normalised to peak vehicle control response (0.3 µM ATP) and represented as percentage of vehicle control response. All data points represent the mean ± SEM.

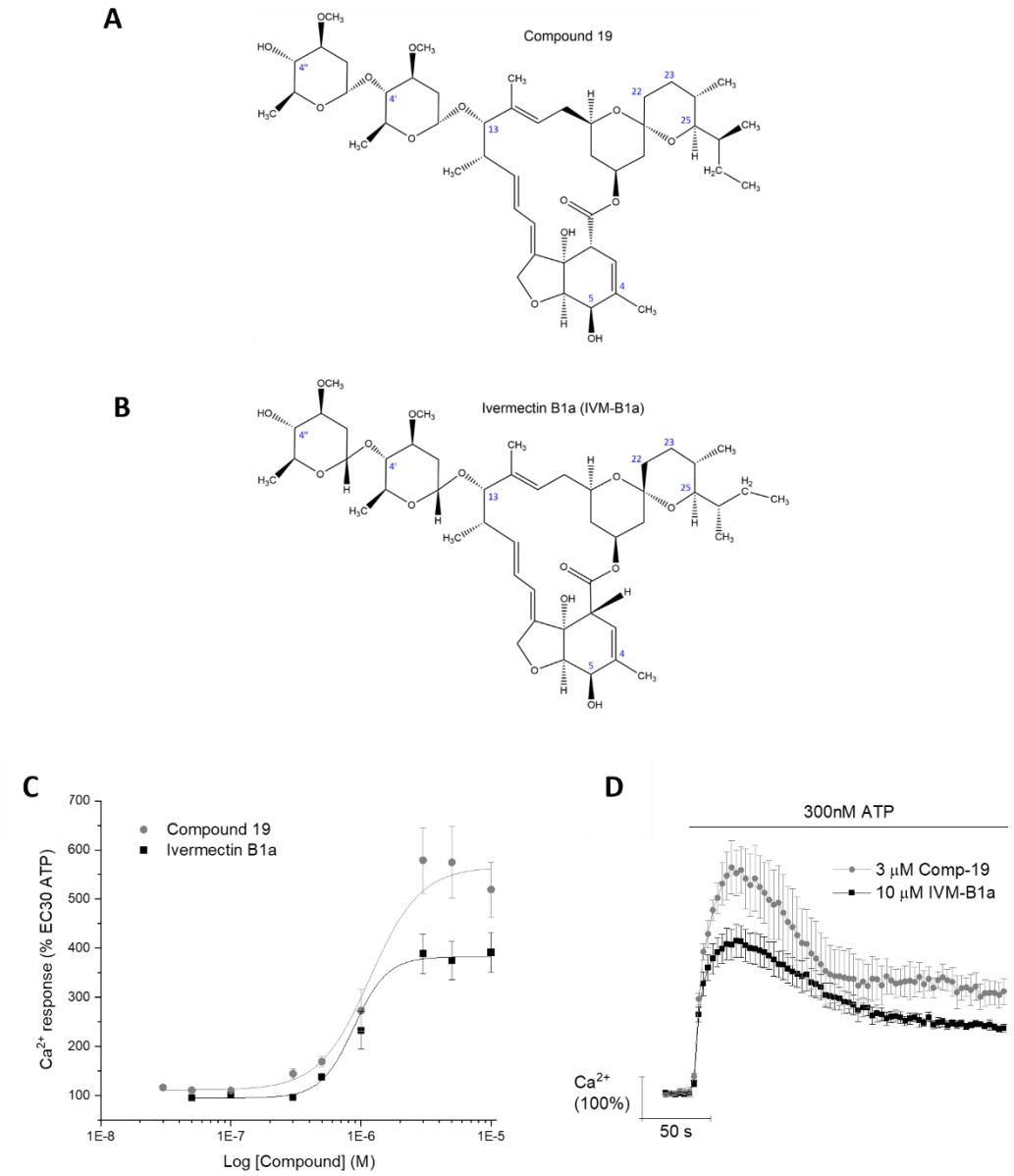

Figure 3.16. Effects of compound 19 on the human P2X4 receptor response in 1321N1 cells. (A and B) Comparison of the chemical structure of compound 19 (top) and IVM-B1a (bottom). Blue numbers represent the C-positions. (C) Concentration-response curve of compound 19 (0.03 – 10 µM; grey circles; n=3) compared to IVM-B1a (0.05 – 10 µM; black squares; n=6) when the cells are stimulated with a submaximal EC_{30} ATP concentration (0.3 µM). (D) Representative Ca^{2+} time-response of compound 19 (n=3) and IVM-B1a (n=6) at maximal concentrations when stimulated with submaximal ATP (0.3 µM). Data is normalised to peak vehicle control response (0.3 µM ATP) and represented as percentage of vehicle control response. All data points represent the mean ± SEM.

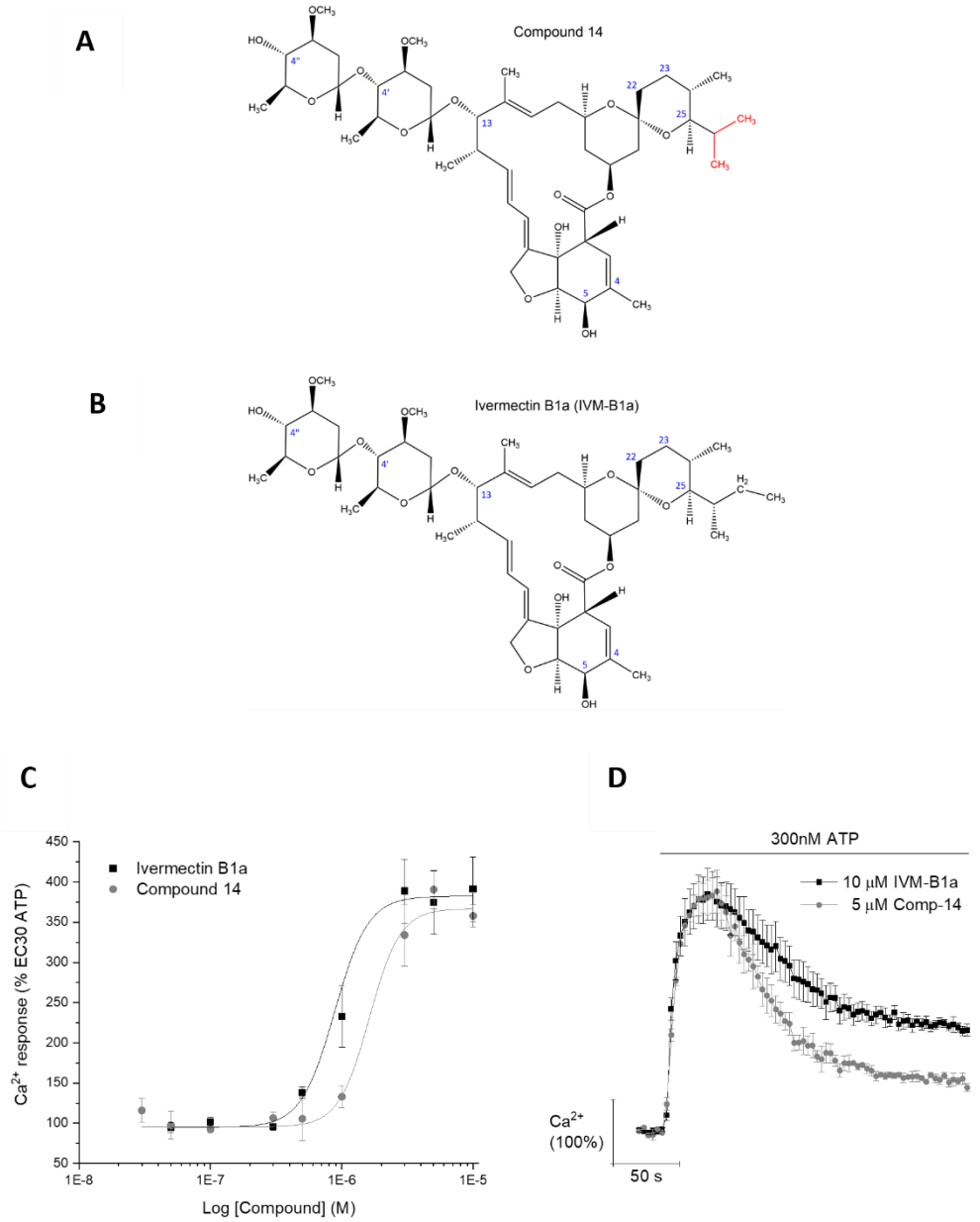

Figure 3.17. Effects of compound 14 on the human P2X4 receptor response in 1321N1 cells. (A and B) Comparison of the chemical structure of compound 14 (top) and IVM-B1a (bottom). Structural differences are highlighted in red. Blue numbers represent the C-positions. (C) Concentration-response curve of compound 14 (0.03 – 10 µM; grey circles; n=4) compared to IVM-B1a (0.05 – 10 µM; black squares; n=6) when the cells are stimulated with a submaximal EC_{30} ATP concentration (0.3 µM). (D) Representative Ca^{2+} time-response of compound 14 (n=4) and IVM-B1a (n=6) at maximal concentrations when stimulated with submaximal ATP (0.3 µM). Data is normalised to peak vehicle control response (0.3 µM ATP) and represented as percentage of vehicle control response. All data points represent the mean ± SEM.

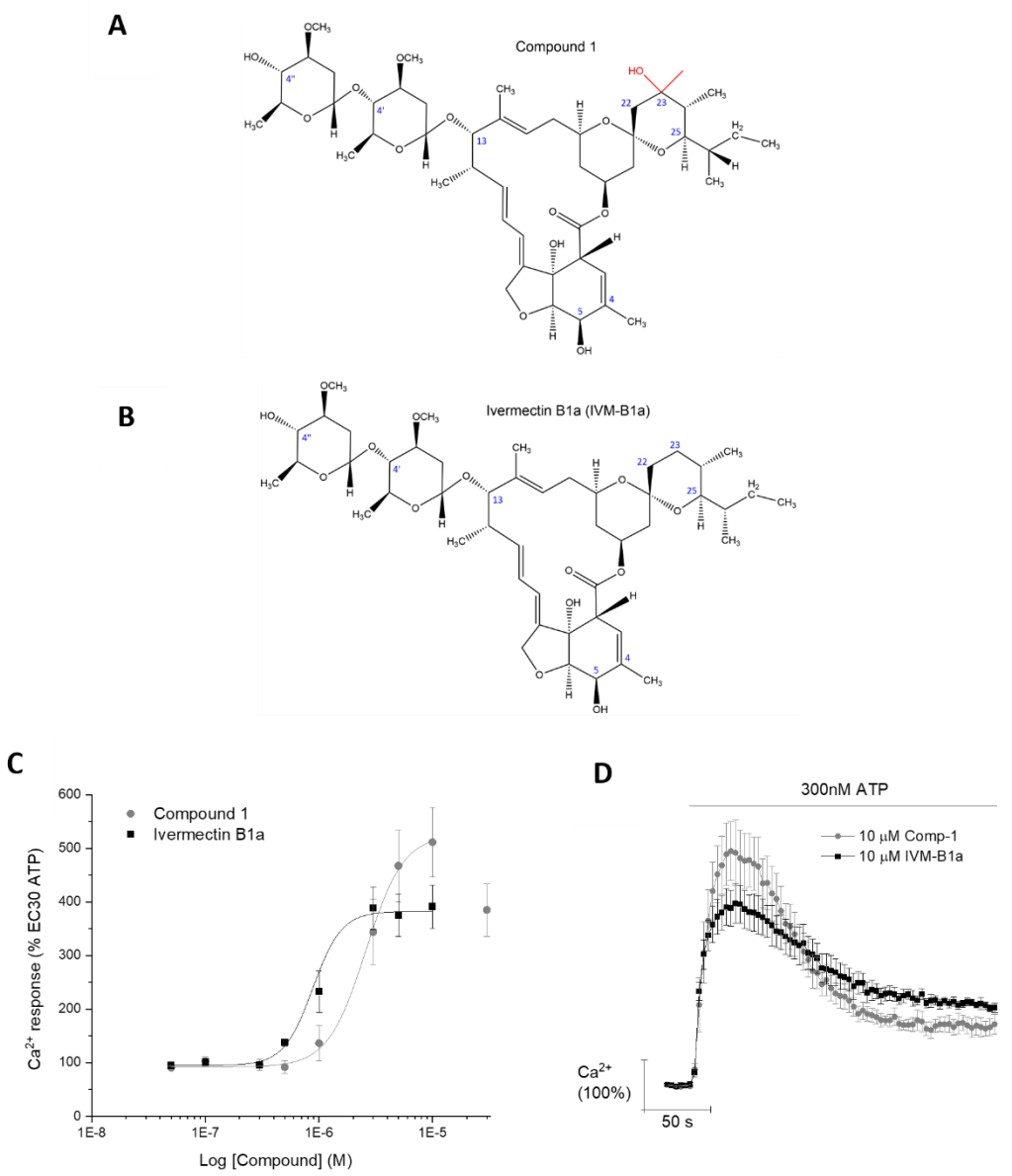

Figure 3.18. Effects of compound 1 on the human P2X4 receptor response in 1321N1 cells. (A and B) Comparison of the chemical structure of compound 1 (top) and IVM-B1a (bottom). Structural differences are highlighted in red. Blue numbers represent the C-positions. (C) Concentration-response curve of compound 1 (0.05 – 30 µM; grey circles; n=4) compared to IVM-B1a (0.05 – 10 µM; black squares; n=6) when the cells are stimulated with a submaximal EC_{30} ATP concentration (0.3 µM). (D) Representative Ca^{2+} time-response of compound 1 (n=4) and IVM-B1a (n=6) at maximal concentrations when stimulated with submaximal ATP (0.3 µM). Data is normalised to peak vehicle control response (0.3 µM ATP) and represented as percentage of vehicle control response. All data points represent the mean ± SEM.

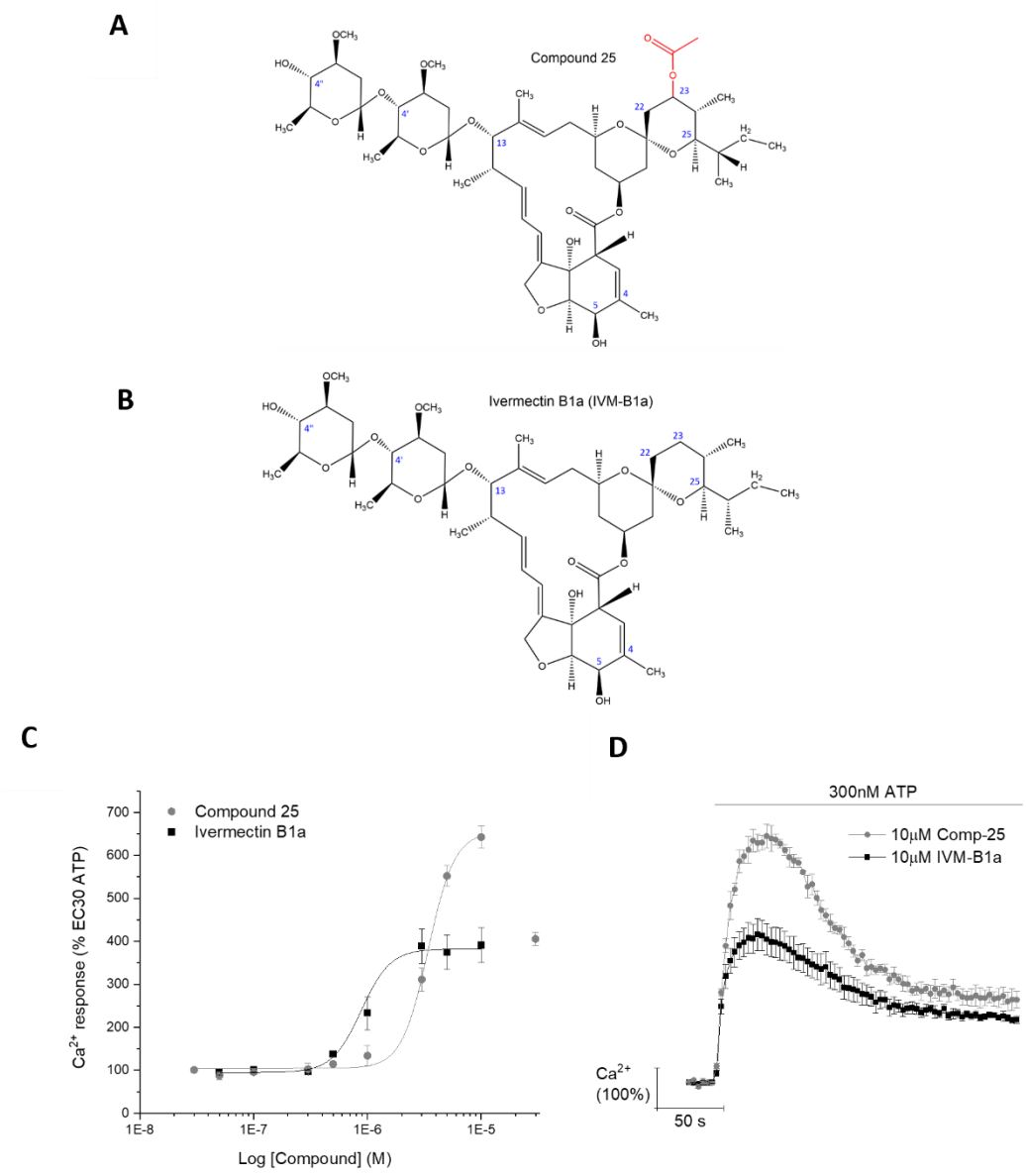

Figure 3.19. Effects of compound 25 on the human P2X4 receptor response in 1321N1 cells. (A and B) Comparison of the chemical structure of compound 25 (top) and IVM-B1a (bottom). Structural differences are highlighted in red. Blue numbers represent the C-positions. (C) Concentration-response curve of compound 25 (0.03 – 10 µM; grey circles; n=3) compared to IVM-B1a (0.05 – 10 µM; black squares; n=6) when the cells are stimulated with a submaximal EC_{30} ATP concentration (0.3 µM). (D) Representative Ca^{2+} time-response of compound 25 (n=3) and IVM-B1a (n=6) at maximal concentrations when stimulated with submaximal ATP (0.3 µM). Data is normalised to peak vehicle control response (0.3 µM ATP) and represented as percentage of vehicle control response. All data points represent the mean ± SEM.

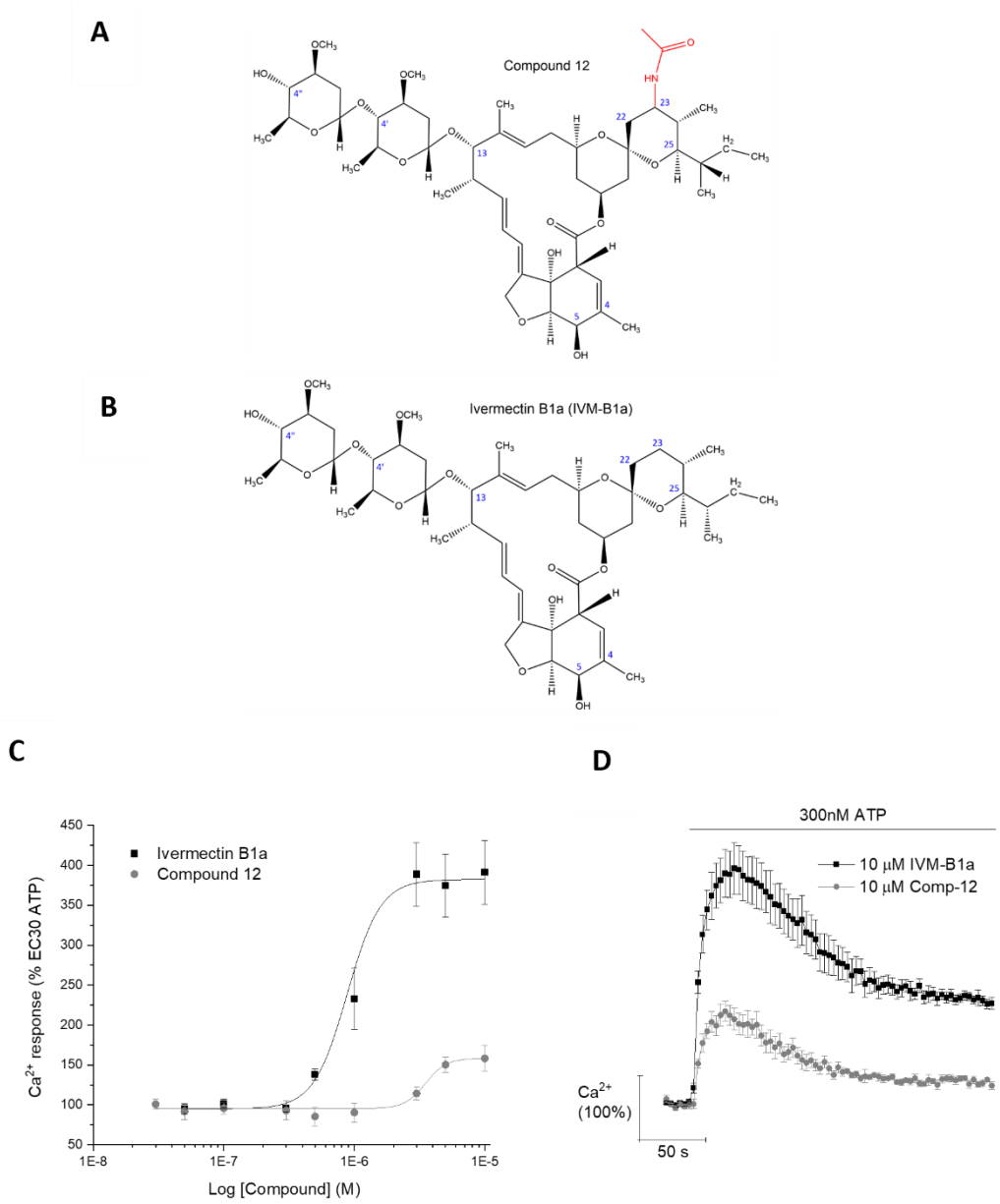

Figure 3.20. Effects of compound 12 on the human P2X4 receptor response in 1321N1 cells. (A and B) Comparison of the chemical structure of compound 12 (top) and IVM-B1a (bottom). Structural differences are highlighted in red. Blue numbers represent the C-positions. (C) Concentration-response curve of compound 12 (0.03 – 10 µM; grey circles; n=4) compared to IVM-B1a (0.05 – 10 µM; black squares; n=6) when the cells are stimulated with a submaximal EC_{30} ATP concentration (0.3 µM). (D) Representative Ca^{2+} time-response of compound 12 (n=4) and IVM-B1a (n=6) at maximal concentrations when stimulated with submaximal ATP (0.3 µM). Data is normalised to peak vehicle control response (0.3 µM ATP) and represented as percentage of vehicle control response. All data points represent the mean ± SEM.

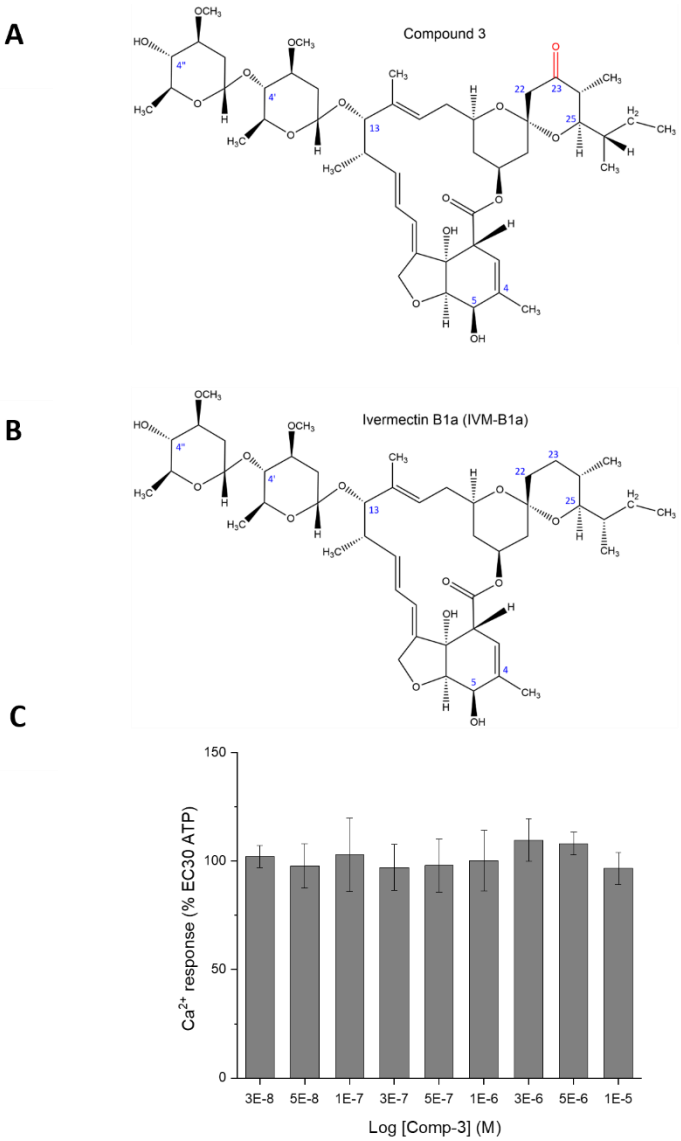

Figure 3.21. Effects of compound 3 on the human P2X4 receptor response in 1321N1 cells. (A and B) Comparison of the chemical structure of compound 3 (top) and IVM-B1a (bottom). Structural differences are highlighted in red. Blue numbers represent the C-positions. (C) Each bar chart illiterates the degree of Ca^{2+} response when the cells are treated with varying concentrations of compound 3 (0.03 – 10 µM) and stimulated with submaximal EC_{30} ATP (0.3 µM). Data is normalised to peak vehicle control response (0.3 µM ATP) and represented as percentage of vehicle control response (n=4). All data points represent the mean ± SEM.

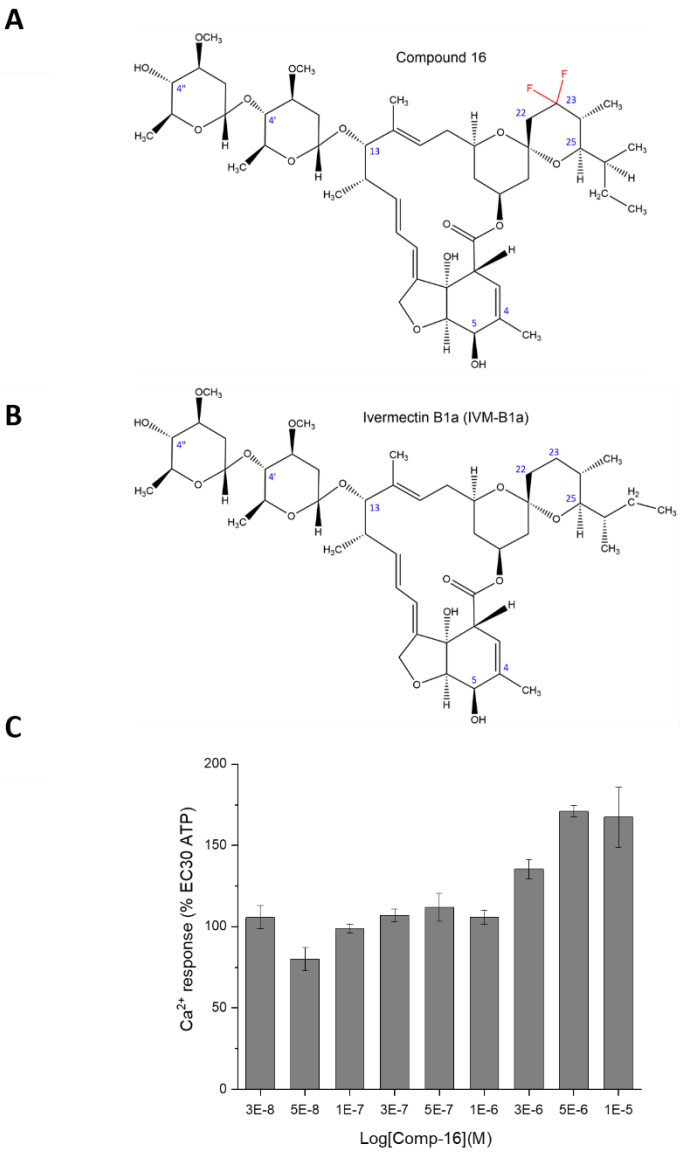

Figure 3.22. Effects of compound 16 on the human P2X4 receptor response in 1321N1 cells. (A and B) Comparison of the chemical structure of compound 16 (top) and IVM-B1a (bottom). Structural differences are highlighted in red. Blue numbers represent the C-positions. (C) Each bar chart illiterates the degree of Ca^{2+} response when the cells are treated with varying concentrations of compound 16 (0.03 – 10 µM) and stimulated with submaximal EC_{30} ATP (0.3 µM). Data is normalised to peak vehicle control response (0.3 µM ATP) and represented as percentage of vehicle control response (n=4). All data points represent the mean ± SEM.

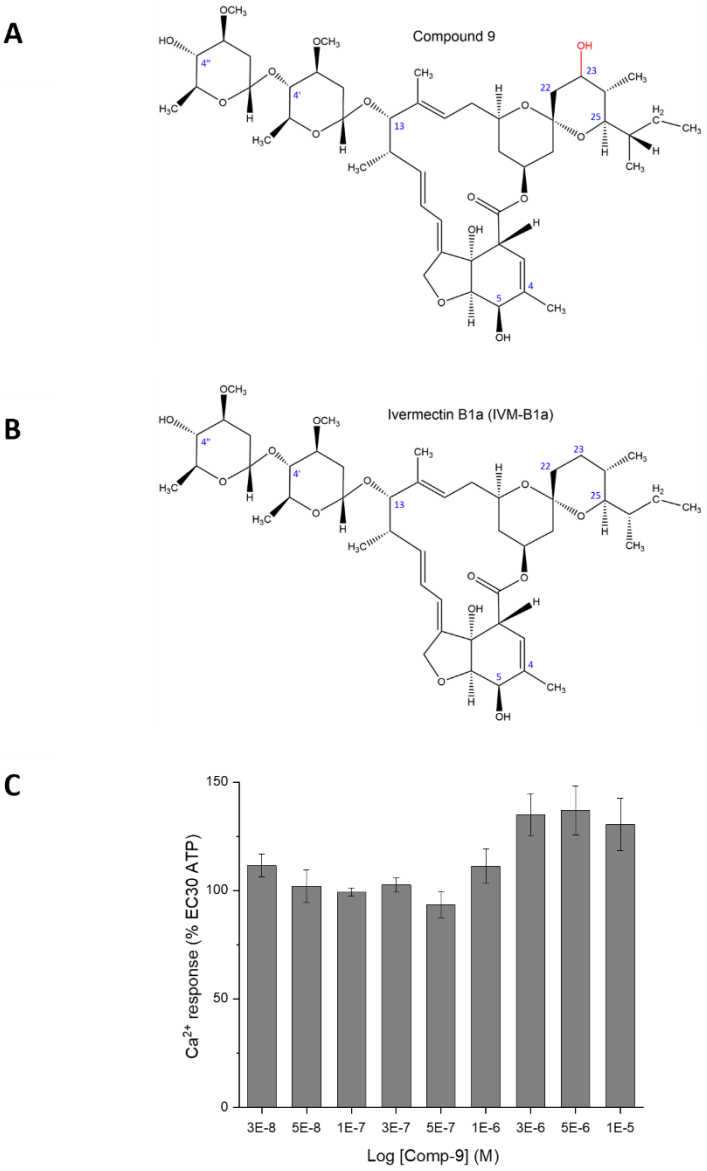

Figure 3.23. Effects of compound 9 on the human P2X4 receptor response in 1321N1 cells. (A and B) Comparison of the chemical structure of compound 9 (top) and IVM-B1a (bottom). Structural differences are highlighted in red. Blue numbers represent the C-positions. (C) Each bar chart illiterates the degree of Ca^{2+} response when the cells are treated with varying concentrations of compound 9 (0.03 – 10 µM) and stimulated with submaximal EC_{30} ATP (0.3 µM). Data is normalised to peak vehicle control response (0.3 µM ATP) and represented as percentage of vehicle control response (n=3). All data points represent the mean ± SEM.

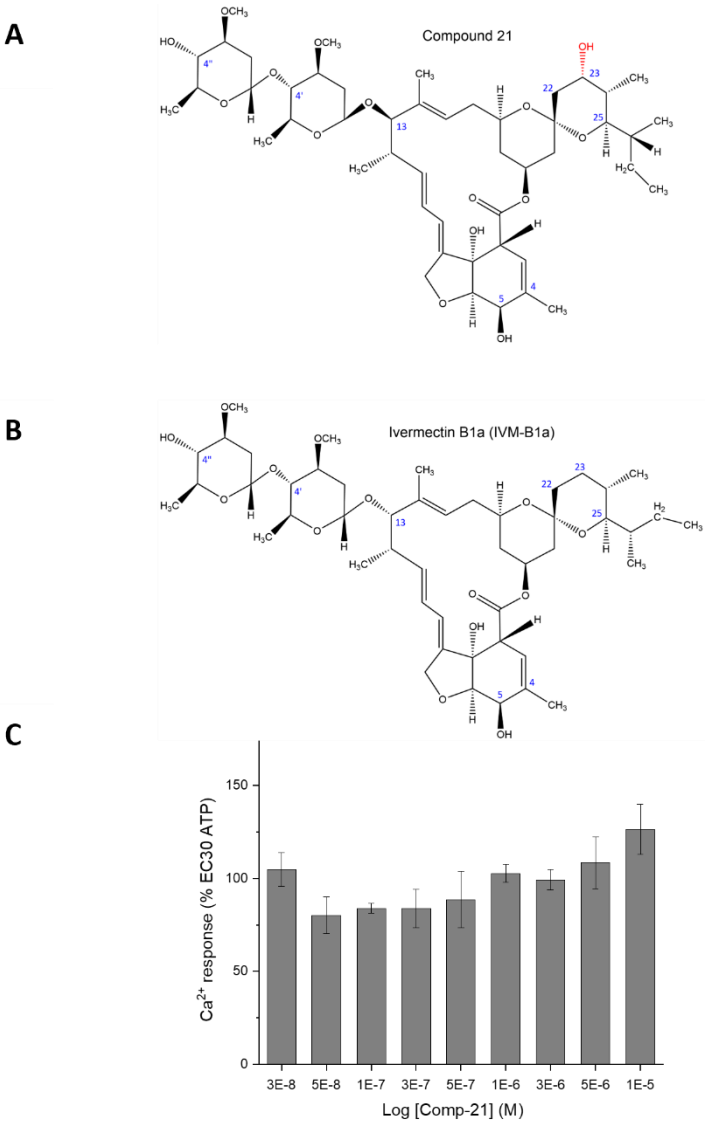

Figure 3.24. Effects of compound 21 on the human P2X4 receptor response in 1321N1 cells. (A and B) Comparison of the chemical structure of compound 21 (top) and IVM-B1a (bottom). Structural differences are highlighted in red. Blue numbers represent the C-positions. (C) Each bar chart illiterates the degree of Ca^{2+} response when the cells are treated with varying concentrations of compound 21 (0.03 – 10 µM) and stimulated with submaximal EC_{30} ATP (0.3 µM). Data is normalised to peak vehicle control response (0.3 µM ATP) and represented as percentage of vehicle control response (n=3). All data points represent the mean ± SEM.

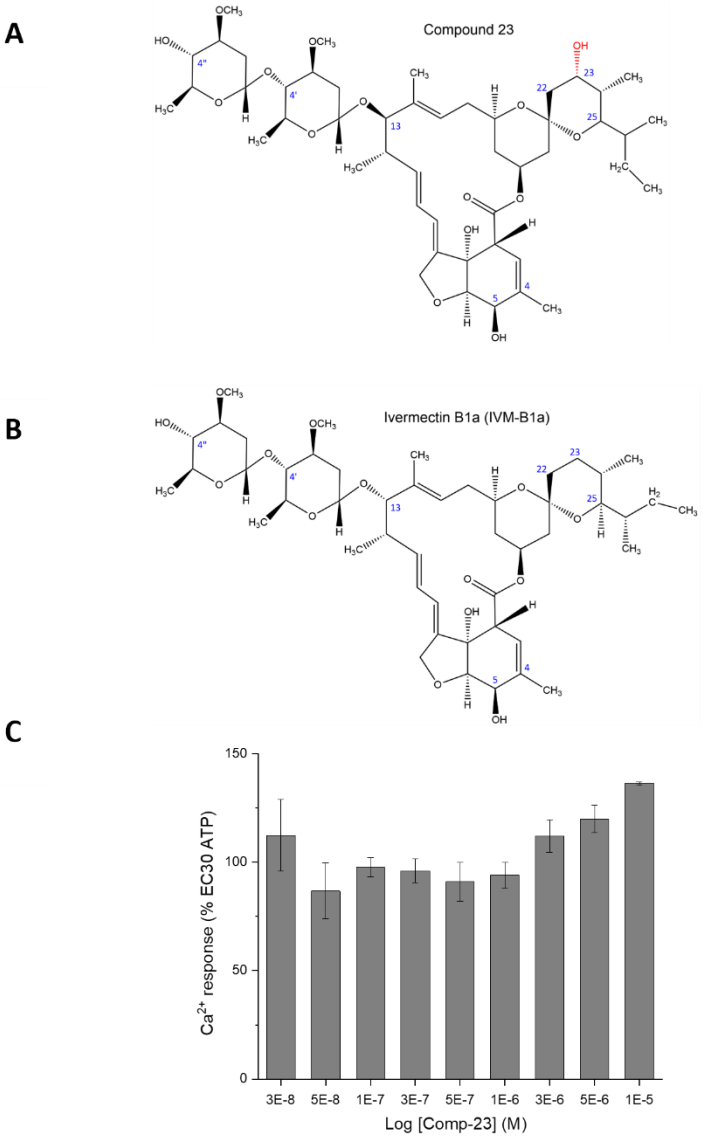

Figure 3.25. Effects of compound 23 on the human P2X4 receptor response in 1321N1 cells. (A and B) Comparison of the chemical structure of compound 23 (top) and IVM-B1a (bottom). Structural differences are highlighted in red. Blue numbers represent the C-positions. (C) Each bar chart illiterates the degree of Ca^{2+} response when the cells are treated with varying concentrations of compound 23 (0.03 – 10 µM) and stimulated with submaximal EC_{30} ATP (0.3 µM). Data is normalised to peak vehicle control response (0.3 µM ATP) and represented as percentage of vehicle control response (n=3). All data points represent the mean ± SEM.

3.3.3.5 Structural modifications at R3 (Benzofuran)

Focusing on the last region of the molecule, the benzofuran region (R3), the potency and efficacy of the following IVM-analogues were investigated. This includes two minor and five larger structural alterations at the C5 position and the C4 side chain within the benzofuran ring.

First, looking at the smallest modifications of compounds **22** and **24**, Figure 3.26A illustrates a methoxy group at the C5 position, replacing a hydroxyl group at compound **22**. Whilst Figure 2.27A shows a hydroxyl group addition to the C4 side chain for compound **24**. Both compounds were able to potentiate the intracellular ATP-evoked Ca^{2+} response to a similar extent, at 390.05 ± 30.21% (10 µM; n=6; $p<0.01$; Figure 3.26C) and 321.94 ± 52.22% (5 µM; n=3; $p<0.001$; Figure 3.27C), respectively. This makes both compounds equally efficacious to IVM-B1a ($p>0.05$). The calculated EC_{50} value for compound **22** was 2.72 ± 0.29 µM (n=6), a significant drop in potency in comparison to IVM-B1a ($p<0.001$). The EC_{50} value for compound **24** was after found to be higher, but not to a significant degree, at 1.89 ± 0.59 µM (n=3), making it equipotent to the reference compound, IVM-B1a ($p>0.05$).

Figure 3.28 illustrates a concentration-response curve and representative time-response curve for compound **4**. This compound has a 2-methoxyethoxymethyl ether (MEM) group attached to the side chain of C4 in the benzofuran ring (Figure 3.28A). Maximum potentiation of the ATP-evoked Ca^{2+} response was recorded at 337.40 ± 8.66% (3 µM; n=3; $p<0.05$), and the calculated EC_{50} value was 0.90 ± 0.02 µM (n=3); making compound **4** equally as efficacious and potent as IVM-B1a ($p>0.05$). Furthermore, at high concentrations (≥3 µM), the loading values for the cells exposed to compound **4** were significantly higher than those incubated with control buffer ($p<0.05$).

Next, compounds **8** (Figure 3.29A) and **27** (Figure 3.30A) have succinic acid additions to the C5 position and the C4 side chain, respectively. At maximal concentration (3 µM), both compounds were able to potentiate the ATP-evoked Ca^{2+} response to a similar extent at 424.54 ± 89.50% (n=3, $p<0.05$; Figure 3.29C) and 409.73 ± 34.03% (n=3; $p<0.001$; Figure 3.30C), respectively. Likewise, both compounds generated similar EC_{50} values at 1.00 ± 0.19 µM and 0.65 ± 0.06 µM, respectively. Overall, both compounds demonstrated similar effects on the ATP-evoked Ca^{2+} response, with no significant change in efficacy or potency to the reference compound, IVM-B1a ($p>0.05$). At high concentrations (≥5 µM) there was an abrupt drop in Ca^{2+} response for compounds 8 and 27 and coincidingly high loading values for the cells exposed to higher concentrations (≥3 µM) of these compounds ($p<0.05$ vs. control buffer).

Lastly, looking at the two largest modifications to R3, Figure 3.31A demonstrates a tris(2,2,2 tri-chloroethyl) phosphate group addition in compound **6,** and Figure 3.32A demonstrates a tris(2,2,2 tri-chloroethyl) phosphate ester group addition to compound **20**, both at the C5 position of the benzofuran ring. Compound **6** could not significantly potentiate the ATP-evoked Ca^{2+} response at the concentrations tested ($p>0.05$). However, a concentration-response curve could be plotted (Figure 3.31C). Compound **20** had a reasonable effect, with maximal potentiation recorded at 5 µM at 252.50 ± 10.11% (n=3; $p<0.05$; Figure 3.32C) and an EC_{50} value recorded at 1.99 ± 0.52 µM (n=3), making

compound **20** equally efficacious and potent as IVM-B1a ($p>0.05$). In addition, at high concentrations (≥5 μM), the loading values for the cells exposed to compounds **6** and **20** were significantly higher than those incubated with control buffer ($p<0.05$).

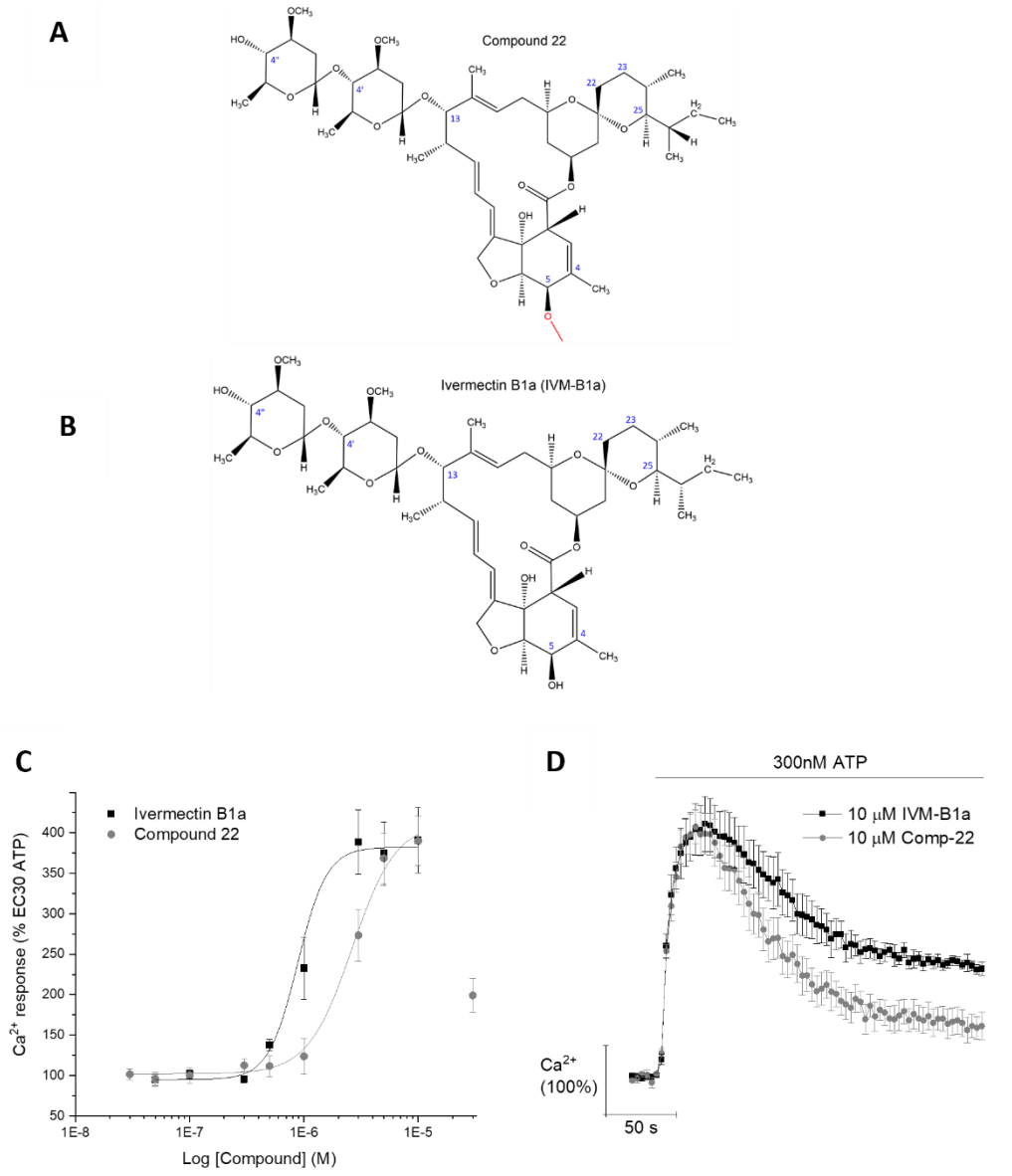

Figure 3.26. Effects of compound 22 on the human P2X4 receptor response in 1321N1 cells. (A and B) Comparison of the chemical structure of compound 22 (top) and IVM-B1a (bottom). Structural differences are highlighted in red. Blue numbers represent the C-positions. (C) Concentration-response curve of compound 22 (0.03 – 10 µM; grey circles; n=6) compared to IVM-B1a (0.05 – 10 µM; black squares; n=6) when the cells are stimulated with a submaximal EC_{30} ATP concentration (0.3 µM). (D) Representative Ca^{2+} time-response of compound 22 (n=6) and IVM-B1a (n=6) at maximal concentrations when stimulated with submaximal ATP (0.3 µM). Data is normalised to peak vehicle control response (0.3 µM ATP) and represented as percentage of vehicle control response. All data points represent the mean ± SEM.

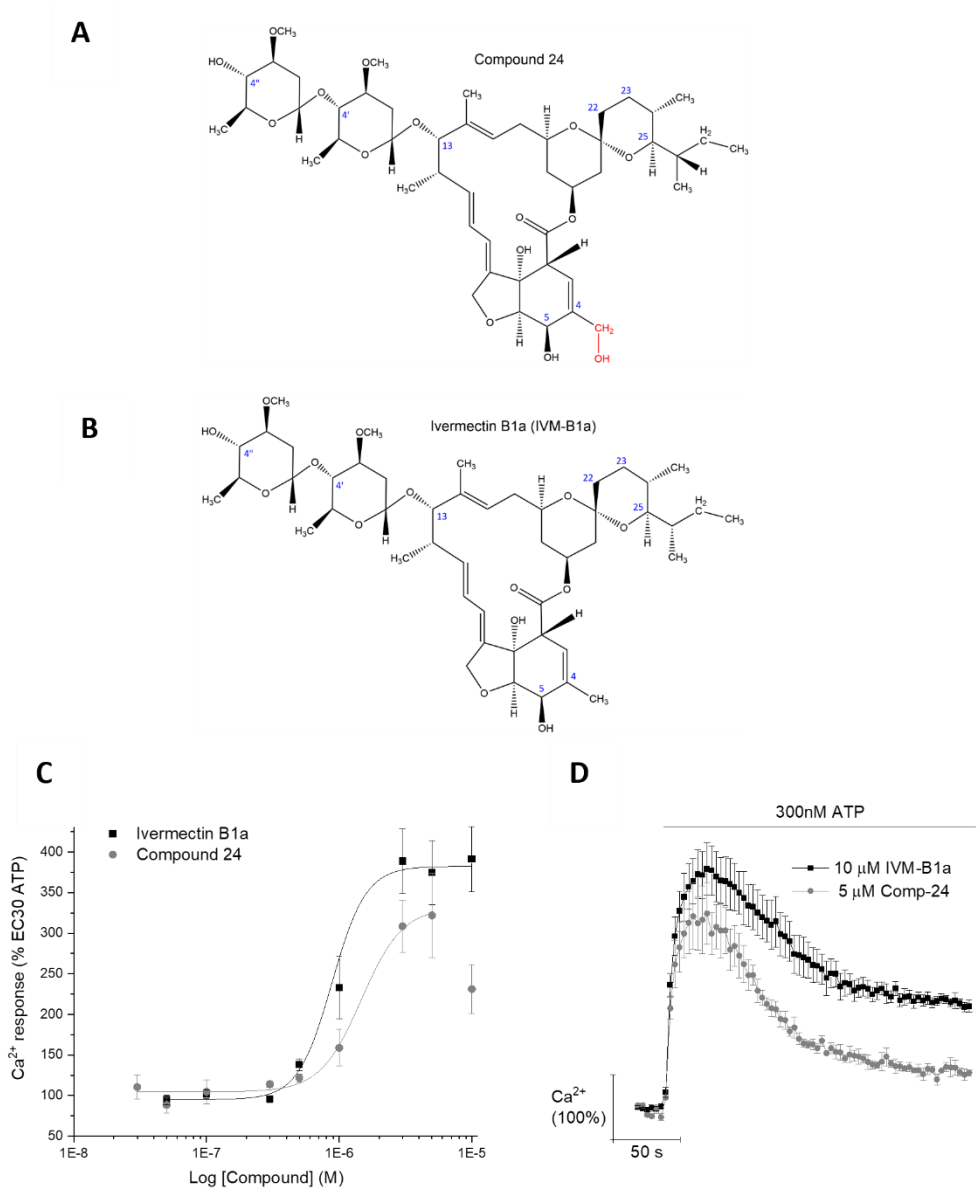

Figure 3.27. Effects of compound 24 on the human P2X4 receptor response in 1321N1 cells. (A and B) Comparison of the chemical structure of compound 24 (top) and IVM-B1a (bottom). Structural differences are highlighted in red. Blue numbers represent the C-positions. (C) Concentration-response curve of compound 24 (0.03 – 10 µM; grey circles; n=3) compared to IVM-B1a (0.05 – 10 µM; black squares; n=6) when the cells are stimulated with a submaximal EC_{30} ATP concentration (0.3 µM). (D) Representative Ca^{2+} time-response of compound 24 (n=3) and IVM-B1a (n=6) at maximal concentrations when stimulated with submaximal ATP (0.3 µM). Data is normalised to peak vehicle control response (0.3 µM ATP) and represented as percentage of vehicle control response. All data points represent the mean ± SEM.

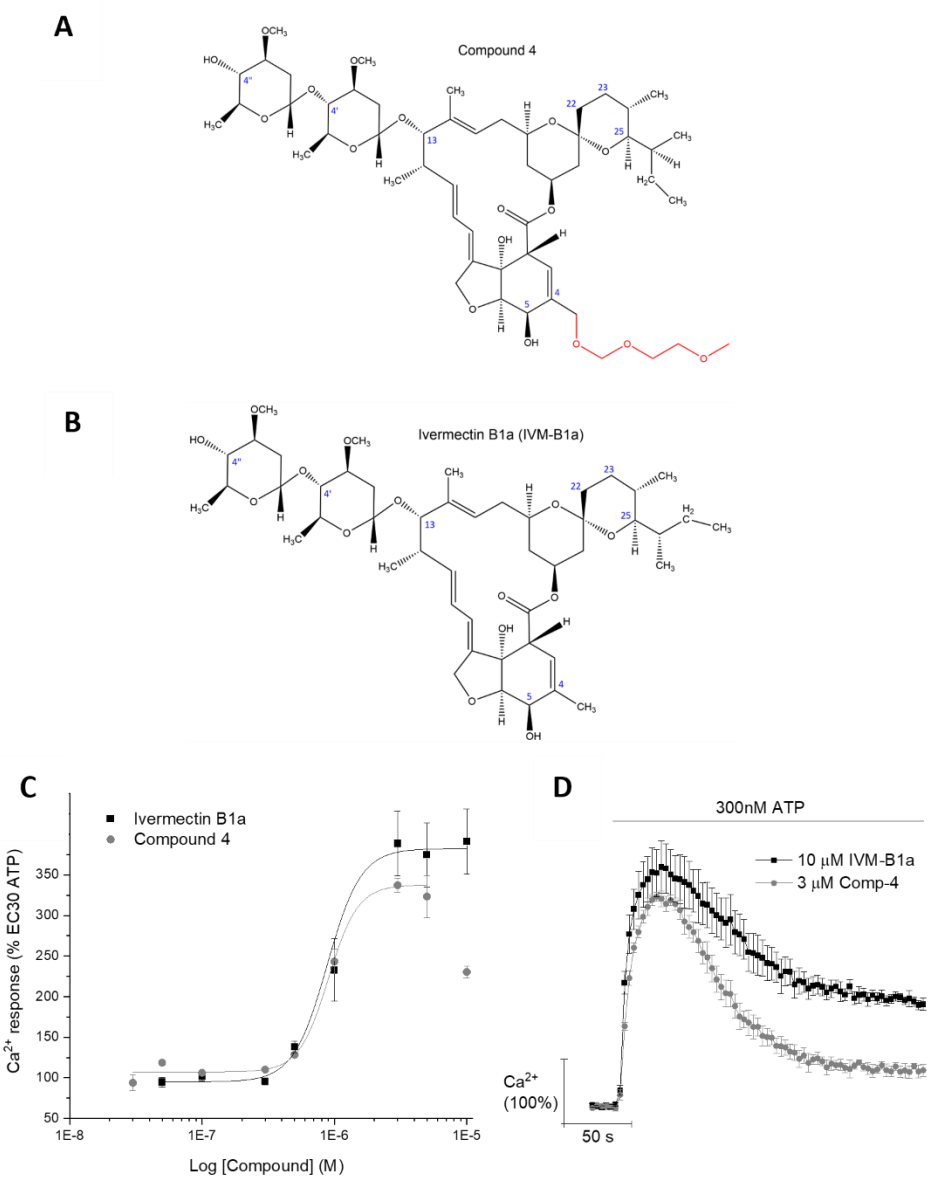

Figure 3.28. Effects of compound 4 on the human P2X4 receptor response in 1321N1 cells. (A and B) Comparison of the chemical structure of compound 4 (top) and IVM-B1a (bottom). Structural differences are highlighted in red. Blue numbers represent the C-positions. (C) Concentration-response curve of compound 4 (0.03 – 10 µM; grey circles; n=3) compared to IVM-B1a (0.05 – 10 µM; black squares; n=6) when the cells are stimulated with a submaximal EC_{30} ATP concentration (0.3 µM). (D) Representative Ca^{2+} time-response of compound 4 (n=3) and IVM-B1a (n=6) at maximal concentrations when stimulated with submaximal ATP (0.3 µM). Data is normalised to peak vehicle control response (0.3 µM ATP) and represented as percentage of vehicle control response. All data points represent the mean ± SEM.

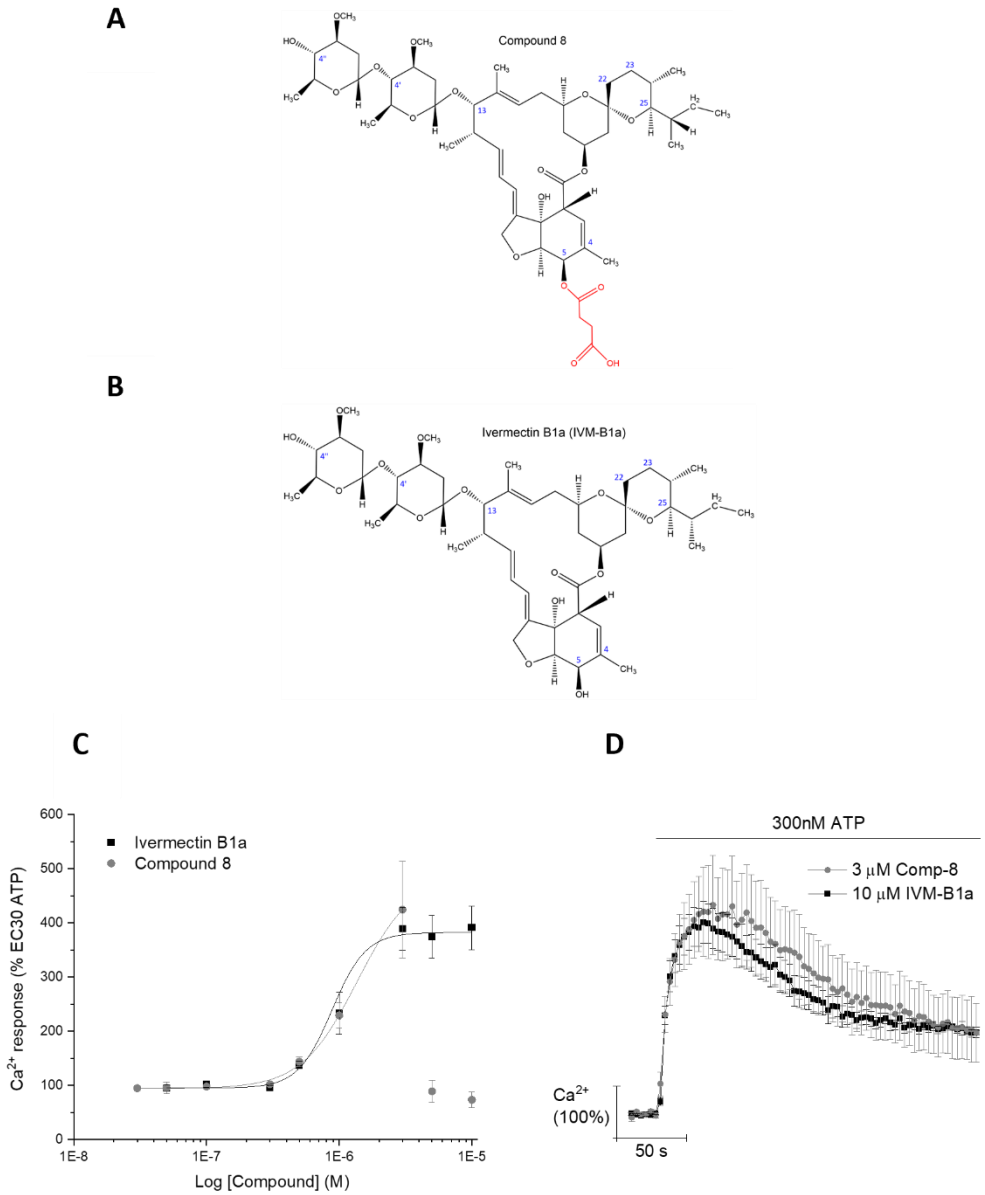

Figure 3.29. Effects of compound 8 on the human P2X4 receptor response in 1321N1 cells. (A and B) Comparison of the chemical structure of compound 8 (top) and IVM-B1a (bottom). Structural differences are highlighted in red. Blue numbers represent the C-positions. (C) Concentration-response curve of compound 8 (0.03 – 10 µM; grey circles; n=3) compared to IVM-B1a (0.05 – 10 µM; black squares; n=6) when the cells are stimulated with a submaximal EC_{30} ATP concentration (0.3 µM). (D) Representative Ca^{2+} time-response of compound 8 (n=3) and IVM-B1a (n=6) at maximal concentrations when stimulated with submaximal ATP (0.3 µM). Data is normalised to peak vehicle control response (0.3 µM ATP) and represented as percentage of vehicle control response. All data points represent the mean ± SEM.

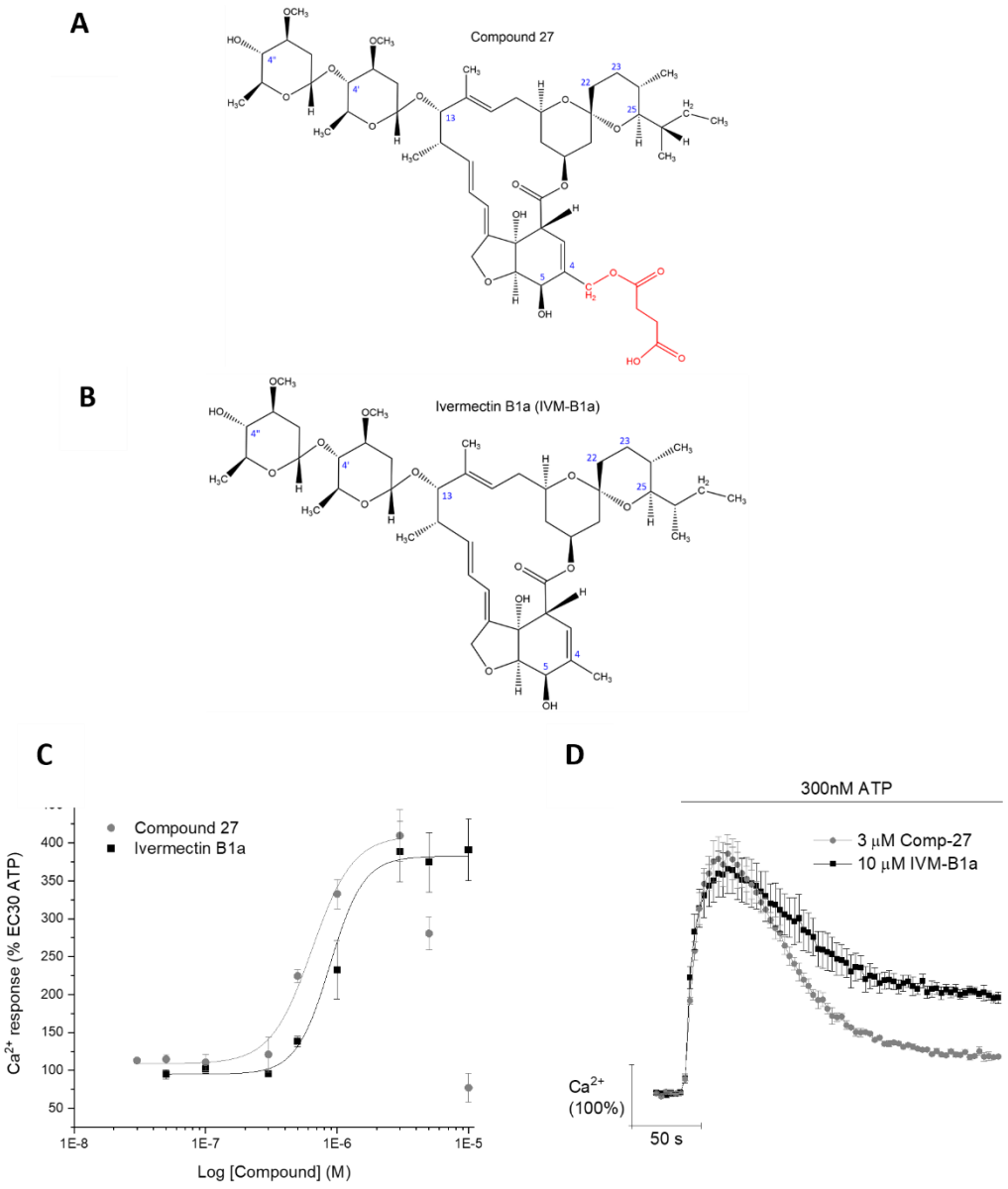

Figure 3.30. Effects of compound 27 on the human P2X4 receptor response in 1321N1 cells. (A and B) Comparison of the chemical structure of compound 27 (top) and IVM-B1a (bottom). Structural differences are highlighted in red. Blue numbers represent the C-positions. (C) Concentration-response curve of compound 27 (0.03 – 10 µM; grey circles; n=3) compared to IVM-B1a (0.05 – 10 µM; black squares; n=6) when the cells are stimulated with a submaximal EC^{30} ATP concentration (0.3 µM). (D) Representative Ca^{2+} time-response of compound 27 (n=3) and IVM-B1a (n=6) at maximal concentrations when stimulated with submaximal ATP (0.3 µM). Data is normalised to peak vehicle control response (0.3 µM ATP) and represented as percentage of vehicle control response. All data points represent the mean ± SEM.

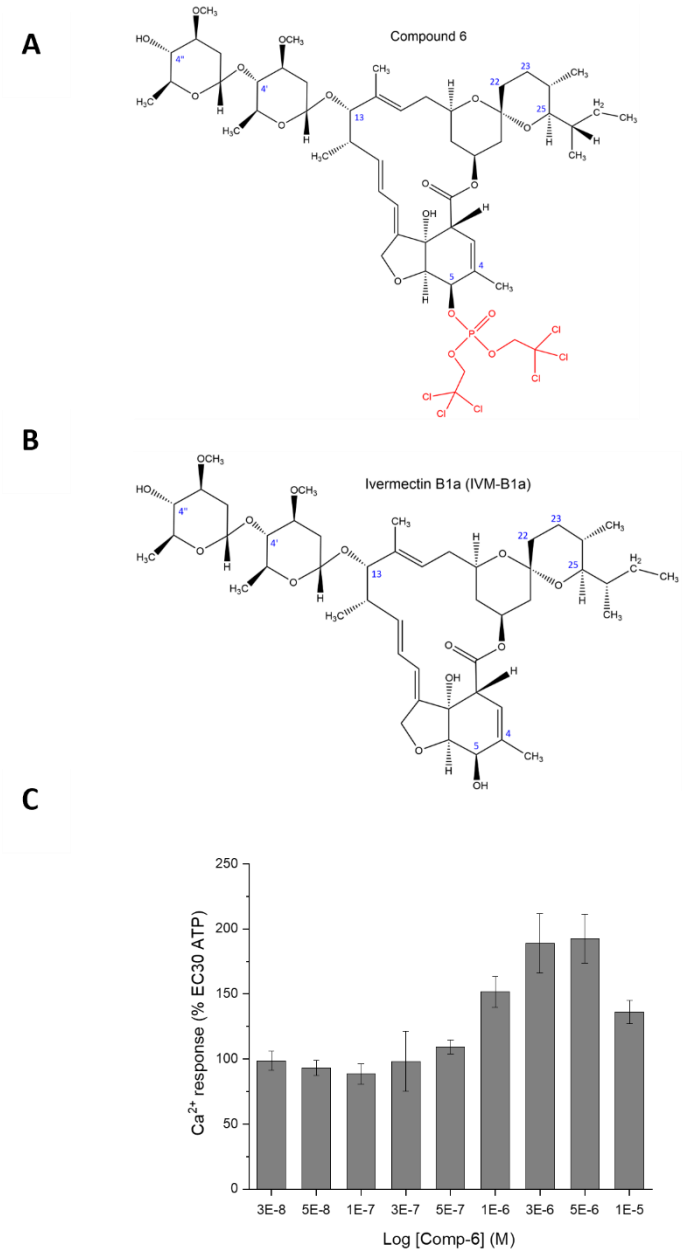

Figure 3.31. Effects of compound 6 on the human P2X4 receptor response in 1321N1 cells. (A and B) Comparison of the chemical structure of compound 6 (top) and IVM-B1a (bottom). Structural differences are highlighted in red. Blue numbers represent the C-positions. (C) Each bar illiterates the degree of Ca^{2+} response when the cells are treated with varying concentrations of compound 6 (0.03 – 10 µM) and stimulated with submaximal EC_{30} ATP (0.3 µM). Data is normalised to peak control response (0.3 µM ATP) and represented as percentage of control response. All data points represent the mean ± SEM.

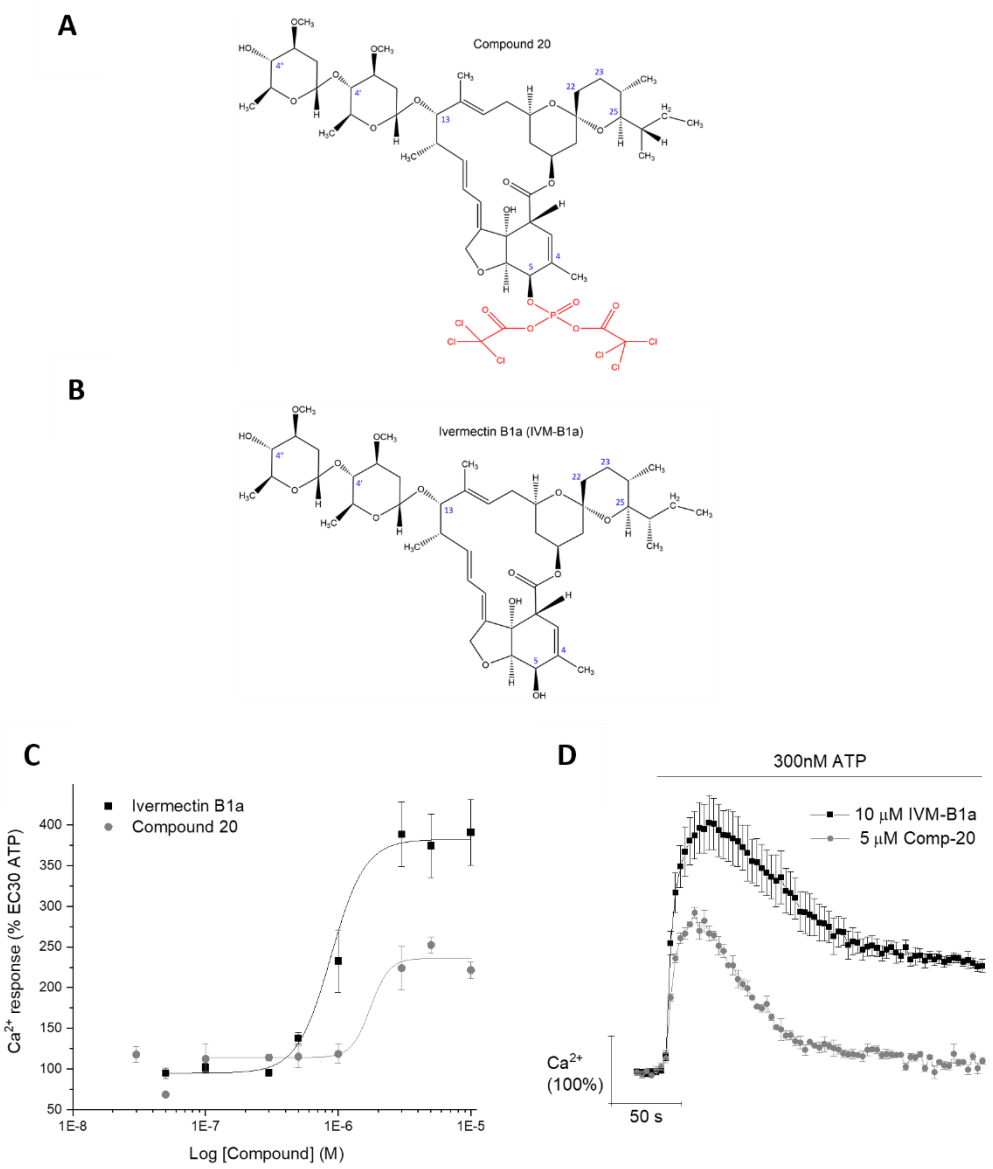

Figure 3.32. Effects of compound 20 on the human P2X4 receptor response in 1321N1 cells. (A and B) Comparison of the chemical structure of compound 20 (top) and IVM-B1a (bottom). Structural differences are highlighted in red. Blue numbers represent the C-positions. (C) Concentration-response curve of compound 20 (0.03 – 10 µM; grey circles; n=3) compared to IVM-B1a (0.05 – 10 µM; black squares; n=6) when the cells are stimulated with a submaximal EC_{30} ATP concentration (0.3 µM). (D) Representative Ca^{2+} time-response of compound 20 (n=3) and IVM-B1a (n=6) at maximal concentrations when stimulated with submaximal EC30 ATP (0.3 µM). Data is normalised to peak vehicle control response (0.3 µM ATP) and represented as percentage of vehicle control response. All data points represent the mean ± SEM.

3.3.3.6 Multiple structural modifications at two or more regions (R1, R2, and R3)

Among the compounds evaluated for modifications in two or more regions, four were commercially available analogues and the first to be assessed. This included two avermectins, eprinomectin (EPM) and selamectin (SLM), and two milbemycins, moxidectin (MOX) and nemadectin (NEM). The first of which, EPM, shares the closest structure to IVM-B1a, the difference being a double bond in the C22-23 position (R2) and an acetamide instead of the alcohol group present off carbon 4" at the end of the molecule (R1) (Figure 3.33A). EPM is a mixture of two homologues, the major component being EPM-B1a. On the other hand, SLM shows the most structural variation from IVM-B1a, with three structural differences in all three regions of the molecule. Firstly, SLM lacks the second carbohydrate unit present in the disaccharide group (R1), there is a cyclohexyl group at the C25 position in the place of an aliphatic moiety (R2), and a ketoxime at the C5 position, which has displaced a hydroxyl group in the benzofuran ring (R3) (Figure 3.34A).

At maximal concentration (10 µM), EPM and SLM were able to potentiate the ATP-evoked Ca^{2+} response to a similar extent at 472.634 ± 27.86% (n=6, $p<0.001$; Figure 3.33C) and 423.29 ± 28.08 % (n=5; $p<0.05$; Figure 3.34C), respectively. Likewise, both compounds generated similar EC_{50} values at 1.36 ± 0.22 µM (n=6) and 0.89 ± 0.12 µM (n=5), respectively. Overall, EPM and SLM were well tolerated and demonstrated similar effects on the ATP-evoked Ca^{2+} response as IVM-B1a, with no significant change in efficacy or potency ($p>0.05$).

Since MOX and NEM are both members of the milbemycin group, they lack the disaccharide unit (R1). In addition, MOX has a methoxime moiety at the C23 position and a dimethylbutyl group at the C25 position (R2) (Figure 3.35A). NEM, the precursor molecule to MOX, is structurally identical to MOX, except there is a hydroxyl group at the C23 position, displacing the methoxime group (Figure 3.36A). At maximal concentration (10 µM), MOX and NEM were able to potentiate the ATP-evoked Ca^{2+} response by 491.91 ± 25.36% (n=6; $p<0.01$; Figure 3.35C) and 803.40 ± 103.47% (n=5; $p<0.001$; Figure 3.36C), respectively. Interestingly, the intracellular Ca^{2+} levels remain elevated for cells pre-incubated with MOX over 250 seconds, whilst cells exposed to IVM-B1a enter a steady decline phase, as shown in the representative time-response trace (Figure 3.35D). NEM was found to be the second most efficacious compound tested (Table 3.2), reaching 205% of the IVM-B1a response at maximum concentration ($p<0.01$), as illustrated in the representative time-response curve (Figure 3.36D). From the respective concentration-response curves, MOX and NEM were found to be more potent than IVM-B1a (EC_{50} = 1.01 ± 0.51 µM, n=6), with calculated EC_{50} values of 0.52 ± 0.06 µM ($p<0.001$; n=6) and 0.71 ± 0.07 µM ($p<0.05$; n=5), respectively. In addition, at the highest concentration tested (10 µM), the loading values for the cells exposed to NEM for 30 minutes were significantly higher than those incubated with control buffer ($p<0.05$).

Lastly, compound **10** has a methoxy group addition to the side chain of C4 in the benzofuran ring (R3) and at the C4" position (R1), the latter due to methylation of the hydroxyl group present at the end of the molecule (Figure 3.37A). Figure 3.37C demonstrates that compound **10** (5 µM) was able to

potentiate the ATP-evoked Ca^{2+} response at 285.85 ± 22.69% ($p<0.01$; n=3), 73% of the IVM-B1a response. The calculated EC_{50} value was 1.01 ± 0.26 µM (n=3), making compound **10** equally as potent as the reference compound IVM-B1a ($p>0.05$).

The remaining five compounds in this category had little or no effect on the ATP-evoked Ca^{2+} response at the concentrations tested. This includes compound **5** (Figure 3.38A), which has three large tert-butyldimethylsilyloxy groups attached to all three hydroxyl groups in the molecule. This includes the hydroxyl group at the C7 position (R3), as well as the C4" (R1) and C5 position (R3). In addition, compound **5** has a carbonyl group at the C23 position (R2). Compound **7** (Figure 3.39A) has a hydroxyl group at the carbon 23 position (R2) and phenoxy acetate substituents displacing the hydroxyl groups at the C4" (R1) and C5 (R3) positions. Compounds **15** and **17** (Figure 3.40A and 3.41A, respectively) both have a carbonyl group at the C23 position (R2), while compound **15** has a phenyl group attached to the oxygen at the C5 position, and compound **17** has transformed the same hydroxyl group into a methyl ester group at the C5 position (R3). Lastly, compound **18** (Figure 3.42A) has a tert-butyldimethylsilyloxy group attached to the oxygen at the C5 position (R3) and a large 2,2,2 tri-chloroethyl succinate group attached to the C4" position at the end of the molecule (R1).

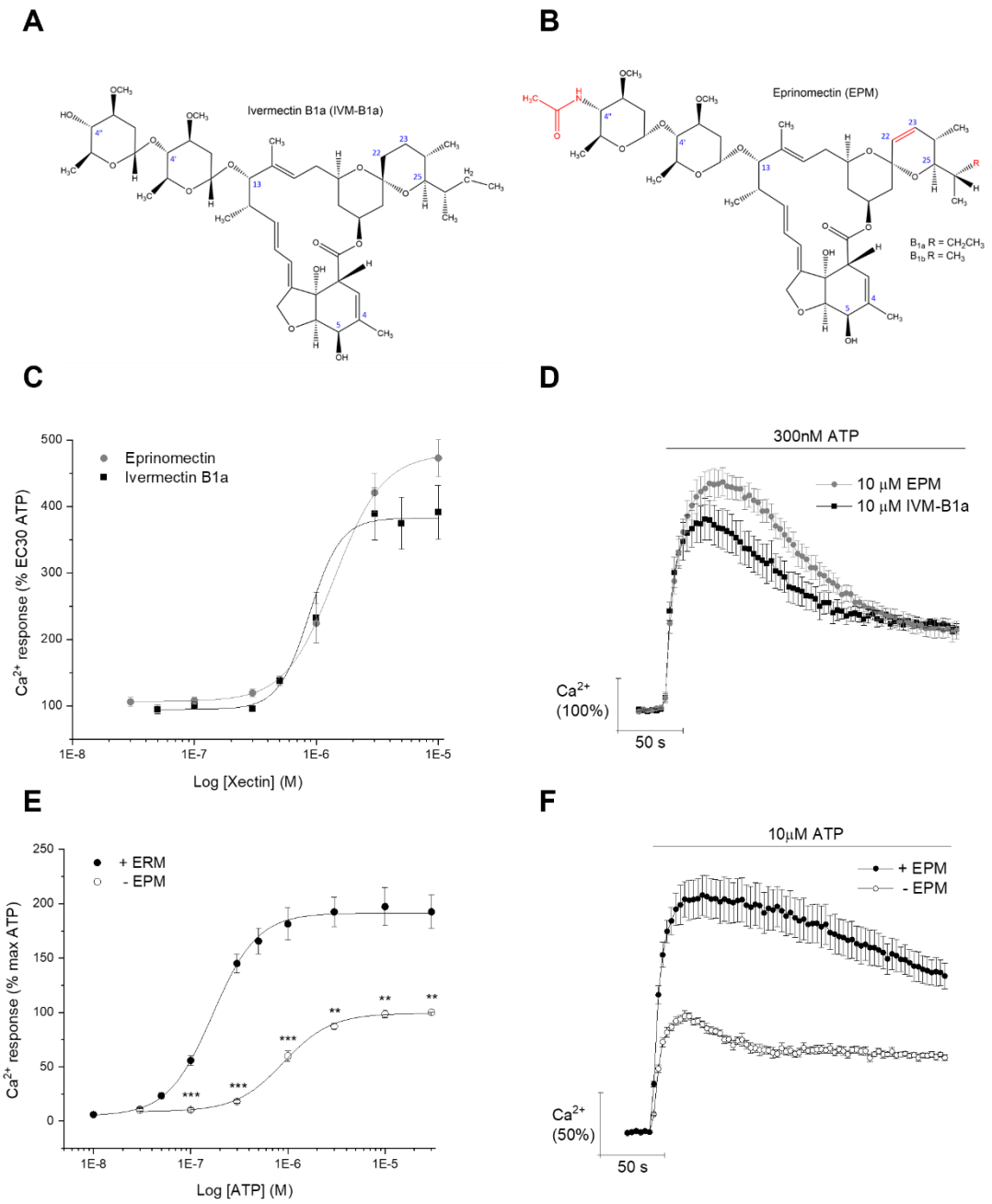

Figure 3.33. Effects of eprinomectin (EPM) on the human P2X4 receptor response in 1321N1 cells. (A and B) Comparison of the chemical structure of IVM-B1a (left) and EPM (right). Structural differences are highlighted in red. Blue numbers represent the C-positions. (C and D) Concentration-response curve of EPM (0.03 – 10 µM; grey circles; n=6) compared to IVM-B1a (0.05 – 10 µM; black squares; n=6) when the cells are stimulated with a submaximal EC_{30} ATP concentration (0.3 µM) and representative Ca^{2+} time-response trace of EPM (10 µM) and IVM-B1a (10 µM) at maximal concentrations, respectively. Data is normalised to peak vehicle control response (0.3 µM ATP) and represented as percentage of vehicle control response. (E and F) ATP concentration-response curve (0.01 – 30 µM) in the presence (closed circles) and absence (open circles) of 10 µM EPM and representative Ca^{2+} time-response trace elicited by maximal ATP (10 µM) in the presence and absence

of 10 μM EPM, respectively. Data is normalised to 30 μM ATP in the absence of EPM (n=5). Asterisks show significant differences between equivalent ATP concentrations in the presence verses the absence of EPM (*p<0.05, **p<0.01, ***p<0.001). All data points represent the mean ± SEM.

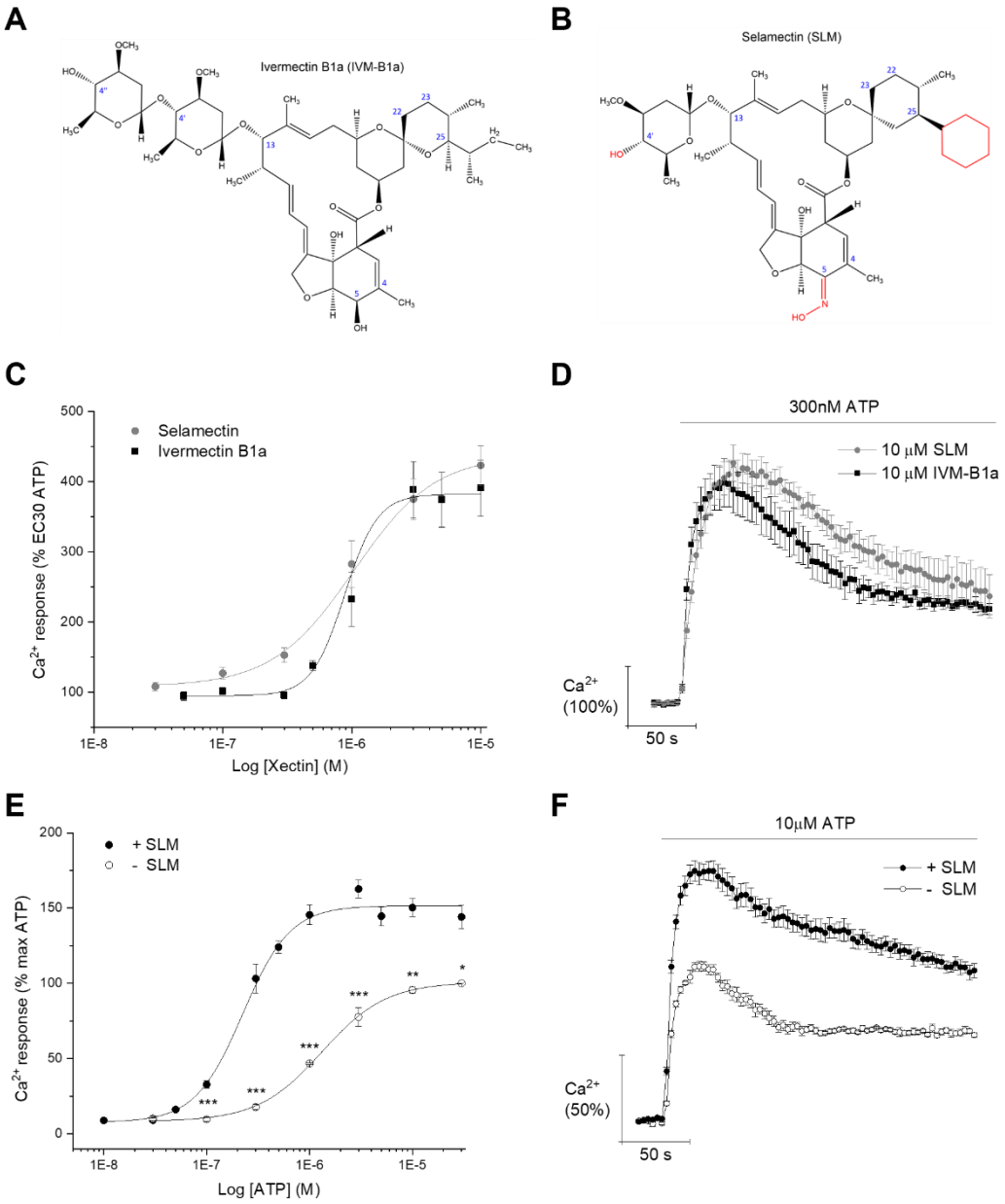

Figure 3.34. Effects of selamectin (SLM) on the human P2X4 receptor response in 1321N1 cells. (A and B) Comparison of the chemical structure of IVM-B1a (left) and SLM (right). Structural differences are highlighted in red. Blue numbers represent the C-positions. (C and D) Concentration-response curve of SLM (0.03 – 10 µM; grey circles; n=5) compared to IVM-B1a (0.05 – 10 µM; black squares; n=6) when the cells are stimulated with a submaximal EC_{30} ATP concentration (0.3 µM) and representative Ca^{2+} time-response trace of SLM (10 µM) and IVM-B1a (µM) at maximal concentrations, respectively. Data is normalised to peak vehicle control response (0.3 µM ATP) and represented as percentage of vehicle control response. (E and F) ATP concentration-response curve (0.01 – 30 µM) in the presence (closed circles) and absence (open circles) of 10 µM SLM and representative Ca^{2+} time-response trace elicited by maximal ATP (10 µM) in the presence and absence of 10 µM SLM, respectively. Data is normalised to 30 µM ATP in the absence of SLM (n=5). Asterisks show significant

differences between equivalent ATP concentrations in the presence verses the absence of SLM (*p<0.05, **p<0.01, ***p<0.001). All data points represent the mean ± SEM.

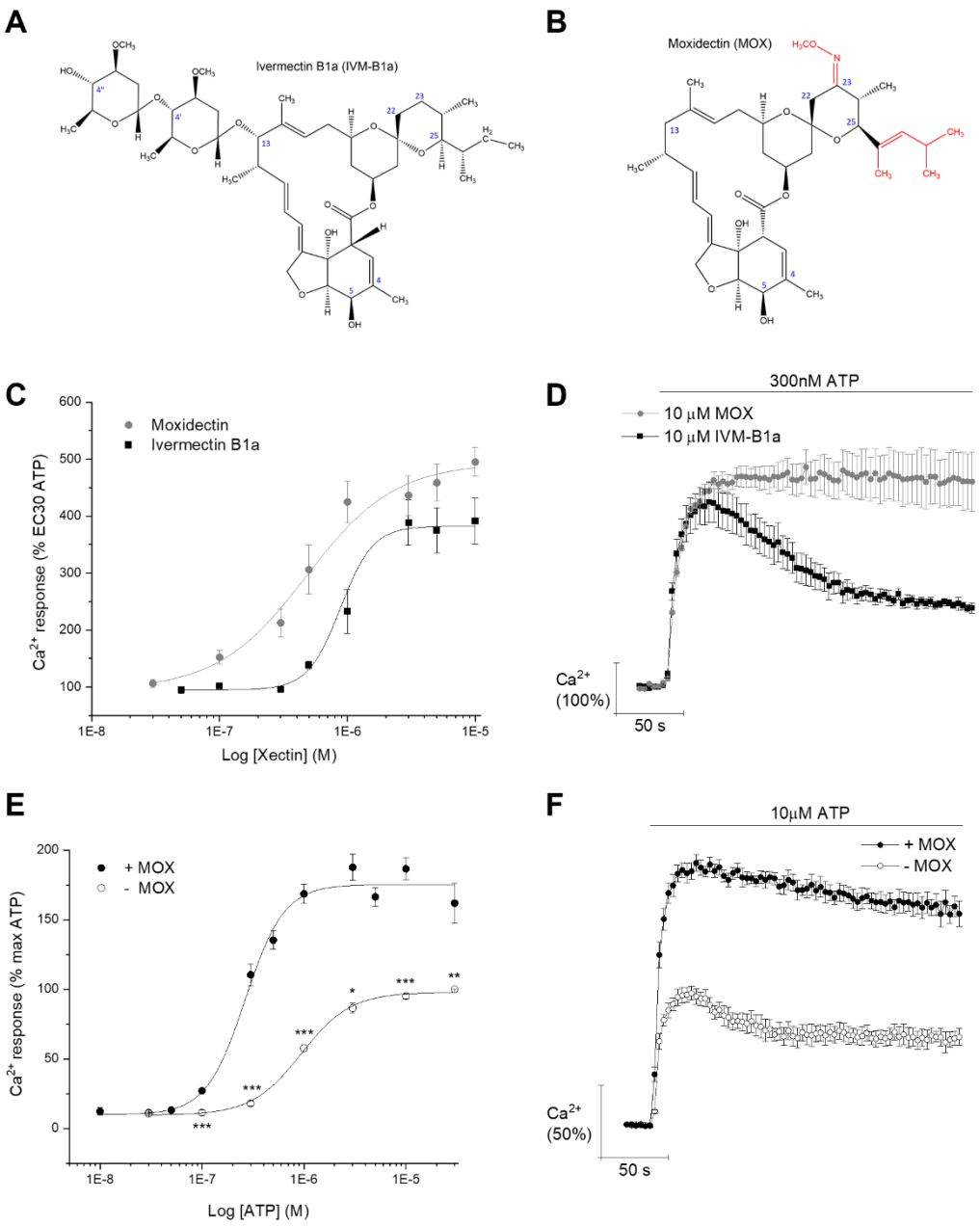

Figure 3.35. Effects of moxidectin (MOX) on the human P2X4 receptor response in 1321N1 cells. (A and B) Comparison of the chemical structure of IVM-B1a (left) and MOX (right). Structural differences are highlighted in red. Blue numbers represent the C-positions. (C and D) Concentration-response curve of MOX (0.03 – 10 µM; grey circles; n=6) compared to IVM-B1a (0.05 – 10 µM; black squares; n=6) when the cells are stimulated with a submaximal EC30 ATP concentration (0.3 µM) and representative Ca^{2+} time-response trace of MOX and IVM-B1a at maximal concentrations, respectively. Data is normalised to peak vehicle control response (0.3 µM ATP) and represented as percentage of vehicle control response. (E and F) ATP concentration-response curve (0.01 – 30 µM) in the presence (closed circles) and absence (open circles) of 10 µM MOX and representative Ca^{2+} time-response trace elicited by maximal ATP (10 µM) in the presence and absence of 10 µM MOX,

respectively. Data is normalised to 30 µM ATP in the absence of MOX (n=5). Asterisks show significant differences between equivalent ATP concentrations in the presence verses the absence of MOX (*p<0.05, **p<0.01, ***p<0.001). All data points represent the mean ± SEM.

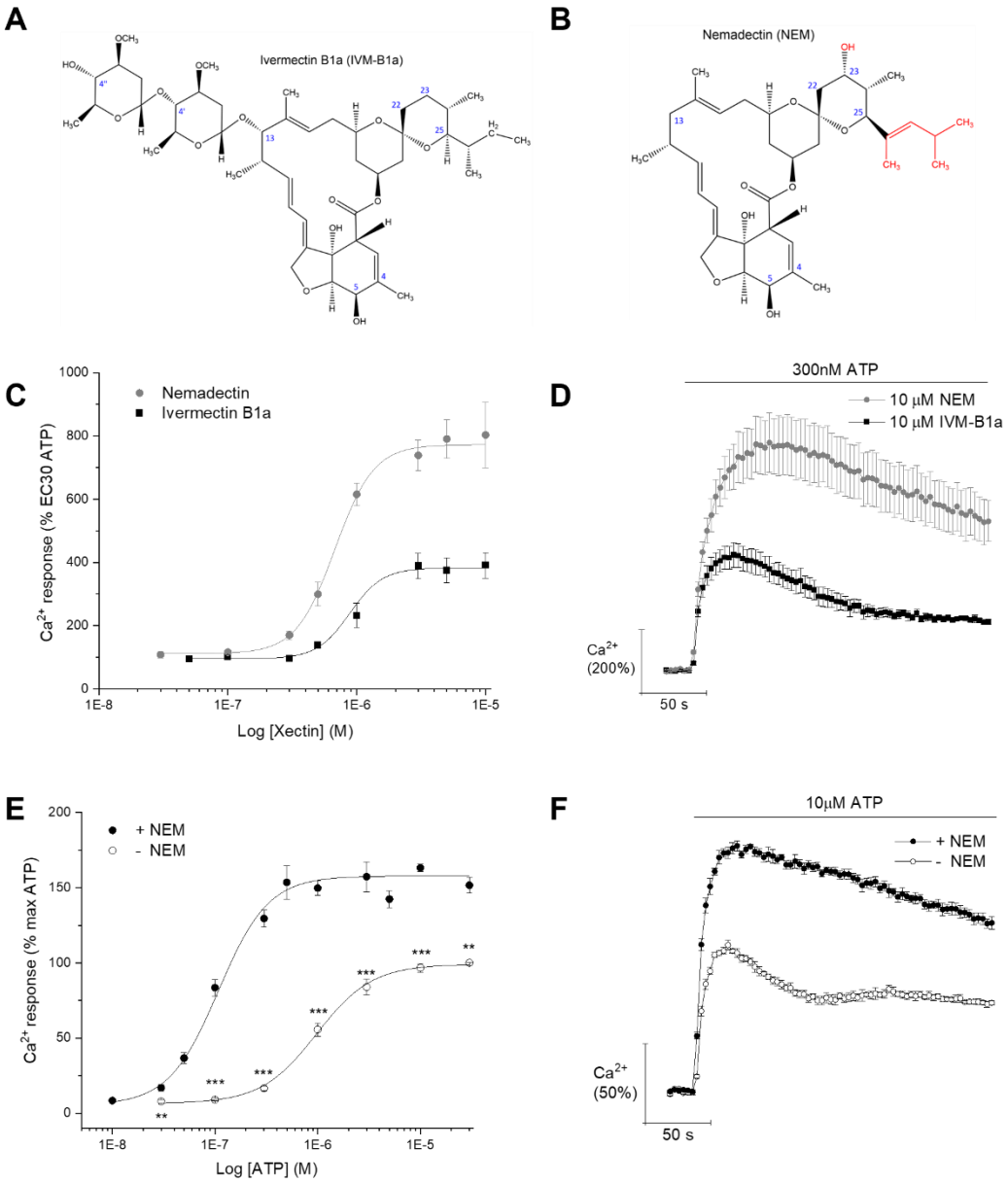

Figure 3.36. Effects of nemadectin (NEM) on the human P2X4 receptor response in 1321N1 cells. (A and B) Comparison of the chemical structure of IVM-B1a (left) and NEM (right). Structural differences are highlighted in red. Blue numbers represent the C-positions. (C and D) Concentration-response curve of NEM (0.03 – 10 µM; grey circles; n=5) compared to IVM-B1a (0.05 – 10 µM; black squares; n=6) when the cells are stimulated with a submaximal EC_{30} ATP concentration (0.3 µM) and representative Ca^{2+} time-response trace of NEM and IVM-B1a at maximal concentrations, respectively. Data is normalised to peak vehicle control response (0.3 µM ATP) and represented as percentage of vehicle control response. (E and F) ATP concentration-response curve (0.01 – 30 µM) in the presence (closed circles) and absence (open circles) of 10 µM NEM and representative Ca^{2+} time-response trace elicited by maximal ATP (10 µM) in the presence and absence of 10 µM NEM, respectively. Data is normalised to 30 µM ATP in the absence of NEM (n=5). Asterisks show significant differences between

equivalent ATP concentrations in the presence verses the absence of NEM (*p<0.05, **p<0.01, ***p<0.001). All data points represent the mean ± SEM.

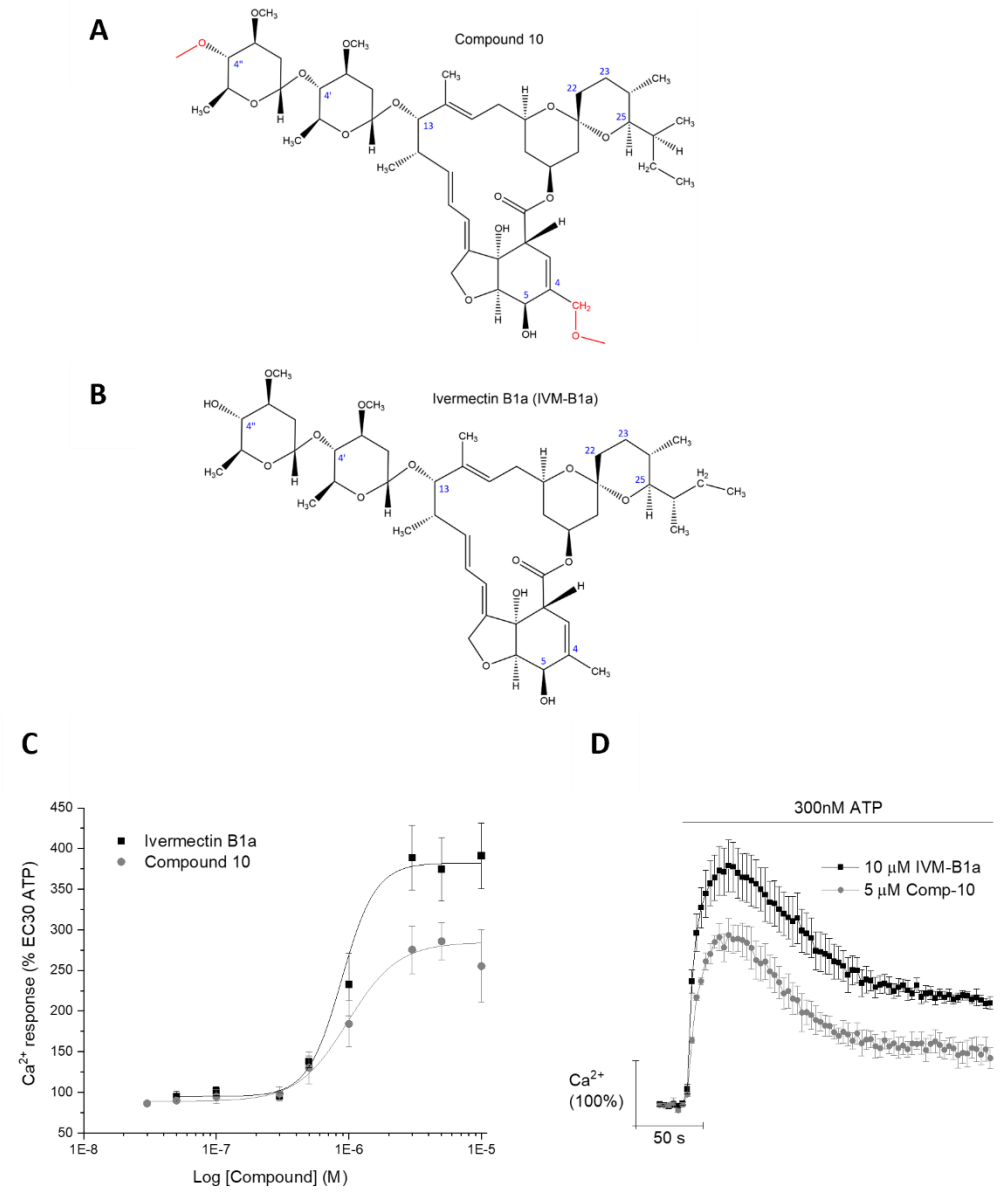

Figure 3.37. Effects of compound 10 on the human P2X4 receptor response in 1321N1 cells. (A and B) Comparison of the chemical structure of compound 10 (top) and IVM-B1a (bottom). Structural differences are highlighted in red. Blue numbers represent the C-positions. (C) Concentration-response curve of compound 10 (0.03 – 10 µM; grey circles; n=3) compared to IVM-B1a (0.05 – 10 µM; black squares; n=6) when the cells are stimulated with a submaximal EC_{30} ATP concentration (0.3 µM). (D) Representative Ca^{2+} time-response of compound 10 (n=3) and IVM-B1a (n=6) at maximal concentrations when stimulated with submaximal ATP (0.3 µM). Data is normalised to peak vehicle control response (0.3 µM ATP) and represented as percentage of vehicle control response. All data points represent the mean ± SEM.

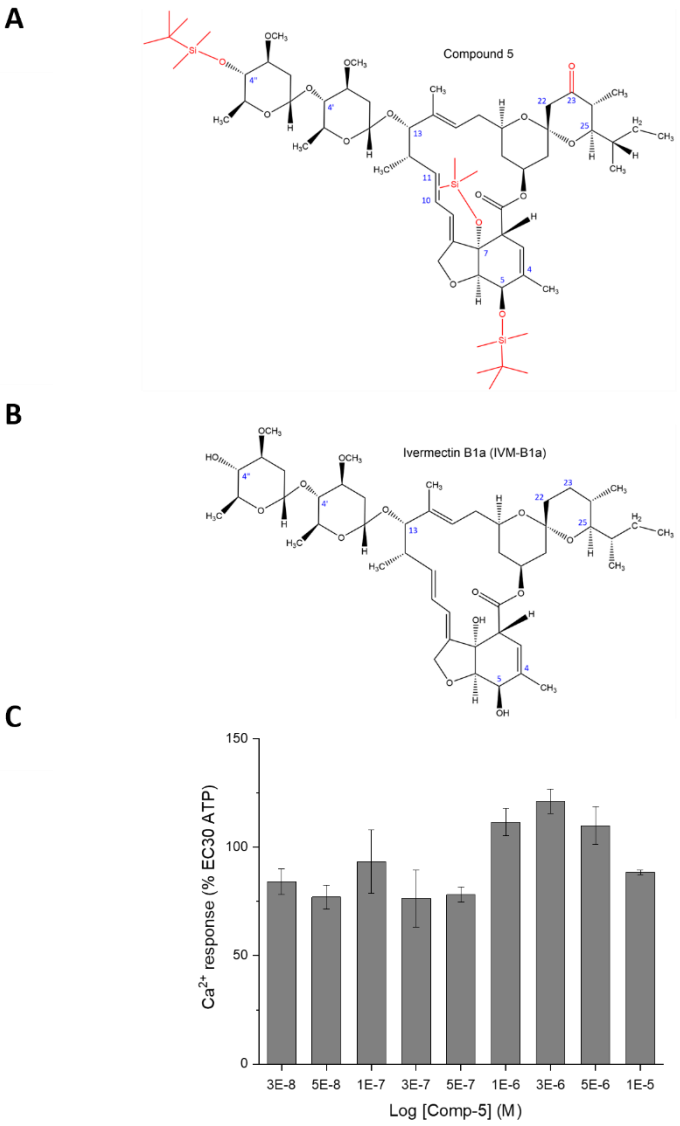

Figure 3.38. Effects of compound 5 on the human P2X4 receptor response in 1321N1 cells. (A and B) Comparison of the chemical structure of compound 5 (top) and IVM-B1a (bottom). Structural differences are highlighted in red. Blue numbers represent the C-positions. (C) Each bar chart illiterates the degree of Ca^{2+} response when the cells are treated with varying concentrations of compound 5 (0.03 – 10 µM) and stimulated with submaximal EC_{30} ATP (0.3 µM). Data is normalised to peak vehicle control response (0.3 µM ATP) and represented as percentage of vehicle control response (n=3). All data points represent the mean ± SEM.

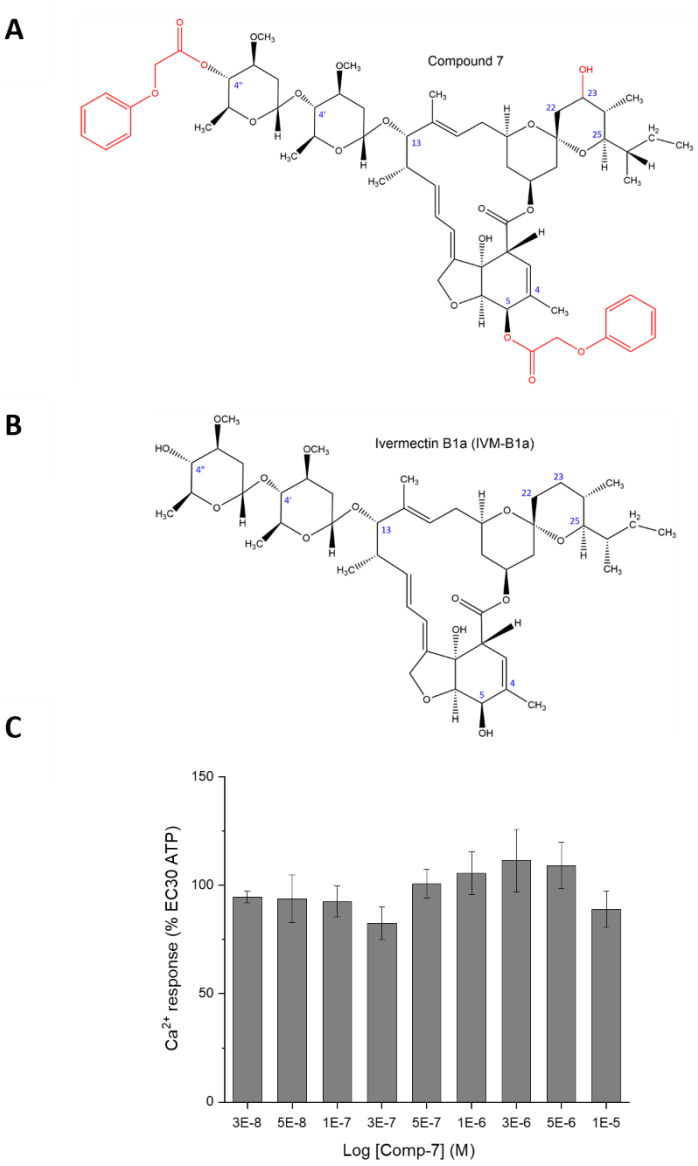

Figure 3.39. Effects of compound 7 on the human P2X4 receptor response in 1321N1 cells. (A and B) Comparison of the chemical structure of compound 7 (top) and IVM-B1a (bottom). Structural differences are highlighted in red. Blue numbers represent the C-positions. (C) Each bar chart illiterates the degree of Ca^{2+} response when the cells are treated with varying concentrations of compound 7 (0.03 – 10 µM) and stimulated with submaximal EC_{30} ATP (0.3 µM). Data is normalised to peak vehicle control response (0.3 µM ATP) and represented as percentage of vehicle control response (n=3). All data points represent the mean ± SEM.

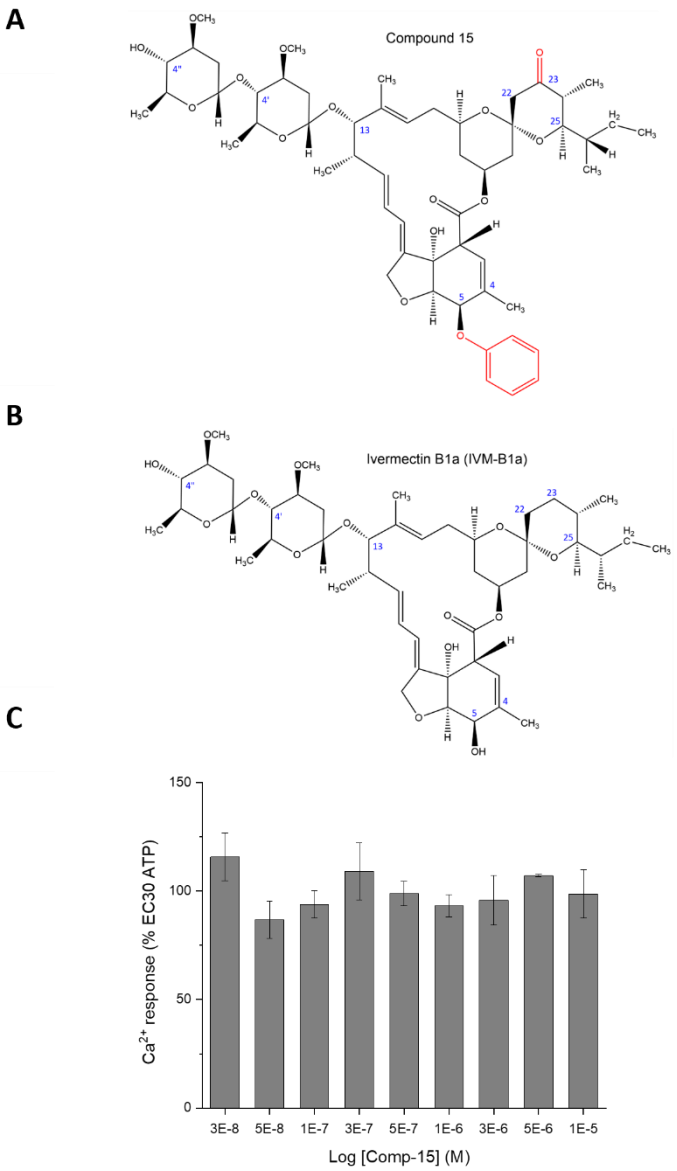

Figure 3.40. Effects of compound 15 on the human P2X4 receptor response in 1321N1 cells. (A and B) Comparison of the chemical structure of compound 15 (top) and IVM-B1a (bottom). Structural differences are highlighted in red. Blue numbers represent the C-positions. (C) Each bar chart illiterates the degree of Ca^{2+} response when the cells are treated with varying concentrations of compound 15 (0.03 – 10 µM) and stimulated with submaximal EC_{30} ATP (0.3 µM). Data is normalised to peak vehicle control response (0.3 µM ATP) and represented as percentage of vehicle control response (n=3). All data points represent the mean ± SEM.

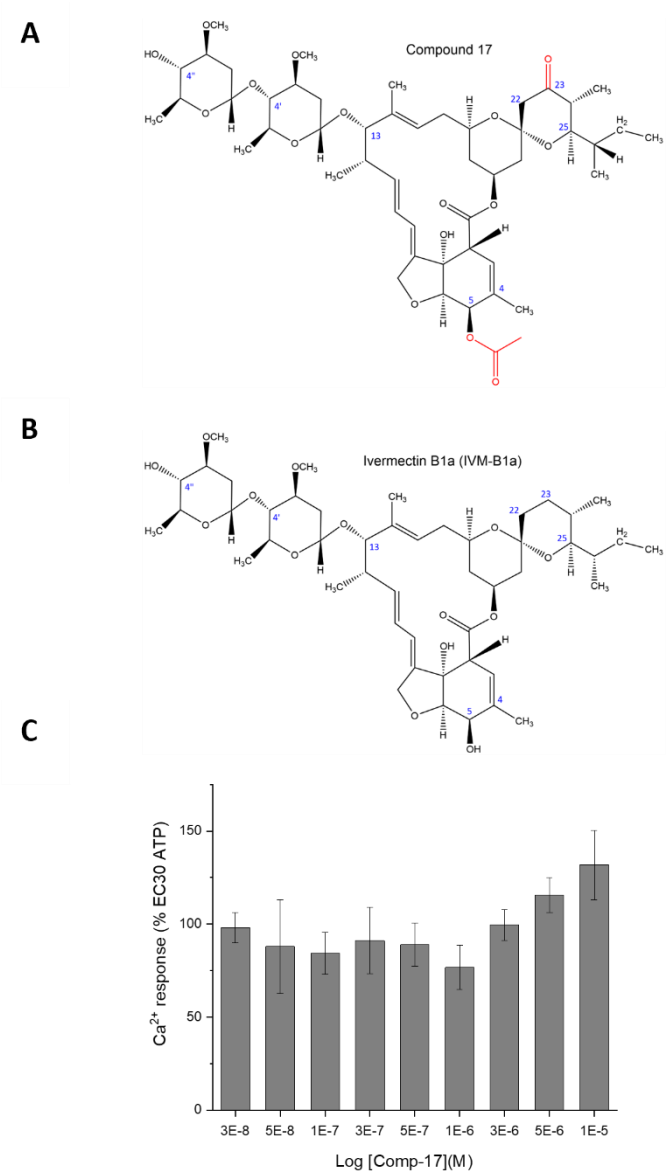

Figure 3.41. Effects of compound 17 on the human P2X4 receptor response in 1321N1 cells. (A and B) Comparison of the chemical structure of compound 17 (top) and IVM-B1a (bottom). Structural differences are highlighted in red. Blue numbers represent the C-positions. (C) Each bar chart illiterates the degree of Ca^{2+} response when the cells are treated with varying concentrations of compound 17 (0.03 – 10 µM) and stimulated with submaximal EC_{30} ATP (0.3 µM). Data is normalised to peak vehicle control response (0.3 µM ATP) and represented as percentage of vehicle control response (n=3). All data points represent the mean ± SEM.

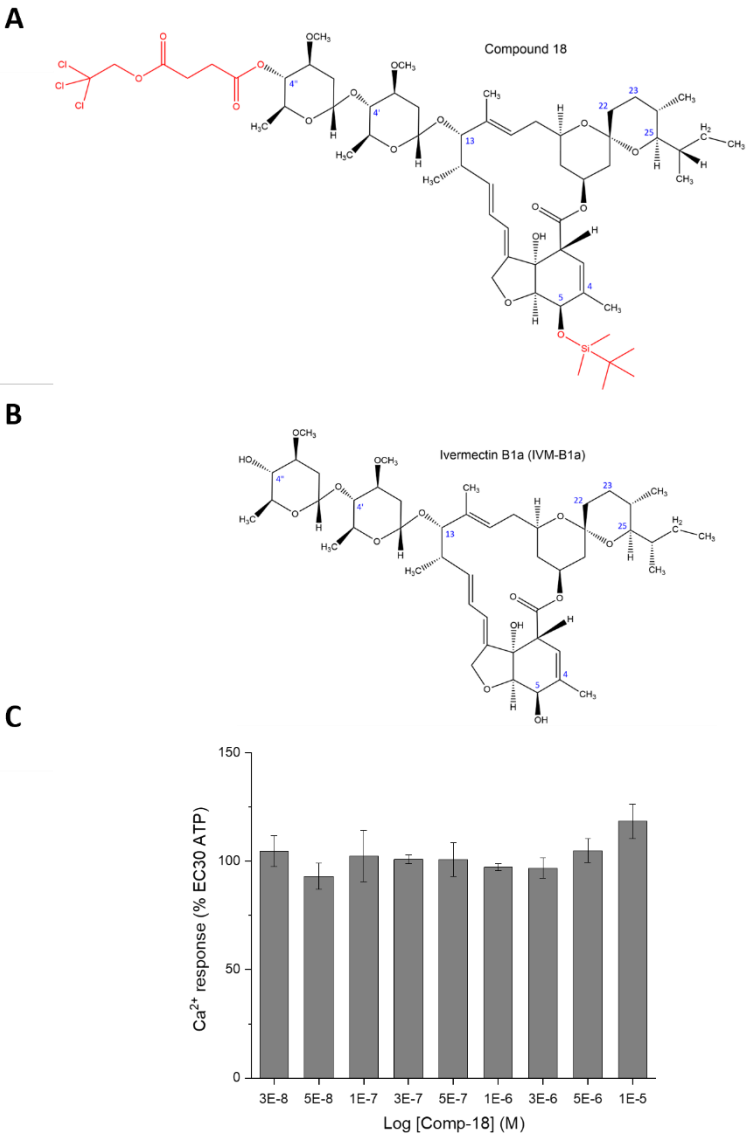

Figure 3.42. Effects of compound 18 on the human P2X4 receptor response in 1321N1 cells. (A and B) Comparison of the chemical structure of compound 18 (top) and IVM-B1a (bottom). Structural differences are highlighted in red. Blue numbers represent the C-positions. (C) Each bar chart illiterates the degree of Ca^{2+} response when the cells are treated with varying concentrations of compound 18 (0.03 – 10 µM) and stimulated with submaximal EC_{30} ATP (0.3 µM). Data is normalised to peak vehicle control response (0.3 µM ATP) and represented as percentage of vehicle control response (n=3). All data points represent the mean ± SEM.

3.3.4 Investigating the selectivity of the IVM analogues for the GABA(A) receptor

In addition to the activity of IVM at P2X4 receptors, previous studies have shown IVM to act as an agonist or allosteric modulator, or both, for other mammalian channels. These include gamma-aminobutyric acid type A ($GABA_A$) receptors (Adelsberger et al., 2000; Krůšek & Zemková, 1994) and glycine receptors (Shan et al., 2001), both of which mediate fast inhibitory neurotransmitter transmission in the central nervous system (CNS). Multiple studies have reportedly observed neurological side effects in humans receiving IVM treatment, including confusion and encephalopathy, as reviewed by Chandler (2018). Furthermore, in veterinary science, it has been well established that certain breeds of dogs, including Collies, are susceptible to neurotoxic side effects following IVM treatment (Mealey et al., 2001). This IVM-induced neurotoxicity often results from overdosing or when the blood-brain barrier function is impaired (Edwards et al., 2003) and is linked to the activation of GABA(A) receptors (Merola et al., 2012; Ménez et al., 2012).

To investigate the selectivity of IVM-B1a and its analogues for P2X4 receptor, an activity screen was performed using a human recombinant GABA(A)R expressing cell line. This study intended to provide information regarding the potential toxicities of the IVM-analogues and insight into how to structurally optimise IVM for selective targeting of P2X4 receptors for future medications. The cell line used was mouse L(tk-) cells (mouse connective tissue) expressing human recombinant GABA(A) (α1β3γ2) receptors. This isoform was chosen as it has the closest composition to GABA(A) (α1β2γ2) channels. This is the most common GABA(A)R isoform found in the brain (Feng and Forman, 2018) and has been linked to IVM activation (Adelsberger et al., 2000), providing a good model to assess IVM-induced neurotoxicity.

To induce GABA(A)R expression, the cells must be treated with dexamethasone (DEX). To assess GABA(A)R activity, a fluorescence-based assay was applied using fluorometric imaging plate reader (FLIPR) membrane potential dye (Molecular Devices). The dye detects GABA(A) receptor modulation by monitoring membrane potential change across the cell. Based on previous literature using the FMP-Red-Dye in an L(tk-) cell expression model, activation of GABA(A) receptors will cause an increase in fluorescence (Nik et al., 2017).

3.3.4.1 Optimisation and Characterisation of the GABA(A)R (α1β3γ2) overexpressing cell line

Having chosen a suitable cell line expressing human GABA(A)R, a feasibility and optimisation study was conducted to assess GABA(A)R activity using the FLIPR membrane potential assay. Initially, the cells were loaded with FMP-Red-Dye, as described in the materials and methods (section 2.3.2) and subjected to the natural agonist GABA to assess the fluorescent signal and thus, GABA(A)R activity. As demonstrated in Figure 3.45B, in cells pre-treated with DEX (1 μM), stimulation with a high concentration of GABA (30 μM) causes an increase in fluorescence. Molecular devices, developers of the FLIPR membrane potential dye, state that an increase in fluorescence corresponds to membrane depolarising. This is surprising as GABA(A) receptors are associated with hyperpolarising effects due to the conductance of chloride ions into the cell following receptor activation. However, another study that employed this technique to study GABA(A) (α1β2γ2) receptor activation in the same cell expression model (L-tk cells) also reported a "positive" fluorescent response when the cells were stimulated with GABA (Nik et al., 2017). Therefore, this readout for GABA(A) receptor activity was accepted, once the cell model was validated with further studies, as discussed below.

To demonstrate the fluorescent signal is GABA(A)R dependant, the cells were stimulated with a range of GABA concentrations (0.01-500 μM) in the absence of DEX (1 μM) treatment (Figure 3.43). GABA-induced increases in fluorescence were noted only in cells treated with DEX ($p<0.001$ vs blank control) but not in the untreated cells. This indicates that the fluorescence signal generated by membrane potential changes is dependent on GABA(A)R expression and that they are correctly localised and functional in the plasma membrane.

To ensure the recommended culturing protocol, provided by Infinity BiologiX (now called Sampled), was optimal for GABA(A)R expression, the level of GABA(A) receptor activity was measured following a 24-, 48- and 72-hour incubation with either 1 μM or 10 μM DEX in the 96-well plate. This test was conducted with the aim of discovering the optimal DEX concentration and DEX incubation time for promoting GABA(A)R activity. As shown in Figure 3.44, it was found that there was no significant difference in fluorescent signal at 150 seconds when the cells were treated with either concentration of DEX, nor was there a discernible difference between the three incubation times (24h, 48h and 72h; $p>0.05$). As a result, GABA(A)R expression was induced with 1 μM DEX for 24 hours for all FLIPR membrane potential assays.

Further characterisation of the L(tk-) cell line was performed through concentration-response studies with the GABA agonist. As shown in Figure 3.45A, GABA promoted the fluorescent signal in a concentration-dependant manner (0.01-500 μM), with maximal activity at 30 μM. The calculated EC_{50} was 0.66 ± 0.10 μM (n=6) which is close to a previous study that found the GABA EC_{50} value to be 0.92 ± 0.19 μM for human GABA(A) (α1β2γ2L) in HEK293 cells using electrophysiological techniques (Estrada-Mondragon and Lynch, 2015). As demonstrated in the fluorescence time-response trace (Figure 3.45B), stimulation of L(tk-) cells with maximal GABA (30 μM) agonist results in an increase in fluorescent signal to 181.27 ± 10.93 RFUs (n=6) that begins to plateau at approximately 150 seconds.

However, a fluorescence artefact can be observed upon the addition of any liquid to the wells, clearly demonstrated in the buffer control. This transient drop in fluorescence is suspected to be a caveat of injecting liquid into the well, effectively diluting the FMP-Red-Dye and causing a drop in fluorescence. To account for this, each experimental plate contained dye-treated wells that would be injected with buffer only and subtracted from all experimental values to counter this drop in fluorescence.

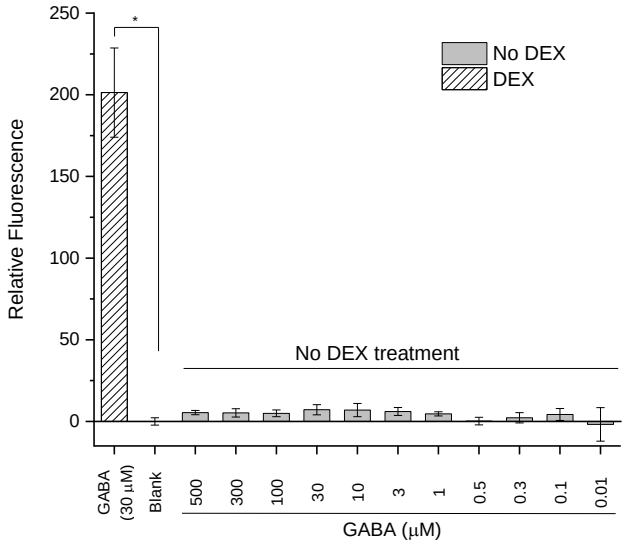

Figure 3.43. GABA-mediated fluorescence is dependent on dexamethasone (DEX) treatment in mouse L(tk-) cells. Bars represent fluorescent signal responses in the presence (striped) and absence (grey) of DEX (1 μM) when the cells are stimulated with GABA agonist (0.01-500 μM) (n=3). Asterisks show statistical significance relative towards blank (buffer control) which contains DEX (*p<0.05). Each bar represents the mean of three independent biological assays; error bars are SEM.

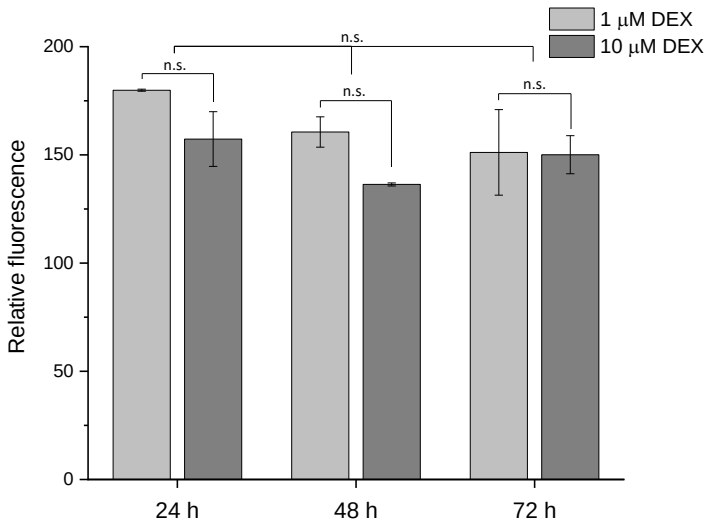

Figure 3.44. Optimisation of mouse L(tk-) cells expressing human recombinant GABA(A) (α1β3γ2) receptors. (A) Bars represent the fluorescent signal responses measured after 24-, 48- and 72- hours of dexamethsome (DEX) exposure to the cells at 1 μM (light grey) and 10 μM (dark grey) concentration. All experiments were done in a 96-well plate and stimulated with 100 μM GABA agonist (N=3). Each bar represents the mean of three technical repeats on the plate; error bars are SEM. n.s. = p>0.05 (not significant).

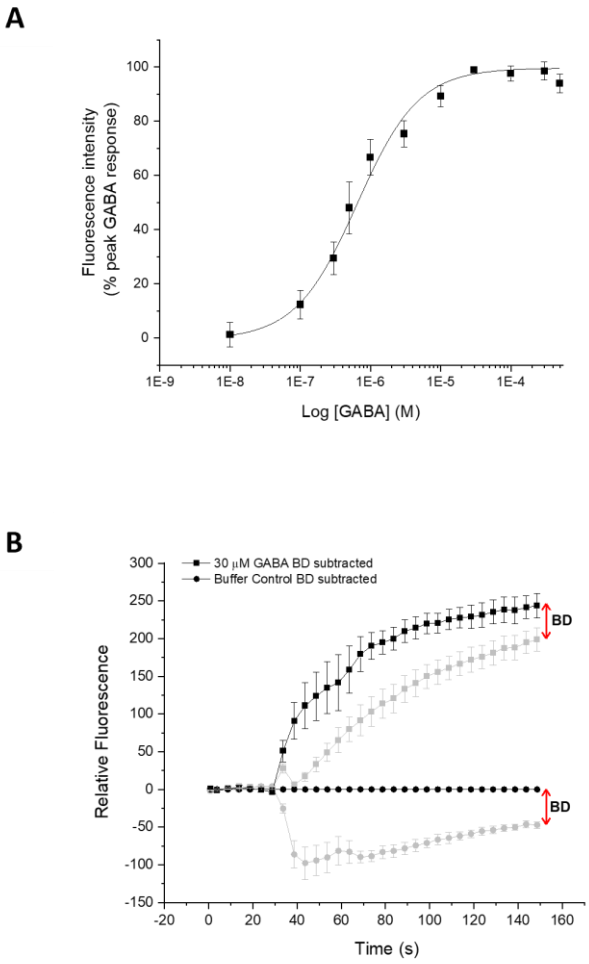

Figure 3.45. GABA-mediated fluorescent changes monitored via the FMP-Red-Dye in mouse L(tk-) cells expressing human GABA(A) (α1β3γ2) receptors. (A) GABA concentration-response curve (0.01-500 µM) for human GABA(A)R based on fluorescent signal responses. All data was normalised to peak GABA response (30 µM) and fit to the Hill1 equation with the following EC_{50} value: 0.66 ± 0.10 µM (n=6). (B) Representative fluorescence time-response trace demonstrating the transient drop in fluorescence upon addition of liquid and subsequent data analysis. Baseline was established by reading the plate for 30 seconds. BD represents the drop in fluorescence from baseline following the addition of any solution to the wells, including buffer control (grey circle) and agonist (grey square). To account for this drop, BD is subtracted from all data points to generate new fluorescence values (black traces). All data points represent the mean ± SEM.

3.3.4.2 Pharmacological characterisation of Ivermectin B1a at the human GABA(A) overexpressing cell line

Given that IVM is known to activate human GABA(A) receptors, IVM-B1a was first tested and characterised as an agonist in the mouse L(tk-) cell line. As shown in Figure 3.46A, stimulating the cells with IVM-B1a increased the fluorescent signal in a concentration-dependant manner (0.01-500 µM), with maximal activity at 30 µM. The calculated EC_{50} was 1.74 ± 0.22 µM (n=7), making IVM significantly less potent as an agonist compared to GABA ($p<0.01$).

At a maximal concentration, IVM-B1a (10 µM) can elicit a fluorescent signal of 184.45 ± 12.74 FRUs (n=7) at 101.42% of the GABA (30 µM) response. The representative fluorescence time-response trace (Figure 3.46B) demonstrates that at a high concentration IVM-B1a (10 µM) can elicit an increase in fluorescent signal equivalent to GABA (30 µM), suggesting it acts as a full agonist at human GABA(A) receptor ($p>0.05$).

To further validate IVM-B1a as an agonist in the L(tk-) cells, another experiment was conducted to test that the fluorescent signal was dependent on GABA(A) receptor activity. To test this, cells were stimulated with a range of IVM-B1a concentrations (0.01-30 µM) in the absence of DEX (1 µM) treatment (Figure 3.47). All the IVM-B1a concentrations tested had a negligible effect ($p>0.05$ vs blank) on the fluorescent signal in L(tk-) untreated cells, whilst stimulation with GABA (30 µM) or IVM-B1a (10 µM) agonists significantly increased the fluorescent signal in DEX treated cells ($p<0.001$).

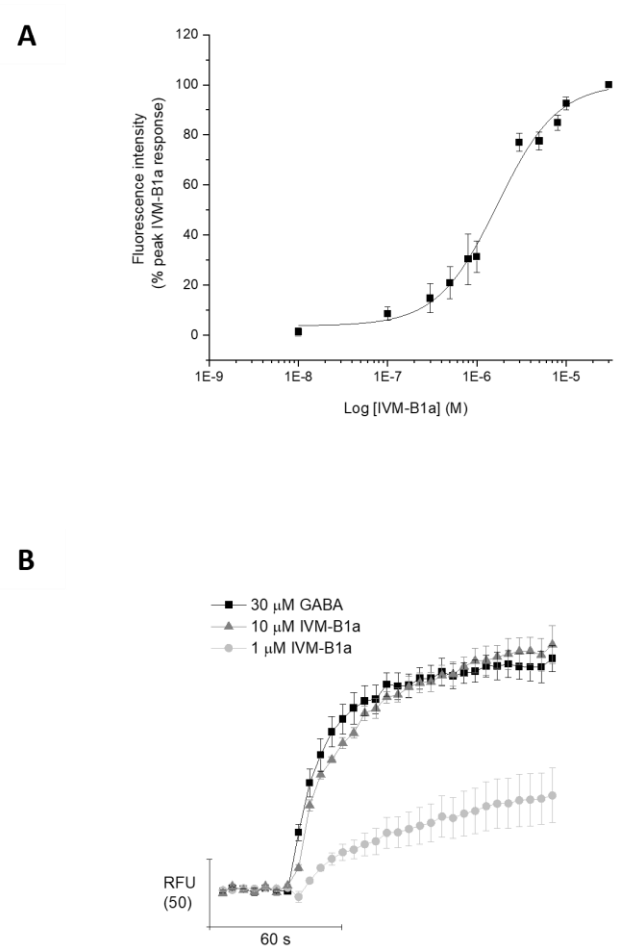

Figure 3.46. IVM-B1a activates human GABA(A) (α1β3γ2) receptor in mouse L(tk-) cells. (A) IVM-B1a concentration-response curve (0.01-30 μM) for human GABA(A) receptor based on fluorescent signal responses. All data was normalised to peak IVM-B1a response (30 μM) and fit to the Hill1 equation with the following EC_{50} value: 1.74 ± 0.22 μM (n=7). (B) Comparison of representative fluorescence time-response traces for cells stimulated with the agonists GABA (30 μM) and IVM-B1a (1 μM and 10 μM) for approx. 150 seconds (n=3). All data points represent the mean ± SEM.

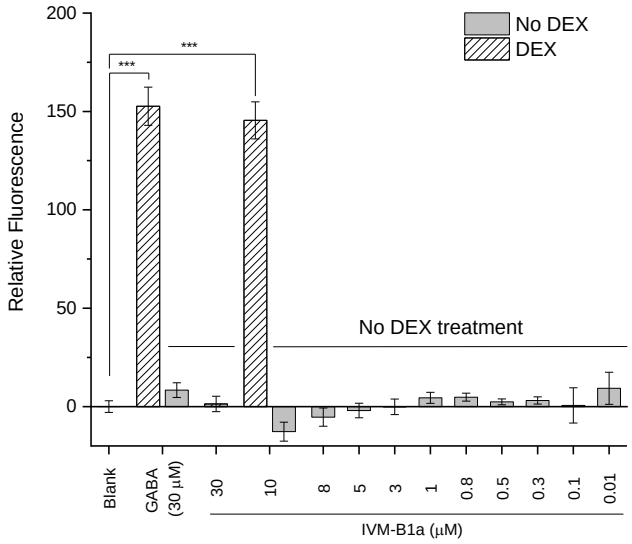

Figure 3.47. IVM-B1a-mediated fluorescence is dependent on dexamethasone (DEX) treatment in mouse L(tk-) cells. Bars represent fluorescent signal responses in the presence (striped) and absence (grey) of DEX (1 µM) when the cells are stimulated with either IVM-B1a (0.01-30 µM) or maximal GABA agonist (30 µM) (n=3). Asterisks show statistical significance relative towards blank (buffer control) with DEX treatment (***p<0.001). Each bar represents the mean of three independent biological assays; error bars are SEM.

3.3.4.3 Testing the selectivity of the IVM-analogues on the GABA(A) overexpressing cell line

Since both GABA and IVM-B1a have been validated and characterised as full agonists at the human GABA(A) receptor using the FMP-Red-Dye, the FLIPR assay was implemented to screen the IVM-analogue library. These compounds are listed in Table 3.4.

Each compound was screened at two fixed concentrations (1 µM and 10 µM) with a 10-fold difference to better indicate compound activity at the GABA(A) receptor. All compounds were tested using the same procedure outlined in the materials and methods section. E_{max} values were then calculated and summarised in Table 3.4 and described the degree of functional activity for each compound compared to 100% for the full agonist GABA (30 µM). For IVM-B1a, stimulating the cells with 1µM and 10 µM concentration generated fluorescent responses with a 2.9-fold activity difference at the GABA(A) receptor (34.65 ± 7.01% and 101.42 ± 1.65%, respectively).

In total, 33 IVM analogues were screened for agonist activity, as shown in Figure 3.48. It was found that over half of the compounds (54%) could increase the fluorescent signal by >70% at a high concentration (10 µM), suggesting they may be acting as full agonists at the human GABA(A) receptor. Interestingly, approximately 20% of the compounds had no activity at the human GABA(A) receptor. Of these compounds, two were identified as having activity at the human P2X4 receptor. This included compound **11** (Figure 3.11) and compound **12** (Figure 3.20). In addition, of those compounds that had limited activity at the human GABA(A) receptor (<70%), six had no activity at the P2X4 receptor.

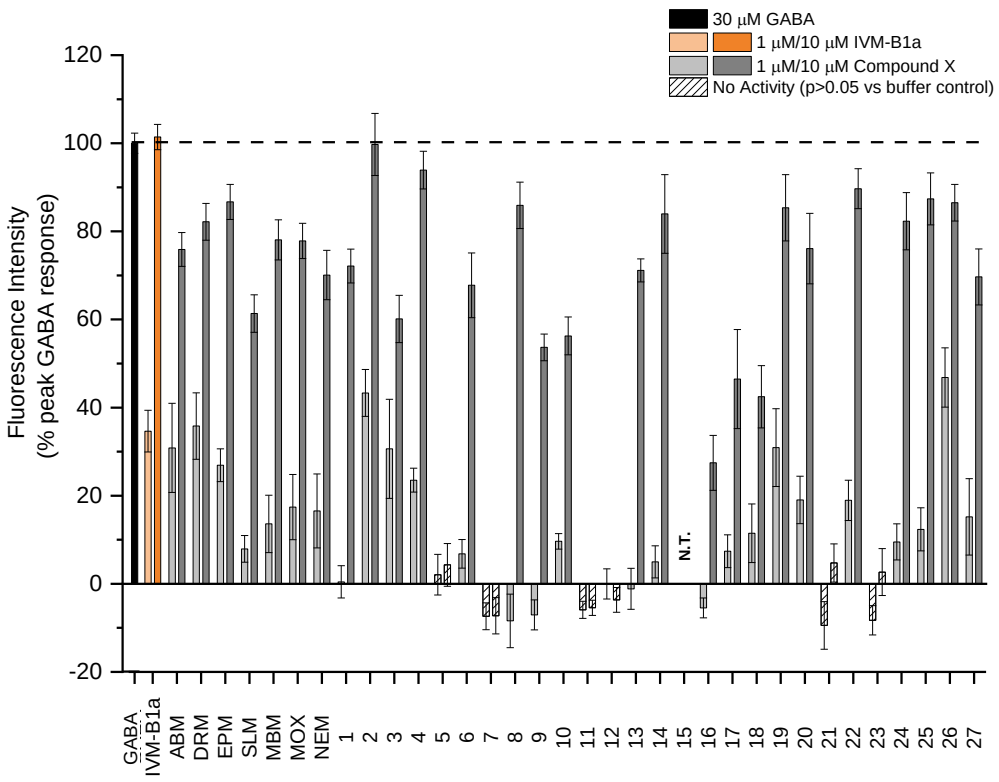

Figure 3.48. Activity screen of IVM-B1a and its analogues at the human GABA(A) (α1β3γ2) receptor in mouse L(tk-) cells. Bar chart showing the efficacy (E_{max}) of all IVM-analogues tested and the reference compound IVM-B1a (orange) at two fixed concentrations (1 μM and 10 μM). All cells were normalised to peak GABA response (30 μM; black). Compounds that did not potentiate the fluorescent signal (p>0.05 vs buffer control) were considered to have no activity at the human GABA(A) receptor (striped) (N=3-21). Each bar represents the mean of at least three technical repeats; error bars are SEM. N.T. = not tested.

Table 3.4. Functional activity data for the IVM-analogues at the human GABA(A) receptor (N=3-21).

Compound ID	Compound concentration (µM)	Efficacy (Maximal Fluorescence Intensity/E_{max}) (%) [α]	Significance (p-value) [β]
GABA	30	**100 ± 2.29**	p<0.001
IVM-B1a	1	34.65 ± 7.01	p<0.001
	10	**101.42 ± 1.65**	p<0.001
ABM	1	30.85 ± 10.12	p<0.05
	10	**75.90 ± 3.85**	p<0.001
DRM	1	35.81 ± 7.54	p<0.001
	10	**82.17 ± 4.16**	p<0.001
EPM	1	26.93 ± 3.72	p<0.001
	10	**86.68 ± 3.97**	p<0.001
SLM	1	7.92 ± 3.02	p<0.05
	10	61.35 ± 4.25	p<0.001
MBM	1	13.60 ± 6.53	n.s.
	10	**78.07 ± 4.56**	p<0.001
MOX	1	17.42 ± 7.40	n.s.
	10	**77.85 ± 4.00**	p<0.001
NEM	1	16.55 ± 8.40	n.s.
	10	**70.08 ± 5.61**	p<0.001
1	1	0.45 ± 3.66	n.s.
	10	**72.14 ± 3.84**	p<0.001
2	1	43.33 ± 5.34	p<0.001
	10	**99.73 ± 7.05**	p<0.001
3	1	30.63 ± 11.24	p<0.05
	10	60.12 ± 5.38	p<0.001
4	1	23.52 ± 2.71	p<0.001
	10	**93.90 ± 4.28**	p<0.001
5	1	2.07 ± 4.61	n.s.
	10	4.30 ± 4.84	n.s.
6	1	6.79 ± 3.24	n.s.
	10	67.77 ± 7.35	p<0.001
7	1	-7.37 ± 3.04	n.s.
	10	-7.24 ± 4.11	n.s.
8	1	-8.42 ± 6.07	n.s.
	10	**85.90 ± 5.27**	p<0.001
9	1	-7.05 ± 3.40	n.s.
	10	53.66 ± 3.02	p<0.001

n.s. = not significant (p>0.05); N.T. = not tested.

α = Activation compared to GABA (% of 30 µM GABA response). Data is presented as mean ± SEM. Compounds with E_{max} >70% are displayed in **bold**.

β = p-value is the statistical comparison between efficacy (E_{max}) of respected compound and blank response (buffer only) (*p<0.05, **p<0.01, ***p<0.001).

Table 3.4 (cont). Functional activity data for the IVM-analogues at the human GABA(A) receptor (N=3-21).

Compound ID	Compound concentration (µM)	Efficacy (Maximal Fluorescence Intensity/E_{max}) (%) [α]	Significance (p-value) [β]
10	1	9.64 ± 1.77	p<0.01
	10	56.27 ± 4.29	p<0.001
11	1	-5.90 ± 1.93	n.s.
	10	-5.44 ± 1.72	n.s.
12	1	-0.01 ± 3.42	n.s.
	10	-3.65 ± 2.78	n.s.
13	1	-1.14 ± 4.63	n.s.
	10	71.15 ± 2.61	p<0.001
14	1	4.989 ± 3.63	n.s.
	10	**83.96 ± 8.93**	p<0.001
15	1	N.T.	N.T.
	10	N.T.	N.T.
16	1	-5.48 ± 2.26	n.s.
	10	27.46 ± 6.24	p<0.01
17	1	7.40 ± 3.73	n.s.
	10	46.46 ± 11.25	p<0.01
18	1	11.47 ± 6.66	n.s.
	10	42.46 ± 7.06	p<0.001
19	1	30.93 ± 8.83	p<0.01
	10	**85.37 ± 7.52**	p<0.001
20	1	19.03 ± 5.39	p<0.05
	10	**76.08 ± 7.99**	p<0.001
21	1	-9.44 ± 5.39	n.s.
	10	4.73 ± 4.32	n.s.
22	1	18.94 ± 4.56	p<0.01
	10	**89.68 ± 4.53**	p<0.001
23	1	-8.27 ± 3.33	n.s.
	10	2.66 ± 5.31	n.s.
24	1	9.51 ± 4.09	n.s.
	10	**82.30 ± 6.50**	p<0.001
25	1	12.36 ± 4.86	p<0.05
	10	**87.39 ± 5.90**	p<0.001
26	1	46.84 ± 6.74	p<0.01
	10	**86.51 ± 4.17**	p<0.001
27	1	15.19 ± 8.68	n.s.
	10	69.66 ± 6.35	p<0.001

n.s. = not significant (p>0.05); N.T. = not tested.

α = Activation compared to GABA (% of 30 µM GABA response). Data is presented as mean ± SEM. Compounds with E_{max} >70% are displayed in **bold**.

β = p-value is the statistical comparison between efficacy (E_{max}) of respected compound and blank response (buffer only) (*p<0.05, **p<0.01, *** p<0.001).

3.4 Discussion

3.4.1 Validating the 1321N1-hP2X4R expressing cell line

The focus of this study was to determine the SAR of IVM-B1a against the human P2X4 receptor using a range of structural analogues and identify important functional groups for PAM activity. As previously discussed, the cellular model used in this study was the human 1321N1 astrocytoma cell line, chosen since it is one of the few cell lines that does not express functional P2 receptors (Filtz et al*.,* 1994). Due to this reason, the potentiating effect of ATP on intracellular Ca^{2+} was specific to human P2X4, which has been stably expressed in the parental 1321N1 cell line (Figure 3.1). Construction of an ATP concentration-response curve using the calcium mobilisation assay generated an EC_{50} of 0.5 ± 0.03 µM. This agreed with the literature, with ATP EC_{50} values reported between 0.2 µM to 1 µM for human P2X4 receptor expressed in 1321N1 cells (Bianchi et al*.,* 1999; Abdelrahman et al*.,* 2017; Sophocleous et al*.*, 2020; Weinhausen et al., 2022). Further cell line validation was carried out using planar patch-clamp electrophysiology, generating an ATP EC_{50} value of 2.61 ± 1.0 µM. Previous studies that used electrophysiological approaches produced similar EC_{50} values for both human (1.4 µM) and rat (2.3 µM) P2X4 receptors in HEK293 cells (Jones et al*.,* 2000; Zemkova et al., 2015). Both techniques measure P2X4 activity differently but are often used interchangeably in science to investigate ion channel activity. Electrophysiology measures the electrical current across the membrane, whilst Ca^{2+} mobilisation assays measure intracellular Ca^{2+} influx. Encouragingly, both techniques have generated an ATP EC_{50} value at the low micromolar range, the small difference between them likely reflecting the varying assay conditions.

At present, Ivermectin (IVM) is the best-known PAM of the P2X4 receptor. In this study, IVM-B1a has been shown to potentiate the ATP-evoked Ca^{2+} response in a concentration-dependent manner (Figure 3.4B). The calculated EC_{50} value was 0.79 ± 0.07 µM. This is close to previous studies that, using electrophysiology, showed IVM could amplify the ATP-evoked current of P2X4 receptors with an EC_{50} value of approximately 0.3 µM (Khakh et al., 1999; Priel and Silberberg, 2004; Gao et al., 2015; Weinhausen et al., 2022). Ivermectin is a mixture of two homologues; C25-ethyl (95%) and C25-methyl (5%), referred to as IVM-B1a and IVM-B1b. Most of the compound library investigated in this study are structural derivates of the primary component, IVM-B1a. This led to the characterisation of both IVM components at the P2X4 receptor, with the intention of making IVM-B1a the reference compound. Both compounds could potentiate the ATP-evoked Ca^{2+} response and were found to be equal in both potency and efficacy ($p>0.05$). Interestingly, both compounds were proven to be equipotent to IVM. However, the maximal response was significantly lower, only potentiating the ATP-evoked Ca^{2+} response to 70.35% and 64.08% of the IVM response for IVM-B1a and IVM-B1b, respectively. This suggests that combining IVM-B1a and IVM-B1b has a synergic effect and could be investigated further by mixing the individual compounds to the same ratio as IVM. A possible explanation for this could be that each homologue is binding to a different allosteric binding site within the P2X4 receptor, and a mixture of both molecules results in optimal PAM activity.

In addition, several compounds investigated in this study promoted high fluorescent values (loading values) in the cells at high concentrations. These measurements are taken by the FlexStaton-3 reader after the cells have been incubated with the corresponding compound for approximately 30 minutes at the start of the experiment, giving an indication of the resting intracellular calcium level in the cell before ATP-stimulation. Elevation of these values suggests that the compounds are affecting the resting intracellular Ca^{2+} levels. A possible explanation for this is that the compound is acting as an agonist for the P2X4 receptor at high concentrations, promoting the influx of calcium ions into the cell before ATP can be applied. In addition, the literature states that IVM can modulate other calcium-handling proteins in the cell (Ahern et al., 1999; Bilmen et al., 2002). This includes inhibiting the Ca^{2+}-ATPase (SERCA) pumps in the endoplasmic reticulum (Bilmen et al., 2002). By blocking Ca^{2+} reuptake from the stores, IVM might be triggering a rise in intracellular calcium in the cell which might explain the high loading values observed for some of the IVM-analogues. Although this response is not seen following IVM-B1a incubation, some of the IVM-analogues (specifically MBM and NEM, and compounds **2**, **4**, **6**, **8**, **11**, **13**, **20** and **27**) might have high affinity for the SERCA pumps. To test if this effect on cytosolic calcium is P2X4-dependant, the identified compounds could be incubated for 30 minutes in the parental cell line, which is devoid of the P2X4 receptor. If the resulting loading values remain elevated, then the effect of these compounds on cytosolic calcium would be independent of P2X4 and would warrant further investigation to understand the mechanism involved.

3.4.2 Investigating the structure-activity relationship (SAR) of IVM-B1a against the human P2X4 receptor

This study aimed to characterise the SAR of IVM-B1a by looking at a library of structural analogues which introduce different substituents to three areas of the molecule (R1, R2 and R3) (Figure 3.6). As detailed earlier in the chapter, the biological activity of these compounds as PAMs for the P2X4 receptor was measured using fluorescent calcium mobilisation assays. For each analogue, the potency (EC_{50}) and efficacy (E_{max}) from the resulting concentration-response curve were calculated and statistically compared to the reference compound IVM-B1a. Any trends relating the chemical structure to the biological activity among the collection of compounds were documented and assessed to determine the SAR between IVM-B1a and the human P2X4 receptor.

3.4.2.1 Structural modifications at R1 (Disaccharide)

Firstly, a limited set of compounds were studied with different substituents on the disaccharide moiety (Figure 3.49) (R1). The most helpful finding in defining a SAR for IVM-B1a at P2X4 was that the disaccharide substituent is not essential for P2X4 activity. This was demonstrated through milbemectin (MBM), a structurally related milbemycin that lacks the disaccharide substituent, which was found to be equally potent and efficacious as IVM-B1a. This suggests that the disaccharide moiety isn't making any important contacts with the binding site and could be pointing out into the solvent. Therefore, the disaccharide moiety could be removed from the IVM-B1a scaffold in the design of novel drug candidates.

The remaining three compounds investigated in this section have substituent groups added to the end of the disaccharide moiety, displacing the polar hydroxyl group, and have neutral, beneficial, and detrimental impacts on P2X4 activity. Compound **2** and compound **11** have phosphate group additions to C4" and were found to be equipotent to IVM-B1a. In terms of potentiating the ATP-evoked Ca^{2+} response, compound **2**, which has a monosodium phosphate group at C4", displayed equal efficacy to IVM-B1a. In contrast, compound **11**, which has a methyl phosphate group at C4", could only potentiate the Ca^{2+} response to 52% of the IVM-B1a response ($p<0.05$). The reduced activity of this compound suggests a less favourable drug-receptor interaction and, thus, a significantly reduced maximal response. If the disaccharide is pointing out into the solvent, this reduced activity could be because the methyl phosphonate is introducing a hydrophobic moiety, making the solvent-exposed disaccharide less favourable. Lastly, compound **26** has a relatively neutral succinic acid addition to C4" and significantly potentiated the ATP-evoked calcium response to 141% of the IVM-B1a response ($p<0.05$). However, compound **26** was discovered to have markedly lower potency than IVM-B1a ($p<0.001$), making it both beneficial and detrimental to efficacy and potency at the P2X4 receptor. This suggests that the disaccharide moiety is making contacts with the binding pocket to some degree when structural modifications are added and influences drug activity.

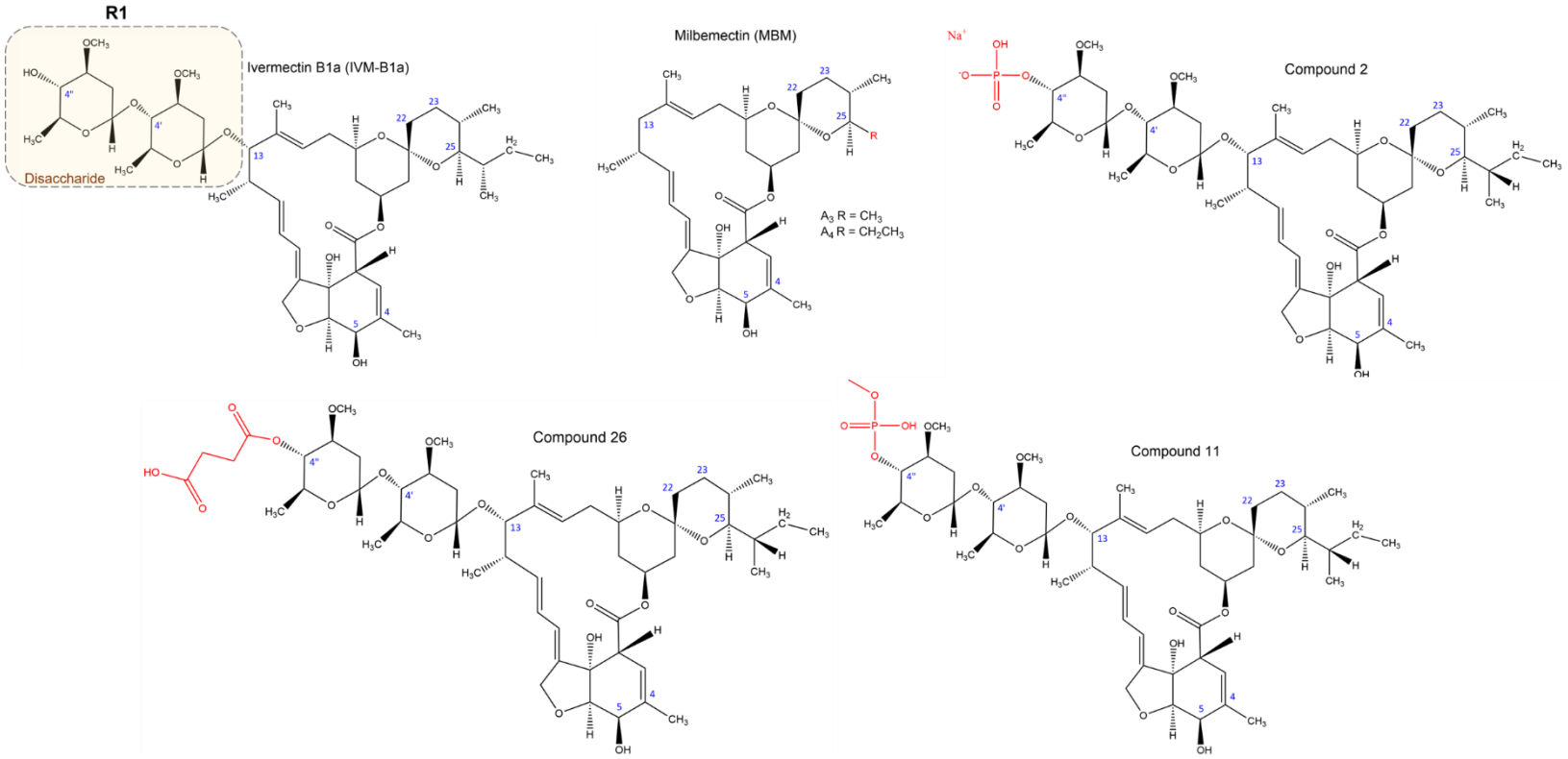

Figure 3.49. Structures of the IVM-analogues with structural modifications within the disaccharide moiety (R1). Structural changes from the reference compound IVM-1a are highlighted in red. Blue numbers represent the C-positions, based upon IVM-B1a numbering.

3.4.2.2 Structural modifications at R2 (Spiroketal)

Next, thirteen IVM-analogues were investigated with different substituents to the spiroketal group (R2) (Figure 3.50). Interestingly, it was found that a double bond in the C22-23 position confers significantly greater biological activity at the P2X4 receptor. Abamectin (ABM) is structurally identical to IVM-B1a and differs only by having a double bond at the C22-23 position. ABM was found to be significantly more potent than IVM-B1a ($p<0.01$) and, at high concentrations, could potentiate the ATP-evoked Ca^{2+} response to 247% of the IVM-B1a response ($p<0.001$), making it one of the highest-ranking compounds tested in terms of efficacy and potency (Table 3.2 and 3.3, respectively). Given that the double bond is the only structural change, it suggests that it is crucial for enhanced activity at the P2X4 receptor. This could be due to a distortion of the shape of the 6-membered ring, making it more planar, which may result in the compound fitting better into the pocket.

The importance of the double bond is also demonstrated by doramectin (DRM), which possesses a double bond in the C22-23 position and a cyclohexane group displacing the side chain of C25. DRM was found to be significantly more potent ($p<0.01$) and efficacious ($p<0.01$) compared to IVM-B1a, potentiating the ATP-evoked calcium response to 164% of the IVM-B1a response. However, unlike ABM, the response drops off at high concentrations (3, 5 and 10 μM). This data suggests that while the double bond confers greater biological activity at the P2X4 receptor, the additional cyclohexane ring could hinder DRMs ability to potentiate the ATP-evoked Ca^{2+} response to the same degree as ABM at high concentrations. Tolerance of the bulky cyclohexane ring supports the hypothesis that the spiroketal group is buried in the binding site since it is highly hydrophobic and could be filling a spacious centre of the pocket.

It was also discovered that the stereochemistry of IVM-B1a has an apparent effect on the PAM activity. IVM-B1a has a total of 20 stereocenters (Serafini et al., 2020). These are carbon atoms attached to four different groups, giving non-superimposable centres that lead to the formation of a pair of stereoisomers. Both compounds **13** and **19** are stereoisomers of each other. In addition, both compounds have the same formula and constitutional structure as IVM-B1a and could also be stereoisomers of IVM-B1a. Interestingly, this subtle change in the spatial orientation of the molecules leads to two very different effects on compound activity at the P2X4 receptor. Compound **19** had a more beneficial stereochemical configuration, as it was found to be equal in potency to IVM-B1a and significantly more efficacious, potentiating the Ca^{2+} response to 148% of the IVM-B1a response ($p<0.05$). On the other hand, compound **13** was found to be equally efficacious but suffered a significant loss in potency ($p<0.01$). Since IVM-B1a has an unusually high number of chiral centres, careful considerations regarding the 3D molecular structure must be taken when developing new drugs, as different stereoisomers can lead to substantial differences in biological activity.

Compound **14** appears to have the same structure as the minor component of IVM (IVM-B1b), which has a methyl group (CH_3) attached to the C25 side chain within the spiroketal group. Not surprisingly,

compound **14** did not differ in terms of potency or efficacy from IVM-B1b, suggesting they have identical structures, both in terms of stereochemistry and physical and chemical properties.

Furthermore, several structural derivates show a trend that upon the addition of a hydroxyl or carbonyl group to C23, the drug loses all biological activity at the P2X4 receptor. A compound is considered to have no activity at the P2X4 receptor if it cannot significantly potentiate the Ca^{2+} response upon stimulation with submaximal ATP (0.3 μM). This is the case for compounds **9**, **21** and **23**, which have a hydroxyl group addition to C23, and compound **3**, which has a carbonyl group addition to C23. Both functional groups are highly hydrophilic, supporting the hypothesis that R2 is pointing into the hydrophobic binding pocket. If this is the case, disrupting the spiroketal group's hydrophobic nature would be highly unfavourable for compound-receptor binding and its biological activity. A loss of activity is also observed for compound **16**, which incorporates two fluorine atoms at carbon 23. In general, halogen substituents increase the lipophilicity of a drug, but fluorine atoms can have varying effects on the solubility and are highly electronegative. Due to its electron-withdrawing properties, fluorine is widely used in medicinal chemistry to boost a drug's biological activity and metabolic stability (Shah and Westwell, 2007; Gillis et al., 2015). In this study, the fluorine substituents at C23 were not tolerated. This could be due to steric hindrance, but given the small size of these atoms, it is more likely to be a result of fluorine's electronegativity disrupting molecular interactions within the binding site, especially since the spiroketal group appears to be critical for influencing the primary pharmacology of IVM-B1a at the P2X4 receptor.

Three compounds investigated had substituents added to C23 and retained PAM activity at the P2X4 receptor. This included compound **1**, which has a hydroxyl group and methyl group addition at C23 and was found to have a similar biological activity to IVM-B1a ($p>0.05$). This could be because of the presence of the hydrophobic methyl group, masking any unfavourable polar interaction from the hydroxyl group. Compound **25** has a methyl ester group addition to C23 and experienced a significant drop in potency ($p<0.001$). This was countered by a significant increase in drug efficacy, potentiating the ATP-evoked Ca^{2+} response to 164% of IVM-B1a response ($p<0.01$). Although ester groups are lipophilic, they are still polar molecules that could interfere with hydrophobic interactions, making the initial binding less favourable. However, once the drug has bound to the allosteric site, adding an ester group to the C23 position leads to an increase in maximal response (efficacy), which could result from new intermolecular interactions. Lastly, compound **12** has relatively poor biological activity with a significant reduction in both compound potency ($p<0.05$) and efficacy ($p<0.01$). Compound **12** has an acetamide group at C23. As with the methyl ester substituent, acetamide groups are considered lipophilic but capable of forming hydrogen bonds due to their polarity. However, the acetamide group is less favourable than the methyl ester substituent. This could be because acetamide groups are less reactive and therefore, cannot form any new interactions at the binding site. Overall, the C23 position can tolerate additions but only if they retain some of the hydrophobic nature of the spiroketal group (R2). Again, this supports the hypothesis that R2 is situated deep in the ligand-binding pocket of the P2X4 receptor.

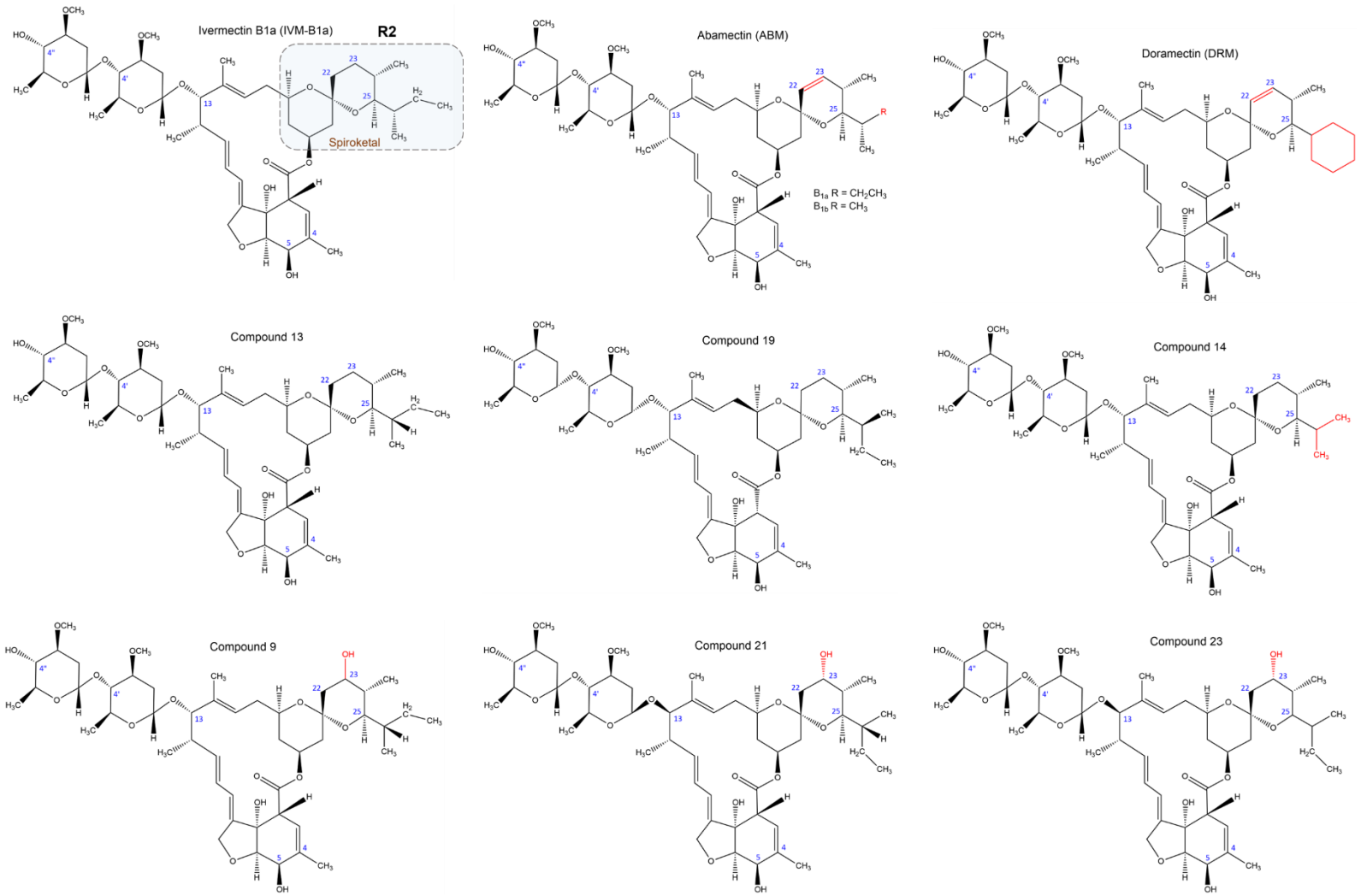

Figure 3.50. Structures of the IVM-analogues with structural modifications within the spiroketal moiety (R2). Structural changes from the reference compound IVM-1a are highlighted in red. Blue numbers represent the C-positions, based upon IVM-B1a numbering.

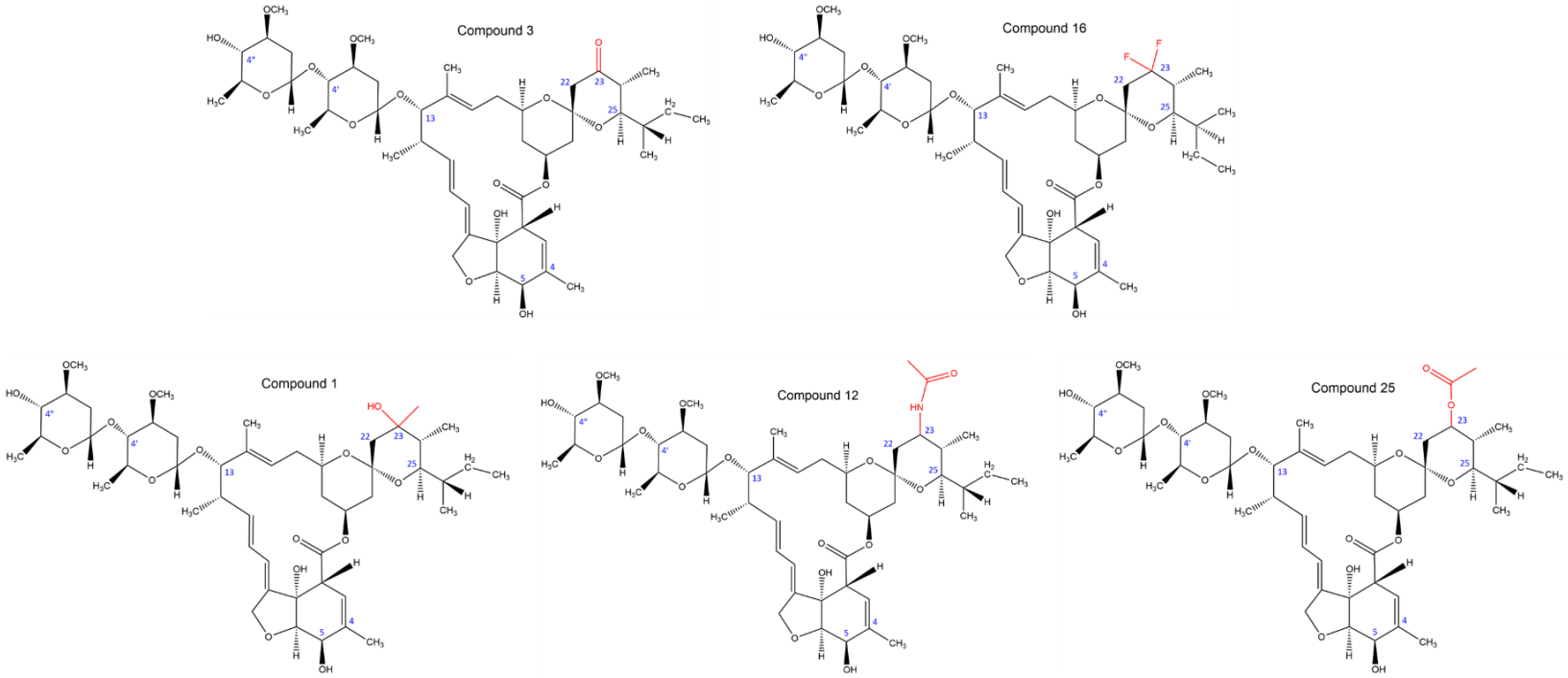

Figure 3.50 (cont.). Structures of the IVM-analogues with structural modifications within the spiroketal moiety (R2). Structural changes from the reference compound IVM-1a are highlighted in red. Blue numbers represent the C-positions, based upon IVM-B1a numbering.

3.4.2.3 Structural modifications at R3 (Benzofuran)

For the last region of the molecule, the benzofuran moiety (R3), it was discovered that large additions are well tolerated and that the C5-hydroxyl group might play a role in maintaining drug potency (Figure 3.51). Firstly, looking at the relevance of the C5 position on the benzofuran ring, compound **22** has displaced the hydroxyl group with a methyl ether (methoxy group). Compound **22** was found to potentiate the ATP-evoked Ca^{2+} response to a similar extent as IVM-B1a but suffered a significant loss in drug potency ($p<0.001$). Since hydroxyl groups are commonly involved in hydrogen bonding, this suggests that the methyl ether disrupts or prevents this interaction with the binding site, hence a drop in drug potency. One explanation is that the hydrogen (hydrogen bond donor) in the original hydroxyl group plays a role in hydrogen bonding which is lost when substituted for the methyl ether. Another reason could be that the methyl group hinders the region from getting close enough to the binding site to establish hydrogen bonding via the oxygen (hydrogen bond acceptor) (Clayden and Greeves, 2012).

Furthermore, compounds **8** and **27** have succinic acid additions to the C5 position and C4 side chain, respectively. Notably, both drugs retained their PAM activity at the P2X4 receptors and were close in potency and efficacy to IVM-B1a. If the benzofuran group is involved in hydrogen bonding, then swapping out the original C5-hydroxyl group with another polar functional group would be expected to have little consequence on drug activity. However, succinic acid is bulkier than an alcohol group, and its acceptance suggests space within the binding pocket to accommodate bulkier additions. This hypothesis is supported by compound **4,** which has a long ester chain, called a 2-Methoxyethoxymethyl (MEM) group attached to the C4 side chain, yet it maintains similar biological activity to IVM-B1a ($p>0.05$). These groups are commonly used in organic chemistry to protect a more reactive site, such as a hydroxyl group. The last derivative to have a substitution at the C4 side chain, compound **24**, also maintains similar biological activity to IVM-B1a at the P2X4 receptor ($p>0.05$). The compound has a hydroxyl group at the end of the alkyl C4 side chain. Since compounds **24** or **4** did not result in any gain of biological activity, it suggests that substituting the methyl group (CH_3) at the C4 side chain for an oxygen-containing substituent (hydroxyl group or a MEM group, respectively) does not promote any new molecular interactions, nor did it disrupt any essential interactions for drug activity. Moreover, tolerance of the MEM protecting group supports the existence of ample space within the binding pocket.

The two derivatives with the largest structural modifications to the benzofuran region (R3) are compounds **20** and **6**. Compound **20** has a sizeable lipophilic group, a tris (2,2,2 tri-chloroethyl) phosphate ester group, attached to the C5 position, but its biological activity was only slightly diminished compared to IVM-B1a ($p>0.05$). This supports the hypothesis that the benzofuran group could point out of the binding pocket to accommodate such a large addition. However, compound **6** does not conform to this trend. Interestingly, compound **6** has a similar substituent, a tris(2,2,2 tri-chloroethyl) phosphate group, attached to the same position but could not significantly potentiate the ATP-evoked Ca^{2+} response. A possible explanation could be that the ester linkage, the only

structural difference between compounds **20** and **6**, is involved in a critical molecular interaction. By removing it, this interaction is lost.

To conclude, the benzofuran region can tolerate large structural additions with various chemical properties, suggesting that R3 can accommodate large functional groups without disrupting critical binding interactions. In addition, the C5 position might be involved in hydrogen bonding with the binding pocket, as substituting this site with less polar substituents was detrimental to the drug's biological activity, as seen in compounds **22** and **6**. Altogether this suggests that the benzofuran group is participating in molecular interactions at the C5 position and could be partially pointing out of the binding pocket to accommodate large structural additions.

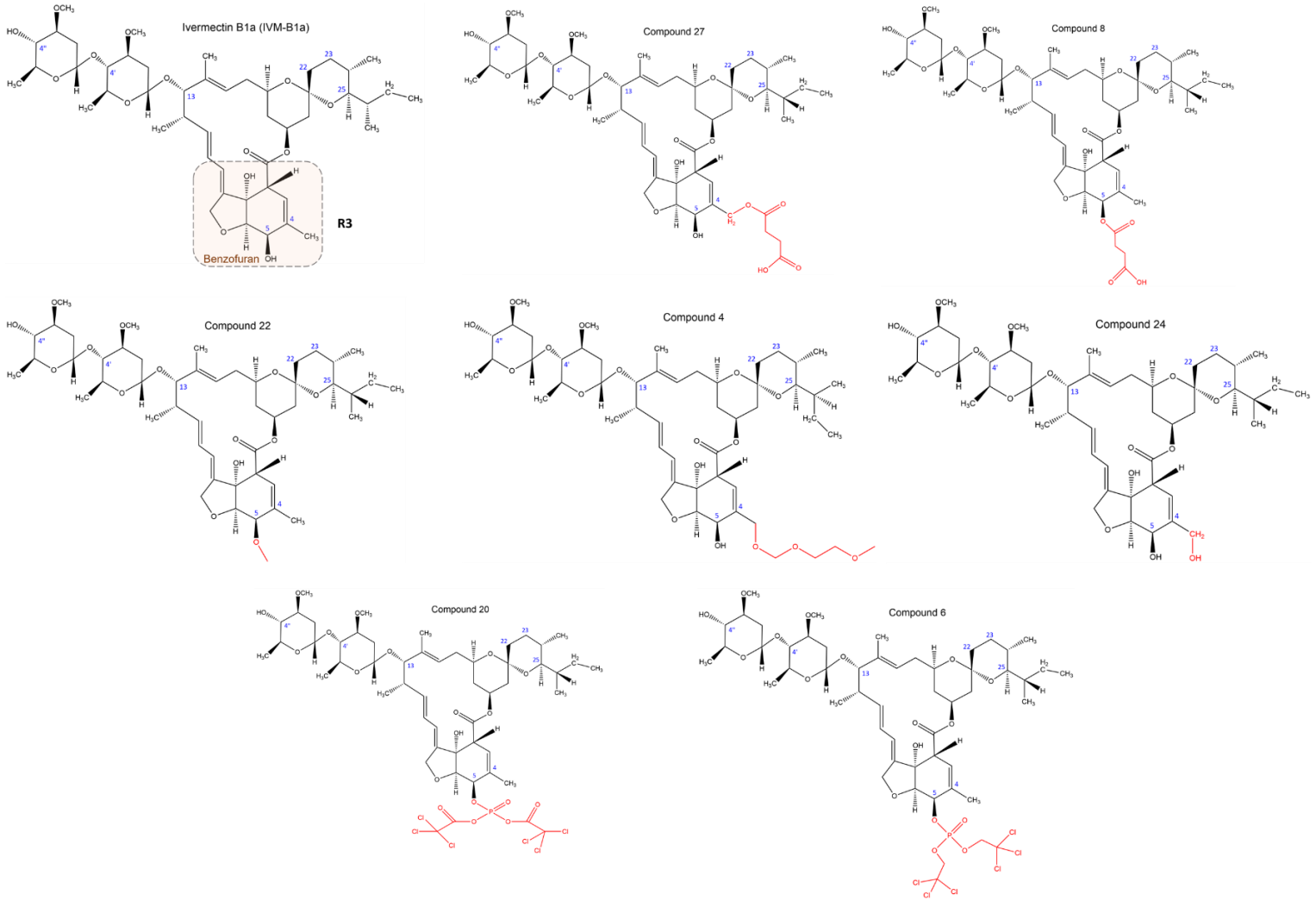

Figure 3.51. Structures of the IVM-analogues with structural modifications within the benzofuran moiety (R3). Structural changes from the reference compound IVM-1a are highlighted in red. Blue numbers represent the C-positions, based upon IVM-B1a numbering.

3.4.2.4 Multiple structural modifications at two or more regions (R1, R2, and R3)

Lastly, focusing on those compounds with structural modifications in two or more regions, several SAR trends identified earlier in the study were reinforced. Eprinomectin (EPM) differs structurally from IVM-B1a through a double bond at the C22-23 position and an acetamide group displacing the hydroxyl at the C4" position. Based on ABM and DRM, the other two commercial analogues with a double bond in this position, a substantial gain of biological activity would be expected through enhanced potency and efficacy at the P2X4 receptor. However, for EPM, the biological activity was maintained. An earlier trend was found that additions to the disaccharide moiety are tolerated and can have various effects on drug activity. Moreover, the removal of the disaccharide group did not affect the biological activity at the P2X4 receptor, suggesting that this group is pointing out of the binding pocket into the solvent. If this hypothesis is correct, substituting a hydroxyl group for an acetamide, with reduced polarity and overall low hydrophilicity, would be unfavourable. For EPM, this could be cancelling out any additional activity gained through the presence of the double bond.

Selamectin (SLM) also maintained biological activity at the P2X4 receptor. Notably, SLM had three structural changes in all three regions of the molecule. The largest is a cyclohexane addition to C23 (R2). As with DRM, adding a large aliphatic ring to the spiroketal group is well-tolerated, supporting the hypothesis that the spiroketal group is buried deep in the hydrophobic binding site. In addition, SLM lacks one of the sugar moieties (R1). Despite this, the polar and hydrophilic nature of R1 is maintained with a hydroxyl group at the C4" position, and earlier results have shown the removal of the disaccharide moiety to have no impact on the PAM activity. This implies that removing one of the sugar moieties would have little impact on drug activity. Lastly, SLM displaces the hydroxyl group at the C5 position in the benzofuran group (R3) with a ketoxime. Since this group retains much of the same chemical properties and can still potentially interact with the binding site via hydrogen bonding, minimal impact on drug activity would be expected.

Next, the last two milbemycins were investigated, moxidectin (MOX) and nemadectin (NEM). Both compounds lack the entire disaccharide moiety (R1) and have structural modifications within the spiroketal group (R2). MOX has enhanced activity at the P2X4 receptor, achieving significantly higher potency than IVM-B1a ($p<0.001$). Likewise, NEM was found to be significantly more potent than IVM-B1a ($p<0.05$) but was also able to potentiate the ATP-evoked Ca^{2+} response to 205% of the IVM-B1a response, making it the second most efficacious compound tested ($p<0.01$; Table 3.2). As well as missing the disaccharide moiety, both compounds possess a dimethyl-butyl group at the C25 position, which appears beneficial for PAM activity. This could be because the dimethyl-butyl group contains a double bond and multiple methyl groups. This makes the spiroketal group (R2) more stable and lipophilic, strengthening any hydrophobic interactions with the binding site. This agrees with the trends outlined so far. First, the disaccharide moiety is not required to achieve optimal PAM activity at the P2X4 receptor. Second, the spiroketal group favours lipophilic additions because it is located deep in the hydrophobic binding pocket.

The last structural modification for MOX and NEM occurs at the C23 position within the spiroketal group. Previous data from this study has shown that adding a polar, hydrophilic substituent to the C23 is highly unfavourable. Specifically, hydroxyl and carbonyl groups at this position are not tolerated. NEM, a naturally occurring milbemycin, has a hydroxyl group at the C23 position and is an exception to the trend. The lack of the disaccharide could be changing how the compound fits within the binding pocket. Likewise, MOX, the semi-synthetic derivative of NEM, has a methoxime group addition to the C23 position. This functional group has similar properties to the hydroxyl group, being a polar molecule, and is well tolerated.

So far, for the non-commercial compounds, when looking for SAR trends, substituents have been altered or added one at a time to the molecule. This systematic approach provides a way to identify which substituents are beneficial and which are not. However, in this case, due to the compounds having varying substituents, it is harder to pinpoint which substituents are good for activity. It is also possible for two substituents that are individually bad for the activity to have a synergistic beneficial effect when they are both present and vice versa. This needs to be considered when analysing these compounds.

In total, for the non-commercial compounds, six of the structural derivates investigated had substituents in all three regions of the molecule (R1, R2 and R3). Five of these failed to significantly potentiate the ATP-evoked Ca^{2+} response and, thus, were considered to have lost all biological activity at the P2X4 receptor. Notably, three of these drugs had a carbonyl group (compounds **5**, **15** and **17**), and one a hydroxyl group (compound **7**) at the carbon 23 position. This agrees with the SAR trend previously highlighted; the presence of either a hydroxyl or carbonyl group in the C23 position is not tolerated. However, due to these drugs having changes in multiple regions of the molecule, it is difficult to discern if this modification alone was responsible for the loss of PAM activity.

Focussing on the other modifications within these compounds, compound **17** had the smallest number of varying substituents, with only a carbonyl group at the C23 position and a methyl ester group at the C5 position, displacing the hydroxyl group. In medicinal chemistry, polar functional groups can be masked by converting an alcohol group into a less polar ether or ester group, along with an alkyl group, to act as a steric shield, which might disrupt important binding interactions between the drug and its target (Clayden and Greeves, 2012). This was thought to occur in compound **22** by substituting a hydroxyl group with an ester which resulted in a significant drop in drug potency (see section 3.4.2.3). This could also be happening in compound **17**. Furthermore, compound **15** has a larger addition to the C5 position, a phenyl ring attached by an oxygen atom. This substituent would have a much greater hydrophobic effect and likely contribute to the loss of drug activity.

On the other hand, compounds **5** and **7** have structural additions to the disaccharide (R1) and the benzofuran (R3) moiety in addition to the carbonyl/hydroxyl group at carbon 23 (R2). Compound **5** has the largest additions, with three tert-butyldimethylsilyloxy groups displacing all three hydroxyl groups in the molecule (C4”, C7 and C5 position). This modification consists of a bulky alkyl group

covalently bound to a central silicone atom and is highly hydrophobic. Likewise, compound **7** has two bulky aromatic groups (phenoxy acetate) substituting the hydroxyl groups at the C4" and C5 position. To conclude, both compounds **5** and **7** have hydrophobic substituents that will increase the overall size and hydrophobicity of the molecule and likely interfere with ligand-drug interactions. This suggests that the unfavourable interaction at C23 might not be the sole determinant for the loss of drug activity for compounds **5** and **7** at the P2X4 receptor.

The last compound found to have no activity at the P2X4 receptor was compound **18**. Interestingly this compound did not have a carbonyl or hydroxyl addition at the C23 position, but two large substituents, a tert-butyldimethylsilyloxy group and a 2,2,2 tri-chloroethyl succinate group, attached to the C5 (R3) and C4" (R1) position, respectively. An earlier hypothesis was that the disaccharide group was pointing out of the binding site. By substituting a polar hydroxyl group with a 2,2,2 tri-chloroethyl succinate group, the lipophilicity of the molecule increases due to the extra alkyl groups and the chlorine atoms, making any hydrophilic interactions between the solvent and the molecule less favourable. Likewise, substituting another polar hydroxyl group at the C5 position for a bulky hydrophobic group is likely hindering any polar interactions between the compound and the binding site, changing how the molecule fits inside the binding pocket, if at all. Together, both substituents reduce the overall hydrophilicity of the molecule and are both likely contributing to the loss of PAM activity at the P2X4 receptor.

The only compound in this group that was able to retain biological activity to a similar extent as IVM-B1a was compound **10**. This is not surprising since it only has two small methyl ether groups attached to the side chain of the C4 position in the benzofuran ring (R3) and displacing the hydroxyl at the C4" position of the disaccharide moiety (R1). Based on previous SAR trends identified in this study, these changes would not be expected to affect drug activity significantly. For example, compound **4** (see section 3.4.2.3) maintains full biological activity at the P2X4 receptor despite having a more extended ester group at the C4 position. Likewise, although results so far indicate that masking the polar hydroxyl group with a lipophilic group at the C4" position is unfavourable, the methyl ether is a very small and, albeit weak, polar modification. Therefore, it would be expected to have little or no impact on drug activity.

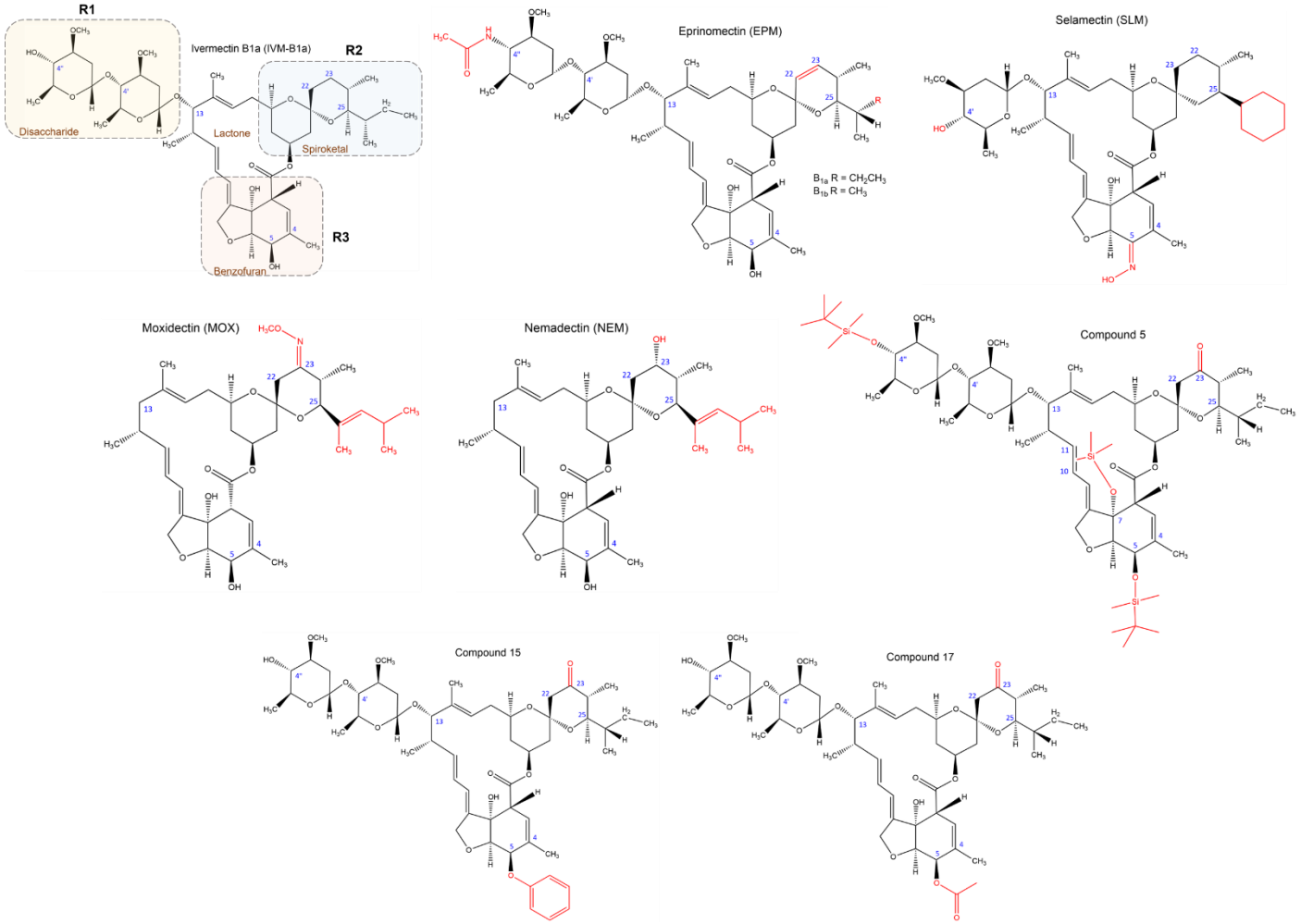

Figure 3.52. Structures of the IVM-analogues with multiple structural modifications at two or more regions (R1, R2, and R3). Structural changes from the reference compound IVM-1a are highlighted in red. Blue numbers represent the C-positions, based upon IVM-B1a numbering.

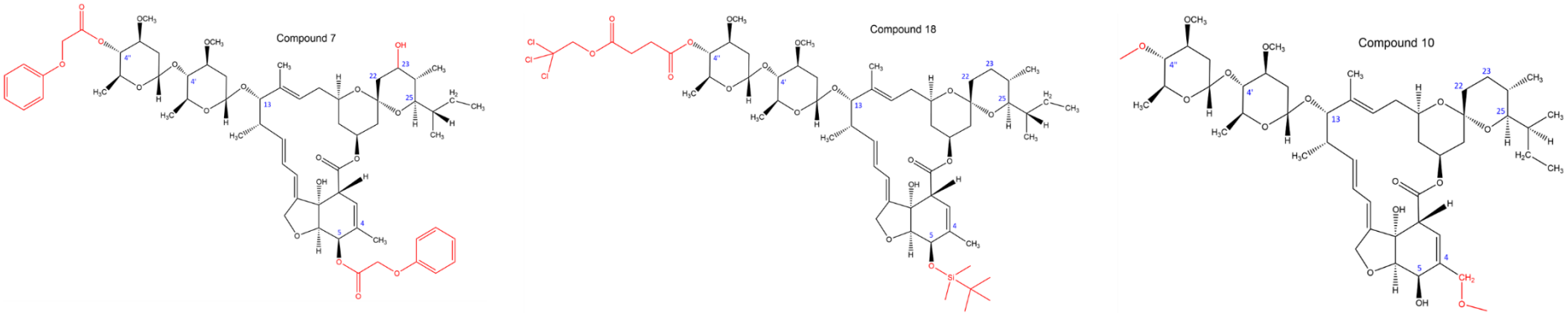

Figure 3.52 (cont.). Structures of the IVM-analogues with multiple structural modifications at two or more regions (R1, R2, and R3). Structural changes from the reference compound IVM-1a are highlighted in red. Blue numbers represent the C-positions, based upon IVM-B1a numbering.

3.4.2.5 Summary of the SAR analysis

Overall, the general trends of the SAR analysis of IVM-B1a are summarised in Figure 3.53. Firstly, with respect to the disaccharide moiety (R1) of IVM-B1a, the following SARs were found:

I. The disaccharide substituent is not essential for drug activity at the P2X4 receptor
II. Structural additions to the end of the disaccharide moiety are tolerated.

Regarding the spiroketal moiety (R2) of IVM-B1a, the following SARs were identified:

I. A double bond in the C22-23 position confers significantly greater potency and efficacy at the P2X4 receptor.
II. Addition of a hydroxyl or carbonyl group to the C23 position is not tolerated.
III. Structural additions to the C23 position are tolerated, but hydrophobic substituents are more favourable.

Lastly, concerning the benzofuran moiety (R3), the following SARs were found:

I. Large structural additions to this region were well tolerated.
II. The hydroxyl group at the C5 position might play a role in drug potency.

Overall, the SAR analysis suggests that the spiroketal group (R2) encompasses the most active part, the pharmacophore, of the molecule. This refers to the minimal part of the molecule responsible for producing a particular biological effect, in this case, allosteric potentiation of the human P2X4 receptor. This region appears to be the most sensitive to structural changes. It favours hydrophobic additions, such as cyclohexane rings, alkyl chains and double bonds, which could participate in hydrophobic interactions with the binding site. Conversely, adding polar functional groups such hydroxyl, carbonyl and fluorine atoms to the spiroketal group, specifically to C23, is highly unfavourable. Identifying and fully comprehending how the pharmacophore interacts with the binding site is critical in designing novel drugs. A future step would be to find or synthesise analogues that contain the same pharmacophore with improved properties, such as better biological activity and selectivity. In this study, 7 compounds were found to be significant more efficacious then IVM-B1a, this included four of the commercial analogues (ABM, NEM, DRM and IVM), and three of the non-commercial analogues (compounds **19**, **25** and **26**). For potency ranking, only four compounds were significantly more efficacious then IVM-B1a, all being commercial analogues (DRM, ABM, MOX, and NEM). Based on the SAR analysis in this study, an obvious first step would be to simplify the structure of IVM-B1a by removing any non-essential regions, such as the disaccharide group, and reducing the size of the carbon skeleton at the benzofuran group and central lactone ring. This could be carried out systematically to ensure that essential groups are not accidentally removed. It may also be beneficial to incorporate structural features from the compounds identified to be significantly more efficacious and/or potent, such as a double bond at C22-23 in the spiroketal group (R2), as demonstrated by ABM and DRM. Another factor that needs to be considered is the chirality of IVM-B1a, which, based on the

SAR study, does have an impact on biological activity. For example, the stereochemical configuration of compound **19**, which is identical to IVM-B1a in terms of molecular formula and connectivity, appears to be beneficial for PAM activity, potentiating the Ca^{2+} response to 148% of the IVM-B1a response ($p<0.05$). Given the number of chiral centres in IVM-B1a, this would dramatically increase the number of tests that need to be carried out, as all enantiomers would need to be tested for activity.

There are a few exceptions to the identified trends. For example, NEM has enhanced activity at the P2X4 receptor compared to IVM-B1a but has a hydroxyl group addition at the C23 position (R2). All other compounds investigated with this structural change have lost biological activity. However, NEM is much smaller than IVM-B1a as it lacks the bulky disaccharide group (R1). This dramatic change in structure suggests that NEM fits differently into the binding pocket, rendering the C23-hydroxyl less detrimental to drug activity. Compounds with two or more structural modifications, such as NEM, make it harder to identify which are beneficial and detrimental to activity and could be explored further by widening the structural library.

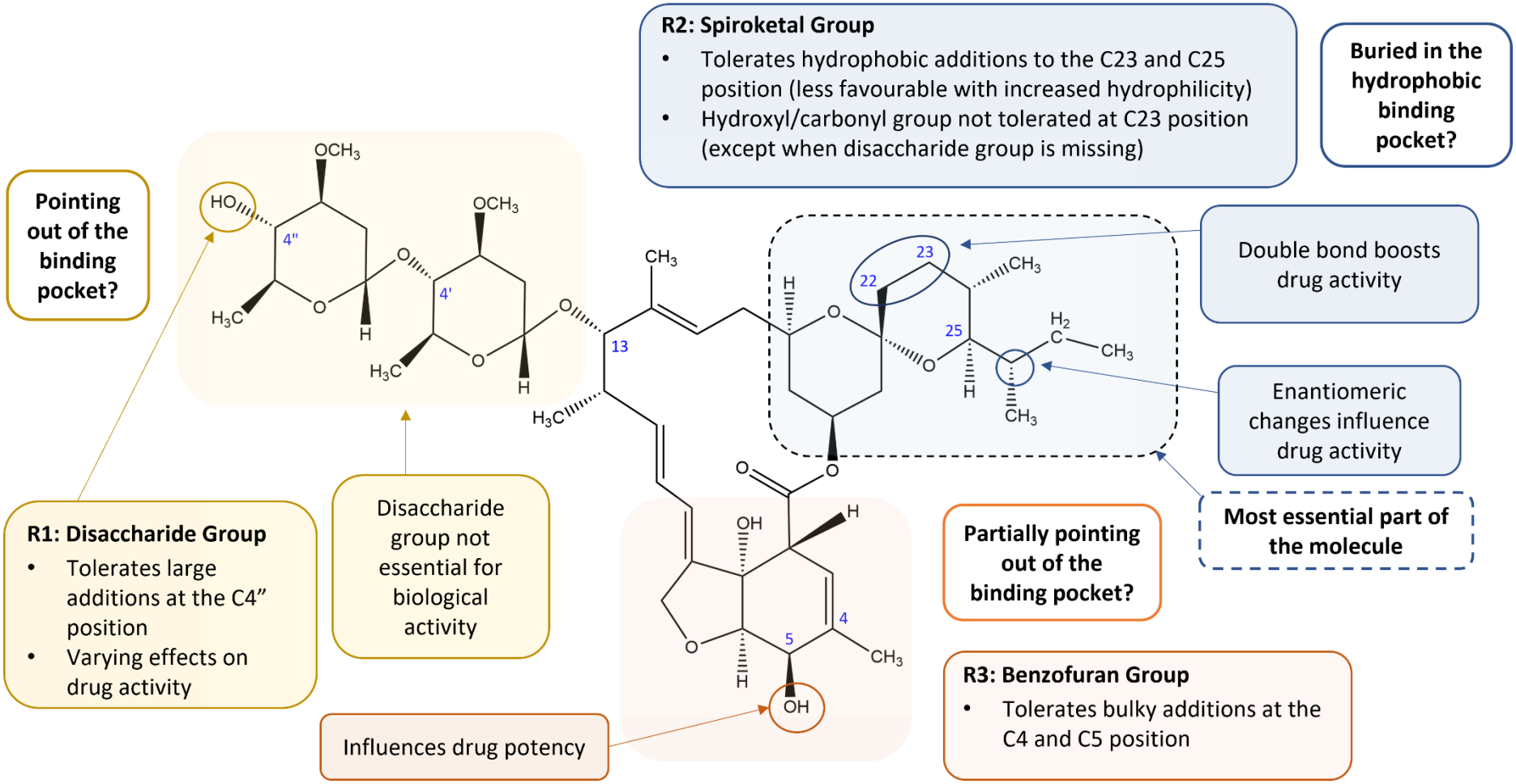

Figure 3.53. Summary of structure-activity relationships of IVM-B1a against the human P2X4 receptor.

3.4.3 Investigating the selectivity of the IVM-analogues against the GABA(A) receptor

Another objective of this study was to test the selectivity of the IVM-analogues against the GABA(A) receptor. This study was based on previous reports that show IVM and its analogues to act as activators of human GABA(A) receptors at high concentrations, as well as multiple studies that relate IVM treatment to adverse neurological side effects in humans and animals (Krusek and Zemkova, 1994; Chandler et al., 2018). As previously discussed, the cellular model chosen for this study was a mouse L(tk-) cell line expressing GABA(A) receptors comprising the α1β3γ2 submoiety combination. This is very close to the GABA isoform α1β2γ2 that is predominately expressed in the CNS and is activated by IVM, making it a good cellular model to test drug selectivity and potential neurotoxicity *in vitro* (Adelsberger et al., 2000).

To assess GABA(A) receptor expression, a fluorescence-based assay was conducted using the FLIPR-membrane potential red dye (FMP-Red-Dye). The dye detects changes in membrane potential by increasing or decreasing the fluorescent signal upon cell depolarisation or hyperpolarisation, respectively. This provides an indirect measure of GABA(A) receptor activity. Initially, the cells were exposed to various concentrations of GABA to assess the FMP-red dye for fluorescent signal detection. Stimulating the cells with GABA resulted in a concentration-dependent increase in fluorescence, suggesting cell depolarisation. This was surprising as activation of GABA(A) receptors is usually associated with a hyperpolarising response (Estrada-Mondragon and Lynch, 2015) and therefore a reduction in fluorescence was expected. However, a "positive" fluorescent response is consistent with multiple studies testing membrane potential dyes to study GABA(A) receptor activation, including a report using the same cell expression model (Nik et al., 2017), and is attributed to GABA-mediated depolarisation of the cells (Joesch et al., 2008). A possible explanation could be related to the ionic constitution of the assay buffers used in these experiments which might alter the chloride gradient. Another theory could be the downregulation or absence of the outward potassium-chloride cotransporter, which would lower the intracellular chloride concentration in the cell and potentially switch GABAs effects from inhibitory (hyperpolarising) to excitatory (depolarising) transmission (Stokes et al., 2017).

Additionally, the resulting pharmacology from this technique matches what would be expected for GABA(A) receptors. The generated EC_{50} value for GABA in this study was 0.66 ± 0.10 µM. Previous studies in HEK cells using electrophysiological techniques have generated comparable GABA potencies in the low micromolar range (EC_{50} = 0.9-7 µM) for human (Estrada-Mondragon and Lynch, 2015; Nik et al., 2017) and rat (Adelsberger et al., 2000) GABA(A) receptors with similar isoform conformations. In addition, L(tk-) cells that were not exposed to dexamethasone (DEX), the promoter to induce GABA(A) receptor expression, did not respond to GABA at any concentration tested (0.01-500 µM). In the absence of DEX treatment, the lack of GABA response suggests that the GABA(A) channels are not being expressed and indicates that the fluorescent signal is GABA(A) receptor-dependant.

Furthermore, exposure to IVM led to a concentration-dependent increase in fluorescence, with IVM at high concentrations (10 uM) behaving as a full agonist at 101.42 ± 1.65% of the maximal GABA response (30 µM). The generated EC_{50} value was 1.74 ± 0.22 µM. This agrees with a previous study showing IVM to be a potent agonist of the rat GABA(A) (α1β2γ2s) receptor with an EC_{50} value of 2.3 µM (Adelsberger et al., 2000). Again, L(tk-) cells that were not exposed to DEX did not respond to IVM at any concentration tested (0.01-30 µM), indicating that the fluorescent response upon IVM stimulation is GABA(A) receptor-dependant.

Once the FMP-Red-Dye had been validated for its use as a rapid throughput indicator of GABA(A) receptor activity, the FLIPR assay was employed to screen the IVM-analogue library. Each compound was screened at two fixed concentrations (1 µM and 10 µM), and the degree of agonist activity was measured as a percentage of the GABA response at 30µM. For the reference compound IVM-B1a, these fixed concentrations generated a fluorescent signal equal to 101.42 ± 1.65% and 34.65 ± 7.01% of the maximal GABA response (30uM) and, therefore, should provide a good indication of compound activity at the GABA(A) receptor.

In total, 33 IVM-analogues were screened, with 80% showing activity as GABA(A) receptor activators and 54% increasing the fluorescent signal by >70% at high concentrations (10 µM). This suggests that most of the IVM-analogues tested are acting as full agonists at the GABA(A) receptor. Interestingly, many of these compounds have chemical additions in all three regions of the IVM-B1a molecule, making it difficult to discern any clear patterns regarding chemical structure and the ability of these compounds to interact with GABA(A) receptors. The remaining 20% could not significantly increase the fluorescent signal, suggesting that they do not act as agonists at the GABA(A) receptor at the concentrations tested. This included compounds **5**, **7**, **11**, **12**, **21** and **23**. Of these compounds that showed no activity at the GABA(A) receptor, compounds **11** and **12** were identified as positive allosteric modulators of the human P2X4 receptor earlier in the study. Compound **11** had a methyl phosphate displacing the hydroxyl group at the C4" position in the disaccharide moiety (R1), and compound **12** possessed an acetamide addition to the C23 position in the spiroketal group (R2). In terms of enhancing P2X4 activity, both compound **11** (3 µM) and **12** (10 µM) could significantly potentate the ATP-evoked Ca^{2+} response, but only to 52.02% and 40% of the IVM-B1a response at maximal concentration, respectively. Likewise, concentration-response curves at the P2X4 receptor revealed EC_{50} values of 1.10 ± 0.51 µM for compound **11** and 4.24 ± 0.75 µM for compound **12**, the latter of which was significantly less than IVM-B1a (EC_{50} = 1.04 ± 0.12 µM). This data suggests that the structural modifications of compounds **11** and **12** to the disaccharide and spiroketal moiety, although partially detrimental to PAM activity at the P2X4 receptor, confer selectivity to P2X4 receptors over the GABA(A) receptor. A promising advantage to these compounds is the reduction of potential toxicity in the CNS. However, the identified compounds may still act as GABA(A) receptor activators at higher concentrations. Therefore, it is important to test a broader range of concentrations and support this using other approaches, such as patch-clamp electrophysiology.

In addition, two of the compounds tested (compound **5** and **7**) that failed to activate the GABA(A) receptor have a molecular weight of over 1000 g/mol due to bulky hydrophobic substitutions in both the disaccharide (R1) and benzofuran (R3) group, in addition to a hydroxyl/carbonyl substitution in the spiroketal group (R2). Given the dramatic change in hydrophobicity and size, it is not surprising that these two molecules do not activate the GABA(A) receptor at the concentrations tested, neither did they potentiate the ATP-evoked Ca^{2+} response at the P2X4 receptor. In addition, compounds **21** and **23** showed no activity as GABA(A)R agonists, but compound **9** (10 μM) was able to activate the GABA(A) receptor to 53.66 ± 3.02% of the GABA response (30 μM). All three compounds have a hydroxyl group addition to the C23 position within the spiroketal group, differing only in stereochemistry. This suggests that the stereochemical composition of IVM-B1a impacts its ability to act as a GABA(A) receptor activator.

Lastly, five of the IVM-analogues tested were effective as GABA(A) receptor activators but displayed no PAM activity at the human P2X4 receptor. This included compounds **3**, **6**, **9**, **16** and **17**, all of which have small structural modifications, except for compound **6**, within the spiroketal (R2) and benzofuran (R3) moiety of the IVM-B1a. In addition to targeting the P2X4 receptor, the structure-function data reported in this study could help elucidate the mechanism of IVM activation at the GABA(A) receptor and assist in designing novel therapeutics that target GABA(A)ergic channels.

Chapter 4. Activity of IVM on endothelial cells and mouse mesenteric arteries

4.1 Introduction

As detailed in the introduction (section 1.2.4.2), Yamamoto and colleagues (2000b, 2006) were the first to provide evidence to support the contribution of P2X4 receptors to the flow-dependent regulation of vascular tone. They demonstrated that the P2X4 is a major contributor to shear-stress mediated calcium signalling in vascular endothelial cells in humans and mice. They also showed P2X4 knockout mice to have suppressed nitric oxide (NO) production and hypertensive characteristics (Yamamoto et al., 2000b, 2006). Given that the P2X4 receptor is a potential route to flow-dependent vasodilation via Ca^{2+} influx and NO production, targeting this pathway with a pharmacological tool such as IVM, a known positive allosteric modulator of P2X4 receptor, would be hypothesised to enhance this response.

To investigate this hypothesis, pressure myography studies were performed on the isolated second-order mesenteric arteries of male mice. This technique provides an *ex-vivo* model for evaluating the role of P2X4 receptors in the vasculature, at physiological pressures and rates of luminal flow. In addition, human vascular endothelial cells were investigated as potential *in vitro* model to study the mechanism of endothelial-dependant vasodilation.

4.2 Aims

- Explore the activity of IVM on flow dependant vasodilation in mouse mesenteric arteries.
- Investigate the effect of IVM on ATP-evoked calcium in a human endothelial cell line.

4.3 Results

4.3.1 Exploring the activity of IVM in mouse mesenteric arteries

4.3.1.1 Testing artery viability through agonist-induced contraction and relaxation

Before running the myography protocol, the pressurized second-order mesenteric mouse artery must be subjected to a series of viability tests. These tests ensure contractile and endothelial integrity of the artery. Following the equilibration step, the artery is first challenged with three consecutive exposures to a high potassium buffer (60 mM KPSS) to test contractile integrity. This step is often called the “standard-start” protocol and ‘wakes’ the artery by triggering membrane depolarisation, causing an influx of Ca^{2+} ions and activating contractile machinery. If the muscle is functional, this should trigger a strong and reproducible contraction that is immediately reversed when the artery is washed with PSS buffer, as seen in Figure 4.1A. The upper panel shows images of a mouse mesenteric artery pressurized to 60 mmHg before (left image; outer diameter = 255 µm) and after (right image; outer diameter = 130 µm) exposure to 60 mM KPSS. The lower panel of Figure 4.1A shows a representative myography trace of the same vessel following application of 60 mM KPSS to the chamber and the subsequent wash steps that return the diameter to baseline.

Towards the end of every experiment, another test is performed to assess the integrity of the endothelium, which can become damaged during the protocol. This involves monitoring the endothelium-dependent vasodilatory response to Acetylcholine (ACh) following a PE-induced contraction. Phenylephrine (PE) triggers a vasoconstrictive response by binding to Alpha-1 adrenergic receptors on the smooth muscle membrane, triggering a rise of intracellular Ca^{2+} and subsequent contraction of the artery. Once stable, ACh is added to trigger an instant vasodilatory response by stimulating the synthesis of NO, a potent vasodilator, from the endothelial cells. The artery is considered functional if exposure to ACh triggers relaxation to >50% of the maximal artery diameter. The upper panel of Figure 4.1B shows images of a mouse mesenteric artery pre-constricted with 300 nM PE (left image; outer diameter = 155 µm) and relaxed following treatment with 10 µM ACh (left image; outer diameter = 255 µm), achieving 100% recovery to baseline diameter. The lower panel of Figure 4.1B shows a representative myography trace of the same artery showing the contraction and dilation response to PE (300 nM) and ACh (10 µM) treatment, respectively.

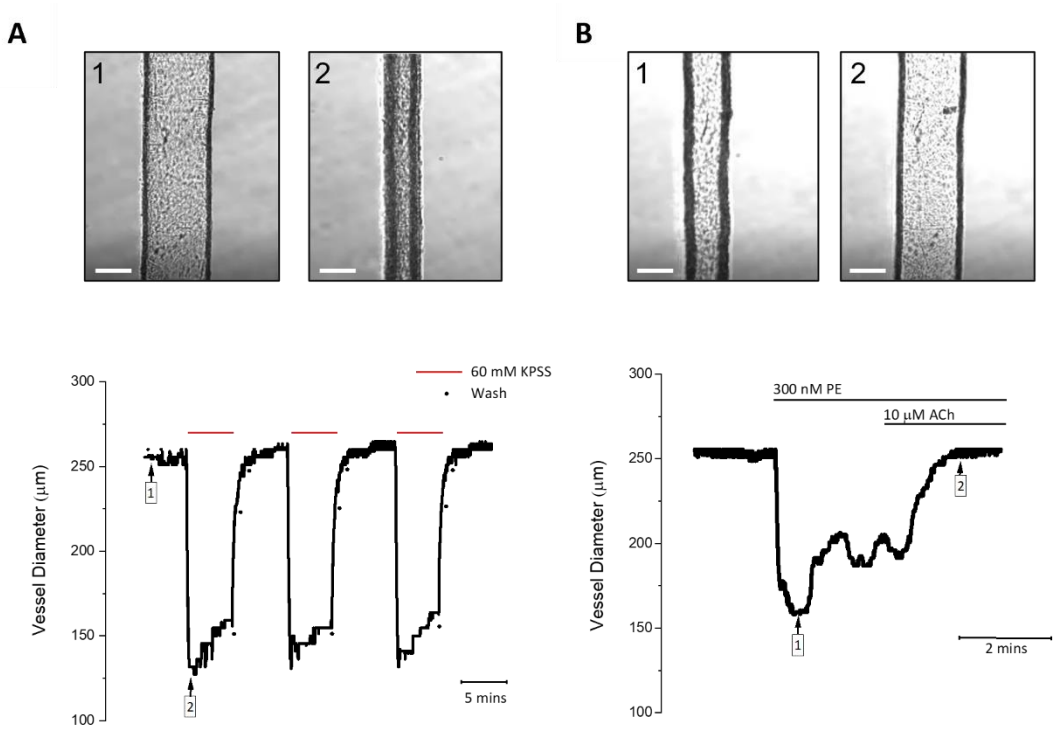

Figure 4.1. Tracking of the outer wall diameter of a pressurized vessel during viability tests. (A) Real-data of a second-order mesenteric mouse artery (60 mmHg) in response to KPSS (60 mM) to assess muscle integrity at the start of the protocol. The top two panels show the artery before (1) and after (2) the chamber was flooded with KPSS. This protocol was repeated three times as shown by the representative trace (bottom panel). Red lines indicate when the artery was exposed to high potassium buffer. (B) Real-data of a second-order mesenteric mouse artery (60 mmHg) looking at ACh-induced dilation (10 µM) in PE-constricted vessels (300 nM), as shown in the top two images (1 and 2, respectively). The representative trace shows a full return to baseline diameter in response to ACh. This test is performed towards the end of the protocol to assess endothelium function. Vessels that achieve >50% of the peak vessel diameter (D_{max}) are considered viable. Representative artery was obtained from a male (8-10 week old) mouse. Scale bar 130 µm.

4.3.1.2 The effect of IVM on flow-dependant vasodilation

In total, 3 mesenteric arteries with a mean maximal external diameter of 260 µm were used in this study and maintained at 60mmHg of luminal pressure to keep within physiological range. The arteries were incubated for 15 minutes with either vehicle control (0.03% DMSO) or IVM (3 µM) before being constricted with U46619 (40 nM), a thromboxane receptor agonist, to approximately 60% of the initial diameter. The arteries were then challenged with a flow gradient (4, 8 or 10 mmHg) to elicit submaximal vasodilation (approximately 70% of initial diameter). Finally, the vessel was re-constricted with U46619 under non-flow conditions before being washed three times with PSS buffer. For each artery, the protocol was repeated at least twice for the control and IVM conditions.

As shown in Figure 4.2B, pre-incubated with IVM (3 µM), resulted in a significant increase in percentage dilation under flow conditions (4-10 mmHg) in comparison to control (81.64 ± 3.55% vs 50.31 ± 3.26%, respectively; n=3; $p<0.05$). Figure 4.2A shows the overlaid representative traces of an artery under control (black line) and IVM (red line) treated conditions and demonstrates the enhanced flow-dependant vasodilatory effect of IVM (3 µM). The time points labelled 1 and 2 correspond to images 1 and 2 on the right panel. These images show a representative mouse mesenteric artery under flow conditions (8 mmHg) in the absence (left image; outer diameter = 191 µm) and presence (right image; outer diameter = 237 µm) of IVM (3 µM) following pre-constriction with U416619 (40 nM). Overall, this data demonstrates that IVM significantly increases flow-dependent vasodilation in mouse mesenteric arteries.

In addition to investigating the flow-dependant effect of IVM, the resting diameter of the vessel and size of the U46619-evoked constriction was examined. Under non-flow conditions, there was no significant difference ($p>0.05$) in the resting vascular tone of the artery when incubated for 15-minutes with vehicle control (100.08 ± 0.84% of vessel diameter before DMSO addition; n=3) and IVM (101.54 ± 0.40% of vessel diameter before IVM addition; n=3) (Figure 4.2C). Likewise, there was no significant difference ($p>0.05$) in the size of the U46619-evoked contraction between the vehicle control (68.58 ± 11.17 % of maximal diameter; n=3) and IVM (58.70 ± 1.16% of maximal diameter; n=3) conditions.

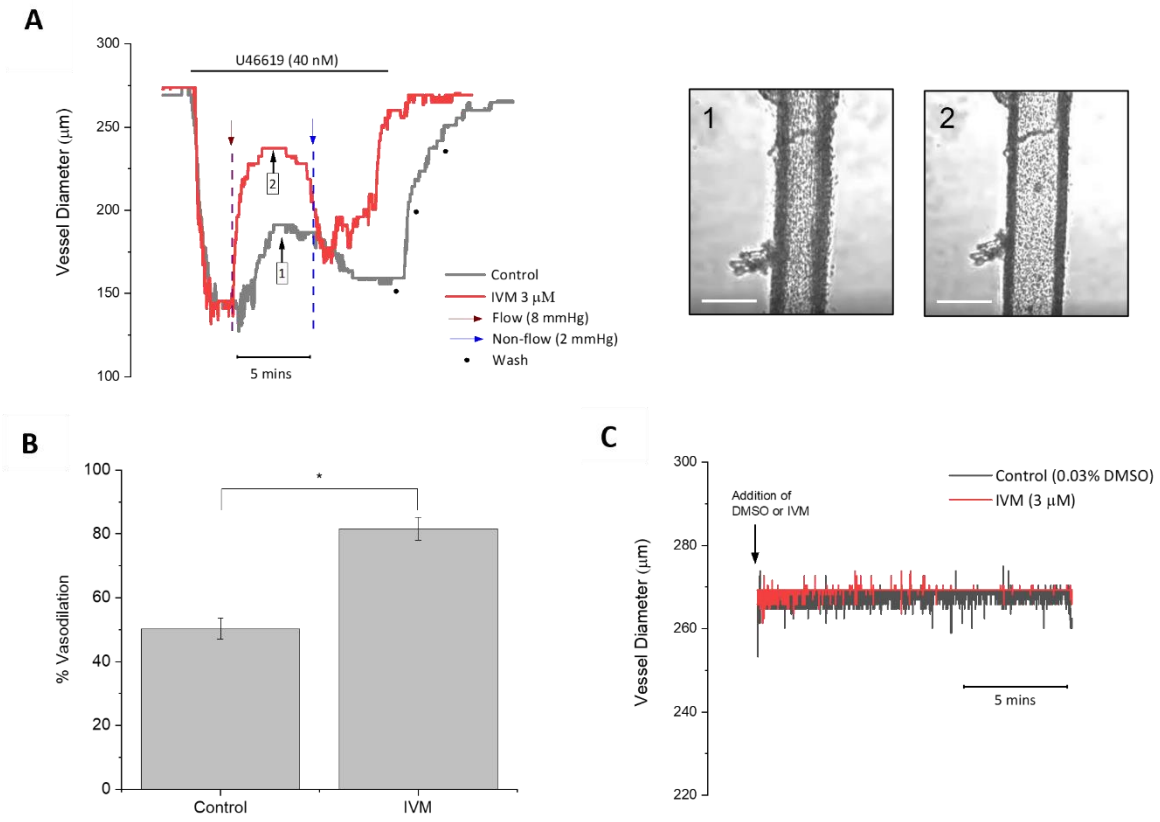

Figure 4.2. IVM (3 µM) potentiates flow-induced vasodilation in mouse mesenteric arteries. (A) Representative trace showing second-order mesenteric artery (60 mmHg) in response to flow challenge. Vessels were pre-incubated with vehicle control (0.03% DMSO; grey) or IVM (3 µM; red) for 15 minutes before the vessel is constricted with U4166 (40 nM) and flow is applied (8 mmHg; dark red arrow). After 5 minutes non-flow conditions are applied to the vessel (2 mmHg; blue arrow) and the artery constricts again before three wash steps (circles) return the vessel diameter to baseline. The two right images show peak vasodilation of the artery under flow conditions following pre-incubation with control (1) and IVM (2). Scale bar 200 µm. (B) Summarised data showing the effect of IVM (3 µM) pre-incubation on flow-dependant vasodilation in mouse mesenteric arteries (n=3). Asterisk denotes statistical significance (*p<0.05). Each bar chart represents the mean of three male mice arteries (8-32 weeks); error bars are SEM. (C) Representative trace of vessel diameter during a 15-minute incubation with control (0.03% DMSO; grey) and IVM (3 µM; red), demonstrating no effect on resting vascular tone.

4.3.2 Investigating the contribution of P2X4-mediated calcium responses in human umbilical vein endothelial cells (HUVECs)

In the previous section (4.3.1), a pressure myography set-up was used to demonstrate the potential role of the P2X4 receptor in the regulation of vascular tone in mouse mesenteric arteries. After exposing the intact vessel preparations to IVM (3 µM), a significant increase in the flow-dependant vasodilatory response was observed, suggesting IVM could enhance endothelial function.

The next step was to investigate the role of P2X4 receptors in human endothelial cells. The cell line chosen for this purpose was human umbilical vein endothelial cells (HUVECs). HUVECS are a well-known in-vitro model for studying human vascular endothelial cell physiology and, most importantly, have been shown to predominantly express P2X4 receptors (Yamamoto et al., 2000a). This study aimed to isolate the P2X4 response using a combination of pharmacological tools and to measure the downstream signalling effects linked to P2X4 activation, including elevation of intracellular Ca^{2+} response. If these cellular processes can be enhanced in HUVECS with the use of IVM, then it might provide novel insight into the mechanism of endothelial-dependant vasodilation.

4.3.2.1 Effect of IVM and BX-430 on the ATP-evoked calcium response in HUVECs

In this study, the extracellular nucleotide ATP was used to evoke an intracellular Ca^{2+} response in HUVECs. HUVECS are primary cells isolated from the vein of the umbilical cord and are known to have an endogenous P2Y response. As previously discussed, ATP is a full agonist for P2X receptors, but some P2Y receptors are also ATP-sensitive. The lack of selective agonists means additional pharmacological tools must be employed to isolate the P2X4 response. In this study, the P2X4 subtype-selective PAM molecule IVM was utilised, as well as the P2X4-selective antagonist, BX-430.

Initially, to investigate the global Ca^{2+} response in HUVECs to an exogenous agonist the cells were treated with ATP. As expected, stimulating the cells with ATP (100 µM) led to a large initial peak (F ratio 1.91 ± 0.09; n=4) and subsequent sustained phase in Ca^{2+} response. This maximal concentration of ATP (100 µM) was used throughout the study to ensure P2X4 activation. Next, to investigate the contribution of P2X4 receptors to the global Ca^{2+} response in HUVECs, the cells were treated with 100 µM ATP in the presence and absence of IVM (3 µM). In this study, both the magnitude of the ATP-evoked calcium response and the net Ca^{2+} movement were assessed. The latter was derived from area under the curve (AUC) data and represents both the initial rise in Ca^{2+} and the sustained Ca^{2+} phase. Interestingly, pre-treatment of cells with IVM (3 µM) did not affect the magnitude of the ATP-evoked calcium response (100 ± 2.20% to 95.42 ± 4.84%; $p>0.05$; n=4; Figure 4.3A) but did significantly inhibit net Ca^{2+} movement (100 ± 1.36% to 69.92 ± 3.83%; $p<0.05$; n=4; Figure 4.3B). The representative Ca^{2+} time-response trace (Figure 4.3C) demonstrates this decrease in sustained Ca^{2+} response for HUVECs pre-treated with IVM (3 µM) compared to agonist stimulation alone (100 µM ATP).

To confirm if this reduction in the Ca^{2+} sustained phase is P2X4-dependant, the P2X4-selective antagonist BX-430 was used. Pre-treatment with both IVM and BX-430 generated a similar response to IVM-treatment alone with no effect on the magnitude of the ATP-evoked Ca^{2+} response (100 ±

2.20% for ATP alone and 104.75 ± 4.32% for IVM and BX-430 co-incubation; $p>0.05$; n=4; Figure 4.3A) but significant inhibition of the net Ca^{2+} movement (100 ± 1.36% to 69.92 ± 3.83%, $p<0.05$, n=4, Figure 4.3B). This suggests that inhibition of the ATP-evoked net Ca^{2+} movement in the presence of IVM is likely to be independent of P2X4.

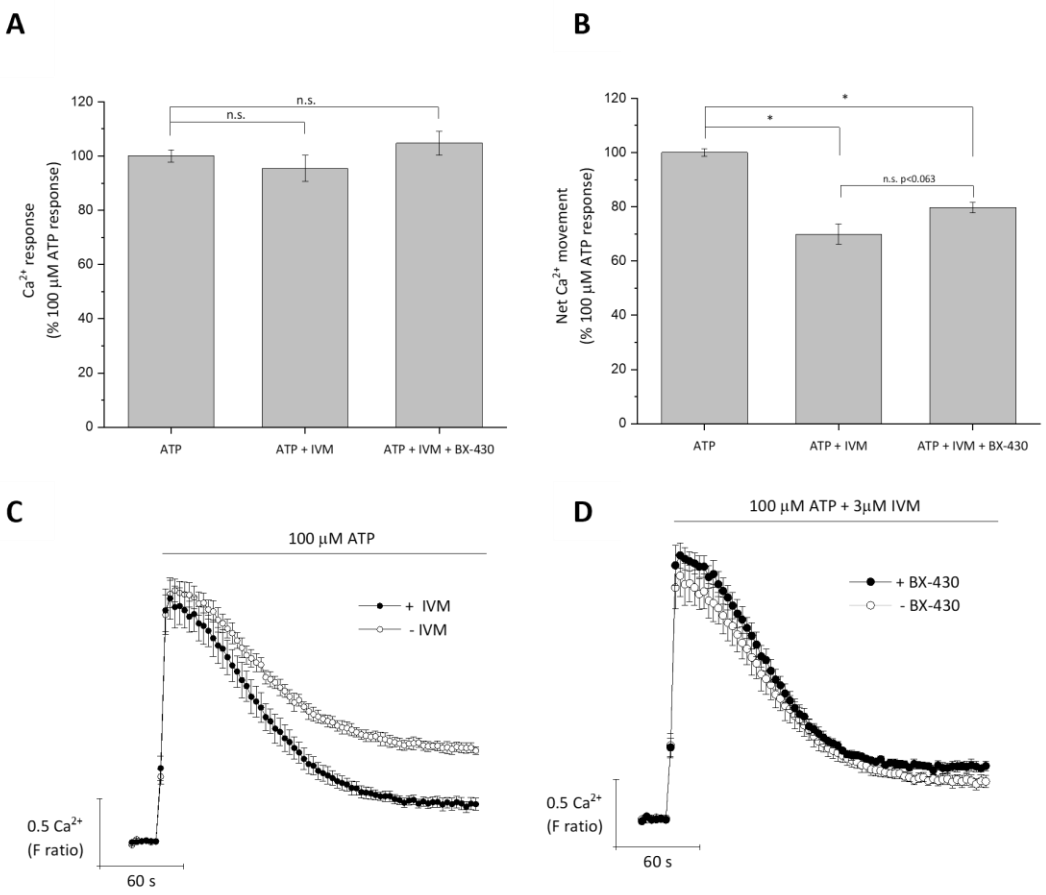

Figure 4.3. Effect of IVM (3 µM) and BX-430 (5 µM) on ATP-evoked calcium response in HUVECS. (A and B) Effect of IVM (3 µM) on the magnitude of the ATP-evoked (100 µM) intracellular Ca^{2+} response and net Ca^{2+} movement after a 30-minute incubation, with and without the addition of BX-430 (5 µM), respectively. All data was normalised to 100 µM ATP (n=4). Asterisk denotes statistical significance (*p<0.05). n.s. = p>0.05 (not significant). (C and D) Representative Ca^{2+} time-response traces showing the effect of IVM (3 µM) and the co-application of IVM (3 µM) plus BX-430 (5 µM) on the response to 100 µM ATP, respectively (n=4). All data points represent the mean ± SEM.

4.3.2.2 Blocking the metabotropic P2Y contribution with Thapsigargin

Thapsigargin (Tg) is a potent non-competitive Ca^{2+}-ATPase (SERCA) inhibitor. SERCA pumps are responsible for transporting Ca^{2+} into the sarco/endoplasmic reticulum. By blocking Ca^{2+} uptake, Tg triggers the depletion of the Ca^{2+} stores and increases intracellular Ca^{2+} levels in the cell (Pimenta et al., 2010). Since P2Y receptors induce Ca^{2+} release from intracellular stores, depleting the stores with Tg should prevent any metabotropic-induced Ca^{2+} response, thereby isolating any Ca^{2+} response caused by the ionotropic P2X receptors.

Pre-treatment of cells with Tg (5 µM) completely abolished the ATP-evoked Ca^{2+} response (100 ± 2.20% to 4.16 ± 0.16%; $p<0.001$; n=4; Figure 4.4), as demonstrated in the representative Ca^{2+} trace (Figure 4.4B). This suggests that the ATP-evoked Ca^{2+} response in HUVECs is predominantly due to metabotropic P2Y receptor activation. Following this, to confirm there is no contribution of P2X4 receptors to the ATP-evoked Ca^{2+} response, IVM was utilised in combination with Tg-treatment. As expected, pre-treatment of cells with IVM (3 µM) and Tg (5 µM) significantly reduced the magnitude of the ATP-evoked Ca^{2+} response (100 ± 2.20% to 7.37 ± 1.49%; $p<0.001$; n=4; Figure 4.5A), as well as the net Ca^{2+} movement in the cell (100 ± 1.36% to 1.91 ± 0.86; $p<0.001$; n=4; Figure 4.5B).

However, as shown in Figure 4.5C, Tg pre-treatment in the presence of IVM did not appear to completely abolish the ATP-evoked Ca^{2+} response in HUVECs. This data demonstrates a possible small contribution of P2X4 towards the ATP-evoked Ca^{2+} response in HUVECs that can only be isolated when the large metabotropic response is blocked with Tg.

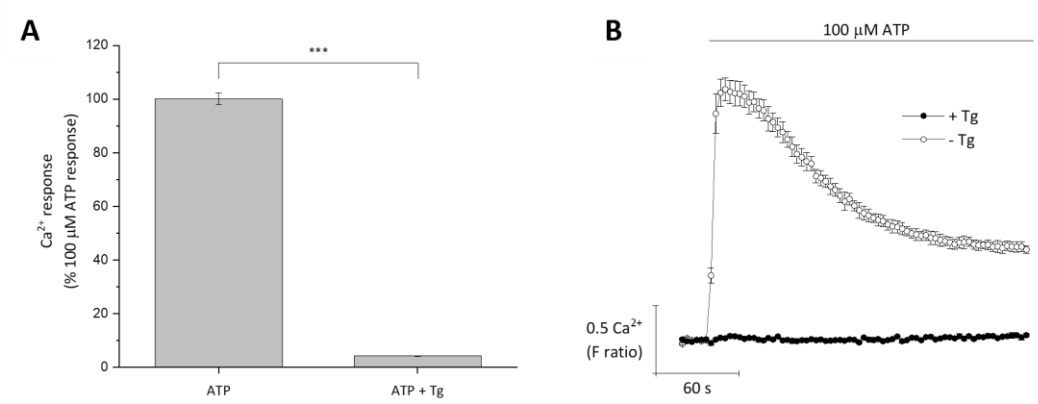

Figure 4.4. Effect of Thapsigargin (5 µM) on the ATP-evoked calcium response in HUVECs. (A) Effect on the magnitude of the intracellular Ca^{2+} response after a 30-minute incubation in the presence and absence of Tg (5 µM) upon stimulation with ATP (100 µM). All data was normalised to 100 µM ATP in the absence of Tg (n=4). Asterisk denotes statistical significance (***p<0.001). (B) Representative Ca^{2+} time-response trace elicited by ATP (100 µM) in the presence (closed circle) and absence (open circle) of 5 µM Tg (n=4). All data points represent the mean ± SEM.

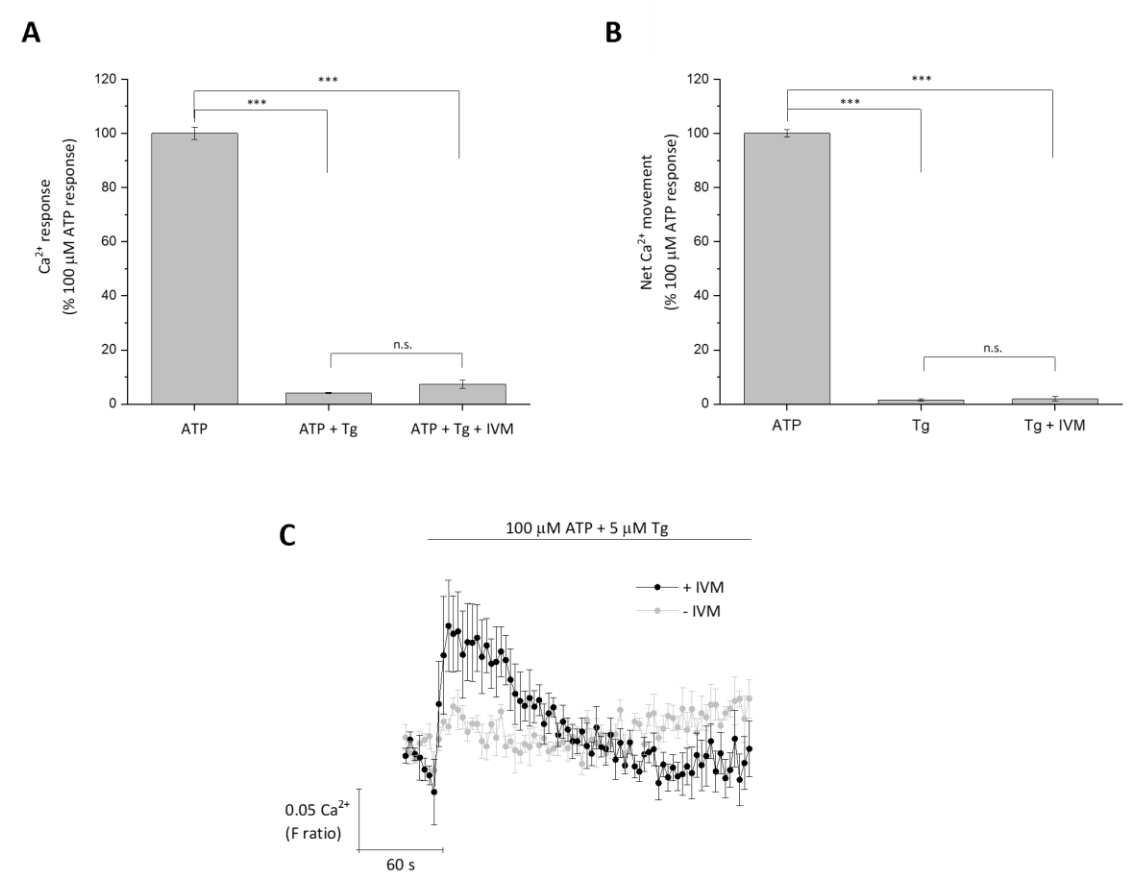

Figure 4.5. Effect of Tg (5 µM) and IVM (3 µM) on the ATP-evoked calcium response in HUVECs. (A and B) Effect of IVM (3 µM) on the magnitude of the intracellular Ca^{2+} response and net Ca^{2+} movement in Tg-treated cells, respectively. All data was normalised to 100 µM ATP in the absence of Tg (n=4). Asterisk denotes statistical significance (*p<0.05). n.s. = p>0.05 (not significant). (C) Representative Ca^{2+} time-response trace elicited by ATP (100 µM) in the presence (black) and absence (grey) of IVM in Tg-treated cells (n=4). All data points represent the mean ± SEM.

4.3.2.3 Testing the effects of TNF-alpha at upregulating the P2X4 response

To simulate a pro-inflammatory environment and potentially up-regulate the expression of the P2X4 receptor in HUVECs, the cells were pre-treated for 48 hours with Tumour Necrosis Factor-alpha (TNF-α). TNF-alpha is a cytokine produced during acute inflammation by immune cells (microglia/macrophages) and plays an integral role in the pro-inflammatory signalling cascade. Previous studies have shown TNF-α to trigger cytotoxicity in HUVECs through oxidative stress, inflammation, and apoptosis, thus making a model system for endothelial cell-based inflammation (Zhou et al., 2017).

Pre-treatment of the cells for 48 hours with TNF-α (10 ng/mL) did not affect the Ca^{2+} response when stimulated with 100 µM ATP (F ratio 1.91 ± 0.09 without TNF-α versus 1.89 ± 0.23, with TNF-α; $p>0.05$; n=3). Likewise, in HUVECs pre-treated with TNF-α, pre-incubating with IVM (3 µM) did not affect the magnitude of the ATP-evoked Ca^{2+} response (100 ± 4.89% to 87.46.42 ± 14.92%; $p>0.05$; n=3; Figure 4.6A). As shown in Figure 4.6B, IVM also reduced the net Ca^{2+} movement in the cells, but not significantly (100 ± 3.68% to 62.30 ± 11.47%; $p>0.05$; n=3). This may be a limitation of the number of repeated experiments. Likewise, co-application of IVM (3 µM) and BX-430 (5 µM) in HUVECs treated with TNF-α had no significant effect on the magnitude or net movement of Ca^{2+} in the cell ($p>0.05$).

Pre-incubation of Tg (5 µM) in TNF-α-treated cells completely abolished the ATP-evoked Ca^{2+} response (100 ± 4.89% to 3.71 ± 0.24%, $p<0.05$; n=3; Figure 4.6C). Co-application of Tg (5 µM) and IVM (3 µM) also completely attenuated the magnitude of the ATP-evoked Ca^{2+} response and net Ca^{2+} movement to a similar extent, as shown in Figures 4.6C and 4.6D, respectively. The representative Ca^{2+} trace (Figure 4.6E) shows this abolished response with no apparent increase in ATP-evoked Ca^{2+} in the presence of IVM. This suggests P2Y receptor activation contributes significantly to the ATP-evoked Ca^{2+} response in HUVECs and that subjecting the cells to TNF-α-induced injury did not upregulate the P2X4 response.

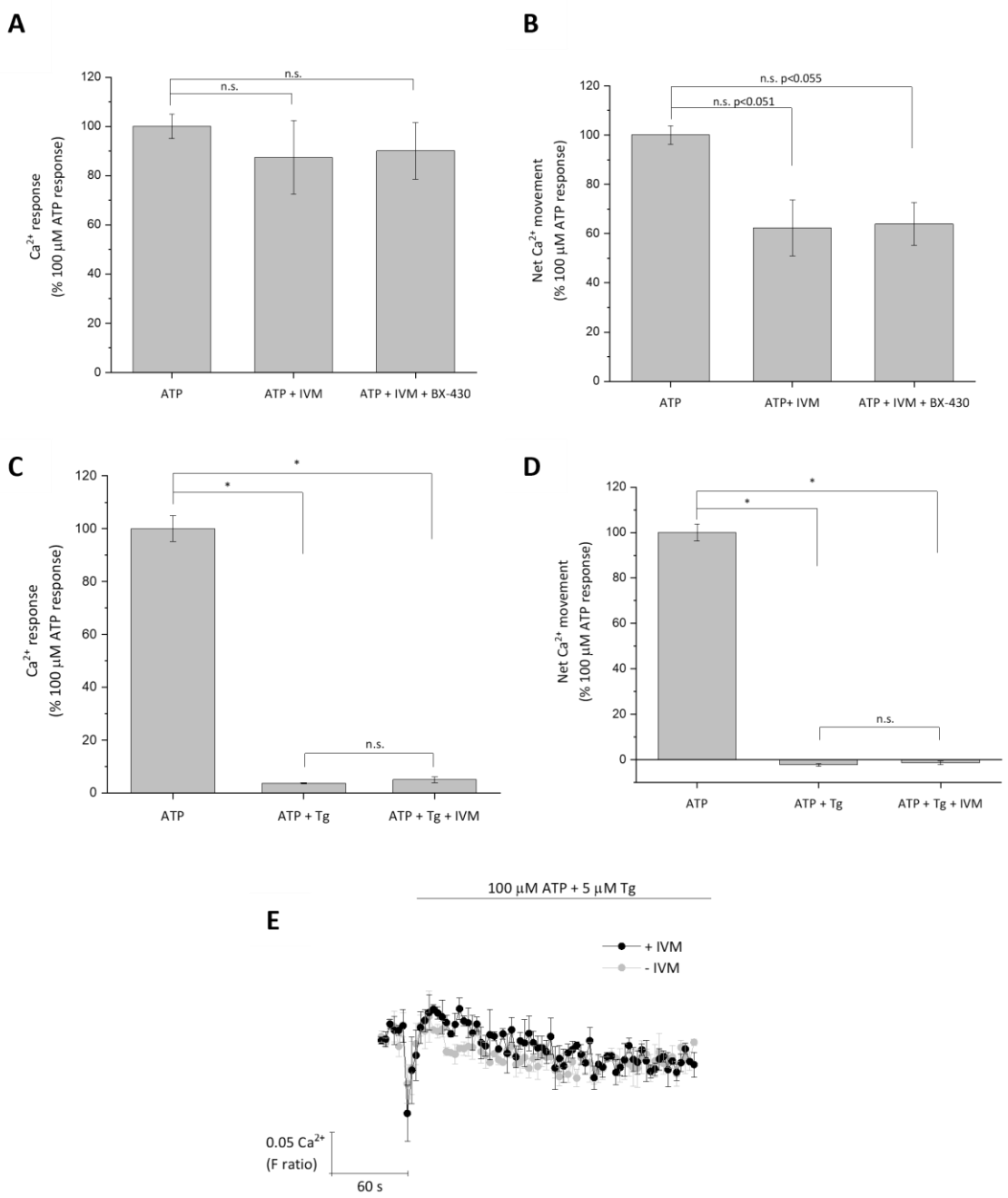

Figure 4.6. Investigating the effect of Tg (5 µM), IVM (3 µM) and BX-430 (5 µM) on HUVECS treated with tumour necrosis factor-alpha (TNF-α) for 48 hours. (A and B) Effect of IVM (3 µM) on the magnitude of the ATP-evoked (100 µM) intracellular Ca^{2+} response and net Ca^{2+} movement after a 30-minute incubation, with and without the addition of BX-430 (5 µM), respectively (n=3). (C and D) Effect of IVM (3 µM) on the magnitude of the intracellular Ca^{2+} response and net Ca^{2+} movement in Tg-treated cells, respectively. All data was normalised to 100 µM ATP in the absence of Tg (n=3). Asterisk denotes statistical significance (*p<0.05). n.s. = p>0.05 (not significant). (E) Representative Ca^{2+} time-response trace elicited by ATP (100 µM) in the presence (black) and absence (grey) of IVM in Tg-treated cells (n=3). All cells were treated for 48 hours with TNF-α (10 ng/mL) prior to the start of the experiment. All data points represent the mean ± SEM.

4.3.2.4 Testing the effects of fibronectin at upregulating the P2X4 response

Lastly, in a pilot study the HUVEC cells were cultured on 96-well plates coated with the extracellular-matrix component fibronectin (100 μg/mL) in an attempt to elevate the P2X4 receptor response. Fibronectin is a multifunctional glycoprotein that plays a role in processes such as wound repair by controlling cellular behaviour (Parisi et al., 2020). Following peripheral nerve injury, previous studies have shown that fibronectin can stimulate P2X4 receptor upregulation at the mRNA and protein level in cultured microglial cells (Nasu-Tada et al., 2006; Tsuda et al., 2008). Fibronectin also plays an important role during extracellular matrix (ECM) remodelling in endothelial cells by acting as an inflammatory mediator during processes such as angiogenesis (Baeyens et al., 2016). This suggests that exposing HUVECs to fibronectin may enhance endothelial activation and potential expression of the P2X4 receptor.

So far, growing HUVECs in fibronectin-coated plates appeared not to affect the magnitude of the ATP-evoked Ca^{2+} response in the presence of IVM (3 μM) (Figure 4.7A) and, as before, caused a drop in the net Ca^{2+} movement that could not be reversed with the use of BX-430 (5 μM) (Figure 4.7B). Most importantly, fibronectin did not increase that global Tg-resistant ATP-evoked Ca^{2+} response in the presence of IVM (3 μM), as shown in Figure 4.7E. This suggests that under these culturing conditions (see section 2.2.3.5), fibronectin does not stimulate P2X4 upregulation in HUVECs.

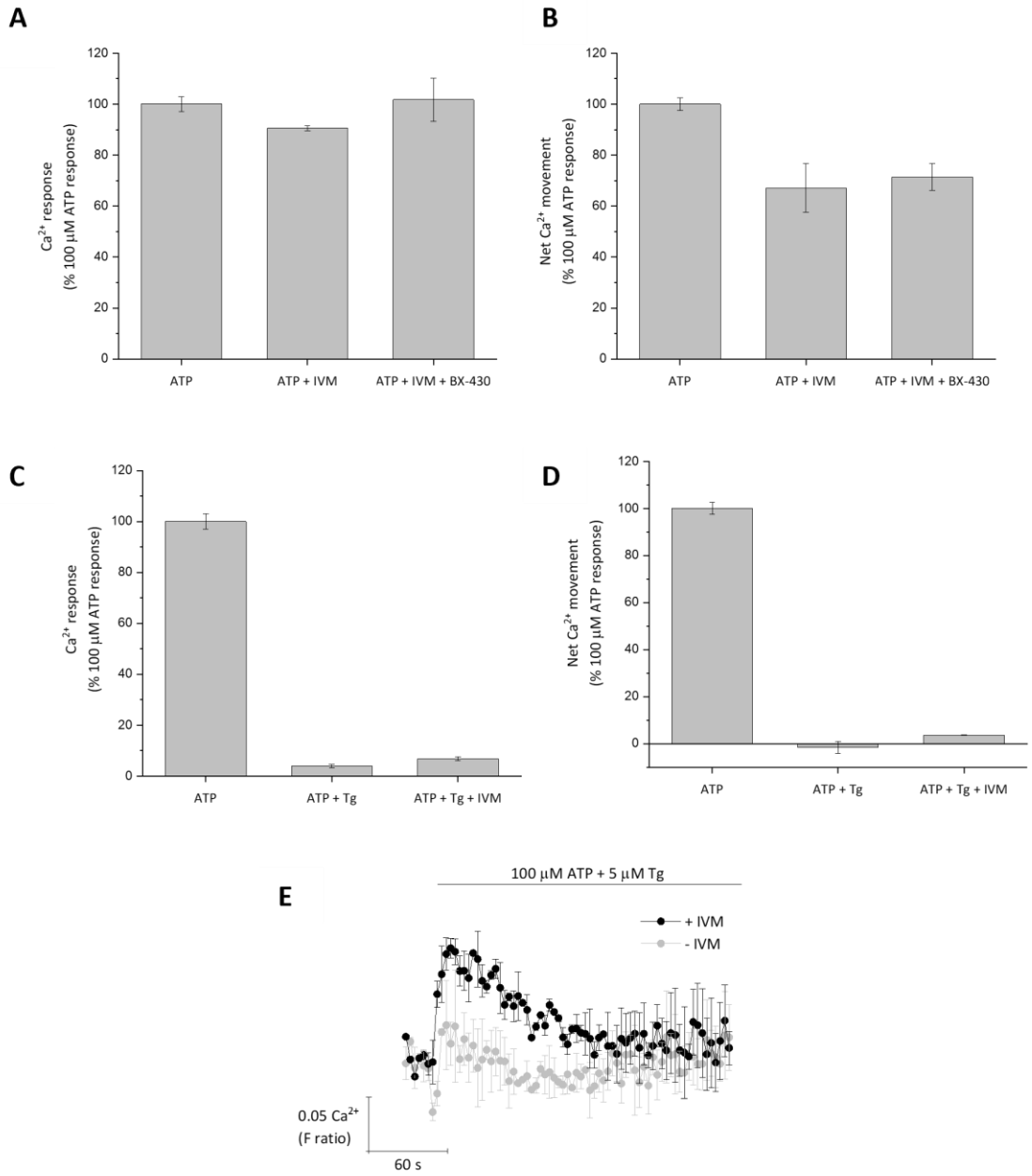

Figure 4.7. Investigating the effect of Tg (5 µM), IVM (3 µM) and BX-430 (5 µM) on HUVECS cultured on fibronectin-coated 96-well plates (100 µg/mL). (A and B) Effect of IVM (3 µM) on the magnitude of the ATP-evoked (100 µM) intracellular Ca^{2+} response and net Ca^{2+} movement after a 30-minute incubation, with and without the addition of BX-430 (5 µM), respectively (n=2). (C and D) Effect of IVM (3 µM) on the magnitude of the intracellular Ca^{2+} response and net Ca^{2+} movement in Tg-treated cells, respectively. All data was normalised to 100 µM ATP in the absence of Tg (n=2). (E) Representative Ca^{2+} time-response trace elicited by ATP (100 µM) in the presence (black) and absence (grey) of IVM in Tg-treated cells (n=2). All data points represent the mean ± SEM.

4.4 Discussion

4.4.1 IVM potentiates flow-dependent vasodilation in mouse mesenteric arteries

At present, the molecular mechanisms involved in the regulation of vascular tone still need to be fully understood. However, it has been shown that P2X4 receptors are highly expressed in vascular endothelial cells, and multiple studies have linked this receptor to the regulation of vascular tone in mice and humans. In the present study, application of IVM (3 μM) to mouse mesenteric arteries significantly potentiated the flow-mediated vasodilatory effect in pre-constricted vessels. Since IVM is a known PAM of the P2X4 receptor, this data suggests that P2X4 receptors are involved in the flow-sensitive mechanism that regulates blood pressure. This data agrees with Yamamoto et al. (2006), who used P2X4-deficient mice to investigate the role of P2X4 receptors in blood pressure and flow-dependent vasodilation. They found that the P2X4 knockout mice had higher blood pressure and reduced endothelial cell responses to blood flow, such as reduced flow-induced Ca^{2+} influx and NO production. Together, this suggests that the P2X4 receptor plays a key role in how endothelial cells respond to changes in blood flow. In addition, this study found that, under non-flow conditions, IVM pre-incubation did not affect the resting vascular tone (resting diameter) of the vessel compared to vehicle control (DMSO), nor did it influence the size of the U46619-evoked contraction. This suggests that the vasodilatory effect of IVM does not occur without changes in the luminal flow conditions (blood flow). This agrees with Yamamoto, who proposed that when exposed to changes in blood flow (shear stress), ECs release intrinsic ATP which activates human P2X4 receptors. This is supported by multiple studies showing P2X4 receptors facilitating fluid shear stress mediated Ca^{2+} influx and nitric oxide release (Yamamato et al., 2000a; 2000b; 2006). Together this data suggests that the potentiation of P2X4 receptors by IVM leads to the relaxation of vascular tone under flow-mediated conditions. These results are novel and add to the understanding of P2X4-mediated vasodilation by being the first to show potentiation of the endothelium-dependent response to blood flow in mouse mesenteric arteries via the application of IVM. However, further physiological studies will be needed to fully understand the mechanism by which IVM promotes flow-induced vasodilation in mice arteries. This data demonstrates positive allosteric modulation of P2X4 as a novel route to pharmacological control of arterial tone and presents a promising start in the development of P2X4 modulators for the treatment of cardiovascular diseases such as hypertension or ischemia.

One caveat to this study is that the *in vivo* model uses mouse arteries instead of human arteries. However, previous studies have shown the physiological profile of mouse P2X4 to be very similar to human P2X4, which is not surprising given their high sequence identity (86.9%) (Jones et al., 2000; Abdelrahman et al., 2017). In addition, IVM has also been shown to potentiate ATP-evoked currents and prolong receptor deactivation in rat P2X4 receptors, which share 87.4% sequence identity with human P2X4 receptors, so IVM would be expected to have a similar positive allosteric modulatory effect at the mouse P2X4 receptor (Khakh et al., 1999; Jelínkova et al., 2006; Abdelrahman et al., 2017).

4.4.2 Investigating the effect of IVM on ATP-evoked calcium response in HUVECs

Human Umbilical Vein Endothelial Cells (HUVECs) are a human cell type isolated from the vein of umbilical cords and are commonly used as an *in vitro* model to study vascular physiology and pathologies, such as inflammatory diseases and atherosclerosis. This study aimed to use HUVECs as a model to investigate how P2X4 receptors might be regulating vasodilatory responses in blood vessel endothelium. Past *in vitro* studies have used HUVECs to study purinoceptor function in endothelial cells and have demonstrated that the P2X4 receptor is the most highly expressed compared to other P2X receptor subtypes (Yamamoto et al., 2000a; Wilson et al., 2007; Tang et al., 2008).

In this study, 100 µM ATP was used to maximally activate the P2X4 receptor. As expected, ATP elicited a biphasic Ca^{2+} response involving a rapid increase in intracellular Ca^{2+}, reflected in the peak magnitude and a sustained Ca^{2+} phase, corresponding to slow Ca^{2+} decay in the cell. This study conveyed the sum of the two Ca^{2+} responses as the net Ca^{2+} movement (derived from the area under the curve data). To isolate the contribution of the P2X4 receptors in these cells, two pharmacological tools were employed to positively modulate (IVM) and inhibit (BX430) the P2X4-mediated Ca^{2+} responses. Interestingly, the application of ATP and IVM did not affect the magnitude of the ATP-evoked Ca^{2+} response but significantly inhibited the net Ca^{2+} movement. In addition, the inhibitory effect of IVM could not be reversed with P2X4 inhibitor BX430, suggesting that the inhibitory response is independent of P2X4.

The potent (SERCA) inhibitor, thapsigargin, was also employed to block the *metabotropic* P2Y response. Pre-treating the cells with thapsigargin completely abolished the ATP-evoked Ca^{2+} response, suggesting that the ATP-evoked Ca^{2+} response in HUVECs is predominantly due to metabotropic P2Y receptor activation. However, in the presence of thapsigargin and IVM, there appeared to be a small recovery in the ATP-evoked Ca^{2+} response ($p>0.05$). This apparent sensitivity towards IVM could be due to the potentiation of the P2X4 response, previously masked by the predominant P2Y response. Notably, IVM and thapsigargin pre-incubation was not enough to isolate the P2X4 response and suggests that the P2X4 receptor is not highly expressed at the cellular surface. A review by Surprenant and North (2009) draws attention to the fact that multiple studies have provided evidence to suggest that P2X4 receptors predominantly localise to the intracellular compartments in other cell types. This could be the case with HUVEC and warrants further investigation.

In the interest of promoting the up-regulation of human P2X4, a number of conditions were tested. First, the cells were pre-treated with Tumour Necrosis Factor-alpha (TNF-α) for 48 hours. However, the co-application of thapsigargin and IVM did not significantly potentiate the thapsigargin-resistant Ca^{2+} response that was seen in the untreated cells. This suggests that pre-treatment of HUVECs with TNF-α does not promote the up-regulation of the P2X4 receptor. This is contradictory to the literature which proposes that pro-inflammatory states upregulate P2X4 receptor expression in endothelial cells. For example, multiple studies have shown that pre-treating HUVECs with pro-inflammatory cytokines causes the up-regulation of the P2X4 receptor (Wilson et al., 2007; Tang et al., 2008).

Specifically, Wilson et al. (2007) found that combined treatment of interferon-γ (IFN-γ) and TNF-α for 48 hours significantly up-regulated the P2X4 receptor at the RNA and protein levels. However, Wilson et al. (2007) failed to detect any electrophysiological responses attributed to P2X4 activation in response to ATP (low micromolar concentrations) or through the addition of IVM under both basal and stimulated conditions (IFN-γ and TNF-α treatment). In contrast, Tang et al. (2008) demonstrated that IFN- γ increased ATP-induced Ca^{2+} response in HUVECS and attributed this effect to P2X4 receptor activation. A review by Ralevic (2012) highlights the mismatch between the *in vitro* studies which point to high expression of the P2X4 receptor in HUVECs, but contradictory results when it comes to measuring P2X4 receptor function. Notably, this study could not isolate the ATP-evoked Ca^{2+} response attributed to the P2X4 receptor in HUVECs, despite previous reports of high expression at the mRNA and protein level.

Secondly, a pilot study was conducted to test the effect of fibronectin in upregulating the P2X4 receptor. The HUVEC cells were cultured on 96-well plates coated with fibronectin for 24 hours. As with TNF-α conditions, fibronectin did not appear to elevate the ATP-evoked Ca^{2+} response in the presence of IVM or thapsigargin, alone or in combination. This suggests that fibronectin cannot up-regulate P2X4 receptor expression in HUVECs under the conditions tested. In contrast, Tsuda et al. (2008) found that in cultured microglia fibronectin/integrin signalling was crucial for the increased expression of the P2X4 receptor.

Taken together, this research reflects the discrepancy in the literature regarding P2X4 function in HUVEC cells. Under basal conditions, the results presented in this study suggest HUVECs are a poor model for studying P2X4-mediated responses in blood vessel endothelium. As for promoting P2X4 function in inflammatory conditions, further cytokines, alone or in combination, could be tested in the hope of promoting the expression of functional P2X4 receptors in HUVECs, as seen by Tang et al. (2008). However, although these conditions might promote P2X4 receptor expression at the cell surface, the model would be more representative of endothelial dysfunction associated with vascular disease states rather than healthy endothelial-mediated processes.

Chapter 5. General Discussion

5.1 Structure-activity relationship of IVM-B1a against the P2X4 receptor

Over the last two decades, growing evidence has implicating P2X4 as a feasible therapeutic target in several cardiovascular and neurological disorders. However, the lack of selective modulators for P2X4 channels has hindered research advancement. At present, the best-known P2X4 positive modulator is IVM, a large semi-synthetic lactone. Within the P2X family, IVM is selective for P2X4 and is routinely used as a pharmacological tool to identify the contribution of P2X4 receptors in a range of physiological and pathophysiological processes. However, there are various drawbacks to using IVM to target P2X4 receptors, one being that the full mechanism of allosteric modulation is yet to be elucidated and, second, its ability to bind and modulate other mammalian ion channels. In the current study, key structure-activity trends were observed between IVM-B1a and its PAM activity at the human P2X4 receptor. Some of the most important findings include: (1) the disaccharide moiety was not essential for IVM-B1a activity; (2) the spiroketal moiety appears to be the most active part of the molecule, and (3) the benzofuran moiety plays a role in drug potency. This led to the hypothesis that the spiroketal group is forming hydrophobic interactions and is buried within the allosteric binding site, whilst the disaccharide group is pointing out of the pocket. The benzofuran group is thought to partially point away from the binding site as it can tolerate large structural modifications but is likely participating in hydrogen bonding at the C5-hydroxyl group (Figure 5.1).

Since the crystal structure of human P2X4 with IVM bound has yet to be solved, many studies have utilised techniques such as site-directed mutagenesis and molecular docking to identify the allosteric site and any important residues involved in ligand-receptor binding. Early work proposed that IVM modulates P2X4 receptor activity by binding between the TM domains of the receptor, directly influencing the re-arrangement of the TM domain during channel gating (Silberberg et al., 2007). Multiple alanine, tryptophan and cysteine scanning mutagenesis studies have gone on to identify important IVM-sensitive residues within TM1 and TM2. This includes a specific region in TM1 between **Ile39** – **Trp50** and TM2 between **Asn338** – **Val348**, as well as **Val357** at the C-terminal end of TM2 (Jelinkova et al., 2006; Silberberg et al., 2007; Jelinkova et al., 2008). Further insights into the IVM binding site were spurred by discovering that IVM could reverse the inhibitory effects of alcohol at the P2X4 receptor. The link between the two modulators was first made when Popova and colleagues (2013) discovered that two critical residues at the top of TM2, specifically **Asp331** and **Met336**, were important in ethanol binding and close to the proposed IVM-binding site. Subsequently, other residues thought to play a role in IVM/ethanol action were identified (**Try46** and **Trp50**), and a molecular model was made of IVM bound to the open-state rat P2X4 receptor from the crystal structure of zebrafish (Asatryan et al., 2010; Popova et al., 2013). In the model, IVM is shown to sit between two receptor subunits close to the interface between the extracellular and transmembrane domain. This agrees with Silberberg et al. (2007) as it supports the possibility of three IVM binding sites existing within the P2X4 receptor, with each IVM molecule "sandwiched" between two neighbouring subunits. Specifically, Popova et al. (2013) predicts that the benzofuran (R3) and

spiroketal (R2) group of IVM binds close to aromatic residues **Try46** and **Trp50**, while the disaccharide (R1) points away. This agrees with this study's hypothesis that the spiroketal group forms important hydrophobic interactions with the binding site, whilst the disaccharide group does not appear to be essential to IVM modulation. The allosteric site identified in the model by Popova et al. (2013) has been linked to the lateral portals, otherwise known as the lateral fenestrations in the P2X4 receptor. These portals are thought to allow the passage of ions through the pore of the P2X4 channel, as well as being important for IVM modulation (Samways et al., 2011 and 2012).

Based on past site-directed mutagenesis and structure-function experiments, two groups performed IVM docking studies based on the rat P2X4 model. In the molecular model by Pasqualetto et al. (2018), IVM-B1a is positioned between two adjacent subunits within the extracellular-TM domain interface, interacting with the upper region of TM1 and TM2 of one subunit, and the lower region of TM2 in the adjacent subunit. This docking simulation explains IVMs ability to stabilise the channel open state following the application of ATP and reduce receptor deactivation. In the docking simulation the IVM-B1a molecule is positioned with the disaccharide group near the extracellular face forming hydrophobic/stacking interactions with **Tyr42**, **Trp46**, and **Val47** at the upper region of TM1. They also identified a potential hydrogen bond formation between the hydroxyl group of the terminal sugar unit (C4'') within the disaccharide group and the oxygen within the side chain of **Asn338** near the upper region of TM2 of the same subunit. Although it is not possible to rule out hydrogen bonding interactions occurring between the disaccharide group and TM1, this study has demonstrated that the disaccharide is not essential to PAM activity at the P2X4 receptor. In addition, substituting the hydroxyl group at the C4" position for a methyl ester would likely disrupt any hydrogen bonding. Yet compound **10**, a compound investigated in this study where this substitution takes place, retains all biological activity at the P2X4 receptor. This does not support the hypothesis proposed by Pasqualetto et al. (2018) of a hydrogen bond forming between the **Asn338** side chain and the terminal hydroxyl group at C4".

Furthermore, in the molecular model proposed by Pasqualetto et al. (2018), the benzofuran group of IVM-B1a forms hydrophobic interactions with **Leu345** and **Val348** (ratP2X4 numbering) close to the C-terminal end of TM2 of the adjacent subunit. In this study, it was found that benzofuran could tolerate a range of substituents that differed in both size and polarity to both the C4 and C5 positions, suggesting that the benzofuran group is partially pointing out of the binding pocket. Notably, substituting the C5-hydroxyl group for a methyl ether was the only structural change within the benzofuran moiety that resulted in a significant decrease in drug potency (compound **22**). This suggests that C5-hydroxyl is important for IVM-B1a binding and could participate in hydrogen bond interactions within the binding site. If this is the case, it would suggest the involvement of other polar groups instead of, or in addition to, the aliphatic side chains of **Leu345** and **Val348**.

Around the same time, another model of IVM bound to rat P2X4 receptor showing a similar docking simulation was published by Latapiat et al. (2017). They concluded that the upper parts of TM1,

enriched with aromatic residues (**Trp50**, **Tyr42** and **Trp46**), helps to assist in the positioning of IVM into the binding pocket by creating a favourable non-polar environment. They also identify **Asp331** and **Met336** in TM2 of the adjacent subunit as sites for potential hydrogen bonding with IVM, which agrees with the predicted action pocket for both ethanol and IVM proposed by Popova et al. (2013). Interestingly, neither model by Pasqualetto et al. (2018) nor Latapiat et al. (2017) mentioned the spiroketal group, the proposed pharmacophore for IVM-B1a in this study. The SAR trends identified in this study suggest that the hydrophobic, non-polar nature of the spiroketal group must be maintained to retain drug activity at the P2X4 receptor and that this region of the molecule is very sensitive to structural modifications. Overall, the results from this study suggest that the spiroketal group might be buried deeper in the binding pocket and forming hydrophobic contacts, potentially with the aromatic residues at the upper region of TM1 (**Trp50**, **Tyr42** and **Trp46**) (coloured blue in Figure 5.1) or with hydrophobic residues in TM2 in the adjacent subunit, such as **Met336, Leu345** and/or **Val348** (coloured yellow in Figure 5.1). The latter orientation would twist the IVM-B1a molecule so that the spiroketal group was facing down towards the cytoplasm and the benzofuran closer to the lateral portals and aromatic residues at the upper region of TM1. This might allow for hydrogen bonding between the C5-hydroxyl group within the benzofuran and the phenolic hydroxyl of **Tyr42** or the side-chain oxygen of **Asn338** at the upper region of TM1 and TM2 of the same subunit, respectively (coloured blue in Figure 5.1).

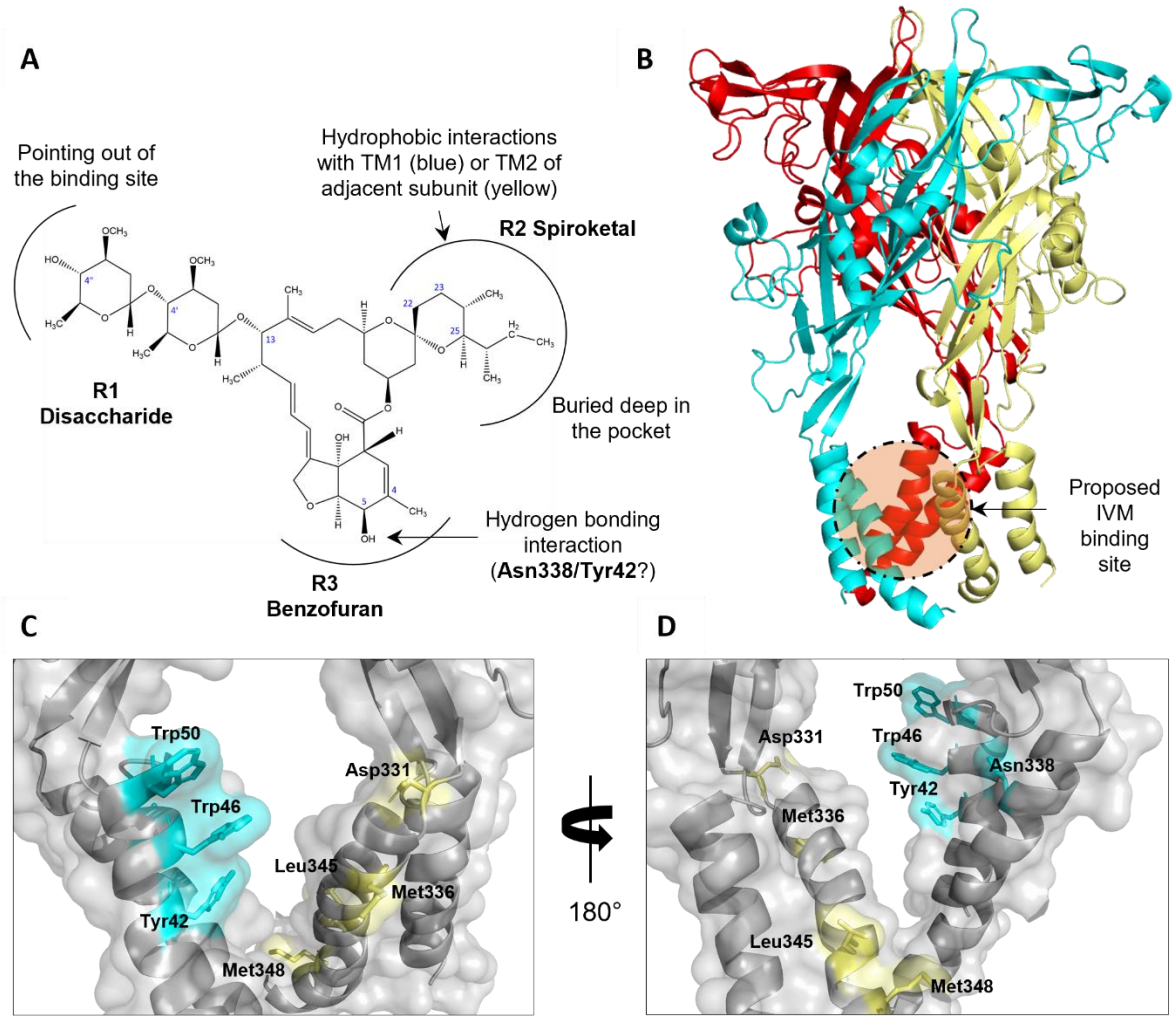

Figure 5.1. Proposed allosteric binding pocket for IVM-B1a at the P2X4 receptor in the open state. (A) Chemical structure of IVM-B1a. Structure-activity trends have been summarised to propose how IVM-B1a might be orientated in the pocket and interacting with the P2X4 receptor. (B) Location of the predicted IVM-B1a binding site in the P2X4 receptor. The receptor has been represented in ribbons, each colour representing a different P2X4 subunit, as viewed from the plane of the membrane. The proposed allosteric site lies between two adjacent subunits close to the interface between the extracellular and transmembrane domain. (C) A close-up view of the proposed IVM binding site, as viewed from the plane of the membrane. Residues suspected to be important for IVM binding and modulation at the rat P2X4 receptor have been coloured according to the receptor subunit, shown here in the corresponding position in the zfP2X4 receptor. The receptor surface and ribbons of the transmembrane helices are represented in grey; the coloured areas correspond to highlighted residues. (D) 180° rotation of the proposed IVM-B1a binding site. Structure was obtained from the SWISS-MODEL Repository (PDB accession number 4DW1).

Recently a homology model of the human P2X4 receptor bound to IVM in the open-state was published based on the crystal structure of the zebrafish P2X4 receptor (Weinhausen et al., 2022). They propose that the main binding site is situated in the extracellular domain of the P2X4 receptor, and that it is responsible for the potentiating effect of IVM. Weinhausen et al. (2022) lists a series of residues that might interact with IVM in the proposed binding site but does not go into extensive detail on the predicted interactions or binding orientation of IVM in the pocket. Although this proposed allosteric site seems contradictory to previous literature, they support the hypothesis that IVM could bind to two binding sites based on experimental results with chimeric P2X4(P2X2) receptors. Given that the literature implicates many different regions in IVM binding through chimeric and mutagenesis approaches, including the involvement of the extracellular domain (Silberberg et al., 2007), both TM domains (Priel and Silberberg, 2004; Zemkova et al., 2014) and the lateral fenestrations (Samways et al,. 201; Gao et al., 2015) it is entirely possible that IVM exerts its effects by binding to two separate binding sites. This hypothesis was originally proposed by Priel and Silberberg (2004) and states that when IVM binds to the high affinity site it amplified the ATP-evoked current by reducing channel desensitisation and increasing ATP efficaicy, whereas binding to the low affinity site reduces receptor deactivation by stabilising the open state of the channel.

Aside from IVM, structure-function experiments have been conducted with the other avermectins to investigate their effects on P2X4 receptors and, more recently, their potential as therapeutics to reduce alcohol consumption. These compounds include abamectin (ABM), doramectin (DRM), selamectin (SLM) and moxidectin (MOX). Silberberg et al. (2007) found abamectin and IVM comparable at potentiating ATP-evoked currents in P2X4 receptors. Notably, abamectin has the smallest structural variation from IVM, with only a double bond at the C22-23 position in the spiroketal group (R2), so a similar biological activity might be expected. In contrast, Asatryan (2014) demonstrated that at high concentrations (≥3 μM) abamectin could enhance ATP-evoked currents significantly more than IVM, with a 10-fold greater activity at 10 μM. This data agrees with what was found in this study. Abamectin demonstrated enhanced potency and efficacy compared to IVM-B1a at the human P2X4 receptor, with a 2.5-fold increase in the ability to potentiate the ATP-evoked Ca^{2+} response at high concentrations (10 μM). Interestingly, Asatryan et al. (2014) also found that at high concentrations, abamectin could enhance P2X4 activity in the absence of ATP, suggesting that abamectin also acts as a direct agonist of the P2X4 receptor.

Moreover, Silberberg et al. (2007) found doramectin to be significantly less efficacious at potentiating ATP-evoked currents than ivermectin and abamectin. Structurally, doramectin has a double bond in the C22-23 position and a cyclohexane group substituting the aliphatic side chain at the C25 position within the spiroketal group (R2). In contrast, this study found doramectin to be significantly more potent and efficacious than IVM, potentiating the ATP-evoked Ca^{2+} response to 164% of the IVM-B1a response at the maximal concentration (1 μM). Likewise, Asatryan (2014) found selamectin (SLM) to be a weak modulator of P2X4 activity compared to IVM at all concentrations tested (0.5–10 μM). It was noted that the greater structural diversity of selamectin could be linked to its reduced activity at

P2X4 receptors, but they did not go into explicit detail. Selamectin has three structural differences from IVM in all three regions of the molecule, including the absence of a sugar moiety in the dissachride group (R1) and the replacement of the hydroxyl group and sec-butyl/isopropyl group with a ketoxime and cyclohexyl group at the C5 (R3) and C25 (R2) position, respectively. However, in this study selamectin and ivermectin were found to have similar potency and efficacy at the human P2X4 receptor, suggesting these structural changes are all well tolerated and do not interfere with any important interactions within the binding site.

The most recent analogue of IVM to be investigated for its effectiveness in treating AUD was moxidectin (MOX). This molecule lacks the disaccharide group (R1) and has a methoxime and a dimethyl-butyl substituent in the spiroketal group (R2) at the C23 and C25 positions, respectively. Huynh et al. (2017) found moxidectin to significantly potentiate the P2X4 receptor-mediated current in *Xenopus oocytes* to a similar degree as IVM (0.5 and 1 μM). This data reflects what was found in this study and supports the theory that the disaccharide group is not essential for effective PAM activity at the P2X4 receptor.

Lastly, IVM is also known to activate and/or modulate other mammalian ligand-gated ion channels at (μM) concentrations, including GABA(A) receptors (Adelsberger et al., 2000); glycine receptors (GlyR) (Shan et al., 2001) and the nicotinic acetylcholine receptor (nAChR) (Krause et al., 1998). These are all members of the cys-loop superfamily, meaning they share similar receptor architecture and are formed from an assembly of five subunits. Of these receptors, only GluCl from *C. elegans* (Hibbs and Gouaux, 2011) and GlyR from zebrafish and human (Du et al., 2015; Huang et al., 2017) have been crystalised with IVM-bound to an allosteric binding site. For both receptors IVM is thought to bind at the interface between the M3 α-helix of the principal subunit and the M1 α-helix of the complementary subunit (Hibbs and Gouaux, 2011; Huang et al., 2017). As for the orientation of IVM in the pocket, the benzofuran group (R3) is shown to face into the hydrophobic pocket with the C5-hydroxyl group forming hydrogen bonds with surrounding residues. Whilst the spiroketal group faces the cytoplasm and the disaccharide is pointing out of the binding pocket (Zemkova et al., 2014; Huang et al., 2017). This orientation is close to what has been proposed for this study at the P2X4 receptor. The fact that IVM can bind to two seemingly unrelated receptor families suggests that it is the hydrophobic character and size of the allosteric pocket that determines IVM modulation, rather than conserved amino acids (Silberberg et al., 2007; Chen and Kubo, 2018). This makes the rational design of novel, selective PAMs for the cys-loop receptors and P2X4 receptors more difficult. Therefore, further crystal structure-based identification, structure-function experiments and mutagenesis approaches will be needed to fully elucidate the binding site(s) and mechanisms involved in IVM modulation.

5.2 Selectivity screen of the IVM-analogues against the GABA(A) receptor

Generally, the use of IVM, and related avermectins, as an anti-parasitic drug is considered to have a large safety margin. This is due to p-glycoproteins associated with the blood-brain barrier that prevent high concentrations of drugs from building up in the brain. However, there have been reports of severe toxic neurological side effects following IVM treatment in humans and animals, specifically during incidences of accidental overdose or when the body's ability to block the penetration of IVM into the CNS is compromised. These neurological effects, ranging from dizziness to coma, have been linked to IVM's ability to penetrate the CNS and directly activate and modulate GABA(A) receptors (Chandler, 2018).

Recently, IVM has been linked to the treatment of alcohol use disorder (AUD), with pre-clinical evidence demonstrating that IVM-treatment in mice reduces alcohol consumption (Asatryan et al., 2014). The role of P2X4 receptors in this process was supported by *in vitro* experiments demonstrating that IVM could attenuate the inhibitor effect of alcohol in P2X4 receptors in *Xenopus oocyte* (Asatryan et al., 2010; 2014). Moreover, a molecular model was proposed of IVM and ethanol occupying an overlapping allosteric site in the P2X4 receptor (Asatryan et al., 2010). However, as a potential treatment for AUD, the low retention time of IVM in the CNS is not ideal. Recent studies have begun structure-function experiments to identify structural modifications that might increase retention time (reduced affinity for P-glycoproteins) but retain the ability to reduce alcohol intake. However, higher retention time in the brain would heighten the risk of neurological side effects due to GABA(A) receptor overstimulation. Recently, studies have looked at the ability of the avermectins to potentiate GABA(A) receptors with the aim of identifying a drug with a more favourable safety profile than IVM (i.e. less potent at the GABA(A) receptor).

Asatryan et al. (2014) found IVM, abamectin (ABM) and selamectin (SLM) to be equally potent at potentiating the GABA(A) (α1β2γ2) response. In this study, both ABM and SLM were tested as agonists at the GABA(A) (α1β3γ2) receptor. Treating the cells with either drug resulted in a significant increase in GABA(A) activity, but they appeared to act as partial agonists at 10 μM, only eliciting a fluorescent response to 75.9 ± 3.9% and 61.4 ± 4.3% of the maximal GABA (30 μM) response, respectively. A later study also investigated Moxidectin (MOX) as a candidate for the treatment AUD (Huynh et al., 2017). This was based on previous research demonstrating MOX to have lower affinity for P-glycoproteins, allowing it to cross the BBB more readily and reach higher concentrations in the CNS (Menez et al., 2012). Interestingly, MOX was also found to be significantly less potent at potentiating the GABA(A) receptor compared to IVM (Huynh et al., 2017). Huynh et al. (2017) suggests that MOX is a better drug candidate for AUD, as there will likely be fewer side effects associated with GABA(A) receptor overstimulation, such as CNS depression. As with ABM and SLM, this study found MOX to act as a partial agonist when tested at 10 μM at the GABA(A) receptor (77.9 ± 4% of the maximal GABA response). However, unlike the avermectins, MOX did not appear to activate the receptor at low concentrations (1 μM). This suggests that, when tested at the low micromolar range, MOX will not overstimulate the GABA(A) receptor either as an agonist or positive modulator, making it a promising

option in the treatment of AUD. Likewise, this trend is seen in the other two milbemycin molecules tested in this study (nemadectin and milbemycin). The milbemycins are a group of compounds that are chemically related to the avermectins but lack the disaccharide substituent (R1), making them considerably smaller than the other IVM-analogues tested in this study. This suggests that removal of the disaccharide hinders the ability of these compounds to act as agonists at the GABA(A) receptor, giving them a more favourable safety profile compared to IVM in the treatment of AUD.

In addition to the above-mentioned compounds, this study screened a library of IVM-analogues against a GABA(A) receptor expressing cell line to test their ability as GABA(A) activators. IVM-B1a was shown to act as a full agonist at 10 μM. Likewise, most of the compound library could increase the fluorescent signal to >70% of the maximal GABA response, suggesting they can activate the GABA(A) receptor. Since most of the IVM-analogues can be tolerated by GABA(A) receptors, all with various sized modifications and physical properties, it hints to the existence of a large IVM binding pocket within the receptor. In total, only compounds **11** and **12** displayed selectivity towards the P2X4 receptor over the GABA(A) receptor. This suggests that the structural features of these compounds confer greater selectivity towards P2X4 receptor modulation and thus might have a broader safety profile as novel therapeutics. These findings help to support the use of IVM as a platform for designing novel drugs for AUD, and for the targeting of other P2X4-mediated processes, currently hindered due to a lack of selective pharmacology and safety concerns regarding GABA(A)R overstimulation.

5.3 Activity of IVM on endothelial cells and mouse mesenteric arteries

Building evidence has linked the role of P2X4 receptors in the regulation of vascular tone and cardiovascular disease. Yamamoto et al. (2006) provided conclusive evidence by reporting flow-induced increases in calcium and NO production in cultured endothelium from mice pulmonary microvessels that were absent in P2X4 knockout mice. Furthermore, the P2X4 knockout mice had significantly higher blood pressure and produced less nitric oxide than wild-type mice. In this study, ivermectin (IVM), an allosteric modulator expected to enhance P2X4 function, was found to significantly potentiate flow-dependent vasodilation in mouse mesenteric arteries. Taken together, this research supports the functional role of P2X4 receptors in regulating flow-mediated vasodilation in mouse arteries. Furthermore, clinical research has demonstrated that a single loss-of-function mutation in the human P2X4 receptor gene can hinder P2X4 function and shows an association with increased pulse pressure in patients (Stokes et al., 2011). However, further research will be needed to fully understand the role of P2X4 receptors in vascular homeostasis and the molecular pathway by which IVM might potentiate flow-induced vasodilation. This research has implications for the possible targeting of P2X4 receptors in the treatment of cardiovascular disease states such as hypertension and atherosclerosis.

It is well documented in the literature that endothelial cells, in response to shear stress and subsequent extracellular ATP release, can modulate cellular signalling through P2 receptors, with P2X4 mediating calcium signalling and vasodilation. In this study, an attempt to explore the P2X4-mediated

effects in endothelial cells was carried out using HUVECs, an *in vitro* model for blood vessel endothelium. Unfortunately, the ATP-evoked calcium response associated with P2X4 receptor activation could not be isolated. This is surprising since HUVECs have been shown by multiple studies to pre-dominantly express P2X4 receptors at the mRNA and protein level (Yamamoto et al., 2000a; Wilson et al., 2007; Tang et al., 2008). However, this discrepancy has been seen before by Wilson et al. (2009) who could not detect any changes in membrane currents in response to ATP nor detect any potentiation of membrane currents in the presence of IVM in untreated or IFN-γ, and TNF-α treated HUVECS. This suggests that HUVECs are a poor model for studying P2X4 receptor function in endothelium-mediated vasodilation.

An unexpected observation was noted in this study. Following stimulation with ATP, the net Ca^{2+} movement in the cell was significantly inhibited in the presence of IVM. This reduction in the Ca^{2+} response could not be reversed with the co-application of IVM and BX430, a P2X4 receptor antagonist, suggesting that the inhibitory response to IVM is independent of P2X4. In addition to acting as a positive allosteric modulator of the P2X4 receptor, IVM has also been shown to inhibit Ca^{2+}-ATPase (SERCA) at the micromolar range (Pimenta et al., 2010). This pump is responsible for Ca^{2+} re-uptake in the sarcoplasmic reticulum of skeletal muscle cells and the endoplasmic reticulum of non-muscle cells. Several isoforms of SERCA exist in mammals and previous studies have shown that IVM can inhibit both the SERCA1 isoform, a skeletal muscle-specific isoform, and SERCA2(a/b), which are expressed in cardiac muscle and non-muscle cell types (Bilmen et al., 2002; Pimenta et al., 2010). Endothelial cells predominantly express the SERCA2b and SERCA3 (non-muscle cell) isoforms, with HUVECs documented to highly express the 2b isoform *in vitro* (Mountian et al., 1999; Keeley et al., 2018). Noël et al. (2011) explains how IVMs lipophilic nature might allow it to cross the plasma membrane and reach the SERCA at the sarco-endoplasmic reticulum in a similar way to thapsigargin (Bilmen et al., 2002). By blocking Ca^{2+} uptake, IVM is triggering the depletion of the Ca^{2+} stores, resulting in reduced Ca^{2+} release from the stores upon activation of the metabotropic P2Y receptors with ATP. This could explain the significant reduction in the net Ca^{2+} movement observed in HUVECs following IVM pre-treatment in this study. In addition, previous studies have demonstrated that thapsigargin is a more potent inhibitor of SERCA than IVM, with a reported IC_{50} value in the nanomolar range (Yatime et al., 2009). This could explain why IVM did not completely abolish the ATP-evoked Ca^{2+} response in HUVECs, as seen with thapsigargin pre-treatment. This action of IVM on Ca^{2+}-ATPase could also explain the raised baselines (high loading vales) observed earlier in the study in the human P2X4 overexpressing astrocytoma cells upon incubation with a selection of the IVM-analogues.

5.4 Concluding remarks

The current project provides novel information on the structure-activity relationship of IVM-B1a in the potentiation of human P2X4 receptors. The detailed investigation of a library of structurally related IVM-B1a derivatives revealed several SAR trends, including the importance of the spiroketal region of the molecule and how the disaccharide region was not essential for IVM-B1a activity,

summarised in Figure 3.53. This information could be used to strip back the chemical structure of IVM and design novel therapeutics that can target the P2X4 receptor with increased efficacy and potency.

In addition, IVM is known to bind to many ligand-gated ion channels in mammals, including GABA(A) receptors. This has been linked to severe neurological side effects following IVM-treatment in humans and animals. To discover if any of the IVM-analogues conveyed selectivity towards the P2X4 receptor, an activity screen was carried out against the GABA(A) receptor. Of the 33 compounds screened, two were identified as having selectivity towards the human P2X4 receptor. Further experiments will be needed to understand what structural features drive IVMs ability to modulate a broad range of mammalian ion channels. However, the results from this study provide a good starting point in this investigation and provide novel insight into the development of drugs that can target P2X4 receptors with increased selectivity and, consequently, fewer adverse side effects.

Lastly, this study was the first to show that IVM can potentiate flow-dependant vasodilation in mouse mesenteric arteries. Although the mechanism of IVM's *in vivo* activity needs to be investigated further, the present study supports the role of P2X4 receptors in the regulation of vascular tone. In terms of therapeutic advancement, this research also supports the targeting of P2X4 receptors for treating hypertension.

5.5 Future directions

The main focus of this study was to investigate the structure-activity profile of IVM using a series of structural derivates at the human P2X4 receptor. This was achieved using fluorescent calcium mobilisation assays. Each analogue was tested for PAM activity by measuring the degree of potentiation on the ATP-evoked Ca^{2+} response in human P2X4 overexpressing cells. One caveat to the Ca^{2+} mobilisation assay is that cytosolic Ca^{2+} level increase can come from various routes, not just P2X4 receptor activation. A series of experiments were conducted to characterise the cell line and demonstrate that the response to ATP was P2X4-dependent. However, this work could be validated further using electrophysiology. Not only would this support the Ca^{2+} work but provide additional information such as the desensitization and deactivation kinetics of the IVM-analogues. In addition, IVM has previously been reported to alter Ca^{2+} permeability of the channel (Samways et al., 2012). By employing electrophysiology, I can measure whole cell current changes for IVM, as well as further characterising some of the IVM-analogues, rather than measuring the calcium component only. It would also be possible to take this further by carrying out single channel recordings which would permit further measurements, such as duration of channel opening and closing as well as frequency of channel gating and changes in channel conductance. This information could be used to make a more informed decision on how IVM and its analogues modulate P2X4 receptor activity and together with site-directed mutagenesis studies we could better characterise the allosteric binding site.

A potential future direction for this project would be to employ molecular docking analysis to identify the allosteric site of IVM and any important residues involved in ligand-receptor binding. It would be interesting to see if any novel docking sites align with the structure-function information discovered in this study, as well as experimental findings from the literature. Unfortunately, the human P2X4 receptor is yet to be crystallised; however, the zebrafish P2X4 has been crystalised in the apo, closed state (Kawate et al., 2009) and holo, ATP-bound open state (Hattori and Gouaux, 2012). Since then, the crystal structures of Gulf Coast tick P2X (Kasuya et al., 2016), panda and chicken P2X7 (Karasawa and Kawate, 2016 and Kasuya et al., 2017, respectively) have been resolved, as well as the NMR structure of the isolated head domain of rat P2X4 (Igawa et al., 2015). Due to the high sequence similarity between P2X receptors, these structures can be used as templates for homology modelling the currently unresolved human P2X4 receptor. This would help to identify the IVM-B1a binding site(s), and any potentially critical binding interactions can be tested using site-directed mutagenesis. Moreover, any novel lead compounds designed based on the SAR analysis could be inserted into the binding site *in silco* to test how they might interact and fit in the pocket before being synthesised.

Regarding the selectivity screen, a potential next step would be to test the activity of the IVM-analogues as PAMs of GABA(A) receptors, rather than activators. This would provide further structure-function information for IVMs potentiation of GABA(A) receptors and ultimately help in the design of novel therapeutics for the selective targeting of either P2X4 or GABA(A) receptors. It would also be interesting to test the selectivity of the IVM-analogues against other known targets of IVM, such as the nicotinic acetylcholine receptor (nAChR).

In this study, a primary human endothelial cell line (HUVEC) was tested to investigate the mechanism of how IVM might enhance flow-dependant vasodilation, as seen in mouse mesenteric arteries. This avenue was investigated as a higher throughput approach to explore downstream endothelium-dependant processes such as a Ca^{2+} influx and NO production in response to the application of IVM and its analogues. Given the challenges of isolating the P2X4 response in HUVECS, a potential next step would be to expand upon the myography work, ideally in human arteries. For example, to demonstrate that IVMs effect is P2X4 dependant, PSB-12062, a selective antagonist for mouse P2X4 receptor, could be employed to reverse the IVM-induced vasodilatory effect observed in the vessels under flow conditions. Furthermore, the proposed mechanism for P2X4-mediated vasodilation is the release of nitric oxide (NO) (Yamamoto et al., 2006). This could be tested in the vessel set-up by blocking nitric oxide release with N-nitro L-arginine methyl ester (L-NAME), a potent NO synthase inhibitor. Another potential direction would be to test more IVM-analogues at potentiating flow-dependant vasodilation. For example, nemadectin (NEM) would be a good candidate to test as it has a very different chemical structure from IVM yet was found to be significantly more potent and efficacious at enhancing P2X4 activity in the calcium assays. It would be interesting to know if this enhanced activity is reflected in a more physiologically relevant system.

Appendix

Table A1. List of the commercially available compounds used in this study. Red indicates structural changes from the reference compound IVM-B1a. Blue numbers represent the C-positions.

Ivermectin B1a 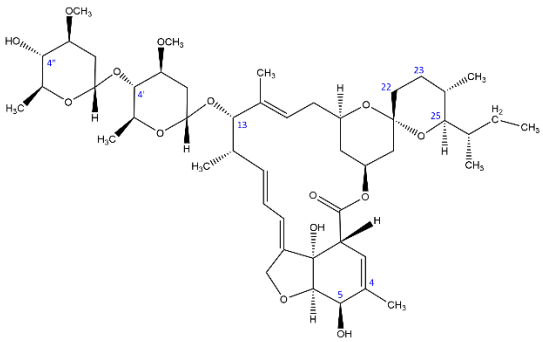	Ivermectin B1b 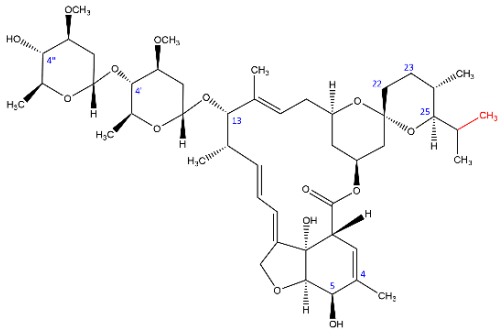
Ivermectin 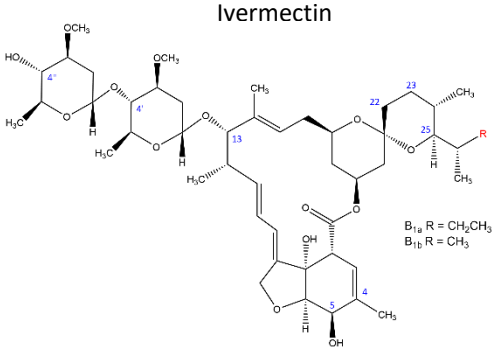 	Abamectin 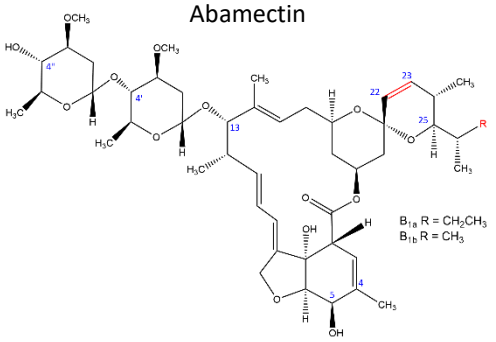
Doramectin 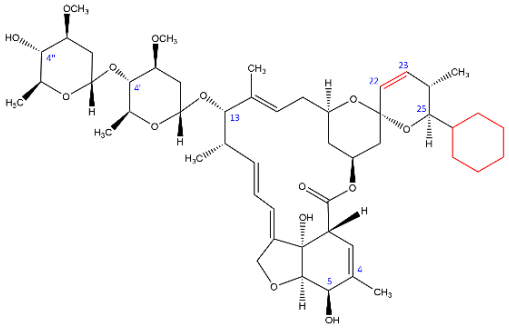	Eprinomectin 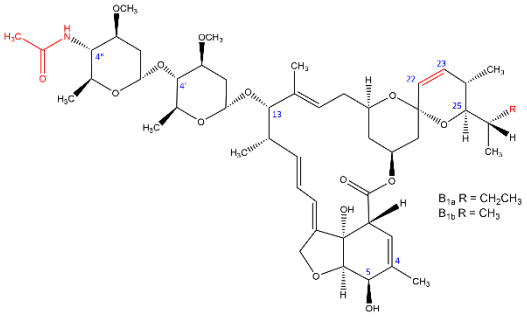
Selamectin 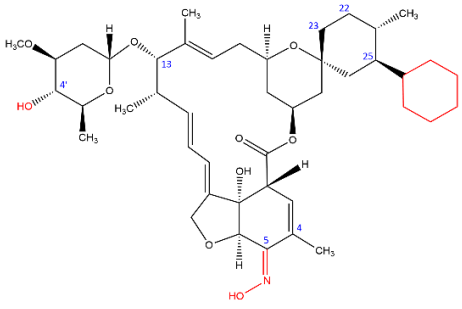	Milbemectin 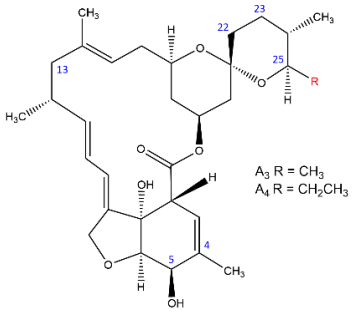

Table A1. (cont.) List of the commercially available compounds used in this study. Red indicates structural changes from the reference compound IVM-B1a. Blue numbers represent the C-positions.

Nemadectin	Moxidectin
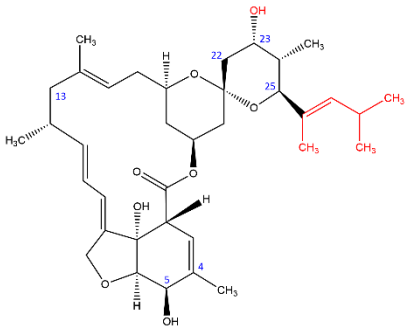	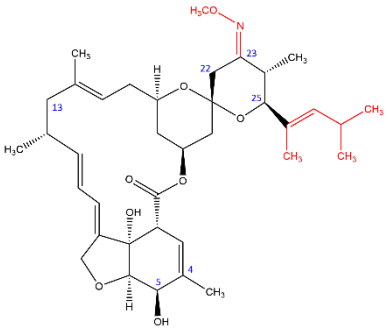

Table A2. List of non-commercial compounds used in this study. Red indicates structural changes from IVM-B1a. Blue numbers represent the C-positions.

1 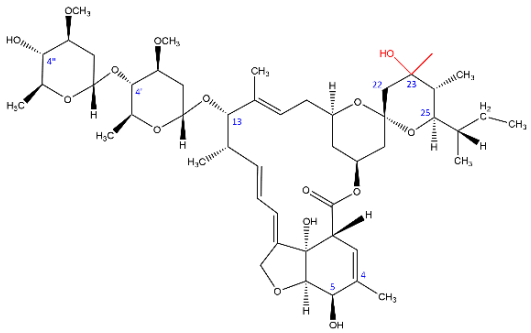	**2** 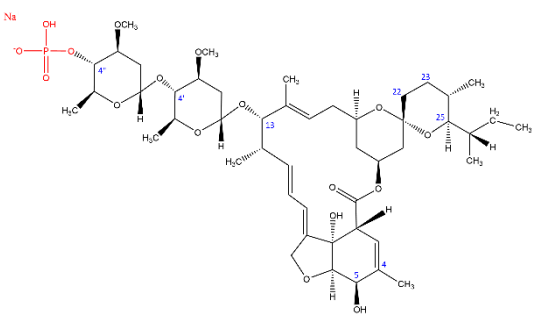
3 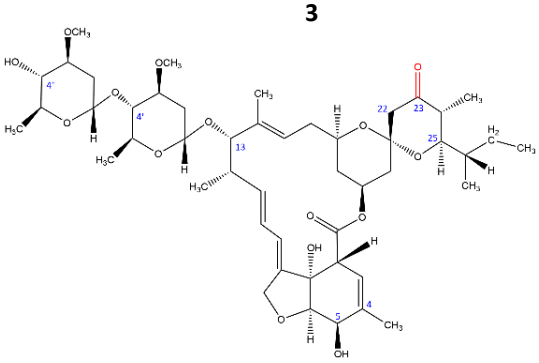	**4** 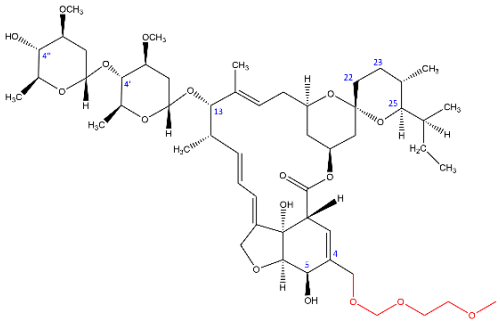
5 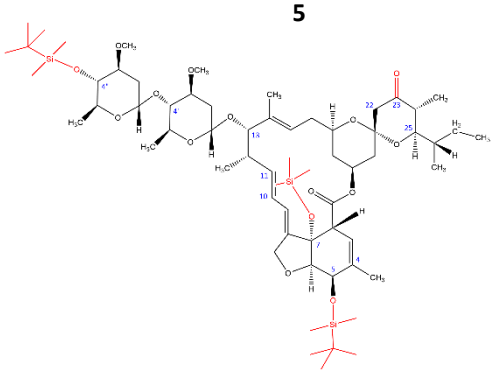	**6** 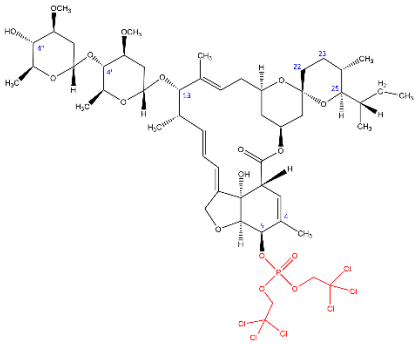
7 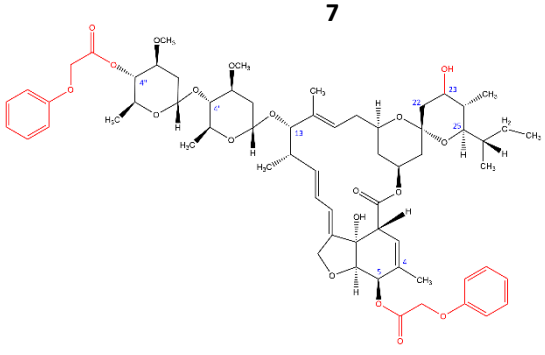	**8** 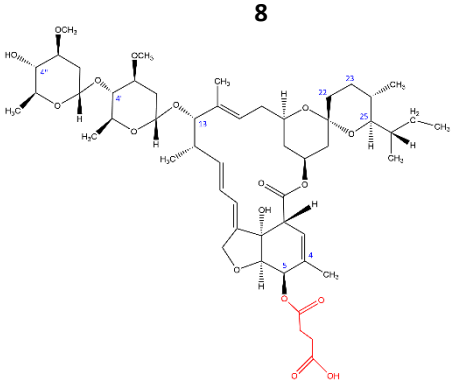

Table A2. (cont.) List of compounds used in this study. Red indicates structural changes from IVM-B1a. Blue numbers represent the C-positions.

9 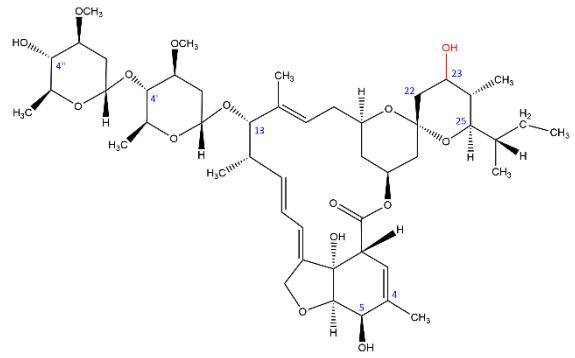	**10** 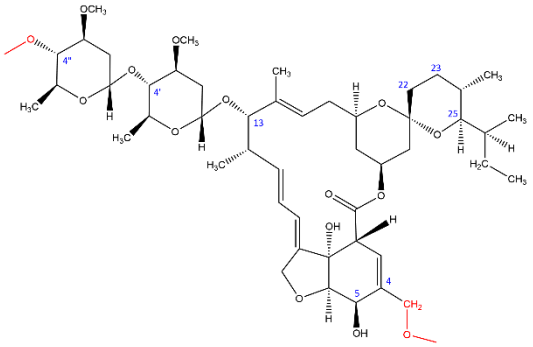
11 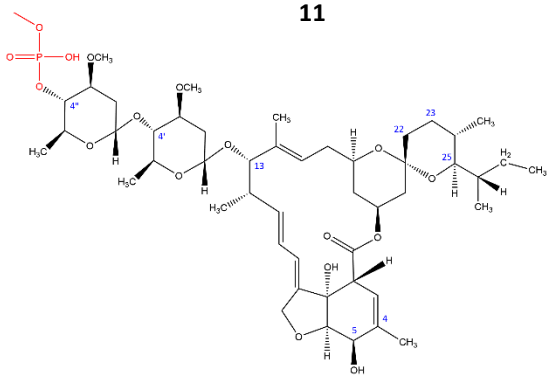	**12** 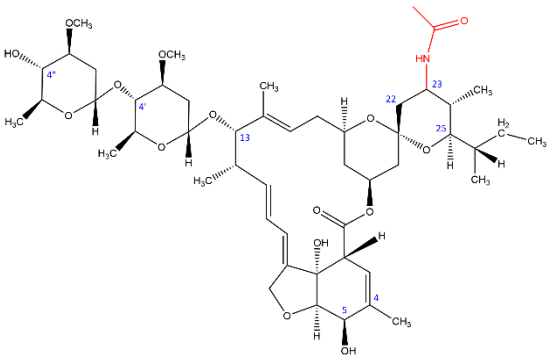
13 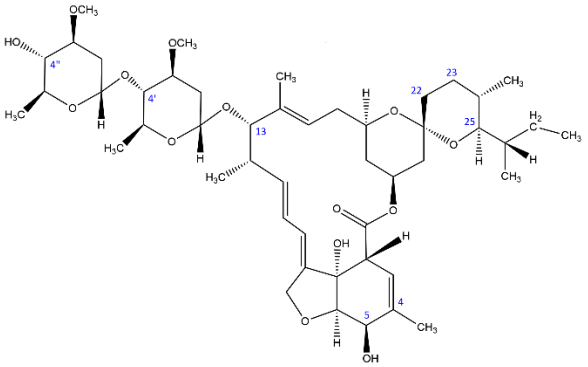	**14** 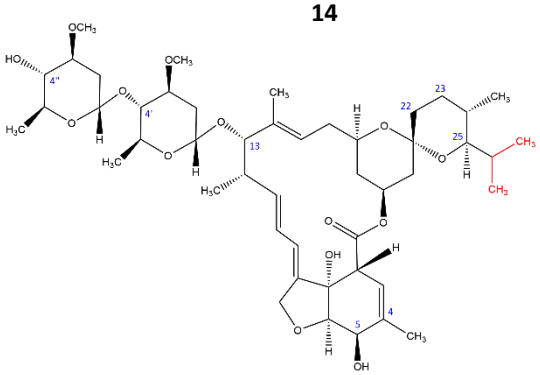
15 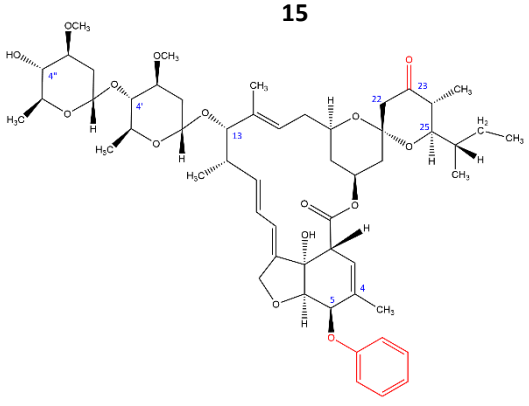	**16** 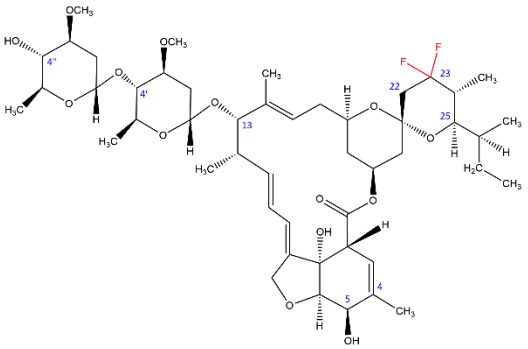

Table A2. (cont.) List of compounds used in this study. Red indicates structural changes from IVM-B1a. Blue numbers represent the C-positions.

17 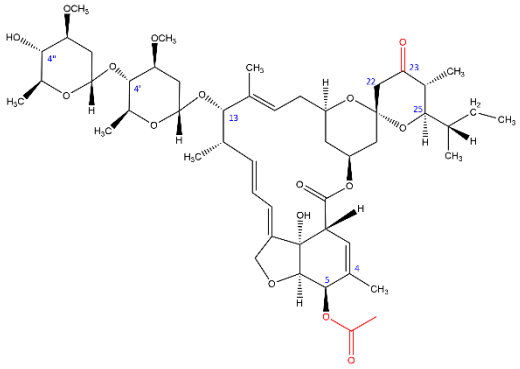	**18** 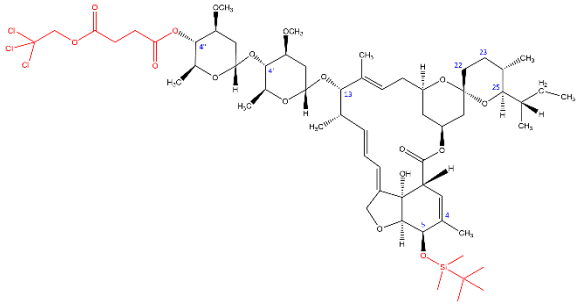
19 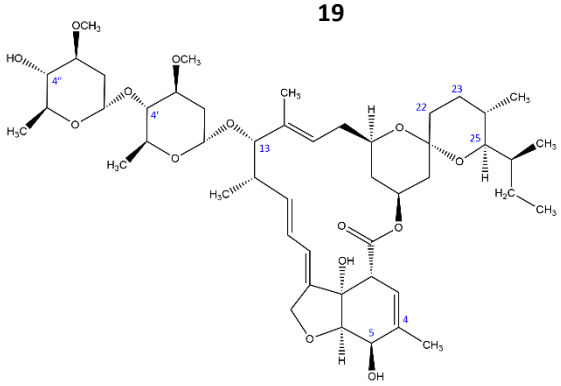	**20** 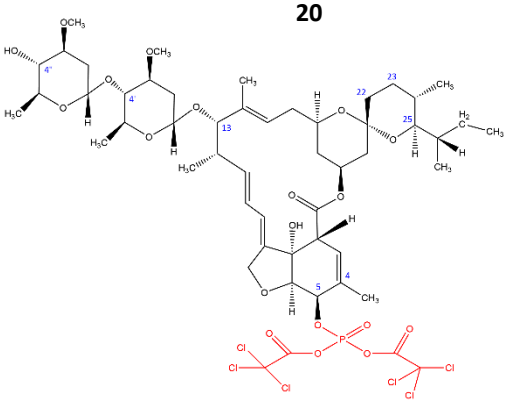
21 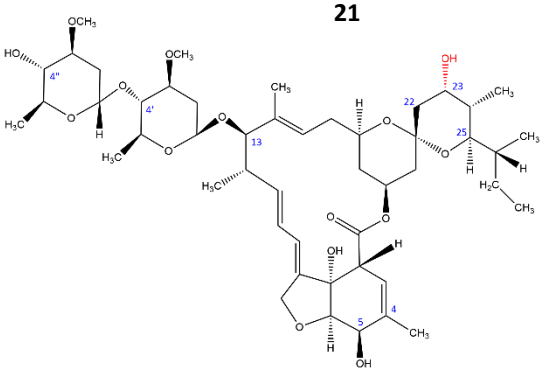	**22** 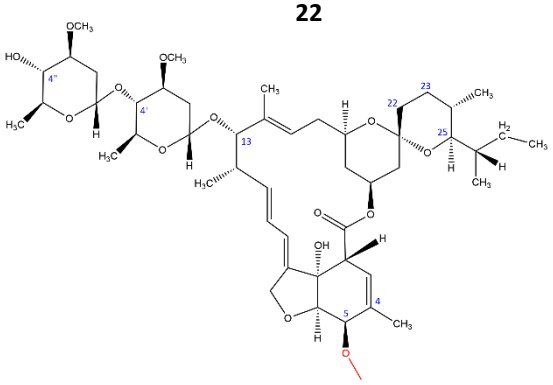
23 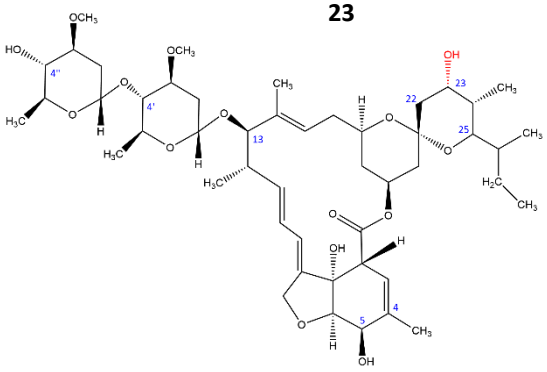	**24** 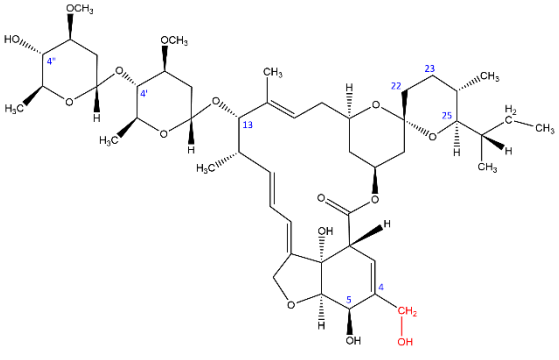

Table A2 (cont.) List of compounds used in this study. Red indicates structural changes from IVM-B1a. Blue numbers represent the C-positions.

25 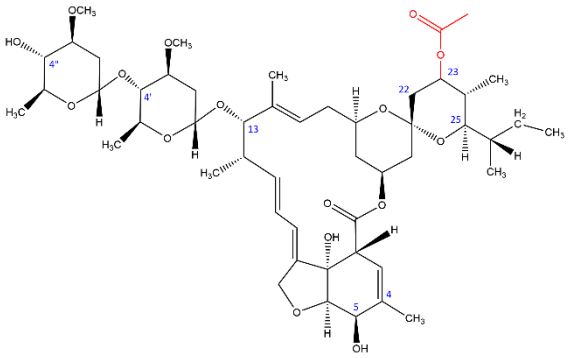	**26** 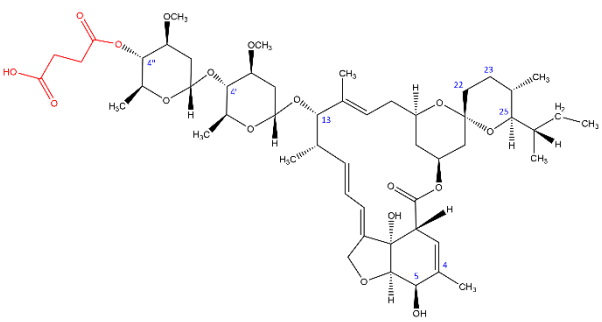
27 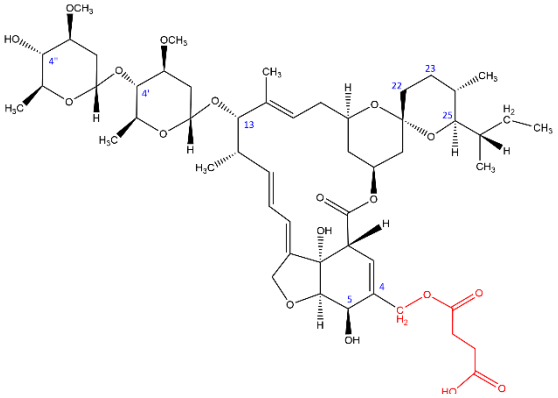	

References

Abdelrahman, A., Namasivayam, V., Hinz, S., Schiedel, A. C., Köse, M., Burton, M., … Müller, C. E. (2017). Characterization of P2X4 receptor agonists and antagonists by calcium influx and radioligand binding studies. *Biochemical Pharmacology*, *125*, 41–54. https://doi.org/10.1016/j.bcp.2016.11.016

Acuña-Castillo, C., Morales, B., & Huidobro-Toro, J. P. (2000). Zinc and copper modulate differentially the P2X4 receptor. *Journal of Neurochemistry*, *74*(4), 1529–1537. https://doi.org/10.1046/j.1471-4159.2000.0741529.x

Adelsberger, H., Lepier, A., & Dudel, J. (2000). Activation of rat recombinant α1β2γ(2S) GABA(A) receptor by the insecticide ivermectin. *European Journal of Pharmacology*, *394*(2–3), 163–170. https://doi.org/10.1016/S0014-2999(00)00164-3

Ahern, G. P., Junankar, P. R., Pace, S. M., Curtis, S., Mould, J. A., & Dulhunty, A. F. (1999). Effects of ivermectin and midecamycin on ryanodine receptors and the Ca^{2+} -ATPase in sarcoplasmic reticulum of rabbit and rat skeletal muscle. *The Journal of Physiology*, *514*(2), 313–326. https://doi.org/10.1111/j.1469-7793.1999.313ae.x

Aia, Brancale, A., & Young, M. T. (2018). The Molecular Determinants of Small-Molecule Ligand Binding at P2X Receptors. *Frontiers in Pharmacology*, *9*, 1–13. https://doi.org/10.3389/fphar.2018.00058

Asatryan, L., Nam, H. W., Lee, M. R., Thakkar, M. M., Saeed Dar, M., Davies, D. L., & Choi, D.-S. (2011). Implication of the Purinergic System in Alcohol Use Disorders. *Alcoholism: Clinical and Experimental Research*, *35*(4), 584–594. https://doi.org/10.1111/j.1530-0277.2010.01379.x

Asatryan, L., Popova, M., Perkins, D., Trudell, J. R., Alkana, R. L., & Davies, D. L. (2010). Ivermectin antagonizes ethanol inhibition in purinergic P2X4 receptors. *Journal of Pharmacology and Experimental Therapeutics*, *334*(3), 720–728. https://doi.org/10.1124/jpet.110.167908

Asatryan, L., Popova, M., Woodward, J. J., King, B. F., Alkana, R. L., & Davies, D. L. (2008). Roles of ectodomain and transmembrane regions in ethanol and agonist action in purinergic P2X2 and P2X3 receptors. *Neuropharmacology*, *55*(5), 835–843. https://doi.org/10.1016/j.neuropharm.2008.06.044

Asatryan, L., Yardley, M. M., Khoja, S., Trudell, J. R., Hyunh, N., Louie, S. G., … Davies, D. L. (2014). Avermectins differentially affect ethanol intake and receptor function: implications for developing new therapeutics for alcohol use disorders. *The International Journal of Neuropsychopharmacology*, *17*(06), 907–916. https://doi.org/10.1017/S1461145713001703

Ase, A. R., Honson, N. S., Zaghdane, H., Pfeifer, T. A., & Seguela, P. (2015). Identification and Characterization of a Selective Allosteric Antagonist of Human P2X4 Receptor Channels. *Molecular Pharmacology*, *87*(4), 606–616. https://doi.org/10.1124/mol.114.096222

Ase, A. R., Therrien, É., & Séguéla, P. (2019). An Allosteric Inhibitory Site Conserved in the Ectodomain of P2X Receptor Channels, *13*, 1–11. https://doi.org/10.3389/fncel.2019.00121

Baeyens, N., Bandyopadhyay, C., Coon, B. G., Yun, S., & Schwartz, M. A. (2016). Endothelial fluid shear stress sensing in vascular health and disease. *Journal of Clinical Investigation*, *126*(3), 821–828. https://doi.org/10.1172/JCI83083

Balázs, B., Dankó, T., Kovács, G., Köles, L., Hediger, M. A., & Zsembery, Á. (2013). Investigation of the inhibitory effects of the benzodiazepine derivative, 5-BDBD on P2X 4 purinergic receptors by two complementary methods. *Cellular Physiology and Biochemistry*, *32*(1), 11–24. https://doi.org/10.1159/000350119

Baxter, D. F., Kirk, M., Garcia, A. F., Raimondi, A., Holmqvist, M. H., Flint, K. K., … Xie, Y. (2002). A Novel Membrane Potential-Sensitive Fluorescent Dye Improves Cell-Based Assays for Ion Channels. *SLAS Discovery*, *7*(1), 79–85. https://doi.org/10.1177/108705710200700110

Bianchi, B. R., Lynch, K. J., Touma, E., Niforatos, W., Burgard, E. C., Alexander, K. M., … Van Biesen, T. (1999). Pharmacological characterization of recombinant human and rat P2X receptor subtypes. *European Journal of Pharmacology*, *376*(1–2), 127–138. https://doi.org/10.1016/S0014-2999(99)00350-7

Bidula, S. M., Cromer, B. A., Walpole, S., Angulo, J., & Stokes, L. (2019). Mapping a novel positive allosteric modulator binding site in the central vestibule region of human P2X7. *Scientific Reports*, *9*(1), 1–11. https://doi.org/10.1038/s41598-019-39771-5

Bilmen, J. G., Wootton, L. L., & Michelangeli, F. (2002). The inhibition of the sarcoplasmic/endoplasmic reticulum Ca2+-ATPase by macrocyclic lactones and cyclosporin A. *Biochemical Journal*, *366*(1), 255–263. https://doi.org/10.1042/bj20020431

Bowler, J. W., Jayne Bailey, R., Alan North, R., & Surprenant, A. (2003). P2X4 , P2Y1 and P2Y2 receptors on rat alveolar macrophages. *British Journal of Pharmacology*, *140*(3), 567–575. https://doi.org/10.1038/sj.bjp.0705459

Burnstock, G. (2006). Purinergic signalling. *British Journal of Pharmacology*, *147*, 172–181. https://doi.org/10.1038/sj.bjp.0706429

Burnstock, G. (2007). Physiology and Pathophysiology of Purinergic Neurotransmission. *Physiological Reviews*, *87*(2), 659–797. https://doi.org/10.1152/physrev.00043.2006

Burnstock, G., Campell, G., Satchell, D., & Smythe, A. (1970). Evidence that adenosine triphosphate or a related nucleotide is the transmitter substance released by non-adrenergic inhibitory nerves in the gut. *British Journal of Pharmacology*, *40*(4), 668–688. https://doi.org/10.1111/j.1476-5381.1970.tb10646.x

Burnstock, G., & Kennedy, C. (1985). Is there a basis for distinguishing two types of P_2-purinoceptor? *Gen Pharmacol*, *16*(5), 433–440.

Burnstock, G., & Ralevic, V. (1998). Receptor for purines and pyrimidines. *Pharmacological Reviews*, *50*(3), 413–492.

Burnstock, G., & Verkhratsky, A. (2012). Purinergic signaling (Review of 1972 paper). *Wiley Interdisciplinary Reviews: Membrane Transport and Signaling*, *1*(2), 116–125. https://doi.org/10.1002/wmts.14

Burton, R., & Marsden, J. (2016). The Public Health Burden of Alcohol and the Effectiveness and Cost-Effectiveness of Alcohol Control Policies An evidence review, (December), 241. Retrieved from http://www.gov.uk/phe%5Cnwww.facebook.com/PublicHealthEngland%5Cnalcoholenquiries@phe.gov.uk%5Cnwww.gov.uk/phe%5Cnwww.facebook.com/PublicHealthEngland%5Cnalcoholenquiries@phe.gov.uk

Chandler, R. E. (2018). Serious neurological adverse events after ivermectin-do they occur beyond the indication of onchocerciasis? *American Journal of Tropical Medicine and Hygiene*, *98*(2), 382–388. https://doi.org/10.4269/ajtmh.17-0042

Chataigneau, T., Lemoine, D., & Grutter, T. (2013). Exploring the ATP-binding site of P2X receptors. *Frontiers in Cellular Neuroscience*, *7*(December), 1–12. https://doi.org/10.3389/fncel.2013.00273

Chen, I. S., & Kubo, Y. (2018). Ivermectin and its target molecules: shared and unique modulation mechanisms of ion channels and receptors by ivermectin. *Journal of Physiology*, *596*(10), 1833–1845. https://doi.org/10.1113/JP275236

Chen, I. S., Tateyama, M., Fukata, Y., Uesugi, M., & Kubo, Y. (2017). Ivermectin activates GIRK channels in a PIP2-dependent, Gβγ-independent manner and an amino acid residue at the slide helix governs the activation. *Journal of Physiology*, *595*(17), 5895–5912. https://doi.org/10.1113/JP274871

Clarke, C. E., Benham, C. D., Bridges, A., George, A. R., & Meadows, H. J. (2000). Mutation of histidine 286 of the human P2X4 purinoceptor removes extracellular pH sensitivity. *Journal of Physiology*, *523*(3), 697–703. https://doi.org/10.1111/j.1469-7793.2000.00697.x

Clayden, J., Greeves, N., & Warren, S. (2012). Organic Chemistry (2nd ed.). Oxford University Press

Coddou, C., Lorca, R. A., Acuña-Castillo, C., Grauso, M., Rassendren, F., & Huidobro-Toro, J. P. (2005). Heavy metals modulate the activity of the purinergic P2X 4 receptor. *Toxicology and Applied Pharmacology*, *202*(2), 121–131. https://doi.org/10.1016/j.taap.2004.06.015

Coddou, C., Stojilkovic, S. S., & Huidobro-Toro, J. P. (2011). Allosteric modulation of ATP-gated P2X receptor channels. *Revneuro*, *22*(3), 335–354. https://doi.org/10.1515/rns.2011.014

Coddou, C., Yan, Z., Obsil, T., Huidobro-Toro, J. P., & Stojilkovic, S. S. (2011). Activation and Regulation of Purinergic P2X Receptor Channels. *Pharmacological Reviews*, *63*(3), 641–683. https://doi.org/10.1124/pr.110.003129

Collins, T., & Millar, N. S. (2010). Nicotinic Acetylcholine Receptor Transmembrane Mutations Convert Ivermectin from a Positive to a Negative Allosteric Modulator. *Molecular Pharmacology*, *78*(2), 198–204. https://doi.org/10.1124/mol.110.064295

Crump, A., & Omura, S. (2011). Ivermectin, 'Wonder drug' from Japan: the human use perspective. *Proceedings of the Japan Academy, Series B*, *87*(2), 13–28. https://doi.org/10.2183/pjab.87.13

Csóka, B., Németh, Z. H., Szabó, I., Davies, D. L., Varga, Z. V, Pálóczi, J., … Haskó, G. (2018). Macrophage P2X4 receptors augment bacterial killing and protect against sepsis, *3*(11), 1–18.

Dao-Ung, P., Skarratt, K. K., Fuller, S. J., & Stokes, L. (2015). Paroxetine suppresses recombinant human P2X7 responses. *Purinergic Signalling*, *11*(4), 481–490. https://doi.org/10.1007/s11302-015-9467-2

Davies, D. L., Kochegarov, A. A., Kuo, S. T., Kulkarni, A. A., Woodward, J. J., King, B. F., & Alkana, R. L. (2005). Ethanol differentially affects ATP-gated P2X3 and P2X4 receptor subtypes expressed in Xenopus oocytes. *Neuropharmacology*, *49*(2), 243–253. https://doi.org/10.1016/j.neuropharm.2005.03.015

Dhuna, K., Felgate, M., Bidula, S. M., Walpole, S., Bibic, L., Cromer, B. A., … Stokes, L. (2019). Ginsenosides Act As Positive Modulators of P2X4 Receptors. *Molecular Pharmacology*, *95*(2), 210–221. https://doi.org/10.1124/mol.118.113696

Du, J., Lü, W., Wu, S., Cheng, Y., & Gouaux, E. (2015). Glycine receptor mechanism elucidated by electron cryo-microscopy. *Nature*, *526*(7572), 224–229. https://doi.org/10.1038/nature14853

Edwards, G. (2003). Ivermectin: does P-glycoprotein play a role in neurotoxicity? *Filaria Journal*, *2*(Suppl 1), S8. https://doi.org/10.1186/1475-2883-2-S1-S8

Egan, T. M., & Khakh, B. S. (2004). Contribution of calcium ions to P2X channel responses. *The Journal of neuroscience : the official journal of the Society for Neuroscience*, *24*(13), 3413–3420. https://doi.org/10.1523/JNEUROSCI.5429-03.2004

Estrada-Mondragon, A., & Lynch, J. W. (2015). Functional characterization of ivermectin binding sites in α1β2γ2L GABA(A) receptors. *Frontiers in Molecular Neuroscience*, *8*(September), 1–13. https://doi.org/10.3389/fnmol.2015.00055

Feng, H.-J., & Forman, S. A. (2018). Comparison of αβδ and αβγ GABAA receptors: Allosteric modulation and identification of subunit arrangement by site-selective general anesthetics. *Pharmacological Research*, *133*(1), 289–300. https://doi.org/10.1016/j.phrs.2017.12.031

Filtz, T. M., Li, Q., Boyer, J. L., Nicholas, R. A., & Harden, T. K. (1994). Expression of a cloned P(2Y) purinergic receptor that couples to phospholipase C. *Molecular Pharmacology*, *46*(1), 8–14.

Franklin, K. M., Asatryan, L., Jakowec, M. W., Trudell, J. R., Bell, R. L., & Davies, D. L. (2014). P2X4 receptors (P2X4Rs) represent a novel target for the development of drugs to prevent and/or treat alcohol use disorders. *Frontiers in Neuroscience*, *8*(8 JUN), 1–12. https://doi.org/10.3389/fnins.2014.00176

Gao, C., Yu, Q., Xu, H., Zhang, L., Liu, J., Jie, Y., … Li, Z. (2015). Roles of the lateral fenestration residues of the P2X4 receptor that contribute to the channel function and the deactivation effect of ivermectin. *Purinergic Signalling*, *11*(2), 229–238. https://doi.org/10.1007/s11302-015-9448-5

Garcia-Guzman, M., Soto, F., Gomez-Hernandez, J. M., Lund, P.-E., & Stühmer, W. (1997). Characterization of Recombinant Human P2X4 Receptor Reveals Pharmacological Differences to the Rat Homologue. *Molecular Pharmacology*, *51*(1), 109–118. https://doi.org/10.1124/mol.51.1.109

Gillis, E. P., Eastman, K. J., Hill, M. D., Donnelly, D. J., & Meanwell, N. A. (2015). Applications of Fluorine in Medicinal Chemistry. *Journal of Medicinal Chemistry*, *58*(21), 8315–8359. https://doi.org/10.1021/acs.jmedchem.5b00258

Gouaux, E., & Hattori, M. (2012). Molecular mechanism of ATP binding and ion channel activation in P2X receptors. *National Institute of Health*, *485*(7397), 207–212. https://doi.org/10.1038/nature11010.Molecular

Grynkiewicz, G., Poenie, M., & Tsien, R. Y. (1985). A new generation of Ca^{2+} indicators with greatly improved fluorescence properties. *Journal of Biological Chemistry*, *260*(6), 3440–3450. https://doi.org/10.1016/S0021-9258(19)83641-4

Habermacher, C., Dunning, K., Chataigneau, T., & Grutter, T. (2016). Molecular structure and function of P2X receptors. Neuropharmacology, 104, 18–30.

https://doi.org/10.1016/j.neuropharm.2015.07.032

Han, S. J., Lovaszi, M., Kim, M., D'Agati, V., Haskó, G., & Lee, H. T. (2020). P2X4 receptor exacerbates ischemic AKI and induces renal proximal tubular NLRP3 inflammasome signaling. *The FASEB Journal*, *34*(4), 5465–5482. https://doi.org/10.1096/fj.201903287R

Helliwell, R. M., Shioukhuey, C. O., Dhuna, K., Molero, J. C., Ye, J. M., Xue, C. C., & Stokes, L. (2015). Selected ginsenosides of the protopanaxdiol series are novel positive allosteric modulators of P2X7 receptors. *British Journal of Pharmacology*, *172*(13), 3326–3340. https://doi.org/10.1111/bph.13123

Hernandez-Olmos, V., Abdelrahman, A., El-Tayeb, A., Freudendahl, D., Weinhausen, S., & Müller, C. E. (2012). N-Substituted Phenoxazine and Acridone Derivatives: Structure–Activity Relationships of Potent P2X4 Receptor Antagonists. *Journal of Medicinal Chemistry*, *55*(22), 9576–9588. https://doi.org/10.1021/jm300845v

Hibbs, R. E., & Gouaux, E. (2011). Principles of activation and permeation in an anion-selective Cys-loop receptor. *Nature*, *474*(7349), 54–60. https://doi.org/10.1038/nature10139

Hu, B., Mei, Q. B., Yao, X. J., Smith, E., Barry, W. H., & Liang, B. T. (2001). A novel contractile phenotype with cardiac transgenic expression of the human P2X4 receptor. *The FASEB Journal : Official Publication of the Federation of American Societies for Experimental Biology*, *15*(14), 2739–2741. https://doi.org/10.1096/fj.01-0445fje

Huang, X., Chen, H., & Shaffer, P. L. (2017). Crystal Structures of Human GlyRα3 Bound to Ivermectin. *Structure*, *25*(6), 945–950.e2. https://doi.org/10.1016/j.str.2017.04.007

Huynh, N., Arabian, N., Naito, A., Louie, S., Jakowec, M. W., Asatryan, L., & Davies, D. L. (2017). Preclinical development of moxidectin as a novel therapeutic for alcohol use disorder. *Neuropharmacology*, *113*, 60–70. https://doi.org/10.1016/j.neuropharm.2016.09.016

Huynh, N., Khoja, S., Asatryan, L., Jakowec, M. W., & Davies, D. L. (2019). *The avermectin family as potential therapeutic compounds for alcohol use disorder: Implications for using P2X4 receptor as a drug-screening platform*. *Neuroscience of Alcohol: Mechanisms and Treatment*. Elsevier Inc. https://doi.org/10.1016/B978-0-12-813125-1.00068-4

Illes, P., Müller, C. E., Jacobson, K. A., Grutter, T., Nicke, A., Fountain, S. J., Kennedy, C., Schmalzing, G., Jarvis, M. F., Stojilkovic, S. S., King, B. F., & di Virgilio, F. (2021). Update of P2X receptor properties and their pharmacology: IUPHAR Review 30. British Journal of Pharmacology, 178(3), 489–514. https://doi.org/10.1111/bph.15299

Jacobson, K. A., Delicado, E. G., Gachet, C., Kennedy, C., von Kügelgen, I., Li, B., … Müller, C. E. (2020). Update of P2Y receptor pharmacology: IUPHAR Review 27. *British Journal of Pharmacology*, *177*(11), 2413–2433. https://doi.org/10.1111/bph.15005

Jacobson, K. A., & Gao, Z. G. (2006). Adenosine receptors as therapeutic targets. *Nature Reviews Drug Discovery*, *5*(3), 247–264. https://doi.org/10.1038/nrd1983

Jelínkova, I., Vávra, V., Jindrichova, M., Obsil, T., Zemkova, H. W., Zemkova, H., & Stojilkovic, S. S. (2008). Identification of P2X4 receptor transmembrane residues contributing to channel gating and interaction with ivermectin. *Pflugers Archiv European Journal of Physiology*, *456*(5), 939–950. https://doi.org/10.1007/s00424-008-0450-4

Jelínková, I., Yan, Z., Liang, Z., Moonat, S., Teisinger, J., Stojilkovic, S. S., & Zemková, H. (2006). Identification of P2X4receptor-specific residues contributing to the ivermectin effects on channel deactivation. *Biochemical and Biophysical Research Communications*, *349*(2), 619–625. https://doi.org/10.1016/j.bbrc.2006.08.084

Jiang, L.-H., Kim, M., Spelta, V., Bo, X., Surprenant, A., & North, R. A. (2003). Subunit arrangement in P2X receptors. The Journal of Neuroscience, 23(26), 8903–8910. https://doi.org/10.1523/JNEUROSCI.23-26- 08903.2003

Jiao, Y., Lu, Y., & Li, X. Y. (2015). Farnesoid X receptor: A master regulator of hepatic triglyceride and glucose homeostasis. *Acta Pharmacologica Sinica*, *36*(1), 44–50. https://doi.org/10.1038/aps.2014.116

Jin, L., Feng, X., Rong, H., Pan, Z., Inaba, Y., Qiu, L., … Li, Y. (2013). The antiparasitic drug ivermectin is a novel FXR ligand that regulates metabolism. *Nature Communications*, *4*, 1–8. https://doi.org/10.1038/ncomms2924

Jin, L., Wang, R., Zhu, Y., Zheng, W., Han, Y., Guo, F., … Li, Y. (2015). Selective targeting of nuclear receptor FXR by avermectin analogues with therapeutic effects on nonalcoholic fatty liver disease. *Scientific Reports*, *5*(1), 17288. https://doi.org/10.1038/srep17288

Joesch, C., Guevarra, E., Parel, S. P., Bergner, A., Zbinden, P., Konrad, D., & Albrecht, H. (2008). Use of FLIPR membrane potential dyes for validation of high-throughput screening with the FLIPR and μARCS technologies: Identification of ion channel modulators acting on the GABAA receptor. *Journal of Biomolecular Screening*, *13*(3), 218–228. https://doi.org/10.1177/1087057108315036

Jones, C. A., Chessell, I. P., Simon, J., Barnard, E. A., Miller, K. J., Michel, A. D., & Humphrey, P. P. A. (2000). Functional characterization of the P2X4 receptor orthologues. *British Journal of Pharmacology*, *129*(2), 388–394. https://doi.org/10.1038/sj.bjp.0703059

Kadry, H., Noorani, B., & Cucullo, L. (2020). A blood–brain barrier overview on structure, function, impairment, and biomarkers of integrity. *Fluids and Barriers of the CNS*, *17*(1), 69. https://doi.org/10.1186/s12987-020-00230-3

Kanellopoulos, J. M., Almeida-da-Silva, C. L. C., Rüütel Boudinot, S., & Ojcius, D. M. (2021). Structural and Functional Features of the P2X4 Receptor: An Immunological Perspective. *Frontiers in Immunology*, *12*(March), 1–21. https://doi.org/10.3389/fimmu.2021.645834

Kawate, T., Michel, J. C., Birdsong, W. T., & Gouaux, E. (2009). Crystal structure of the ATP-gated P2X4 ion channel in the closed state, *460*(7255), 592–598. https://doi.org/10.1038/nature08198.Crystal

Keeley, T. P., Siow, R. C. M., Jacob, R., & Mann, G. E. (2018). Reduced SERCA activity underlies dysregulation of Ca2+ homeostasis under atmospheric O2 levels. *FASEB Journal*, *32*(5), 2531–2538. https://doi.org/10.1096/fj.201700685RRR

Keely, S. J., & Walters, J. R. F. (2016). The Farnesoid X Receptor: Good for BAD. *Cellular and Molecular Gastroenterology and Hepatology*, *2*(6), 725–732. https://doi.org/10.1016/j.jcmgh.2016.08.004

Khakh, B. S., Proctor, W. R., Dunwiddie, T. V, Labarca, C., & Lester, H. A. (1999). Allosteric Control of Gating and Kinetics at P2X4 Receptor Channels. *Channels*, *19*(17), 7289–7299. https://doi.org/10.1016/B978-0-12-374373-2.00014-5

Khoja, S., Shah, V., Garcia, D., Asatryan, L., Jakowec, M. W., & Davies, D. L. (2016). Role of purinergic P2X4 receptors in regulating striatal dopamine homeostasis and dependent behaviors. *Journal of Neurochemistry*, *139*(1), 134–148. https://doi.org/10.1111/jnc.13734

King, B. F. (2022). Rehabilitation of the P2X5 receptor: a re-evaluation of structure and function. Purinergic Signalling. https://doi.org/10.1007/s11302-022-09903-0

Kitazawa, T., Hirama, R., Masunaga, K., Nakamura, T., Asakawa, K., Cao, J., … Taneike, T. (2008). Muscarinic receptor subtypes involved in carbachol-induced contraction of mouse uterine smooth muscle. *Naunyn-Schmiedeberg's Archives of Pharmacology*, *377*(4–6), 503–513. https://doi.org/10.1007/s00210-007-0223-1

Krause, R. M., Buisson, B., Bertrand, S., Corringer, P.-J., Galzi, J.-L., Changeux, J.-P., & Bertrand, D. (1998). Ivermectin: A Positive Allosteric Effector of the α7 Neuronal Nicotinic Acetylcholine Receptor. *Molecular Pharmacology*, *53*(2), 283–294. https://doi.org/10.1124/mol.53.2.283

Krůšek, J., & Zemková, H. (1994). Effect of ivermectin on γ-aminobutyric acid-induced chloride currents in mouse hippocampal embryonic neurones. *European Journal of Pharmacology*, *259*(2), 121–128. https://doi.org/10.1016/0014-2999(94)90500-2

Latapiat, V., Rodríguez, F. E., Godoy, F., Montenegro, F. A., Barrera, N. P., & Huidobro-Toro, J. P. (2017). P2X4 receptor in silico and electrophysiological approaches reveal insights of ivermectin and zinc allosteric modulation. *Frontiers in Pharmacology*, *8*(DEC), 1–13. https://doi.org/10.3389/fphar.2017.00918

Layhadi, J. A., Turner, J., Crossman, D., & Fountain, S. J. (2018). ATP Evokes Ca^{2+} Responses and CXCL5 Secretion via P2X 4 Receptor Activation in Human Monocyte-Derived Macrophages. *The Journal of Immunology*, *200*(3), 1159–1168. https://doi.org/10.4049/jimmunol.1700965

Li, F., Guo, N., Ma, Y., Ning, B., Wang, Y., & Kou, L. (2014). Inhibition of P2X4 suppresses joint inflammation and damage in collagen-induced arthritis. *Inflammation*, *37*(1), 146–153. https://doi.org/10.1007/s10753-013-9723-y

Li, J., & Fountain, S. J. (2012). Fluvastatin suppresses native and recombinant human P2X4 receptor function. *Purinergic Signalling*, *8*(2), 311–316. https://doi.org/10.1007/s11302-011-9289-9

Lovell RA. (1990). Ivermectin and piperazine toxicoses in dogs and cats. *Vet Clin North Am Small Anim Pract*, 20(2), 453-68. https://doi.org/10.1016/s0195-5616(90)50038-8

Mathie, A., Sutton, G. L., Clarke, C. E., & Veale, E. L. (2006). Zinc and copper: Pharmacological probes and endogenous modulators of neuronal excitability. *Pharmacology and Therapeutics*, *111*(3), 567–583. https://doi.org/10.1016/j.pharmthera.2005.11.004

Mealey, Katrina L.a; Bentjen, Steve A.a; Gay, John M.a; Cantor, Glenn H.b. (2001). Ivermectin sensitivity in collies is associated with a deletion mutation of the mdr1 gene. *Pharmacogenetics* 11(8), 727-733. https://doi.org/10.1097/00008571-200111000-00012

Ménez, C., Sutra, J. F., Prichard, R., & Lespine, A. (2012). Relative Neurotoxicity of Ivermectin and Moxidectin in Mdr1ab (-/-) Mice and Effects on Mammalian GABA(A) Channel Activity. *PLoS Neglected Tropical Diseases*, *6*(11). https://doi.org/10.1371/journal.pntd.0001883

Merola, V. M., & Eubig, P. A. (2012). Toxicology of Avermectins and Milbemycins (Macrocylic Lactones) and the Role of P-Glycoprotein in Dogs and Cats. *Veterinary Clinics of North America: Small*

Animal Practice, *42*(2), 313–333. https://doi.org/10.1016/j.cvsm.2011.12.005

Mountian, I., Manolopoulos, V. G., Smedt, H. De, Parys, J. B., Missiaen, L., & Wuytack, F. (1999). Expression patterns of sarco / endoplasmic reticulum Ca^{2+} -ATPase and inositol in vascular endothelial cells, *25*, 371–380.

Musa, H., Tellez, J. O., Chandler, N. J., Greener, I. D., Mączewski, M., MacKiewicz, U., … Dobrzynski, H. (2009). P2 purinergic receptor mRNA in rat and human sinoatrial node and other heart regions. *Naunyn-Schmiedeberg's Archives of Pharmacology*, *379*(6), 541–549. https://doi.org/10.1007/s00210-009-0403-2

Nagata, K., Imai, T., Yamashita, T., Tsuda, M., Tozaki-Saitoh, H., & Inoue, K. (2009). Antidepressants inhibit P2X4 receptor function: A possible involvement in neuropathic pain relief. *Molecular Pain*, *5*, 1–12. https://doi.org/10.1186/1744-8069-5-20

Nasu-Tada, K., Koizumi, S., Tsuda, M., Kunifusa, E., & Inoue, K. (2006). Possible involvement of increase in spinal fibronectin following peripheral nerve injury in upregulation of microglial P2X4, a key molecule for mechanical allodynia. *Glia*, *53*(7), 769–775. https://doi.org/10.1002/glia.20339

Nik, A. M., Pressly, B., Singh, V., Antrobus, S., Hulsizer, S., Rogawski, M. A., … Pessah, I. N. (2017). Rapid throughput analysis of GABAA receptor subtype modulators and blockers using DiSBAC1(3) membrane potential red dye. *Molecular Pharmacology*, *92*(1), 88–99. https://doi.org/10.1124/mol.117.108563

Noël, F., Pimenta, P. H. C., Dos Santos, A. R., Tomaz, E. C. L., Quintas, L. E. M., Kaiser, C. R., … Férézou, J. P. (2011). Δ2,3 -Ivermectin ethyl secoester, a conjugated ivermectin derivative with leishmanicidal activity but without inhibitory effect on mammalian P-type ATPases. *Naunyn-Schmiedeberg's Archives of Pharmacology*, *383*(1), 101–107. https://doi.org/10.1007/s00210-010-0578-6

Nörenberg, W., Sobottka, H., Hempel, C., Plötz, T., Fischer, W., Schmalzing, G., & Schaefer, M. (2012). Positive allosteric modulation by ivermectin of human but not murine P2X7 receptors. *British Journal of Pharmacology*, *167*(1), 48–66. https://doi.org/10.1111/j.1476-5381.2012.01987.x

North, R. A. (2002). Molecular Physiology of P2X Receptors. *Physiological Reviews*, *82*(4), 1013–1067. https://doi.org/10.1152/physrev.00015.2002

North, R. A., & Jarvis, M. F. (2013). P2X receptors as drug targets. *Molecular Pharmacology*, *83*(4), 759–769. https://doi.org/10.1124/mol.112.083758

North, R. A., & Surprenant, A. (2000). Pharmacology of Cloned P2X Receptors. *Annual Review of Pharmacology and Toxicology*, *40*(1), 563–580. https://doi.org/10.1146/annurev.pharmtox.40.1.563

Oken, A. C., Krishnamurthy, I., Savage, J. C., Lisi, N. E., Godsey, M. H., & Mansoor, S. E. (2022). Molecular Pharmacology of P2X Receptors: Exploring Druggable Domains Revealed by Structural Biology. *Frontiers in Pharmacology*, *13*(June). https://doi.org/10.3389/fphar.2022.925880

Õmura, S. (2008). Ivermectin: 25 years and still going strong. *International Journal of Antimicrobial Agents*, *31*(2), 91–98. https://doi.org/10.1016/j.ijantimicag.2007.08.023

Paredes, R. M., Etzler, J. C., Watts, L. T., Zheng, W., & Lechleiter, J. D. (2008). Chemical calcium indicators. *Methods*, *46*(3), 143–151. https://doi.org/10.1016/j.ymeth.2008.09.025

Parisi, L., Toffoli, A., Ghezzi, B., Mozzoni, B., Lumetti, S., & Macaluso, G. M. (2020). A glance on the role of fibronectin in controlling cell response at biomaterial interface. *Japanese Dental Science Review*, *56*(1), 50–55. https://doi.org/10.1016/j.jdsr.2019.11.002

Pimenta, P. H. C., Silva, C. L. M., & Noël, F. (2010). Ivermectin is a nonselective inhibitor of mammalian P-type ATPases. *Naunyn-Schmiedeberg's Archives of Pharmacology*, *381*(2), 147–152. https://doi.org/10.1007/s00210-009-0483-z

Pontén J, Macintyre EH. (1968). Long term culture of normal and neoplastic human glia. Acta Pathol Microbiol Scand, 74(4), 465-86. https://doi.org/10.1111/j.1699-0463.1968.tb03502.x

Popova, M., Asatryan, L., Ostrovskaya, O., Wyatt, L. R., Li, K., Alkana, R. L., & Davies, D. L. (2010). A point mutation in the ectodomain-transmembrane 2 interface eliminates the inhibitory effects of ethanol in P2X4 receptors. *Journal of Neurochemistry*, *112*(1), 307–317. https://doi.org/10.1111/j.1471-4159.2009.06460.x

Popova, M., Trudell, J., Li, K., Alkana, R., Davies, D., & Asatryan, L. (2013). Tryptophan 46 is a site for ethanol and ivermectin action in P2X4 receptors. *Purinergic Signalling*, *9*(4), 621–632. https://doi.org/10.1007/s11302-013-9373-4

Priel, A., & Silberberg, S. D. (2004). Mechanism of Ivermectin Facilitation of Human P2X4 Receptor Channels. *Journal of General Physiology*, *123*(3), 281–293. https://doi.org/10.1085/jgp.200308986

Qureshi, O. S., Paramasivam, A., Yu, J. C. H., & Murrell-Lagnado, R. D. (2007). Regulation of P2X4 receptors by lysosomal targeting, glycan protection and exocytosis. *Journal of Cell Science*, *120*(21), 3838–3849. https://doi.org/10.1242/jcs.010348

Ralevic, V. (2012). P2X receptors in the cardiovascular system. *Wiley Interdisciplinary Reviews: Membrane Transport and Signaling*, *1*(5), 663–674. https://doi.org/10.1002/wmts.58

Robinson, L. E., & Murrell-Lagnado, R. D. (2013). The trafficking and targeting of P2X receptors. *Frontiers in Cellular Neuroscience*, *7*(NOV), 1–6. https://doi.org/10.3389/fncel.2013.00233

Sakaki, H., Fujiwaki, T., Tsukimoto, M., Kawano, A., Harada, H., & Kojima, S. (2013). P2X4 receptor regulates P2X7 receptor-dependent IL-1β and IL-18 release in mouse bone marrow-derived dendritic cells. *Biochemical and Biophysical Research Communications*, *432*(3), 406–411. https://doi.org/10.1016/j.bbrc.2013.01.135

Samways, D. S. K., Khakh, B. S., Dutertre, S., & Egan, T. M. (2011). Preferential use of unobstructed lateral portals as the access route to the pore of human ATP-gated ion channels (P2X receptors). *Proceedings of the National Academy of Sciences of the United States of America*, *108*(33), 13800–13805. https://doi.org/10.1073/pnas.1017550108

Samways, D. S. K., Khakhs, B. S., & Egan, T. M. (2012). Allosteric modulation of Ca 2+ flux in ligand-gated cation channel (P2X4) by actions on lateral portals. *Journal of Biological Chemistry*, *287*(10), 7594–7602. https://doi.org/10.1074/jbc.M111.322461

Samways, D. S. K., Li, Z., & Egan, T. M. (2014). Principles and properties of ion flow in P2X receptors. *Frontiers in Cellular Neuroscience*, *8*(February), 1–18. https://doi.org/10.3389/fncel.2014.00006

Sattelle, D. B., Buckingham, S. D., Akamatsu, M., Matsuda, K., Pienaar, I., Jones, A. K., … Blundell, C. D. (2009). Comparative pharmacology and computational modelling yield insights into allosteric

modulation of human α7 nicotinic acetylcholine receptors. *Biochemical Pharmacology*, *78*(7), 836–843. https://doi.org/10.1016/j.bcp.2009.06.020

Schneider, M., Prudic, K., Pippel, A., & Klapperstück, M. (2017). Interaction of Purinergic P2X4 and P2X7 Receptor Subunits, *8*(November), 1–14. https://doi.org/10.3389/fphar.2017.00860

Serafini, M., Cargnin, S., Massarotti, A., Pirali, T., & Genazzani, A. A. (2020). Essential Medicinal Chemistry of Essential Medicines. *Journal of Medicinal Chemistry*, *63*(18), 10170–10187. https://doi.org/10.1021/acs.jmedchem.0c00415

Shah, P., & Westwell, A. D. (2007). The role of fluorine in medicinal chemistry. *Journal of Enzyme Inhibition and Medicinal Chemistry*, *22*(5), 527–540. https://doi.org/10.1080/14756360701425014

Shan, Q., Haddrill, J. L., & Lynch, J. W. (2001). Ivermectin, an Unconventional Agonist of the Glycine Receptor Chloride Channel. *Journal of Biological Chemistry*, *276*(16), 12556–12564. https://doi.org/10.1074/jbc.M011264200

Shen, J.-B., Pappano, A. J., & Liang, B. T. (2006). Extracellular ATP-stimulated current in wild-type and P2X4 receptor transgenic mouse ventricular myocytes: implications for a cardiac physiologic role of P2X4 receptors. *The FASEB Journal*, *20*(2), 277–284. https://doi.org/10.1096/fj.05-4749com

Silberberg, S. D., Li, M., & Swartz, K. J. (2007). Ivermectin Interaction with Transmembrane Helices Reveals Widespread Rearrangements during Opening of P2X Receptor Channels. *Neuron*, *54*(2), 263–274. https://doi.org/10.1016/j.neuron.2007.03.020

Sivcev, S., Slavikova, B., Ivetic, M., Knezu, M., Kudova, E., & Zemkova, H. (2020). Lithocholic acid inhibits P2X2 and potentiates P2X4 receptor channel gating. *Journal of Steroid Biochemistry and Molecular Biology*, *202*(June), 105725. https://doi.org/10.1016/j.jsbmb.2020.105725

Sivcev, S., Slavikova, B., Rupert, M., Ivetic, M., Nekardova, M., Kudova, E., & Zemkova, H. (2019). Synthetic testosterone derivatives modulate rat P2X2 and P2X4 receptor channel gating. *Journal of Neurochemistry*, jnc.14718. https://doi.org/10.1111/jnc.14718

Sonin, D., Zhou, S. Y., Cronin, C., Sonina, T., Wu, J., Jacobson, K. A., … Liang, B. T. (2008). Role of P2X purinergic receptors in the rescue of ischemic heart failure. *American Journal of Physiology - Heart and Circulatory Physiology*, *295*(3), 1191–1197. https://doi.org/10.1152/ajpheart.00577.2008

Sophocleous, R. A., Berg, T., Finol-Urdaneta, R. K., Sluyter, V., Keshiya, S., Bell, L., … Sluyter, R. (2020). Pharmacological and genetic characterisation of the canine P2X4 receptor. *British Journal of Pharmacology*, *0*(July 2019), bph.15009. https://doi.org/10.1111/bph.15009

Sophocleous, R. A., Ooi, L., & Sluyter, R. (2022). The P2X4 Receptor: Cellular and Molecular Characteristics of a Promising Neuroinflammatory Target. *International Journal of Molecular Sciences*, *23*(10). https://doi.org/10.3390/ijms23105739

Soto, F., Garcia-Guzman, M., Gomez-Hernandez, J. M., Hollmann, M., Karschin, C., & Stuhmer, W. (1996). P2X4: an ATP-activated ionotropic receptor cloned from rat brain. *Proceedings of the National Academy of Sciences*, *93*(8), 3684–3688. https://doi.org/10.1073/pnas.93.8.3684

Stokes, L. (2013). Rab5 regulates internalisation of P2X4 receptors and potentiation by ivermectin. *Purinergic Signalling*, *9*(1), 113–121. https://doi.org/10.1007/s11302-012-9336-1

Stokes, L., Bidula, S., Bibič, L., & Allum, E. (2020). To Inhibit or Enhance? Is There a Benefit to Positive Allosteric Modulation of P2X Receptors? *Frontiers in Pharmacology*, *11*(May), 1–21. https://doi.org/10.3389/fphar.2020.00627

Stokes, L., Layhadi, J. A., Bibic, L., Dhuna, K., & Fountain, S. J. (2017). P2X4 Receptor Function in the Nervous System and Current Breakthroughs in Pharmacology. *Frontiers in Pharmacology*, *8*(MAY), 1–15. https://doi.org/10.3389/fphar.2017.00291

Stokes, L., Scurrah, K., Ellis, J. A., Cromer, B. A., Skarratt, K. K., Gu, B. J., … Wiley, J. S. (2011). A loss-of-function polymorphism in the human P2X4 receptor is associated with increased pulse pressure. *Hypertension*, *58*(6), 1086–1092. https://doi.org/10.1161/HYPERTENSIONAHA.111.176180

Surprenant, A., & North, R. A. (2009). Signaling at Purinergic P2X Receptors. *Annual Review of Physiology*, *71*(1), 333–359. https://doi.org/10.1146/annurev.physiol.70.113006.100630

Suurväli, J., Boudinot, P., Kanellopoulos, J., & Rüütel Boudinot, S. (2017). P2X4: A fast and sensitive purinergic receptor. *Biomedical Journal*, *40*(5), 245–256. https://doi.org/10.1016/j.bj.2017.06.010

Tang, Y., Matsuoka, I., Ono, T., Inoue, K., & Kimura, J. (2008). Selective up-regulation of P2X4-receptor gene expression by interferon-γ in vascular endothelial cells. *Journal of Pharmacological Sciences*, *107*(4), 419–427. https://doi.org/10.1254/jphs.08073FP

Toulme, E. (2006). Functional Properties of Internalization-Deficient P2X4 Receptors Reveal a Novel Mechanism of Ligand-Gated Channel Facilitation by Ivermectin. *Molecular Pharmacology*, *69*(2), 576–587. https://doi.org/10.1124/mol.105.018812

Toulme, E., Garcia, A., Samways, D., Egan, T. M., Carson, M. J., & Khakh, B. S. (2010). P2X4 receptors in activated C8-B4 cells of cerebellar microglial origin. *Journal of General Physiology*, *135*(4), 333–353. https://doi.org/10.1085/jgp.200910336

Tsuda, M., Masuda, T., Tozaki-Saitoh, H., & Inoue, K. (2013). P2X4 receptors and neuropathic pain. *Frontiers in Cellular Neuroscience*, *7*(191). https://doi.org/10.3389/fncel.2013.00191

Tsuda, M., Shigemoto-Mogami, Y., Koizumi, S., Mizokoshi, A., Kohsaka, S., Salter, M. W., & Inoue, K. (2003). P2X4 receptors induced in spinal microglia gate tactile allodynia after nerve injury. *Nature*, *424*, 778–783. https://doi.org/10.1038/nature01786

Tsuda, M., Toyomitsu, E., Komatsu, T., Masuda, T., Kunifusa, E., Nasu-Tada, K., … Inoue, K. (2008). Fibronectin/integrin system is involved in P2X4 receptor upregulation in the spinal cord and neuropathic pain after nerve injury. *Glia*, *56*(5), 579–585. https://doi.org/10.1002/glia.20641

Ulmann, L., Hatcher, J. P., Hughes, J. P., Chaumont, S., Green, P. J., Conquet, F., … Rassendren, F. (2008). Up-Regulation of P2X4 Receptors in Spinal Microglia after Peripheral Nerve Injury Mediates BDNF Release and Neuropathic Pain. *Journal of Neuroscience*, *28*(44), 11263–11268. https://doi.org/10.1523/JNEUROSCI.2308-08.2008

Von Kügelgen, I., & Hoffmann, K. (2016). Pharmacology and structure of P2Y receptors. *Neuropharmacology*, *104*, 50–61. https://doi.org/10.1016/j.neuropharm.2015.10.030

Warnecke, A. M. P., Kang, M. S., Jakowec, M. W., & Davies, D. L. (2020). The macrocyclic lactones ivermectin and moxidectin show differential effects on rotational behavior in the 6-hydroxydopamine mouse model of Parkinson's disease. *Behavioural Brain Research*,

393(March), 112804. https://doi.org/10.1016/j.bbr.2020.112804

Weinhausen, S., Nagel, J., Namasivayam, V., Spanier, C., Abdelrahman, A., Hanck, T., … Müller, C. E. (2022). Extracellular binding sites of positive and negative allosteric P2X4 receptor modulators. *Life Sciences*, *311*(PA), 121143. https://doi.org/10.1016/j.lfs.2022.121143

Werner, S., Mesch, S., Hillig, R. C., Ter Laak, A., Klint, J., Neagoe, I., … Steinmeyer, A. (2019). Discovery and Characterization of the Potent and Selective P2X4 Inhibitor N-[4-(3-Chlorophenoxy)-3-sulfamoylphenyl]-2-phenylacetamide (BAY-1797) and Structure-Guided Amelioration of Its CYP3A4 Induction Profile. *Journal of Medicinal Chemistry*, *8*. https://doi.org/10.1021/acs.jmedchem.9b01304

Whiteaker, K. L., Gopalakrishnan, S. M., Groebe, D., Shieh, C.-C., Warrior, U., Burns, D. J., … Gopalakrishnani, M. (2001). Validation of FLIPR Membrane Potential Dye for High Throughput Screening of Potassium Channel Modulators. *SLAS Discovery*, *6*(5), 305–312. https://doi.org/10.1177/108705710100600504

Wilson, H. L., Varcoe, R. W., Stokes, L., Holland, K. L., Francis, S. E., Dower, S. K., … Crossman, D. C. (2007). P2X receptor characterization and IL-1/IL-1Ra release from human endothelial cells. *British Journal of Pharmacology*, *151*(1), 96–108. https://doi.org/10.1038/sj.bjp.0707213

Wolstenholme, A. J., & Rogers, A. T. (2005). Glutamate-gated chloride channels and the mode of action of the avermectin/milbemycin anthelmintics. *Parasitology*, *131*(SUPPL. 1). https://doi.org/10.1017/S0031182005008218

Xiong, K., Li, C., & Weight, F. F. (2000). Inhibition by ethanol of rat P2X4 receptors expressed in Xenopus oocytes. *British Journal of Pharmacology*, *130*(6), 1394–1398. https://doi.org/10.1038/sj.bjp.0703439

Xu, H., & Ren, D. (2015). Lysosomal Physiology. *Annual Review of Physiology*, *77*(1), 57–80. https://doi.org/10.1146/annurev-physiol-021014-071649

Yamamoto, K., Korenaga, R., Kamiya, A., & Ando, J. (2000). Fluid Shear Stress Activates Ca 2+ Influx Into Human Endothelial Cells via P2X4 Purinoceptors. *Circulation Research*, *87*(5), 385–391. https://doi.org/10.1161/01.RES.87.5.385

Yamamoto, K., Korenaga, R., Kamiya, A., Qi, Z. H. I., Sokabe, M., Ando, J., … Px, J. A. (2000). P2X4 receptors mediate ATP-induced calcium influx in human vascular endothelial cells, 285–292.

Yamamoto, K., Sokabe, T., Matsumoto, T., Yoshimura, K., Shibata, M., Ohura, N., … Ando, J. (2006). Impaired flow-dependent control of vascular tone and remodeling in P2X4-deficient mice. *Nature Medicine*, *12*(1), 133–137. https://doi.org/10.1038/nm1338

Yang, A., Sonin, D., Jones, L., Barry, W. H., & Liang, B. T. (2004). A beneficial role of cardiac P2X4 receptors in heart failure: Rescue of the calsequestrin overexpression model of cardiomyopathy. *American Journal of Physiology - Heart and Circulatory Physiology*, *287*(3 56-3), 1096–1103. https://doi.org/10.1152/ajpheart.00079.2004

Yatime, L., Buch-Pedersen, M. J., Musgaard, M., Morth, J. P., Winther, A. M. L., Pedersen, B. P., … Fedosova, N. (2009). P-type ATPases as drug targets: Tools for medicine and science. *Biochimica et Biophysica Acta - Bioenergetics*, *1787*(4), 207–220. https://doi.org/10.1016/j.bbabio.2008.12.019

Zabala, A., Vazquez-Villoldo, N., Rissiek, B., Gejo, J., Martin, A., Palomino, A., Perez-Samartín, A., Pulagam, K. R., Lukowiak, M., Capetillo-Zarate, E., Llop, J., Magnus, T., Koch-Nolte, F., Rassendren, F., Matute, C., & Domercq, M. (2018). P2X4 receptor controls microglia activation and favors remyelination in autoimmune encephalitis. *EMBO Molecular Medicine*, *10*(e8743), 1–20. https://doi.org/10.15252/emmm.201708743

Zemkova, H., Khadra, A., Rokic, M. B., Tvrdonova, V., Sherman, A., & Stojilkovic, S. S. (2015). Allosteric regulation of the P2X4 receptor channel pore dilation. *Pflügers Archiv - European Journal of Physiology*, *467*(4), 713–726. https://doi.org/10.1007/s00424-014-1546-7

Zemkova, H., Tvrdonova, V., Bhattacharya, A., & Jindrichova, M. (2014). Allosteric modulation of ligand gated ion channels by ivermectin. *Physiological Research*, *63 Suppl 1*(SUPPL.), S215-24. Retrieved from http://www.ncbi.nlm.nih.gov/pubmed/24564661

Zhou, P., Lu, S., Luo, Y., Wang, S., Yang, K., Zhai, Y., … Sun, X. (2017). Attenuation of TNF-α-induced inflammatory injury in endothelial cells by ginsenoside Rb1 via inhibiting NF-κB, JNK and p38 signaling pathways. *Frontiers in Pharmacology*, *8*(AUG), 1–13. https://doi.org/10.3389/fphar.2017.00464